Spring 2015

The relative effect of charge dimensions on elastic vibration attenuation and blast-induced seismic energy concepts

Nathan Thomas Rouse

Department: Mining and Nuclear Engineering

THE RELATIVE EFFECT OF CHARGE DIMENSIONS ON ELASTIC VIBRATION ATTENUATION AND BLAST-INDUCED SEISMIC ENERGY CONCEPTS

by

NATHAN THOMAS ROUSE

A DISSERTATION

Presented to the Faculty of the Graduate School of the

MISSOURI UNIVERSITY OF SCIENCE AND TECHNOLOGY

In Partial Fulfillment of the Requirements for the Degree

DOCTOR OF PHILOSOPY

in

MINING ENGINEERING

2015

Approved
Jason Baird, Advisor
Paul Worsey
Braden Lusk
Dale Preece
Ruilin Yang

ABSTRACT

This dissertation focuses on expanding the blasting industry's current understanding of the effect of charge geometry on blast vibration attenuation. The work includes a multiple regression analysis of a sample population of signature hole blast vibration data. The regression analysis is used to identify the relative effect of the variables that affect blast vibrations at various distances from the charge. The study suggests that the most common vibration models used in the blasting industry do not use all of the statistically significant variables. Therefore, the models neglect to fully describe the relationship between the significant variables and the blast vibration. The results of the statistical study are used as a foundation for a new method of analyzing and presenting blast vibration data that does fully describe this relationship.

Currently, the blasting industry relies on variations of the scaled distance equation and the Z-Curve to predict or illustrate blast vibration characteristics. These methods focus on blast vibration amplitude and frequency, charge weight, and the distance from the charge. However, neither method solely accounts for all of these details. Additionally, both methods omit variables that have a statistically significant effect on blast vibration attenuation. This document shows that the current methods can be improved upon by developing a methodology that focuses on blast vibration energy. Energy, which can account for blast vibration amplitude, frequency, and duration, can be related to all of the statistically significant variables. Energy relationships also have an advantage over the traditional methods since energy is more easily understood by the general public.

ACKNOWLEDGMENTS

Many thanks go to all who have supported me in one way or another throughout the process finishing my PhD. I have been supported on a daily basis by John Morgan and Linda Carroll and all of my peers at Morgan Worldwide and RESPEC. Many thanks to John and Linda for employing me, providing me with the opportunity (and funding) to pursue this degree, and essentially filling in as my Lexington parents. The rest of my peers and friends at the office have also supported me throughout the process. I would not be where I am as an engineer without them.

My committee has been an invaluable asset by advising and assisting me in many ways throughout this process. Jason Baird, Paul Worsey, Braden Lusk, Dale Preece and Ruilin Yang have been valuable resources, and I owe them much for my development as a blasting engineer and researcher. I also owe Ayman Tawadrous equally for his help as an unofficial committee member and the University of Kentucky Applied Statistics Lab staff for their help with the statistics portion of my research.

There are also many individuals and companies that have helped with various aspects of my project by providing technical advice, testing support, and all manners of other support. Namely, I thank Julian Smith of Orica Mining Services; Bob Satterfield and Terry Figgins of Hilltop Natural Resources; and Tyler Acorn of Newmont Mining Corporation, Maggie Hettinger of Barrick Gold Corporation and Jhon Silva of the University of Kentucky for providing much-needed blast vibration data. There are too many others to name; however, I thank them all equally for their help in this endeavor.

Finally, I thank my family and friends for supporting me throughout the process. My sanity has benefited the most from them, and for that, I am greatly indebted.

TABLE OF CONTENTS

PAGE

LIST OF FIGURES

PAGE

LIST OF TABLES

PAGE

NOMENCLATURE

Symbol	Description
D	Distance from the center of a blast to a point of interest.
A	Amplitude of a wave
f	Frequency of a wave.
φ	Phase of a wave.
t	Time.
PPV	Peak particle velocity
PV	Particle velocity.
PD	Particle displacement.
PD_M	Maximum particle displacement.
PA	Particle acceleration.
$VSPV$	Vector sum particle velocity.
R	Radial or longitudinal component of vibration waveform.
V	Vertical component of vibration waveform.
T	Transverse component of vibration waveform.
P wave	Primary wave
S wave	Secondary wave
R wave	Rayleigh wave
W	Maximum weight of explosive per delay
$SRSD$	Square root scaled distance
ρ	Density of the ground or other material
c	Propagation velocity of the ground.

c_R	Radial, or longitudinal, propagation velocity of the ground
PV_R	Radial, or longitudinal, particle velocity
a	Site specific constant
b	Site specific constant
K	Site specific constant
α	Site specific constant
β	Site specific constant
c_P	P wave propagation velocity
UCS	Unconfined compressive strength
E	Young's Modulus
u	Particle velocity
e	Specific internal energy (internal energy per unit mass)
P	Pressure
U	Shock wave propagation velocity
v	Specific volume
C_0	Bulk sound speed
s	Slope value in shock velocity equation
ER	Energy Ratio
F	Force
E_{SR}	Radial Seismic Energy
PE	Potential Energy
KE	Kinetic Energy
x	Distance a spring or material is compressed

k	linear spring constant
r	radius
m	mass of an object
a_m	acceleration of an object
W_k	Work
d	Displacement
P_k	Power
A_R	Area
Φ	Energy flux
λ, μ	Lame's constants
ε	Strain

1. INTRODUCTION

1.1. BACKGROUND

For years, blasting engineers have endeavored to understand and minimize the potentially negative effect of blast-induced seismic vibrations. Due to this effort, many rules-of-thumb, empirical models, and software packages have been made available to the industry to aid in predicting and evaluating blast vibrations. Two such tools commonly used throughout the blasting industry are the scaled distance equation and the Blasting Level Chart, more commonly known as the "Z-Curve" (Ambraseys & Hendron, 1968; Siskind, Stagg, Kopp, & Dowding, 1980). Both of these methods are adopted by the U.S. Office of Surface Mining Reclamation and Enforcement (OSMRE) as tools for defining safe blasting levels in surface coal mining (Use of Explosives: Control of Adverse Effects, 1983). In addition to OSMRE, state regulatory agencies apply these methods to construction blasting and production blasting for other mining types.

The scaled distance equation and the Z-Curve are conservative empirical equations. They are relatively successful predictive tools; however, each method has its own drawbacks. Despite this, they have been in use for over the last few decades, and, in part due to the inclusion in U.S. Federal regulations, are still widely in use today.

In addition to the scaled distance and Z-Curve, there are many other methods used to evaluate blast vibrations. These vary from simple, field calculations to complex computer simulations (Spathis, 2010). Yet to this day, there is not an easy-to-use, empirical method that compares all of the most significant variables that affect blast vibrations to all of the most important features of a blast vibration.

This issue is confounded by the blasting industry's current understanding of some of the variables that affect blast vibrations. Many variables that affect blast vibrations have been studied in detail and are basically understood. These variables include basic geologic factors, explosive charge characteristics, environmental influences, and blast pattern design. Another set of variables, those relating to charge geometry, are not understood to the same extent as any of the aforementioned factors. The blasting industry has overlooked the effects of the charge diameter, or cross-sectional area, and length of the powder column in the blasthole on blast vibrations. Therefore, it is not known how, or to what extent, charge geometry affects blast vibrations.

It is impossible to develop a method for assessing blast vibrations that incorporates *all of the most influencing factors* affecting blast vibrations without a better understanding of the effect of charge geometry on blast vibrations. Therefore, two interrelating problems currently exist in the blasting industry: (a) an inadequate understanding of the effect of charge geometry on blast vibrations and (b) there is not a method of assessing blast vibrations that incorporates the most influential variables and the most important elements of a blast vibration.

1.2. OVERVIEW

This document details the important features of blast vibrations, including amplitude, frequency and duration, and highlights the many variables that affect blast vibrations, such as distance from the charge and charge weight. The effects of many of these variables have been studied over the last few decades; however, a literature review

shows that there is a limited understanding of the effect of charge geometry on blast vibrations.

Additionally, evidence is presented to illustrate that the modern blasting industry requires an updated, empirical blast vibration assessment tool. Current empirical tools, such as the scaled distance model and Z-Curve, do not include all of the significant variables that affect blast vibrations or account for all of the major features of a blast vibration. They also present data in a manner that is not easily understood, and therefore, commonly misunderstood. The modern blasting industry requires a new model that does account for all of these points; however, before the model can be developed, it is important that the effects of all of the significant variables are evaluated.

Therefore, the first purpose of this study is to assess the relative effect of the charge geometry on blast vibrations with respect to the other variables that affect blast vibrations. A statistical approach is presented that is used to analyze the relative effect of each variable on the amplitude, frequency, and duration of a blast vibration waveform using data from a collection of signature hole tests. A multiple regression analysis ultimately identifies the statistically significant variables that affect blast vibrations.

The second purpose of this study is to present estimates for the blast vibration energy, which can be related to the blast vibration amplitude, frequency, and duration. Blast vibration energy is important since it can be understood easily by the general public, applied directly to structural analyses, and used in the same manner as the tools currently used to evaluate blast vibrations.

1.3. SIGNIFICANCE

This research effort expands the industry's knowledge of blast vibration phenomena by assessing the relative effect of charge geometry on blast vibrations and introducing the groundwork for a new tool of assessing blast vibrations.

Understanding the relative effect of the charge geometry on blast vibrations will help blast vibration model developers enhance their models. The method used to analyze the effect of charge geometry is innovative for two reasons: (a) multiple regression has not been used to study blast vibrations to the level of detail it is used in this study and (b) to this point, signature hole data have not been compared between multiple sites due to variability in many of the factors that affect vibrations.

The proposed energy method incorporates the proven aspects of the blast vibration evaluation methods currently in use. The enhancement of calculating vibration energy improves upon those methods by innovatively accounting for all of the important blast vibration features simultaneously. The method is further enhanced by including the effect of all of the statistically significant variables in the analysis.

In summary, this study is significant for the following points:

- A library of historical signature hole data is compiled and a global review and comparison of the data is presented.
- Multiple regression models are developed to determine the relative influence of the charge geometry on vibration attenuation with respect to other factors.

- The blasting industry is presented with evidence of the effect of charge geometry, which, in part, allows members of the industry to update advanced blast vibration models.
- Groundwork for a proposed energy model is presented. The model could be used as a tool to provide a greater understanding of blast vibration attenuation characteristics.
- Overall, a greater insight to vibration control is achieved. This insight will aid in reducing environmental effects of blasting on structures.

1.4. DESCRIPTION

This document describes the multifaceted process taken to develop the groundwork for producing a modern blast vibration evaluation tool. It is arranged in the following manner:

Section 1. Introduction: description of the background behind the dissertation topic and the significance of the analysis and conclusions contained within the document.

Section 2. Literature Review: comprehensive review of the current knowledge and state of the art of the modern blasting industry. This section includes a review of the variables that affect blast vibration and the common vibration models used in the blasting industry.

Section 3. Data Collection: general overview of the data sources and methodology used to identify required data, develop a test matrix, and devise a field test strategy for data gathered during this study. This section

also includes a summary of the test sites, equipment, test procedure, and data analysis procedures.

Section 4. Signature Hole Data Regression Analysis: description of the complete dataset used in the regression analysis and review of the statistical analyses used to study the dataset. This section introduces the statistically important variables that affect blast vibrations, as determined by the regression analysis.

Section 5. Blast-Induced Seismic Energy: proposal for a new blast vibration evaluation tool which evaluates the blast vibration energy. The section includes a comparison of three potential methods for evaluating blast vibration energy.

Section 6. Conclusions: summary of the literature review, testing and statistical results, energy model study, conclusions, and recommendations for further work.

2. LITERATURE REVIEW

This section focuses on the characteristics and features of blast vibrations, the factors that affect blast vibrations, and a number of models and tools that are currently used to evaluate blast vibrations for various applications. The literature review gives the background required to understand the need to evaluate the effect of charge geometry on blast vibrations. Additionally, it proves the need for a modern empirical tool that can be used to evaluate the effect of all of the statistically significant variables on the blast vibration energy. This section is arranged in the following order:

- Characteristics of Blast Vibrations
- Features of a Blast Vibration Waveform
- Variables that Affect Blast Vibrations
- Vibration Models

2.1. CHARACTERISTICS OF BLAST VIBRATIONS

Blast vibrations are the resultant transient seismic waves caused by the detonation of a charge or multiple charges in a blast. Transient refers to blast vibrations occurring as a sudden pulse of energy in the ground, attenuating rapidly as time and distance from the source increase (Bollinger, 1971). Transient waves propagate through the earth and along its surface.

The transient energy pulse originates from the detonation of an explosive charge. When the charge detonates, the ground near the blasthole undergoes dynamic shock due to the force of the detonation. The explosive-generated energy rapidly decays from a

dynamic shock state to elastic vibration as a significant amount of the shock energy is expended by crushing and breaking rock, creating new cracks, and extending existing fractures (Siskind & Fumanti, 1974).

Elastic deformation, which is caused by the elastic vibration, is a temporary change in a material's shape when it undergoes a stress, where the material returns to its original shape upon unloading. A transient elastic vibration can be structurally damaging; therefore, it is common for blasting operations to monitor the elastic vibrations using a blasting seismograph. A seismograph monitors a single point, or particle. The vibration trace, or waveform, produced by the seismograph describes the reaction of the single point to the passing wave. The waveform passing the particle is described by three perpendicular components of the passing vibration: radial, vertical, and transverse.

2.1.1. Components of Seismic Waves. A seismograph produces a vibration waveform for each of the three components since each component is monitored by a separate velocity transducer (Figure 2.1) (Dowding, 1985). Separately, the components do not produce a complete three-dimensional image of the vibration; however, each component does provide insight into the nature of the passing vibration at the monitored location.

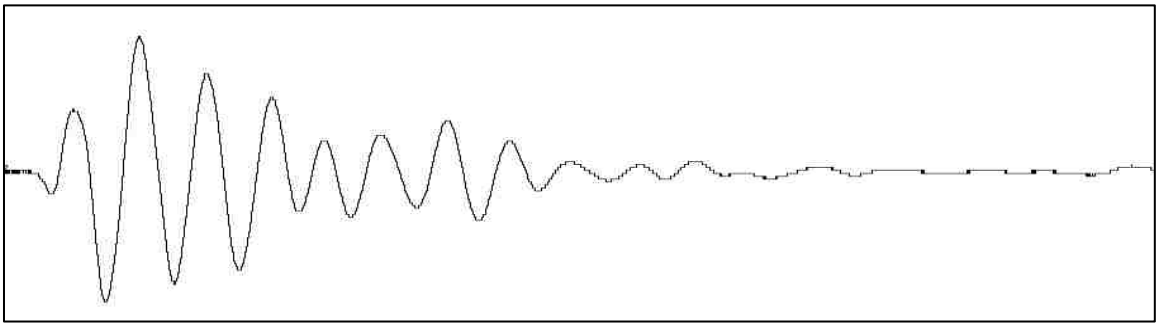

Figure 2.1. Radial component of the particle velocity of a blast vibration waveform.

2.1.1.1. Radial waves. The radial, or longitudinal, component describes vibration along the radial travel path of the seismic wave from the source charge. This component describes the compressive and expansive action of the blast vibration.

2.1.1.2. Vertical waves. The vertical component describes the vertical motion of the vibration as it passes the monitoring location. This component describes the vertical shear action of the blast vibration.

2.1.1.3. Transverse waves. The transverse component describes the horizontal motion perpendicular to the travel path of the vibration as it passes the monitoring location. This component describes the horizontal shear action of the blast vibration.

2.1.2. Types of Seismic Waves. Seismic waves propagate as body waves through the earth's medium or surface waves along the surface of the earth. Body waves are also of interest as they.

2.1.2.1. Body waves. Body waves, which are the faster of the two wave types, are comprised of both compressive (primary) and shear (secondary) waves that move through the earth's medium (Figure 2.2). They dominate blast vibrations at short distances where the vibration has had little influence from the earth's surface or bedding

planes and fractures. Once the body waves reach a surface boundary, surface waves and additional shear waves are produced (Dowding, 1985).

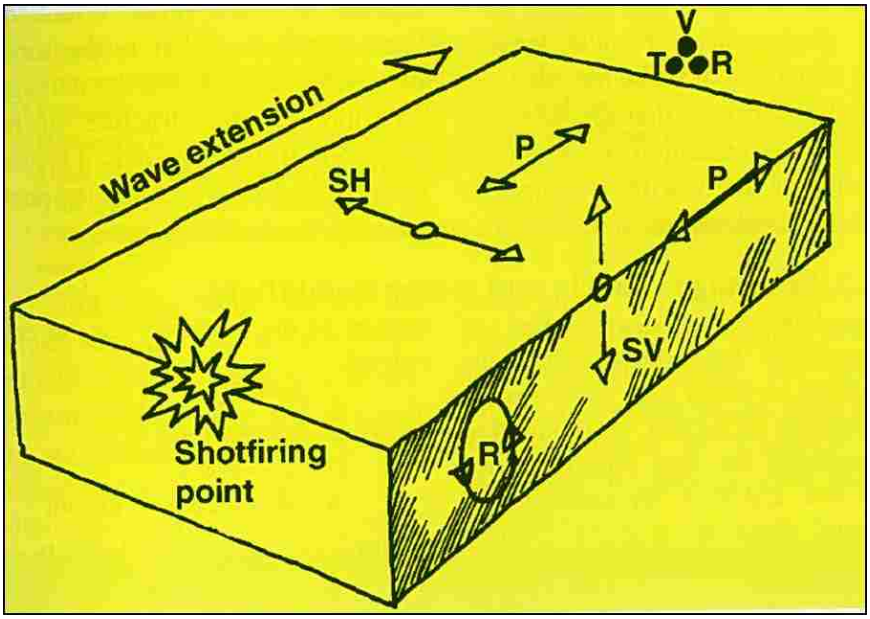

Figure 2.2. Types of seismic waves: primary (P), secondary (SH and SV), and Rayleigh (R) (source: Olofsson, 2002).

2.1.2.2. Surface waves. Surface waves propagate along the surface of the earth, guided by the earth and atmosphere contact (Siskind, Crum, & Plis, 1993). They are slower moving than the body waves, and at great distances from the source, they arrive noticeably later than primary and secondary waves (Siskind, Crum, Otterness, & Kopp, 1989). Near to the source, they are indistinguishable from body waves.

Surface waves can be dangerous to structures due to a concentration of surface wave energy near the earth's interface or other layers. The surface waves exhibit low frequency, long duration, and sometimes repeated nearly sinusoidal waves for multiple

cycles (Siskind et al., 1989). The repeated cycles of low frequency waves can produce excessive structural displacement and strain (Siskind, Stachura, & Nutting, 1985).

2.2. FEATURES OF A BLAST VIBRATION WAVEFORM

A blast-produced seed waveform, like any periodic waveform, can be simplified to a combination of individual sinusoidal waveforms (Silva-Castro, 2012). Periodic sinusoidal waves can be defined by three features, amplitude (*A*), frequency (*f*), and phase (φ), at a specific point in time (*t*):

$$Y(t) = A * sin(2\pi ft + \varphi) \quad (1)$$

However, blast vibrations decay instead of repeating periodically. Therefore, when analyzing blast vibrations, the amplitude, frequency, and duration are of the greatest importance (Stagg & Engler, 1980). A fifth feature, attenuation, describes the changes to the vibration over time and distance as it decays. Each of the five features of a blast vibration is described in the following subsections.

2.2.1. Amplitude. The amplitude is the height of the waveform. In blasting, the amplitude refers to the maximum and minimum values of the waveform with respect to the baseline (zero value). Amplitude can be used to describe particle acceleration, particle velocity, or particle displacement. Any kinematic quantity can be used; however, blast vibrations are most often described by particle velocity, which is measured in units of millimeters per second or inches per second due to requirements of state and federal regulations in the U.S. (Spathis, 2010).

Particle velocity has been identified as the best descriptor of vibration amplitude since particle velocity is more closely related to structural damage than acceleration or

displacement (Duvall & Fogelson, 1962). In contrast, displacement could be argued as being a more effective descriptor of vibration amplitude since displacement directly relates to stress and strain, which can be directly related to physical characteristics of rock and structures. In Duvall and Fogelson's time, displacement was not easily calculated for two reasons: (a) transducers were available which could only measure either acceleration or velocity and (b) desktop computing was not available to integrate the acceleration or velocity waveforms to provide displacement until the mid-1980s. In modern times, displacement waveforms can easily be computed from velocity waveforms using spreadsheets or pre-programmed software packages.

This literature review focuses on particle velocity due to its widespread use throughout the blasting industry in practice and in regulations. Particle velocity can describe the radial, vertical, or transverse components of a vibration. The particle velocity (*PV*) values of each component can also be used together to describe the three-dimensional motion of the three components through the vector sum particle velocity (*VSPV*) waveform:

$$VSPV = \sqrt{PV_R^2 + PV_V^2 + PV_T^2} \tag{2}$$

The subscripts *R*, *V*, and *T* refer to the three components of the vibration. The vector sum waveform can be used to identify the peak vector sum particle velocity, which describes the greatest three-dimensional particle velocity amplitude of that waveform. Due to the calculation, the vector sum is always the absolute value of the three-dimensional amplitude at time *t*; therefore, the vector sum waveform cannot be used to describe the complete three-dimensional motion of the particle.

Regardless of whether a waveform describes a particle's acceleration, velocity, or displacement, the amplitude of the waveform varies between each of the three axial components of the vibration. In the near-field environment, which has never been universally defined but refers to the region near to the blasthole, blast-induced vibrations commonly have a larger vertical amplitude component. Siskind et al. (1989) identified near-field as any location less than 91.4 m (300 ft) from the charge, while Siskind et al. (1985) identified this distance as 152.4 m (500 ft). In the far-field region, at greater distance away from the charge, vibrations have a larger radial component (Yang & Kay, 2011).

Table 2.1 gives the typical ranges for the particle amplitude of a blast vibration, along with each additional blast vibration feature. The table also includes the wavelength, which is not listed as a feature of the vibration waveform in this literature review; however, wavelength, as well as amplitude, frequency, and duration, relates to the attenuation of the vibration, which is discussed.

Table 2.1. Ranges of blast vibration features (after Dowding, 1985).

Feature	Range	Units
Particle Displacement	10^{-4} to 10	mm
Particle Velocity	10^{-4} to 10^{3}	mm/s
Particle Acceleration	10 to 10^{5}	mm/s^2
Frequency	0.5 to 200	Hz
Duration	0.5 to 2	s
Wavelenth	30 to 1500	m

2.2.2. Frequency. Frequency in blasting can describe the period of each cycle of a blast vibration or the most repeated period of a blast vibration; therefore, it plays an essential role in blast vibration analysis. Fundamentally, frequency is a direct indication of the displacement of the ground, meaning the longer the period of each cycle, or lower frequency, the greater the displacement during each cycle of the particle velocity waveform. The effect of frequency on particle displacement (*PD*) is illustrated by the following equation for particle velocity (*PV*) at time, *t*, as a function of particle displacement and frequency, f (Dowding, 1985):

$$PV = PD * (2\pi f) \tag{3}$$

The same logic applies to the equation for particle acceleration (*PA*):

$$PA = PV * (2\pi f) = PD * (2\pi f)^2 \tag{4}$$

These simple equations are derived from a sinusoidal wave; therefore, they can only be used for approximation and can result in estimates that significantly differ from the actual values (Yang, 2012).

The most common blast vibration frequencies of interest are either the dominant frequency or the principal frequency (Taylor, Fourney, & Leiste, 2013). The dominant frequency is the most recurrent frequency value of the entire waveform. It is found by plotting the frequency spectrum, which is the representation of a time domain signal in the frequency domain, using a Fast Fourier Transform (FFT) (Wheeler, 1997). Currently, software packages developed for use with seismographs include a FFT function to determine the dominant frequency of a blast vibration. The dominant frequency can often manifest as two or more dominant frequency zones, which are identified in FFT diagrams with more than one peak (Silva-Castro & Lusk, 2012).

The principal frequency is the frequency associated with the peak amplitude of the vibration. It is found by identifying the peak amplitude of the vibration and calculating the frequency of that cycle using the half cycle estimate. The half cycle estimate, or zero crossing method, is the most common method used to determine the principal frequency of a specific cycle (Wheeler, 1997). For this method, the time difference between the zero crossing values before and after the peak amplitude is multiplied by two and inverted to obtain a frequency estimate. The accuracy of this estimate depends on how closely the peak half cycle approximates a sinusoidal waveform.

The principal frequency of blast vibrations can range from 0.5 Hz to 200 Hz (Table 2.1). Figure 2.3 shows that principal frequencies typically fall within the 0.5 Hz to 40 Hz ranges for quarry and coal mining, while construction blasting typically produces higher frequency blast vibrations. The small distances that are monitored for construction blasting tend to exhibit the higher principal frequencies (Dowding, 1985).

Coal mine blasting tends to produce the lowest principal frequencies due to:

- relatively larger blasts,
- greater monitoring distance for structures since coal mines are typically farther from dwellings than quarries and construction areas, and
- greater effect of geologic factors, which becomes more prevalent at greater distances (Siskind et al., 1985).

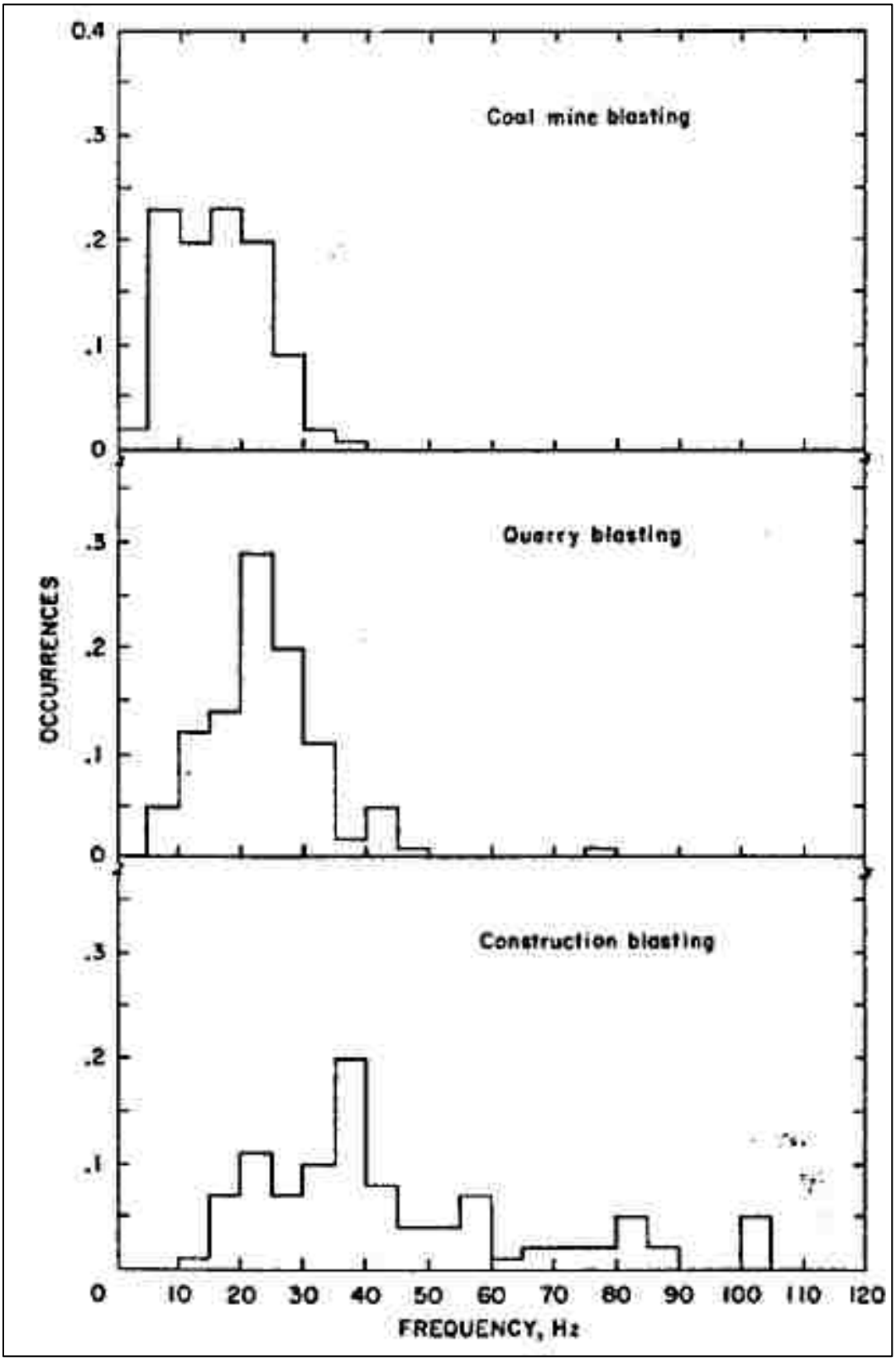

Figure 2.3. Principal frequency ranges for three blasting industries (source: Siskind et al., 1980).

The principal frequency generated by blast vibrations has also been related to ground resonant frequency (Yang, Scovira, & Patterson, 2009). The ground's resonant frequency is location specific due to geology. According the vibration mechanics theory, a single degree of freedom system has one natural frequency, which is found to have a very small difference from the ground's resonant frequency due to the amount of damping in the system (Yang, Whitaker, & Kirkpatrick, 2009). To complicate the scenario, the ground is a continuous deformable body, so there are an infinite number of degrees of freedom of the ground at a blast site. Therefore, only ranges of the ground's resonant frequency can be estimated as opposed to a single specific value. Additionally, as the stiffness effect of the ground and the mass of the system increase with distance from the charge, the resonant frequency range is affected accordingly, meaning frequency values vary over distance.

2.2.3. Phase. The phase is the time difference, or shift, of a sinusoidal wave between the positive peak of the waveform and the positive peak of a reference signal of the same frequency. Phase is not of interest in regulatory compliance monitoring of blast vibrations because the vibrations are single events. However, phase is of interest when modeling various delay patterns of production blasts using vibration waveforms produced by single charges, termed seed waveforms (Anderson, Ritter, Winzer, & Reil, 1985; Crenwelge & Peterson, 1986). Phase can also refer to the lag of the response between the signal output of a geophone and the physical vibration (Farnfield, 1996). The phase response of the seismograph can be corrected using a transfer function; however, this is not common practice in the blasting industry.

2.2.4. Duration. In blasting, the duration of a blast vibration refers to the length of time for a vibration to pass a specific point of interest. A blast vibration event typically lasts for 0.5 to 2 seconds (Table 2.1). The duration of a blast vibration is linearly related to the distance between the monitored point and the charge (Yang & Scovira, 2008). It is also a function of the timing of a blast, charge weight, geology, and other factors.

Blast vibration duration is an important feature to consider when long duration, low frequency vibrations have repeated peaks near a structure's yield point or when modeling to recreate or predict complete blast vibration waveforms. Potentially damaging, low frequency blast vibrations commonly have a long duration at great distances due to wave type separation (Dowding, 1985; Siskind et al., 1985; Siskind et al., 1989). The U.S. Bureau of Mines (USBM) studied the effect of long duration vibrations on residential structures, stating that a structure could resist blast vibrations for years without fatigue affecting the structure. However, the vibrations in the USBM study did eventually affect the test structure with limited amplitude and frequency showing that repeated vibrations around the yield point of a structure cause fracture propagation (Stagg, Siskind, Stevens, & Dowding, 1984).

The duration of a blast vibration is especially important when replicating or predicting blast vibrations (Silva-Castro, 2012). Models that replicate an entire blast vibration waveform, as opposed to only predicting amplitude and/or frequency, must evaluate duration in order to predict the full waveform.

2.2.5. Attenuation. Attenuation refers to the decay of a blast vibration over time. This occurs from two standpoints: (a) the decay of a vibration over time at a constant

location or (b) the decay of a vibration as it propagates with increasing distance. Attenuation is mainly due to three major causes: geometric spreading, material damping, and apparent attenuation, which is the effect of material interfaces on the vibration (Yan, Tham, & Yuen, 2013). The geometric spreading of a blast-induced vibration with distance typically results in an increase in wave front size (Yan et al., 2013).

The decay of a vibration at a specific location can be seen on any blasting seismogram, which is the vibration trace generated by a seismograph. A seismogram will typically show an amplitude peak followed by cycles of decreasing intensity before the vibration decays to equilibrium (Figure 2.1) or another peak amplitude spike occurs.

The second definition of attenuation refers to the decay of the vibration as it propagates with increasing distance. This definition is of most interest to this study. A simple idealization of this process is shown in Figure 2.4. The idealized waveform is a single spike pulse, similar to a shockwave, when very close to the blast (Point A). At this point, the vibration is transmitted directly through the ground. As the pulse propagates away from the source, it attenuates to a sinusoidal-shaped elastic vibration (Point B). By the time the vibration reaches Point B, it has a longer duration and is a combination of direct transmission, reflection, and refraction waves. As the wave propagates, the wave reflects and refracts of fractures and discontinuities and other changes in lithology of the ground, which attenuate the amplitude, frequency, and duration of the wave to varying degrees. Figure 2.4 is oversimplified; however, it serves to illustrate how a blast vibration generally attenuates as it propagates away from the charge.

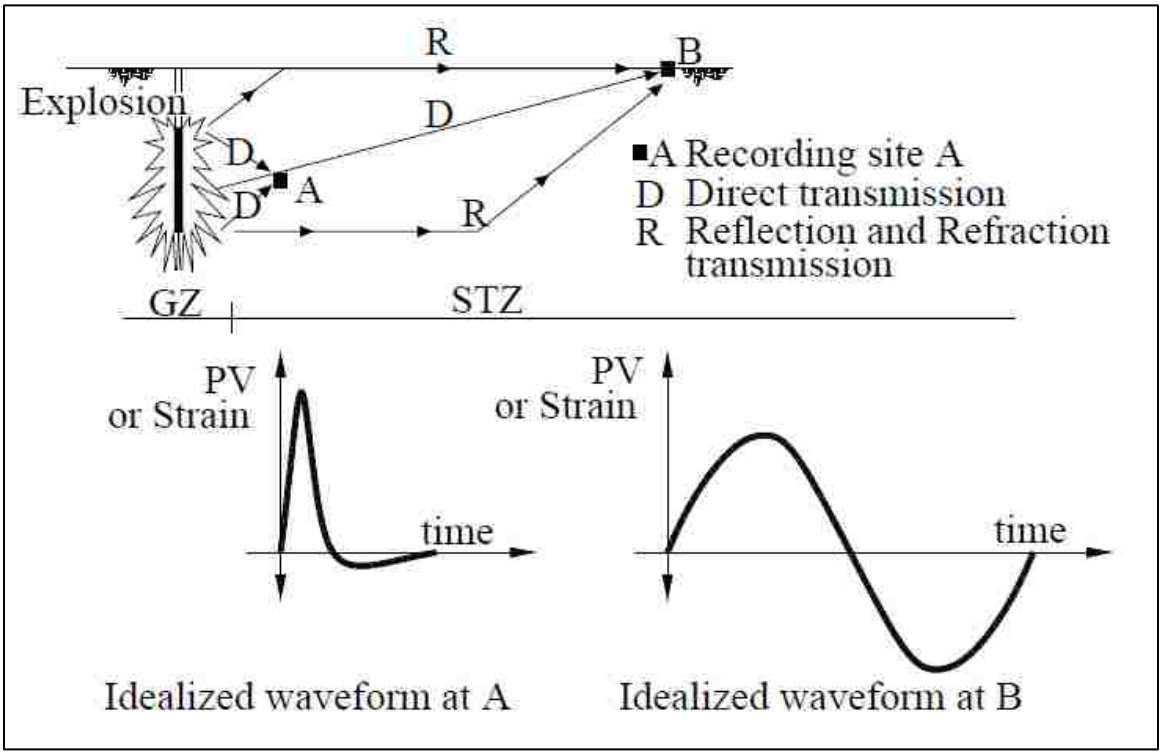

Figure 2.4. Idealized attenuation of seismic vibration (source: Silva-Castro, 2012).

2.3. VARIABLES THAT AFFECT BLAST VIBRATIONS

Many variables affect blast vibration generation and propagation. These variables include blast design characteristics such as charge weight, charge geometry, charge type, blast pattern and timing, and confinement, and environmental influences such as geology, presence of water, direction of propagation, and preconditioning. Additionally, the recorded waveform can be affected by monitoring practices, such as monitoring distance and instrument placement and setup. The effects of these variables can be difficult to predict because even when the effect of a specific variable is understood, the effect of that variable on vibration generation or propagation will still have some variability on a hole-to-hole basis (Silva-Castro, 2012; Yang & Scovira, 2010).

This section briefly covers the current blasting industry knowledge on each of the aforementioned variables but focuses specifically on the charge geometry variables: charge diameter and charge length. The charge geometry variables are the least understood variables; therefore, this review highlights the current understanding of the effect of charge geometry on vibration attenuation and presents the importance of evaluating the relative effect of the charge geometry variables on blast vibrations. The following variables are illustrated in this section:

- Charge Weight
- Charge Geometry
- Charge Type
- Blast Pattern and Timing
- Confinement
- Geology
- Presence of Water
- Direction of Propagation
- Preconditioning
- Monitoring Distance
- Instrumentation Placement and Setup

2.3.1. Charge Weight. The charge weight is one of the most used variables in blast vibration calculations. It is a factor of charge geometry, explosive characteristics, loading conditions, and loading practices.

The peak amplitude of a blast vibration produced by a typical cylindrical blasthole increases linearly with charge weight (Crenwelge, 1988). This relationship changes as

the charge becomes larger and/or relatively less confined to where the amplitude is proportional to the charge weight to the one-half power. The charge weight-particle velocity amplitude relationship also changes as the charge geometry becomes spherical (or can be considered to be spherical) to where the amplitude scales as the cube root of the charge weight. Additionally, for larger charge weights, the shock pulse is thicker (Yang et al., 2009). Thicker shocks require greater distance to attenuate into elastic waves because larger charge weights also produce a greater amount of energy over the full detonation process.

The particle velocity spectra produced by charges with a constant diameter shows that there is little frequency shift as the charge weight ranges from 113 kg to 907 kg (250 lbs to 2000 lbs) (Figure 2.5). This figure displays data produced by four 270 mm (10-5/8 inch) charges with lengths of 2.3, 4.7, 9.3, and 18.6 m (7.5, 15.3, 30.5, and 61 ft). The stacked spectra show that the greater charge weight produces higher particle velocities along the spectrum even though the dominant frequencies are constant.

Charge weight is a function of charge geometry; therefore, the effect of charge weight on vibrations leads to the question of how the geometry of the charge affects vibrations. For example, the Crenwelge (1988) study highlighted in this section used charges of constant diameter. Therefore, the apparent effect of charge weight on amplitude derived by Crenwelge may actually be the effect of charge length on amplitude. The interrelationship between charge weight and geometry can be a confusing topic; however, it is central to this dissertation because the effect of the charge geometry needs to be addressed.

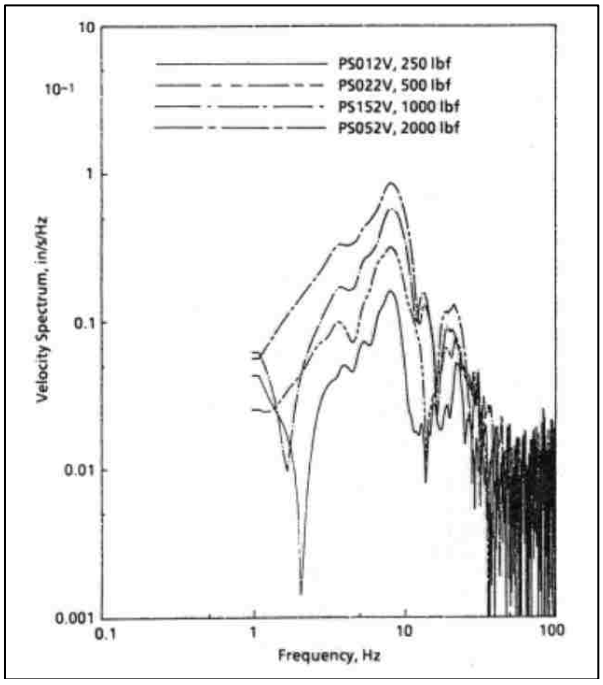

Figure 2.5. Particle velocity spectra for blast vibrations recorded from charges of varying weight and constant diameter (source: Crenwelge, 1988).

2.3.2. Charge Geometry. The charge geometry includes both the charge length and the charge diameter. Theoretically, these two variables, along with charge density, determine the charge weight. Few studies have discussed charge geometry and even fewer still have discussed or studied the effects of the charge geometry on blast vibrations. The goal of this section is to highlight the need for further evaluation of the effect of charge geometry on vibration attenuation and provide a foundation for the analysis that is described later in this document.

2.3.2.1. Charge diameter. The effect of the charge diameter or charge length on vibration attenuation has not been a focus of vibration studies or models for simple reasons. A mine or construction company will typically only have one or two drill bit sizes on a project; therefore, the operator has no interest in altering hole diameter.

Operators are also primarily concerned with production; therefore, the drill bit size is chosen to maximize productivity and efficiency.

Hole diameter has long been known to affect the characteristics of explosive performance (Fleetwood, Villaescusa, & Eloranta, 2012; Kirby, Chan, & Minchinton, 2014; Nicholls & Duvall, 1966). For example, smaller hole diameters decrease explosive performance to a point where the explosive reaches a critical diameter and ceases to detonate (Nicholls & Duvall, 1966).

In some cases, the extent of fracturing around a blasthole has been related to the blasthole diameter. This relationship is relevant because commonly used bulk explosives conform to the blasthole cross-section; therefore, the charge diameter is nominally equivalent to the blasthole diameter for bulk explosives. Charges with larger diameters have a greater tendency than charges with smaller diameters to open up fractures between holes. These fractures have a varying effect on vibration attenuation (Pugliese, 1972). Equations have been developed that relate the blasthole diameter or radius to the extent of the blast fracturing. These equations have been summarized by Siskind and Fumanti (1974). The summary shows that rock can fracture anywhere between three times the blasthole radius to 55 times the blasthole radius, depending on explosive type and geology. Blasts using 165 mm (6.5 inch) diameter holes in Lithonia granite were studied in detail (Siskind & Fumanti, 1974). The study indicates two zones of blast-damage:

- Highly damaged rock: up to eight blasthole radii
- Lesser degree of damaged rock: up to 14 blasthole radii.
- Undamaged rock: beyond 14 radii.

In most cases, blasthole diameter, as well as other factors such as blasthole depth, spacing, burden, and loading procedure, is kept constant (Adhikari et al., 2005; Nicholls, Johnson, & Duvall, 1971). In other cases, the hole diameter is not included as a variable or left out of lists of the most important blast design parameters to study (Crum, Siskind, & Eltschlager, 1992; Siskind et al., 1985). In these cases, the charge weight is assumed to account for the blasthole geometry; however, this is an assumption that is not based on any substantial evidence.

In recently published models, the charge diameter has been assumed to have no effect on explosive performance (Hudaverdi, 2012; Spathis, 2010; Tawadrous & Katsabanis, 2007). The models that do use the charge diameter as a variable only include it as a factor of charge weight (Mueller & Boehnke, 2004) or do not necessarily discuss how it was used in the model, only that it was used (Choudhury & Sitharam, 2010).

In a few models, the charge diameter is given some importance. In one model, blast vibrations have been related to charge distribution, assuming simultaneous pressurization of a section of the blasthole length (Spathis, 2010). The charge distribution can be described by the charge weight per unit length, which is only a function of the charge diameter and charge density. Redpath and Ricketts (1987) also noted in their study that the peak particle velocity for a blasthole array is primarily dependent on charge diameter and not on total charge weight because the linear charge density is solely a function of the charge diameter and explosive density. This approach, which mirrors the Spathis study, is oversimplified for most vibration cases in the elastic region because the detonation and vibration attenuation process is extremely complex.

Another recent model, which focuses on dynamic material response in the shock region near the blasthole, also describes the charge diameter as having an effect on vibration amplitude (Blair, 2014). In this study, a model was used to predict that vibration amplitude increases with increased blasthole diameter. The diameter-amplitude relationship is due to a greater volume of explosive representing greater available energy undergoing simultaneous detonation. The drawback of the Blair study, with respect to this research project, is that it does not focus on elastic material response.

In summary, the questions that follow are how much of the charge length affects the peak vibration amplitude, is the shock period a function of charge length, and does the charge length/vibration relationship in the shock region continue into the elastic vibration region? These questions are important because the charge weight per unit length could be an important factor in the elastic region or the charge weight per unit length could be inconsequential, leaving the total charge weight as the important factor in the elastic region.

2.3.2.2. Charge length. Charge length has been the subject of more attention than charge diameter, although most studies account for variances in charge length with charge weight, assuming constant diameter, such as in the study by Crenwelge (1988) discussed previously. Charge length also has a similar issue as charge diameter: a mining operation or construction operation will have a set face height to blast; therefore, changes in charge length only occur if the face height requires adjusting, the rock requires subdrilling, or other operational requirements dictate the change; therefore, the effect of variability of charge length is not commonly studied.

Crenwelge (1988) and others have pointed out that a cylindrical charge behaves as a point source as the length approaches the same dimension as the diameter. As the charge length changes, it may enhance different frequency values near the charge assuming the geology of the ground doesn't completely filter the frequency spectrum. For example, longer holes produce vibrations with higher peak particle velocities at lower frequencies than short holes, on a pound for pound basis (Worsey, 1986).

In a recent publication by Blair (2014), the effect of charge length was studied using computer modeling. This study contradicts the relationship recognized by most models, which acknowledge that increases in the charge length (causing increase in charge weight) produce vibrations with increased amplitude. Blair's analytical model, using an infinite viscoelastic medium, showed that increases in charge length do not amplify the shock wave produced by the explosive charge. Instead, the length of the shock front increases while the amplitude of the shock front is constant. Of course, the shock front and the realized vibration energy, once the vibration reduces to the elastic realm, are two different phenomena. In practice, as a vibration becomes elastic, the magnitude of vibration energy decreases significantly from that of shock energy.

Blair (2014) also conducted an empirical study and showed that a seismograph on the surface, during a surface blast, showed that the vibration amplitude is sensitive to the volume of the shock wave, implying the vibration amplitude is dependent on total charge weight alone. This is in contrast to his model most likely because the vibration at the seismograph is an elastic vibration, while the model evaluated the effect of the charge length on the shock wave very near to the charge.

2.3.3. Charge Type. The chemical composition of the explosive charge affects the energy, pressure, detonation velocity, and gasses created during the detonation process (Cooper, 1996). These detonation properties are also affected by other variations in the blasting environment. Due to all these effects, the detonation process is never ideal and the detonation properties can vary greatly (Chiappetta, 1994; Mullay, McGinley, & Stancavage, 1995).

The detonation process is typically evaluated using the velocity of detonation (VOD) of the explosive (Chiappetta, 1994; Mohanty & Yang, 1997). For most explosives, the VOD increases asymptotically to a maximum value with increased charge diameter for commercial bulk explosives (Fleetwood et al., 2012; Kirby et al., 2014), although this is not always true (Torrance, 2013).

Density is an example of an explosive characteristic that can be used to estimate performance since the detonation velocity and pressure that develop during the detonation process are affected by the density (Cooper, 1996). It is noted that in practice, cup density, the field method of measuring explosive density, and the density listed on the technical data sheet for an explosive are significantly lower than the average in-hole density by a factor of 7% to 13% (Torrance, 2013).

2.3.4. Blast Pattern and Timing. The blast pattern and timing of a blast affect the interaction of vibrations produced by individual charges in a production blast (Anderson et al., 1985; Crenwelge & Peterson, 1986). This interaction can affect the blast vibrations through superposition of the interacting vibrations or constructive interference or destructive interference, which alters the vibration amplitude and frequency (Siskind et al., 1985; Yang & Scovira, 2007). Due to the complexity of multi-

charge blasts, this study focuses on vibrations produced by single charges, or signature holes. The interaction of the vibrations produced by multiple charges in a production blast could obscure the effect of individual variables; therefore, signature holes have proven to be extremely useful for evaluating the variables that effect blast vibrations. Currently, the signature hole testing method remains the best method for evaluating the effects of the explosive charge and geologic variables on the resulting blast vibrations.

The signature hole method does have limitations when used to model a full blast. One drawback of the signature hole method is that a single hole produces amplitudes two to three times lower than production blasts (Siskind et al., 1989). The amplitude difference can be even greater, at large distances from surface coal mines, such as at those studied by Siskind et. al. (1989).

2.3.5. Confinement. In rock blasting, confinement is the degree to which a charge is buried or covered in the ground; therefore, it is another major variable that affects vibrations (ISEE, 1998). Low confinement typically directs the explosive energy to throw rock or as airblast, while higher confinement typically directs more explosive energy into the ground as seismic vibrations (ISEE, 1998). Higher confinement forces a larger and longer pulse to occur, which equates to higher particle velocity and lower frequency (Worsey, 1986). From a detonation physics standpoint, confinement also affects the VOD of the explosive, thereby making the detonation and subsequent vibration processes more complex (Fleetwood et al., 2012).

Many sources account for confinement with the powder factor, which is the weight of explosive per unit volume of rock (Tawadrous, 2014). In this way, the powder factor can be thought of as the inverse of confinement. However, powder factor can be

an incorrect term to use for confinement when comparing small burden/large spacing shots to standard burden/standard spacing shots. When powder factor is used, the geometry must be kept constant.

Confinement can also be described by the length of stemming. Stemming is the inert material placed on the charge to provide confinement and direct explosive energy and gases toward breaking and heaving rock. The length of stemming is usually a function of the blasthole diameter and burden between the blasthole and the face but is also adjusted to account for geologic variability. Stemming material is usually crushed rock or drill cuttings; crushed rock is a better confining material. Increasing or decreasing the length of stemming in a blasthole can decrease or increase vibrations; although this relationship is not straightforward.

Blastholes that have no free face other than the surface are termed fully confined blastholes. In this scenario, which is not a typical production scenario, confinement is directly related to stemming. For fully confined blastholes, long stemming length equals high confinement, which in turn, causes higher vibration amplitudes than short stemming length. Zhou and Stump (2006) showed that fully confined blasts have two to four times higher seismic energy than free face shots or crater shots. They used 311 mm (12.25 inch) diameter blastholes and defined free face blasts as those with normal burden of 9.1 m (30 ft) and fully confined blasts as those with double normal burden of 18.3 m (60 ft). In reality, the double normal burden blasts were not technically fully confined since the charges still had a free face which gave energy relief.

2.3.6. Geology. Many aspects of the effects of geology on rock blasting have been studied in detail prior to this project. Specific topics include stratification and

bedding, fractures and joints, folds, dip, cavities, rock lenses, and anisotropy (Nicholls et al., 1971; Pugliese, 1972; Ozer, Karadogan, Kalayci, Aksoy, & Keti, 2012; Singh & Narendrula, 2007; Siskind et al., 1985; Walter & Carroll, 1981).

Despite years of research, there is still some disagreement over the effect of some of these parameters. For example, Singh and Narendrula (2007) state that wave attenuation is minimal when the wave incidence is perpendicular or parallel to a joint face but is maximum at 15 to 45 degrees to the face. Wave attenuation has been also said to be the most dramatic in the direction perpendicular to the strike of rock joints because the joints act as low-pass filters by filtering out high frequencies (Wu, Hao, Zhou, & Chong, 1998). At a certain point, joint faces can even have a large enough aperture that the joint acts like a free face (Tariq & Worsey, 1996).

The type of ground also impacts vibration attenuation. In-situ rocks produce lower amplitudes and higher frequencies than overburden on outcrops because weathered material and soils absorb energy differently than in-situ rocks (Nicholls et al., 1971; Singh & Narendrula, 2007). The energy transmission and absorption characteristics of a material can in part be described by the material's impedance value. Impedance is equal to the product of a material's density and longitudinal propagation velocity through the material (Nicholls & Duvall, 1966). Impedance mismatch, which occurs when two materials have dissimilar impedance values, can result in varying magnitudes of reflection and/or transmission of vibration energy at the interface of two materials. An example of impedance mismatch in one study is that fault planes can cause a decrease OR increase in vibration amplitude depending on relative hardness of rock on either side

of the plane (Ozer et al., 2012). Therefore, the effect of a fault plane is most likely dependent on the impedance values of the materials on either side of the plane.

The distance from the charge to the point where geology has a major effect on vibrations is also important to this study. Near the blasthole, vibrations are unaffected by in-situ rock due to the overwhelming nature of explosive charge (Siskind et al., 1989). There has not be a definitive study on the distance at which geology begins to affect vibration attenuation; however, the propagating medium has appeared responsible for determining wave characteristics at distances that range from 91.4 m (300 ft) from the charge (Siskind et al.,1989) to 152.4 m (500 ft) from the charge (Siskind et al., 1985).

Geology, as a whole, may be best accounted for by using a standard distribution type of methodology (Silva-Castro, 2012; Yang & Lownds, 2011). It has also been accounted for by using a rock mass factor to generalize the rock's condition (Mueller & Boehnke, 2004) or a rock quality factor, which is defined in terms of mean stored energy and energy loss during a cycle of sinusoidal deformation (Yang & Ray, 2014; Zhu, Tsvankin, & Dewangan, 2005). Yan, Tham, and Yuen (2013) used material damping and apparent attenuation characteristics to account for the effects of geology, where damping is the intrinsic material losses due to frictional and viscous nature of the medium and apparent attenuation is the characteristic reflection, refraction, and/or transmission of the vibration at material interface. Even given the industry's understanding some of the effects of these variables, most engineering analyses assume the ground media is perfectly elastic or viscoelastic, isotropic, and homogeneous, which essentially assumes geology has no effect on blast vibrations (Bollinger, 1971; Spathis, 2010).

2.3.7. Presence of Water. Water also affects explosive performance, whether in the form of ground water, surface water, or precipitation (ISEE, 1998). In some cases, as with ANFO, water causes the explosive to become inert. In other cases, water can create pockets of decoupled explosive, or floating explosive, if the explosive is loaded incorrectly (Lee, 2011). Water can also act as a coupling agent between explosive and rock, where more energy is transmitted into the rock due to a closer impedance match between explosive, water, and rock than that of explosive, air, and rock (Singh & Narendrula, 2007).

Water also affects vibration propagation. Water channels in rock fractures and the degree of the saturation of soil or rock can affect the vibrations by changing the properties of the transmitting medium (Mohanty & Yang, 1997). Water affects rock and soil by decreasing friction between the particles which reduces compressive and tensile strength (Singh & Narendrula, 2007). Essentially, water can cause the ground vibration amplitude to increase in saturated conditions.

2.3.8. Direction of Propagation. The direction of propagation of blast-induced seismic waves can also affect blast vibrations (Froedge, 1995; Nicholls et al., 1971). Birch, Pegden, and West (2001) account for this by incorporating a vibration path factor into their vibration model. Seismograph arrays have been used to show that vibration amplitude and frequency can attenuate unequally depending on the direction (Froedge, 1995). Vibration amplitude can even increase with increasing distance. This instance, which is not necessarily rare, illustrates the variable effect that geology, mine geometry, groundwater, and other factors have on blast vibration characteristics.

2.3.9. Preconditioning. Preconditioning refers to fractures created from previous blasts or from individual blastholes that are detonated early in a blast (Yang & Scovira, 2010). The previous blasts, or earlier holes, physically alter and fracture the surrounding rock so that the vibrations from the remaining holes must propagate through newly destressed ground (Blair, 2008). The newly fractured ground has characteristics that differ from the original solid rock; therefore, the preconditioned rock affects vibrations differently than unaffected rock. The preconditioning process causes greater vibration attenuation for both amplitude and frequency of each blast vibration (Yang & Scovira, 2010).

In signature hole testing, the effect of preconditioned rock can be minimized by testing with fully confined charges. The only preconditioning that will be encountered by fully confined single charges is backbreak from the bottom of the charges used to break the rock above the grade of the current ground.

2.3.10. Monitoring Distance. Distance is the single most influential variable that affects blast vibrations (Bacci & Landim, 2002; Spathis, 2010). The decay of vibration with distance is inversely proportional to the square of distance. This is called the inverse square law (Oriard, 1992).

The distance field has three ranges: near-field, mid-field, and far-field. Near-field and far-field are the most often discussed categories, although there is no set definition for them. Typically near-field is defined as the area where peak blast vibration amplitude attenuates non-linearly. Near-field has also been defined as the distance from the blast where the vibrations from multiple charges can be identified individually or vibrations propagate in different directions and linear superposition cannot be applied (Bernard,

2012), as a function of the charge length (Andrieux & Heilig, 2000), or as a generic linear distance (Siskind et al., 1989). In this range, many of the variables previously described in this section have a more noticeable effect on the vibrations than at far-field distances. Near-field monitoring is used for blast damage and explosive performance investigations (Mohanty & Yang, 1997). In contrast, the far-field is defined by the linear attenuation of peak vibration amplitude. In this range, the total energy of the explosive is more important, with respect to vibration characteristics. Geology is a primary variable that affects vibrations in the far-field. The mid-field range is not well-defined in any study and is essentially a grey area between the near-field and the far-field. Therefore, the mid-field term is not addressed in this study.

2.3.11. Instrumentation Placement and Setup. Proper choice of instrumentation and mounting procedure are paramount when monitoring blast vibrations, whether for compliance monitoring to ensure vibrations are within regulatory limits or research applications. The measurement of blast vibrations is a major contributor to the scatter of peak particle velocity data, and many times, high variability or scatter of data is due to poor seismograph coupling (Armstrong, 2001; Yang, Kay, & Kim, 2014). Current best practice guidelines for acceleration criteria to select proper coupling methods do not always lead to good quality data (Armstrong, 2001; Segarra et al., 2014). The most accurate and precise data are recorded when instrumentation is anchored to rock or buried and covered with a sandbag and soil (Andrieux & Heilig, 2000; ISEE, 2009; Segarra, Sanchidrián, Castillo, López, & Castedo, 2014). Sandbagged on the surface, freely placed, or protruding instruments can lead to amplification or damping of the signal.

Typically, blasting vibrations are either monitored using geophones or accelerometers (Blair & Duvall, 1954). Geophones, or velocity gauges, are mechanical and made of a magnet mounted in a coil. These sensors have a limited frequency response and limited amplitude range due to the mechanical elements (Andrieux & Heilig, 2000). Geophones suffer amplitude and phase distortions near their resonant frequencies, in the range from 5 to 10 Hertz (Farnfield, 1996). The velocity amplitude limit for geophones is 20 cm/s (7.9 in/s) (Mohanty & Yang, 1997). Geophones have been the most widely used instrumentation for monitoring blast vibrations due to affordability, availability, ease of use, and compliance monitoring to ensure blast vibrations are within regulatory limits.

Accelerometers, which have a small mass attached to a piezoelectric element, are durable and have high frequency and amplitude limits (Andrieux & Heilig, 2000). They have frequency bandwidths between 1 Hz and 20 kHz and can record much higher amplitudes than geophones (Mohanty & Yang, 1997). Though accelerometers are higher priced and more complex, they are the best sensors available to measure vibrations, especially very near to the blasthole (Andrieux & Heilig, 2000; Mohanty & Yang, 1997).

Another aspect of instrumentation setup is sampling rate. The International Society of Explosives Engineers (ISEE) guidelines recommend a sampling rate of 1000 samples per second for standard blast monitoring devices (i.e. geophones) (ISEE, 2009). In near-field monitoring, this is insufficient and a higher sample rate is needed to accurately capture higher frequency components of the vibration event (Andrieux & Heilig, 2000). Andrieux and Heilig (2000) prescribe the required sample rate for near-field monitoring to be at least 5 kHz, although they prefer sample rates of up to 100 kHz.

2.4. VIBRATION MODELS

Silva-Castro (2012) listed five distinct methods for modeling and analyzing blast vibrations:

- Historical data comparison
- Charge weight scaling laws
- Waveform superposition
- Scaled charge weight superposition
- Analytical and/or numerical methods

This review focuses primarily on empirical models, such as scaled distance methods and the Z-Curve, which are common tools used in the blasting industry for vibration evaluation. The scaled distance methods combine historical data comparison with the charge weight scaling laws, while the Z-Curve is a historical data comparison method that was developed using statistical analyses. More sophisticated methods are also briefly discussed; however, these methods are outside of the scope of this study. Finally, vibration energy equations and the equations for conservation of mass, momentum, and energy used in shock analysis are introduced.

2.4.1. Scaled Distance and Related Equations. The scaled distance equation is a tool for normalizing the monitoring distance by the charge weight in order to compare charges of varying weights and similar geometry (Dowding, 1985). The scaled distance is commonly used to compare the distance from the charge and charge weight to the particle velocity of a blast vibration using scaled distance versus peak particle velocity charts. The scaled distance equation weights the distance from the charge with the square root or cube root of the charge weight. Refer to Dowding (1985) for a comparison

between the cube root and square root scaled distance. There is debate over the correct form of the equation, but typically in the United States, square root scaling is associated with ground vibration while cube root scaling is associated with airblast (Spathis, 2010). Therefore, this study uses the square root form of the scaled distance equation (Stagg & Engler, 1980):

$$SRSD = \frac{D}{\sqrt{W}} \tag{5}$$

Where *SRSD* is the square root scaled (ft/lb$^{1/2}$ or m/kg$^{1/2}$), *D* is the distance from the center of the blast to a point of interest (ft or m), and *W* is the maximum weight of explosive per delay (lb or kg). The delay typically refers to an eight millisecond time period, which is a requirement of U.S. Federal and state regulations. The scaled distance equation is plotted against peak particle velocity and displayed on a log-log scale to compare a wide range of charge sizes and sample point distances. The square root scaled distance is typically plotted against peak particle velocity using the following relationship:

$$PPV = a * SRSD^b \tag{6}$$

Where *PPV* is the peak particle velocity (in/sec or mm/sec) and *SRSD* is the square root scaled distance (ft/lb$^{1/2}$ or m/kg$^{1/2}$). The parameters *a* and *b* are site and direction specific, but the units of *a* change continuously; therefore, this relationship is technically not a fundamental equation of vibration, meaning it includes more than the fundamental dimensional units (Silva-Castro, 2012). Figure 2.6 illustrates the SRSD versus PPV relationship.

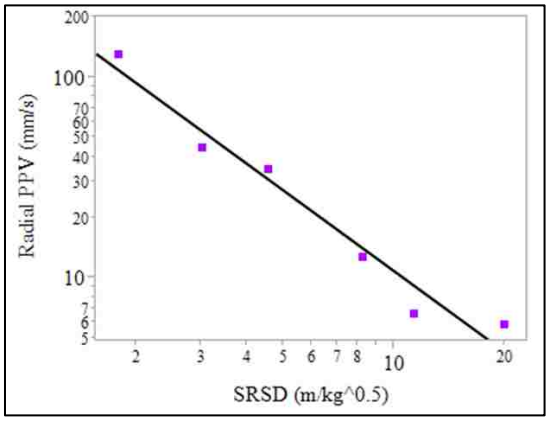

Figure 2.6. Example plot of SRSD versus PPV.

Equation 6 works well for calculating a site-specific regression relationship; however, it does not work well when variability in the input parameters is encountered. For example, the typically limited variability of blasthole dimension and wide variety of geology for a specific site cause the data at that site to conform to a better regression than data from multiple sites. Even within a specific site, this type of model can have poor results from shot to shot. For example, individual blasts monitored by a line of seismographs can produce data with very good correlation; however, the data produced by a combination of blasts at the same site can produce peak particle velocities that vary by an order of magnitude for the same scaled distance (Worsey, Giltner, Drechsler, Ecklecamp, & Inman, 1996). The variation in results can be due to a number of factors such as varying confinement, directional effects, site geometry and geology, variability in explosive performance, and other factors.

Site specific models, such as scaled distance, are mostly only used to model vibrations from charge geometries that do not vary. In other words, modeling scaled

distance with a constant charge weight for scaling is the same as modeling against only distance.

The scaled distance equation is a simplified version of the scaled distance model developed using dimensional analysis. In many cases, it has been further modified to develop blast damage equations and other blast vibration equations. The following sections discuss the origin of the scaled distance equation, which was developed using dimensional analysis in 1915 (Chock, 1996). The sections also briefly review of number of equations that are based on the scaled distance-PPV relationship to show the dependence of current blast vibration equations on the scaled distance equation.

2.4.1.1. Dimensional analysis. Dimensional analysis follows the Buckingham π Theorem, which states that a dimensionless parameter can be constructed from a certain number of physical variables that affect the outcome of a process (Ambraseys & Hendron, 1968). The variables considered in explosion phenomena can be used to generate sets of dimensionless parameters, which can be related to the peak particle velocity. One dimensionless parameter produced by dimensional analysis is $E/\rho c^2 D^3$, which is a function of the energy released by the explosion, E, the density of the rock, ρ, the seismic propagation velocity of the rock, c, and the distance from the charge, D (Ambraseys & Hendron, 1968). In the case of the scaled distance equation used in blasting, all the variables are raised to the 1/3 power to eliminate the distance exponent. The parameter is further altered by approximating the energy with the charge weight. This simplification produces the following cube root scaled distance equation (Dowding, 1985):

$$CRSD = \frac{D*(\rho c^2)^{\frac{1}{3}}}{\sqrt[3]{W}} \quad (7)$$

Where *CRSD* is cube root scaled distance ($ft^{1/3}$ or $m^{1/3}$), *D* is the distance from the center of the blast to a point of interest (ft or m), ρ is the density of the rock (lb-sec^2/ft^4 or kg- sec^2/m^4), *c* is the propagation velocity of the vibration in the rock (ft/s or m/s), and *W* is the maximum weight of explosive per delay (lb or kg). Equation 7 is commonly simplified by removing the rock parameters, which were originally thought to not vary significantly enough to affect the outcome of the equation (Dowding, 1985). The most simplified and commonly used form of Equation 7 for blast vibration evaluation is that of Equation 5, the *SRSD* equation, which substitutes the cube root with the square root.

2.4.1.2. Spathis scaling method. Spathis (2010) introduced an alternative to charge weight scaling, although his method is still based on the scaled distance equation. The approach is basically an altered form of charge weight scaling that includes a time window parameter for charge influence:

$$PPV_t = max\left\{a\left(\sum_{i=1}^{n}\frac{W_i}{D_i^2}\right)^b\right\} \quad (8)$$

Where PPV_t is the peak particle velocity over *n* charges within time window, *t.* The site specific parameters *a* and *b* are estimated from field data. This equation uses full production blasts to estimate over the time window, *t*. Yang and Scovira (2008) have a similar approach by scaling charges within a time window, which is estimated from a waveform broadening factor, and a form of screening.

2.4.1.3. Holmberg-Persson method. The Holmberg-Persson method was developed to control contour blasting and relates rock damage to peak particle velocity. It has been updated by the National Institute for Occupational Safety and Health (NIOSH) to address issues with near-field calculations in the original model (Iverson,

Kerkering, & Hustrulid, 2008). The Holmberg-Persson method is based on the scaled distance equation as:

$$PPV = KW^{\alpha}D^{\beta} \quad (9)$$

Where *W* is charge weight per delay, *D* is distance from the charge, and *K*, *α*, and *β* are constants. NIOSH updated this equation with modifications to the application of the equation in the near-field. However, the equation still has similar issues to those of the scaled distance equation. Namely, the equation is based on an empirical data comparison but is generalized and limited to site specific modeling of signature holes (Fleetwood, Villaescusa, & Li, 2009). These equations are also limited when scaling multiple charge geometries.

2.4.1.4. Rock failure as function of PPV. Another example of modeling rock damage from blast vibrations relates the PPV to engineering parameters of the rock (Fleetwood et al., 2009):

$$PPV_{max} = 0.1 * UCS * \frac{c_P}{E} \quad (10)$$

Where PPV_{max} is the critical PPV (mm/s) above which tensile failure will occur in the rock, *UCS* is unconfined compressive strength (MPa), c_P is the P wave propagation velocity (m/s), and *E* is Young's Modulus (GPa). This equation has a number of limitations:

- Firstly, *0.1*UCS* is an imprecise approximation for tensile strength. Additionally, *UCS* and Young's Modulus are tested under quasi-static conditions. Near the blasthole, rock exhibits dynamic strength characteristics due to the high strain rates that are induced by the explosive. For instance, a study of the BHP Billiton Cannington Mine

showed the dynamic Young's modulus to be 15-50% higher than the quasi-static modulus (Fleetwood et al., 2009). This issue may not be a major limitation of the equation if *UCS/E* is shown to be constant, regardless of the loading condition.

- Secondly, the unconfined strength is conservative and unrealistic of in-situ rock behavior (Fleetwood et al., 2009). The rock realistically has confining pressure; therefore, the overall strength of the rock is increased in the insitu environment. A confined strength value would be more accurate.
- Additionally, the equation also fails to relate the duration of the peak particle velocity over which the waveform acts on the rock. This relationship is defined by the impulse of the wave, which is equivalent to the time integral of the amplitude. The impulse may be of importance while the rock is under stress.
- Finally, the equation uses the PPV to determine the damage point for the rock; however, strain is a more important value. The PPV is related to strain by frequency; therefore, unless frequency does not vary much around a blasthole, the PPV is an incorrect term to use.

2.4.2. Z-Curve. The Z-Curve, or Blasting Level Chart, is a tool that was developed by the USBM in 1980 (Figure 2.7) (Siskind et al., 1980). It is used to determine the potential for a blast vibration to damage a residential structure. The Z-Curve compares particle velocity amplitudes against frequency for each vibration peak, which is calculated using the zero crossing method. Essentially, the values need to be

kept below the limit line for the vibration to be considered safe for residential structures. This method has been a regulatory standard since its adoption by the Office of Surface Mining in 1983 (OSM Blasting Performance Standards, 1983). The Z-Curve is described in greater detail in Section 5 of this document.

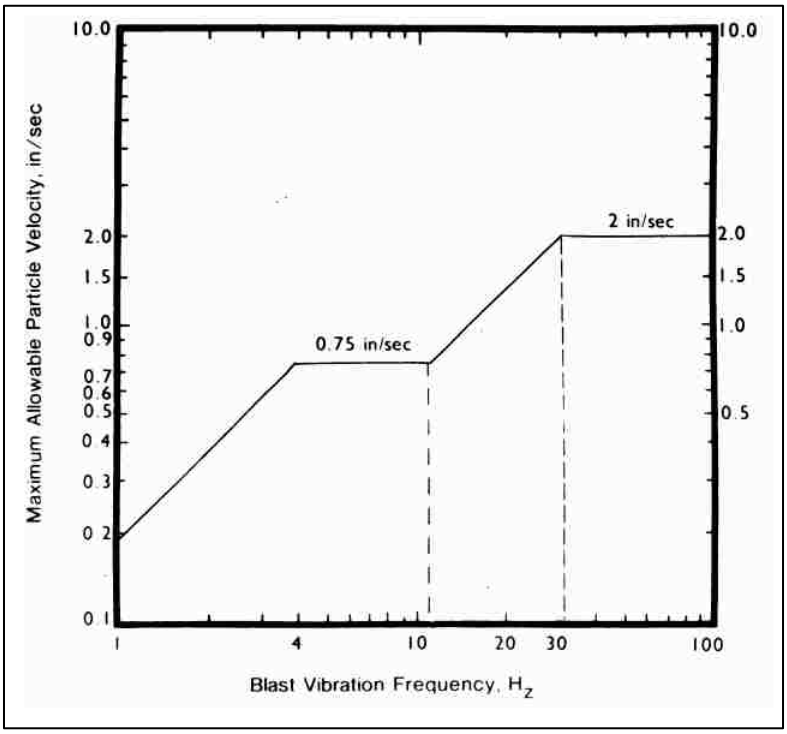

Figure 2.7. Blasting level chart or Z-Curve (source: OSM Blasting Performance Standards, 1983).

2.4.3. Advanced Methods. Advanced methods for evaluating blast vibrations are becoming more common in the blasting industry. However, even these are still not capable of precisely estimating the variability of the geologic medium or vibration propagation. The most common method of modeling vibrations, where geology is considered homogeneous are finite element models (FEM) and boundary element

methods (BEM) (Silva-Castro, 2012). The specifics of these types of models are outside the scope of this project and will not be discussed.

Advanced models can also be simpler than the complex, numerical computational models such as FEM and BEM. For example, the Multiple Seed Waveform (MSW) model and the Silva-Lusk model are relatively simple methods that incorporate many of the phenomena that affect blast vibrations. These models are primarily used to predict vibrations using empirical data rather than evaluate vibrations. They are briefly covered in this literature review to illustrate the complex nature of blast vibration modeling.

2.4.3.1. Multiple Seed Waveform. The MSW method was developed for blast vibration prediction at near and mid-field distances, where the placement of each individual blasthole has a noticeable influence on the resultant blast vibration (Yang & Scovira, 2010).

The MSW model takes into account a number of techniques to process seed waveform data to account for the attenuation of amplitude, frequency, and duration of blast vibrations (Yang & Lownds, 2011). These techniques include the use of a transfer function to model variances in frequency, a screening variable to model the preconditioning effects of neighboring charges, a matrix calculation to account for the depth and three dimensional location of each charge, and a nonlinear relation between PPV and scaled distance (Yang & Lownds, 2011; Yang & Scovira, 2007). The MSW model introduces significant techniques that can be used to account for various influences on vibration attenuation. It does still depend on a scaled distance equation to model particle velocity and must model the frequency and particle velocity using different methods.

A number of peer-reviewed documents have demonstrated the successful application of the MSW model. Even so, this example serves to illustrate the dependence of even modern, advanced models on the scaled distance equation.

2.4.3.2. Silva-Lusk model. The Silva-Lusk model is another recent development in blast vibration modeling. This model focuses on the variability of blast vibrations using Monte Carlo analysis. Blast vibration variables can be treated as random variables with normal probability distributions. The probabilistic approach of Monte Carlo results in a distribution of peak particle velocity values according to each random variable (Silva-Castro, 2012).

The Silva-Lusk model is a methodology that takes into account changes in both amplitude and frequency of a seed waveform. The analysis defines a wave using frequency zones, a decay factor, and an amplitude scaling factor to adjust a basic wave equation. The model uses the statistical distribution of each variable to calculate a vibration envelope that predicts the range of probable values for a vibration (Silva-Castro, 2012).

The model does not use a scaled distance equation, which is uncommon in the blasting industry. It also assumes variability from hole-to-hole. Essentially, this model was developed to produce an envelope that has a high probability of estimating the maximum and minimum vibration amplitude values that are capable of being produced in a given scenario. Therefore, it is primarily used to predict vibrations as opposed to evaluating the effects of variables on measured vibration data.

2.4.4. Energy. A blast vibrations is a transfer of energy from the detonated charge through the ground. The magnitude of the energy in a blast vibration could be of

great importance when evaluating the potential of a blast vibration to damage a man-made or geologic structure.

As described in the beginning of this section, there are two basic zones around an explosive charge. The dynamic zone is near the charge, where material properties are significantly affected by the shock from the explosion and stress in the ground exceeds its elastic strength. The second zone is a quasi-static zone where material properties are constant and the ground behaves elastically. The reaction of the ground in each of these zones varies due to the amount and type of energy the explosive imparts. This section describes the shock and vibration features in these zones.

2.4.4.1. Vibration energy. Seismic vibrations that are most often encountered and studied in the blasting industry are elastic. The description of blast vibration characteristics and features given up to this point pertain to elastic vibrations. Therefore, this section builds on the previous sections and covers vibration energy calculations and the ground response to elastic vibrations.

2.4.4.1.1. <u>Vibration energy calculations.</u> The seismic energy at a specific point is equal to the potential energy at the maximum particle displacement at that point (kinetic energy is zero). The potential energy at the maximum displacement is equal the work done by the force of the vibration to displace the ground from equilibrium to its maximum displacement. By Hooke's Law, the force can be expressed as:

$$F(x) = kx \tag{11}$$

Where *F* is the force needed to compress a spring or elastic material a distance *x*, and *k* is the linear spring constant (Piersol & Paez, 2009). Assuming the resultant

restoring force is equal to the applied force, the potential energy, *PE*, of a system at maximum particle displacement, PD_M, from equilibrium is equal to:

$$PE = \int_0^{PD_M} F(x)dx = \int_0^{PD_M} kxdx = \frac{1}{2}kPD_M{}^2 \quad (12)$$

Therefore, in simplified terms, the seismic energy that passes a point is proportional to the square of the maximum particle displacement at that point. This relationship is relevant to this study since it shows that blast vibration energy is related to the particle displacement amplitude of the blast vibration.

The following sections describe two methods that have been used in the blasting industry to evaluate blast vibration energy. Both show the importance of blast vibration amplitude and frequency when calculating vibration energy.

Energy ratio. Energy ratio (*ER*) has been used to attempt to define the limits of safe blasting (Crandell, 1949). The *ER* is can be defined as a function of particle acceleration, velocity, or displacement (Crandell, 1949; Nicholls et al., 1971):

$$ER = \frac{PA^2}{f^2} \quad (13)$$

$$ER = 4\pi^2 PV^2 \quad (14)$$

$$ER = 16\pi^4 f^2 PD^2 \quad (15)$$

Where *f* is frequency, *PA* is particle acceleration, *PV* is particle velocity, and *PD* is particle displacement. Equations 13-15 are derived from the equation for kinetic energy, *KE*, as opposed to potential energy (Crandell, 1949):

$$KE = \frac{1}{2}mv^2 \quad (16)$$

Where *m* is mass and *v* is velocity. The *ER* is equivalent the term v^2 in Equation 16. In this relationship, the *ER* is considered to be proportional to the kinetic energy.

The energy ratio assumes that the mass is constant and the vibration is a simple harmonic. Technically, Equation 16 applies to the translational motion of a rigid mass as opposed to an oscillatory object (Piersol & Paez, 2009); therefore, frequency does not appear in Equation 14. Crandell (1949) focused on Equation 13, which includes acceleration and frequency since both amplitude and frequency are important to consider when evaluating blast vibration.

Hooke's Law and the Energy Ratio calculations are oversimplifications of the vibration process; however, they show that vibration energy is relatable to both the vibration amplitude and frequency when evaluating the instantaneous energy of a vibration.

Energy flux. Sanchidrián (2007) developed an equation to calculate the seismic energy that passes a spherical surface at radius, D, from the charge:

$$E_{SR} = -4\pi D^2 \rho c_R \int_0^\infty PV_R^2 dt \quad (17)$$

Where ρ is the density of the ground, c_R is the radial, or longitudinal, propagation velocity of the ground, and PV_R is the radial particle velocity. Equation 17 was developed as part of a calculation for explosive energy and includes the entire sphere of vibration propagating from the charge. This equation is derived and discussed in Section 5 of this document; therefore, it is not discussed further in this section.

2.4.4.1.2. <u>Response of the ground to elastic vibrations.</u> The blasting industry typically monitors elastic blast vibrations because residential structures near a blast site that require monitoring are not typically close enough to a blast for the ground to exhibit plastic deformation. Regardless of the distance, the strain, ε, induced in the rock is an

important parameter to consider. Strain induced by a blast vibration can by approximated by the following equation (Dowding, 1985; Fleetwood et al., 2009):

$$\varepsilon = -\frac{PV_R}{c_R} \tag{18}$$

Where ε is strain, PV_R is the radial particle velocity, and c_R is the radial propagation velocity. Equation 18 is a plane wave approximation, which is valid where the blast vibration has traveled a significant distance from the source, which can approximated as greater than five times the charge length (Fleetwood et al., 2009). This equation proves useful in the derivation of the seismic energy equation, as shown in Section 5.

The rate at which a material undergoes strain, $\varepsilon/\Delta t$, determines whether the material will stay within the quasi-static strength range or fall in the dynamic response range. The dynamic response of materials is described in the following section, which focuses on shock energy.

2.4.4.2. Shock energy. Shock dynamics is typically not a focal topic in the blasting industry. The vibrations and waveform features that are focused on by the blasting industry are typically elastic in nature. However, the material around a blasthole does enter a shocked state during the detonation of the charge. While undergoing shock, the strain rates are high, causing the material to exhibit dynamic response characteristics that are not equivalent to the material's quasi-static response characteristics. In the shock zone, there is rapid attenuation of energy around the hole due to rock breakage and the creation of new crack surface areas or extension and opening of existing fractures.

Shock wave propagation can be evaluated following the basic laws of conservation: the conservation of mass, momentum, and energy (Cooper, 1996). These

laws can be used to define the nature of a material before and after a shock front, which is a discontinuity between the original, unshocked state of the material and the shocked state of the material.

2.4.4.2.1. Coordinate system. Seismic waves are typically shown as plots of the particle velocity in the time domain, where the waveform depicts the motion of a single particle over the period of the recording. This system of coordinates, which is used to observe a passing vibration, is referred to as Eulerian (Cooper, 1996). Another coordinate system, which fixes an observation point to a moving object of interest, or the crest of a shock wave in shock systems, is referred to as Lagrangian. The Lagrangian system of coordinates can be used to derive basic "jump" equations to describe shock phenomena, termed Rankine-Hugoniot Jump Equations.

2.4.4.2.2. Rankine-Hugoniot Jump Equations. The Rankine-Hugoniot Equations describe the state of a material on either side of a shock front as a function of the particle velocity, u, material density, ρ, pressure, P, and internal energy (Figure 2.8). Mass is conserved; therefore, internal energy is expressed as specific internal energy, e, in the Rankine-Hugoniot Equations. The equations also include the shock wave propagation velocity, U.

It is important to note that the shock behavior analysis only considers stress and strain in the uniaxial direction of propagation. The Rankine-Hugoniot Equations assume the dimensions perpendicular to the strain axis are infinite, meaning the system has no edge effects (Cooper, 1996).

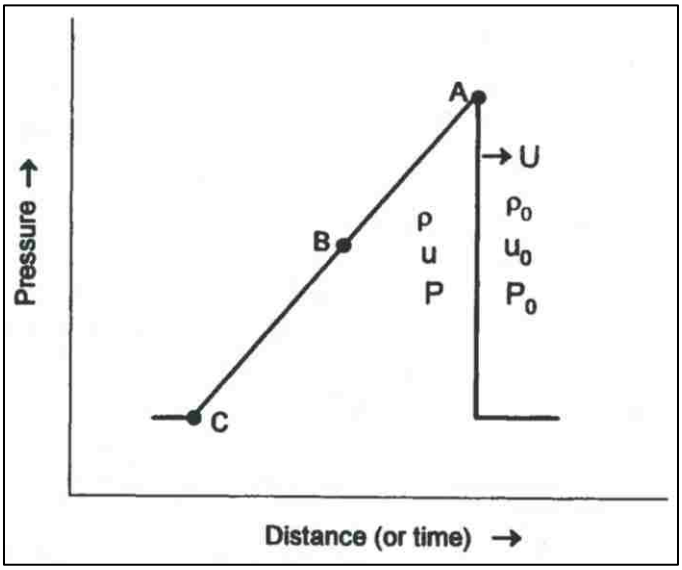

Figure 2.8. Shock wave and rarefaction wave (back end) (source: Cooper, 1996).

Conservation of mass. The conservation of mass states that mass is neither created nor destroyed. Assuming a control volume has an initial mass equal to the final mass, the Rankine-Hugoniot Jump Equation derived from the conservation of mass is as follows (Cooper, 1996):

$$\frac{\rho_1}{\rho_0} = \frac{U-u_0}{U-u_1} = \frac{v_0}{v_1} \tag{19}$$

Where ρ is the material density, u is the particle velocity, U is the shock propagation velocity, v is the specific volume and reciprocal of density, and the subscripts, *0* and *1*, refer respectively to the initial and final states of the material on either side of the shock front. The relationship between shock propagation velocity and particle velocity is linear for most materials, from the following relationship (Cooper, 1996):

$$U = C_0 + su \tag{20}$$

Where C_0 is the bulk sound speed and s is the slope of the linear relationship (Figure 2.9).

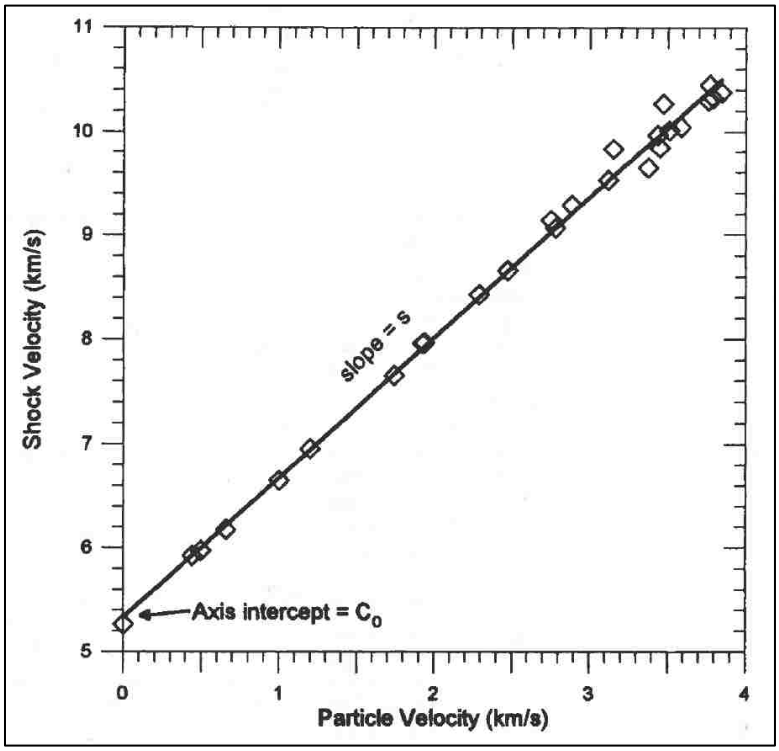

Figure 2.9. Example of linear shock velocity relationship for 6061 aluminum (source: Cooper, 1996).

Conservation of momentum. The conservation of momentum equation addresses the rate of change of momentum during a shock event, stating that the rate of change of momentum of the control mass, from the state before the shock to the state after the shock must be equal to the applied force. The applied force is equal to the pressure difference across the shock front multiplied by the cross-sectional area of the control volume. The momentum equation follows (Cooper, 1996):

$$P_1 - P_0 = \rho_0(u_1 - u_0)(U - u_0) \tag{21}$$

Where *P* is pressure, ρ is density, *u* is particle velocity, and *U* is shock propagation velocity.

Conservation of energy. The conservation of energy relates the rate of energy increase in the control mass to the work being done on it. The energy increase and the work are equal; therefore, the conservation of energy equations describe the specific internal energy difference as follows (Cooper, 1996):

$$e_1 - e_0 = \frac{P_1 u_1 - P_0 u_0}{\rho_0 (U - u_0)} - \frac{1}{2}(u_1^2 - u_2^2) \quad (22)$$

For the case where $u_0 = 0$:

$$e_1 - e_0 = \frac{1}{2}(P_1 + P_0)(v_0 - v_1) \quad (23)$$

Equations of state. Two additional relationships are needed in order to solve the three Rankine-Hugoniot Jump Equations, which are given with five variables (Zhernokletov et al., 2006). These variables can be solved by combining an equation of state and the Hugoniot Planes; however, only the basic laws of conservation are of interest to this study.

2.4.4.2.3. <u>Response of materials to shock.</u> Shock induces very high strain rates in materials. A material under a high strain rate exhibits greater strength characteristics than under quasi-static conditions due to its dynamic response characteristics (Katsabanis, Pascoal, & Rielo, 2011; Tawadrous & Katsabanis, 2007). Dynamic strength characteristics of the ground control the reaction of the ground under shock, and therefore, become important near the blasthole where shock comminutes the rock and drives and creates fractures. The dynamic tensile strength of a rock at high strain rates under shock loading can be an order of magnitude higher than the quasi-static tensile strength of the same rock (Ai & Ahrens, 2004). Table 2.2 displays the tensile strength of

various materials under a range of strain rates. The strain rate increases toward the right side of the table.

Table 2.2. Tensile strengths (MPa) of ice and rocks at a range of strain rates (source: Ai & Ahrens, 2004).

	Tensile Strength (MPa)						
Strain Rate (/s)	1	$2x10^4$	$4.2x10^5$	$7.1x10^5$	$7.7x10^5$	$1x10^6$	$2x10^6$
Coconino Sandstone			17	20			
Donzdonfer Sandstone	3						
Bedford Limestone					35		60
Ice	1.6	17					
San Marcos Gabbro						150	

The effect of high strain rates are further illustrated in Figure 2.10. This figure shows Hopkinson bar and quasi-static failure stress data for two ceramics (Figure 2.10(a)) and Blair dolomite and Climax Stock granodiorite (Figure 2.10(b)). Figure 2.10 shows quasi-static (low strain rate) yield strength of the materials and higher dynamic yield strength for the materials under shock. From the figure, the rock appears to have a dynamic strength that is an order of magnitude higher than the quasi-static strength, although the limited data does not give complete confidence in this estimate. Vibrations that are monitored by standard blasting seismographs only induce strain rates that fall in the quasi-static range of material properties, which is the lower range of values on each diagram shown in Figure 2.10.

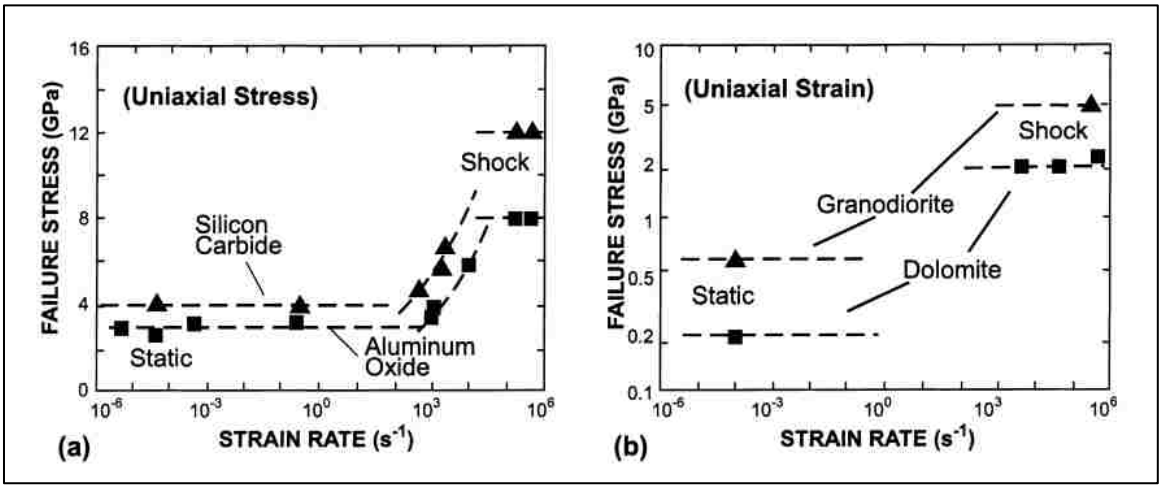

Figure 2.10. Yield stress level versus strain rate for ceramics (a) and rocks (b) (source: Grady, 1998).

2.5. SUMMARY

This literature review covered the characteristics and features of blast vibrations, factors that affect blast vibrations, and common types of models used by the blasting industry to study or estimate blast vibrations.

There are many variables that affect blast vibrations to varying degrees. The charge diameter and charge length are two of these variables that are commonly assumed to have an insignificant effect on blast vibrations. Therefore, there is a need to determine if charge geometry affects blast vibrations and, if so, the nature of that effect.

Vibration models have been developed through the last few decades in the blasting industry, and a majority of those models rely on the scaled distance equation, which has become oversimplified and overly relied upon by the blasting industry. There is no model for blasters to use that incorporates all of the major vibration features and all of the significant variables into one simple model or tool. It is imperative that a blast vibration model be developed that can be easily used in the field and easily understood by

anyone who has an interest in blast vibrations, not just experts in the blasting industry. To do this, all the variables that affect vibration must be evaluated to determine which variables have a statistically relevant effect on the three primary blast vibration features. Then, a model must be developed that accounts for the statistically significant variables and the most important features of blast vibrations.

The following sections present the statistical analyses used to evaluate the variables that affect blast vibrations and the groundwork that has been laid for the development of a model that fulfills the current needs of the blasting industry by accounting for all of the important features of blast vibrations.

3. DATA COLLECTION

3.1. OVERVIEW

The first objective of this work is to determine if charge geometry has a statistically significant effect on any of the three important features of a blast vibration, and if so, to quantify that effect. The best approach to accomplish this task is to use multiple regression analysis on a sample population of signature hole data. The signature hole method eliminates many insignificant variables that would be encountered during a production blast, such as timing and pattern design, influence from multiple holes, and variances in confinement. The signature hole method allows for precise measurements of charge weight, hole/charge diameter, hole depth, charge length, and stemming length to be directly related to the features of the blast vibrations.

This section describes the process used to compile the dataset used in the statistical regression analysis. The complete signature hole dataset is a compilation of data from four sources, totaling 105 signature hole waveforms. Three sets of data were supplied by outside sources; therefore, the details of the tests from these sources are not well documented and are only discussed briefly. The fourth dataset was collected during the process of this study; therefore, the test locations, methodology, and test results for the fourth dataset are discussed in detail.

3.2. GOLD-OPERATOR DATA

The first dataset was supplied by a gold mine operator located in the western United States. This dataset consists of 32 useable signature hole recordings from seven signature hole shots.

The following points are known about the Gold-Operator Dataset:

- Distances between seismographs and signature holes were calculated as three-dimensional straight line distances.
- Only waveforms from seismographs aligned toward the signature holes were used.
- Explosive weights were measured from the truck. The truck scales are assumed to be accurate. The truck operators possibly could have reported back the explosive type incorrectly or used an incorrect blend from the truck, but neither of these scenarios should be the case. Hole depths were calculated as a function of the reported explosive weight, stemming height, charge diameter, and theoretical explosive density.
- Drill cuttings were used for stemming
- Signature holes were detonated using down-hole detonating cord initiation.
- The signature holes were fully confined (no free face).
- Seismographs were all buried in approximately 15 cm (6 inch) deep holes and covered in fines and/or material from the hole.
- The signature hole tests were monitored in the following geologies:

- Colluvium of a combination of fluvial sands and gravels, mudstone, airfall and water lain tuffs, clayey sands and gravels, chert, fine grained sandstone, siltstone, and/or possible back-fill or dump material
- Planar laminated, thin bedded, platy limestone with possible secondary weak silicification
- Thin interbedded and sheared mudstones and chert
- Fine grained sandstone and possible thin bedded argillite

Further statistics on this dataset, and the other three datasets, are included in Section 4.

3.3. COAL-OPERATOR DATA

The coal operator dataset was collected by Dr. Jhon Silva during his PhD research, and is described well in his dissertation titled *Blast Vibration Modeling Using Improved Signature Hole Technique for Bench Blast* (Silva-Castro, 2012). The dataset contains 18 usable signature hole waveforms.

The signature hole tests were conducted at the Guyan surface mine in Logan County, West Virginia. The signature holes were primarily shot in the Coalburg Sandstone, which ranges in thickness from 21.3 m to 30.5 m (70 to 100 feet). The signature hole waveforms were recorded on the mine site and off-site in ridgeline, slope, and bottomland areas. Therefore, the seismic vibrations had complex travel paths through a variety of soil and rock. Despite the complexity of the travel paths, straight

line distances were used. The vibrations were sampled by the seismographs at a sample rate of 1,024 samples per second.

The signature holes were detonated in production blast patterns with long delays between groups of production holes. This allowed the signature hole waveforms to be separated from the production waveforms. Due to this format, the signature holes were not fully confined, unlike the signature holes that were collected from the other three sources.

3.4. GOLD-SUPPLIER DATA

The Gold-Supplier data was collected during a study by an explosives manufacturer and supplier at a gold and copper open pit mine. The data from this source includes a total of 28 useable signature hole waveforms. The waveforms were produced by seven signature holes and recorded with three accelerometers and one geophone.

The geology of the site is sandstone, and the shots were recorded on a solid pit floor that exhibited a P-wave velocity of 2,300 m/s (7,500 ft/s). The dataset was recorded for a research application; therefore, it is assumed to be high quality. Additional information concerning this dataset is unknown.

3.5. LIMESTONE QUARRY DATA

The limestone quarry signature hole data were collected to complete the full signature hole dataset used in the statistical evaluation. For the limestone quarry dataset, 27 signature hole waveforms were collected at two quarries. The limestone quarry dataset is significant for a number of reasons. First, the tests were a tightly controlled set

of signature hole shots that produced data not commonly recorded during conventional signature hole tests. Second, data points were captured near the charge and far from the charge, which provides insight on the variance in vibration features as the vibration propagates from the charge. Finally, the field testing process provided hands-on knowledge required to understand the process of producing this type of dataset, which allowed for a more thorough analysis of the data.

The following section gives details on the test sites that were chosen for this process, the methodology used to design the test matrix, and the approach taken to select the proper equipment and data collection procedures. The section concludes with a brief discussion of the signature hole test results.

3.5.1. Test Locations. The limestone quarry tests were conducted in two quarries in central Kentucky: Butler Quarry and Big Bend Quarry.

3.5.1.1. Butler Quarry. Butler Quarry is an open pit operation that produces crushed rock and aggregates near Butler, KY. The signature hole tests were located in the main pit floor and the north pit floor. This quarry had two drill rigs, which were able to drill holes with diameters ranging from 79 mm to 127 mm (3-1/8 inches to 5 inches).

The main pit floor was in Camp Nelson Limestone at an elevation of approximately 58 m (190 ft) above mean sea level. The Camp Nelson formation is a primary target formation for limestone quarries in the region. The rock, which had a density of 2.6 g/cc, was unweathered, tightly bedded, and competent.

The north pit floor was in Logana Limestone, which is a waste rock composed of shaly limestone. The floor sat at approximately 117 m (385 ft) above mean sea level. The Logana Limestone was unweathered but highly laminated with limestone and shale.

The density, which was not tested, was most likely less than the density of the Camp Nelson due to the interbedded shales. The Camp Nelson and the Logana Limestones did not react similarly to the detonation of the signature hole charges due to high amount of laminations in the Logana Limestone; therefore, to produce more repeatable data, all but one signature hole test was conducted in the Camp Nelson Limestone.

3.5.1.2. Big Bend Quarry. Big Bend Quarry is located near Battletown, KY on the Ohio River. The quarry is a stripping operation that primarily supplies scrubber stone to coal-fired power plants on the Ohio River. The test was conducted at Big Bend Quarry because the pit floor at Big Bend Quarry allowed for greater monitoring distances than the pit floors at Butler Quarry. Additionally, the test at Big Bend Quarry incorporated a larger hole diameter than the tests at Butler Quarry, which allowed for a greater variability in the signature hole dataset. The signature hole at Big Bend Quarry was 140 mm (5.5 inches) in diameter.

The signature hole fired at Big Bend Quarry was located in the St. Genevieve Limestone pit floor. The St. Genevieve Limestone was unweathered and tightly bedded, although there were some stress fractures near the outcrops. The limestone at Big Bend also had a density of approximately 2.6 g/cc.

3.5.2. Methodology. This section describes the variables that were taken into account during the field testing phase of this work and the data that needed collecting during the field testing phase. Additionally, this section discusses the process of developing the final test matrix.

3.5.2.1. Variables. The variables that are addressed by the field testing phase were discussed in the literature review of this document. They include:

- charge weight,
- charge geometry,
- charge type,
- blast pattern and timing,
- confinement,
- geology,
- presence of water,
- direction of propagation,
- preconditioning,
- monitoring distance, and
- instrumentation placement and setup.

3.5.2.1.1. Charge weight. Scaled distance was used to account for charge weight despite the scaled distance limitations that are discussed in the literature review. The use of scaled distance was considered acceptable because the scaled distance was only used to normalize the monitoring distances for each charge weight.

Charge weight was not kept constant since doing so would produce charge dimensions that were impractical. For example, a 8.8 m (29 ft) long, 127 mm (5 inches) diameter charge of ANFO at a density of 0.82 g/cc would have a charge weight of 90.7 kg (200 lbs). The same weight of ANFO in a 79 mm (3-1/8 inches) diameter charge would require a 22.4 m (73 ft) long powder column. In practice, blastholes that are 127 mm in diameter are used for charges that are 8.8 m long; however, a 22.4 m long charge at 79 mm is impractical. There are few charge weight and charge geometry combinations

that would be practical using this methodology, and the range of values for the tested variables would be limited.

3.5.2.1.2. Charge geometry. The goal of this study is to determine if charge length and charge diameter have a statistically significant effect on blast vibrations. The tests were designed to produce data from the widest practicable range of charge diameters and charge lengths available. Charge weight was not a deciding factor in the initial determination of charge diameters and charge lengths because the multiple regression analyses described in Section 4 evaluates the effect of the charge geometry variables independent of charge weight. However, for the final signature hole test, the charge weight was used to determine charge length in order to fill in gaps in the full signature hole dataset.

The charge diameter values were chosen based on the range of available drill bit sizes at each limestone quarry. Butler Quarry had two drills, one capable of drilling holes with diameters as small as 79 mm (3-1/8 inches) and the other capable of drilling holes with diameters as large as 127 mm (5 inches). Big Bend Quarry's drill was capable of drilling holes with a 140 mm (5.5 inch) diameter. All holes were vertical holes.

Two charge length values were chosen for each blasthole diameter to keep the experiment geometrically scalable for each charge diameter. The charge lengths were determined using two arbitrary charge length to charge cross-sectional area ratios: 291.7 m/m^2 and 583.5 m/m^2 (90 ft/ft^2 and 180 ft/ft^2). Using this method, the charge length values were kept within practical limits.

The charge diameter and charge length values that were chosen for the limestone quarry field tests represented a wide range of values that could be expected in the

quarrying industry. The limestone quarry data also filled in noticeable gaps in the signature holes datasets supplied by the gold and coal sources, most noticeably because of the smaller charges had a significant number of monitoring locations in the near-field range.

3.5.2.1.3. Charge type. The explosive type used in each of the limestone quarry signature holes was PowerNel™ 1500, a pumped emulsion with an approximate density of 1.25 g/cc. The technical data sheet lists this emulsion as having a VOD ranging from 5,800 to 6,100 m/sec (19,000 to 20,000 ft/sec) in a 171 mm (6.75 inch) diameter blasthole, an absolute weight strength of 645 cal/g, an absolute bulk strength of 806 cal/cc, and a relative bulk strength of 107% ANFO. The minimum blasthole diameter for this explosive is 50 to 75 mm (2 to 3 inches).

The emulsion was developed to minimize losses in performance in blastholes with smaller diameters; therefore, the emulsion's VOD was expected to be relatively constant over the range of charge diameters tested in this study (Fleetwood & Villaescusa, 2011). All the charges were bottom-primed with one pound boosters because bottom priming is a standard method for priming blastholes in the blasting industry.

3.5.2.1.4. Blast pattern and timing. Blast pattern and timing design were not variables in these experiments due to the use of signature holes.

3.5.2.1.5. Confinement. Confinement was not identified as a variable of interest in the limestone quarry tests. Therefore, the tests were all designed to be fully confined with no open face.

Using the fully confined approach, the only variable relating to confinement was stemming length. Initially, the stemming was calculated as a function of charge length;

however, this configuration resulted in a poorly confined charge in the third field test. Therefore, the fourth and fifth tests were designed with a stemming length to hole diameter ratio of 0.031 m/mm (2.6 ft/inch). This constant stemming length to hole diameter ratio, which is similar to that of the first two tests, optimally resulted in minimal rock heave with minimal variability, for all charges.

3.5.2.1.6. Geology. The tests were conducted in limestone quarry floors. The pit floors had minimal variance in elevation; therefore, topography was not a concern. The rock in the pit floors was solid, unweathered, and exhibited minor layering. Therefore, geology was assumed to have minimal variability in the limestone quarry tests.

3.5.2.1.7. Presence of water. The explosive that was used was a pumped, high density emulsion that is listed as water resistant in the technical data sheet. The explosive was bottom-loaded; therefore, water was assumed to be adequately displaced and a non-factor.

3.5.2.1.8. Direction of propagation. To account for a potential directional effect within each quarry, the string of seismographs was placed on an identical azimuth from each signature hole for every test, except for the test at Big Bend since the quarry locations are different and preference was given to the azimuth that allowed for the greatest monitoring distance. The azimuth direction was dictated by the quarry operator, which was also the direction with the greatest expanse of pit floor from the test location.

3.5.2.1.9. Preconditioning. Each signature hole was placed in a location that was not blasted previously. This minimized the effect of preconditioning by prior blasts. There was the possibility of some preconditioning due to back break from the production blasts shot above the bench; however, the effect of any preconditioning was unavoidable.

3.5.2.1.10. Monitoring distance. Monitoring distances were designed such that both near-field and far-field data could be recorded and compared. Therefore, monitors were set at distances near to the charge and at distances as far as possible from the charge. The furthest monitoring locations were limited by the useable space at each quarry.

The monitoring distances were determined using set scaled distance values (Table 3.1). This was done in order to compare vibrations from multiple charge weights. Even though there are limits to the scaled distance equation, as discussed previously in this document, the set scaled distance values worked well in determining the monitoring distances for the wide range of charge sizes that were tested at the quarries.

Table 3.1. Design SRSD values used to locate the seismographs for the field tests.

Original SRSD Values (Tests 1 - 3)		Final SRSD Values (Tests 4 - 5)	
m/kg^1/2	(ft/lb^1/2)	m/kg^1/2	(ft/lb^1/2)
0.9	(2)	1.8	(4)
1.4	(3)	3.2	(7)
1.8	(4)	4.5	(10)
6.8	(15)	8.1	(18)
13.6	(30)	11.3	(25)

The specific scaled distance for each seismograph was chosen for multiple reasons. It was important to record data as close as practicable to the charge to identify variances in near-field waveforms. Near-field waveforms have been shown to be closer to a single amplitude spike, as opposed to multiple spikes, which occurs in the mid- to far-field ranges (Rouse, Acorn, & Worsey, 2013). Additionally, it was important to

compare the data from near-field seismographs to the data from the far-field seismographs to identify variances between near-field and far-field data.

Originally, the design scaled distance values were set as shown in the left two columns of Table 3.1. They were adjusted to higher values for the final two tests, given in the right two columns of Table 3.1, for two reasons. First, the seismographs closest to the charge showed possible decoupling characteristics at the smaller scaled distance values used in the first three tests. Second, the complete signature hole dataset was missing data in a number of areas and the second set of SRSD values were chosen to fill in those holes. A sixth seismograph was also used in the final two tests to record data at design distances of 182.9 m and 213.4 m (600 ft and 700 ft), which were also chosen to reinforce the signature hole dataset

3.5.2.1.11. Instrument placement and setup. The tests were designed to utilize the best available instrumentation to monitor blast vibrations in the near- and far-field. Care was taken to ensure the proper seismographs were chosen and that the proper mounting methods for the seismographs were used. The process of developing the monitoring plan and equipment setup procedures is described in detail in Section 3.5.2.3.

3.5.2.2. Test matrix. As described in the previous section, the limestone quarry tests were designed to focus on the effect of charge geometry by varying charge length and diameter while minimizing variance of the remaining variables. The test matrix was designed and updated throughout the testing process to make the most of the limited number of signature holes tests. Table 3.2 provides the final "as-built" test matrix, which lists the field-measured hole depth, stemming length, and charge length, theoretical

explosive density, and calculated charge weight for each signature hole test. The location of each test is shown in Table 3.3.

Table 3.2. Experimental "as-built" matrix.

Test #	Hole Diameter		Hole Cross-Sectional Area		Hole Depth		Stemming Length		Charge Length		Expl. Density	Charge Weight		Charge Weight per Unit Length	
	mm	(inch)	sq mm	(sq in)	m	(ft)	m	(ft)	m	(ft)	g/cc	kg	(lbs)	kg/m	(lbs/ft)
1	127	(5)	12,668	(19.6)	11.2	(36.8)	3.8	(12.5)	7.4	(24.3)	1.25	117	(258)	15.8	(10.6)
2	79	(3.125)	4,948	(7.7)	7.5	(24.7)	3.7	(12.0)	3.9	(12.7)	1.25	24	(53)	6.2	(4.2)
3	79	(3.125)	4,948	(7.7)	4.3	(14.3)	1.3	(4.3)	3.0	(9.9)	1.25	19	(41)	6.2	(4.2)
4	127	(5)	12,668	(19.6)	7.3	(24.0)	3.4	(11.0)	4.0	(13.0)	1.25	63	(138)	15.8	(10.6)
5	140	(5.5)	15,328	(23.8)	10.5	(34.4)	4.4	(14.3)	6.1	(20.1)	1.25	117	(258)	19.2	(12.9)

Table 3.3. Location of each signature hole test.

Test #	Quarry	Location	Limestone
1	Butler	Main Pit	Camp Nelson
2	Butler	Main Pit	Camp Nelson
3	Butler	North Pit	Logana
4	Butler	Main Pit	Camp Nelson
5	Big Bend	Main Pit	St. Genevieve

The matrix was originally designed for more than five signature hole tests; however, time and funding constraints limited the number of tests to five. The first four tests were designed to record short and long charges at the smallest and largest hole diameter that was available at Butler Quarry. The final test was added at Big Bend Quarry so that a seismograph could be placed at the farthest distance possible from the signature hole. The only hole diameter available at Big Bend was a 140 mm (5.5 inch) hole. Since the hole diameter did not match any of the first four tests, Test #5 was

designed so that the charge weight matched the charge weight used in Test #1, which was the largest charge weight of the first four tests.

The matrix was also designed with the needs of the signature hole dataset in mind. After the first three tests, the complete dataset was evaluated and a number of gaps were found in the dataset. Therefore, the last two tests were designed to fill in the gaps that were noticed in the complete dataset.

3.5.2.3. Monitoring plan and equipment selection. The limestone quarry tests were designed to capture multiple seed waveforms from each test using a chain of seismographs. Each seismogram was used to identify amplitude, principal frequency and dominant frequency, and duration of the vibration. The seismograms also allowed for a visual inspection of the vibration passing each point.

The limestone quarry tests were also designed to capture as much additional data as possible. Therefore, each test was set up so that the velocity of detonation (VOD) and propagation velocity were recorded, and other factors were noted, including geologic anomalies, presence of water, loading practices, and post-blast results.

3.5.2.3.1. <u>Seismograph selection and placement.</u> The experiments were designed to use both accelerometer-based seismographs and geophones. Accelerometer-based seismographs were used for the closest sampling points, while geophones were used for the monitoring points placed the furthest distances from the charge. This section describes the types of seismograph, the mounting procedure used for each seismograph, and the deployment strategy for each seismograph.

Accelerometer-based seismographs. The accelerometer-based seismographs used in the limestone quarry signature hole tests were White Industrial Seismology Mini-

Seis seismographs with the x1 gain option. These were chosen for this project for their high operating range and availability. The specifications for the Mini-Seis seismographs are given in Table 3.4 and Table 3.5.

Table 3.4. Seismograph specifications.

Sensors	Three seismic channels
Frequency Response	2-500 Hz (-3dB points) at 2048 samples per second
Operating Temp. Range	-18 to 54 C (0 to 130 F)
Sample Rate	32 to 2048 samples per second
Trigger Level	Variable
Duration	1 to 6 seconds

Table 3.5. Seismograph particle velocity operating range.

x2		x1	
0.125 to 64 mmps	(0.005 to 2.5 ips)	0.25 to 127 mmps	(0.01 to 5.0 ips)
0.25 to 127 mmps	(0.01 to 5.0 ips)	0.5 to 254 mmps	(0.02 to 10.0 ips)
0.5 to 254 mmps	(0.02 to 10.0 ips)	1.0 to 508 mmps	(0.04 to 20.0 ips)

The seismographs were set to record at a sample rate of 2,048 Hz, the highest sample rate available. All of the x1 seismographs were set to record amplitudes from 1.0 to 508 mmps (0.04 to 20.0 ips).

Geophone-based seismographs. The geophone-based seismographs were also White Industrial Seismology Mini-Seis models; however, these had the standard x2 gain option (Table 3.4 and Figure 3.1). The standard seismographs were also set to record at 2,048 Hz but were programmed to record in the range from 0.25 to 127 mmps (0.01 to 5.0 ips). The final two tests used a sixth seismograph, which was set to record at a maximum peak particle velocity values of 64 mmps (2.5 ips) at a sample rate of 1024 Hz.

Figure 3.1. Mini-Seis x2 model manufactured by White Industrial Seismology.

Deployment strategy. The seismographs were originally deployed in the near-field and far-field ranges (Table 3.6 and Table 3.7). The three accelerometers were placed at monitoring distances ranging from 4.0 m to 49.6 m (13.1 ft to 162.7 ft). These ranges proved to be within the nonlinear range of the propagating vibration, as shown in Section 4.

Table 3.6. Distance values recorded from the five signature hole tests.

Test #	Distance 1 m	(ft)	Distance 2 m	(ft)	Distance 3 m	(ft)	Distance 4 m	(ft)	Distance 5 m	(ft)	Distance 6 m	(ft)
1	14.8	(48.5)	19.8	(65.1)	27.6	(90.5)	67.4	(221.2)	151.8	(498.1)	-	-
2	5.0	(16.4)	7.3	(23.8)	10.1	(33.0)	37.1	(121.6)	73.9	(242.4)	-	-
3	4.0	(13.0)	6.4	(20.9)	8.4	(27.7)	29.2	(95.8)	57.7	(189.2)	-	-
4	14.5	(47.5)	25.4	(83.4)	35.4	(116.3)	64.0	(209.9)	89.8	(294.7)	147.9	(485.3)
5	19.5	(63.9)	32.9	(108.1)	49.6	(162.7)	89.3	(293.0)	122.9	(403.2)	215.5	(706.9)

Table 3.7. Square root scaled distance values recorded from the five signature hole tests.

Test	SRSD 1		SRSD 2		SRSD 3		SRSD 4		SRSD 5		SRSD 6	
#	M	(I)	M	(I)	M	(I)	M	(I)	M	(I)	M	(I)
1	1.37	(3.0)	1.83	(4.1)	2.55	(5.6)	6.23	(13.8)	14.03	(31.0)	-	-
2	1.02	(2.3)	1.48	(3.3)	2.06	(4.5)	7.58	(16.8)	15.12	(33.4)	-	-
3	0.92	(2.0)	1.47	(3.3)	1.95	(4.3)	6.75	(14.9)	13.34	(29.5)	-	-
4	1.83	(4.0)	3.21	(7.1)	4.48	(9.9)	8.08	(17.9)	11.34	(25.1)	18.67	(41.3)
5	1.80	(4.0)	3.04	(6.7)	4.58	(10.1)	8.25	(18.2)	11.35	(25.1)	19.90	(44.0)

*M: m/kg^1/2 (I: ft/lb^1/2)

The first three signature hole tests used only two of the geophone-based seismographs, leaving a single backup unit. After the first three tests were completed, the need for additional data in the remaining tests necessitated the use of the additional geophone-based seismograph. The geophones were used to monitor at distances ranging from 29.2 m to 215.5 m (95.8 ft to 706.9 ft).

Mounting procedure. To minimize the effect of geology, the seismographs were mounted to the quarry floor where the geology had minimum variability. The extreme vibrations and solid, uncleaned floor made mounting the units difficult. The literature search proved that it is best to bolt the seismographs to solid rock for proper coupling, especially near the charge; however, adhesive bonding has been successfully used as well. For this study, the accelerometer units were anchored to the rock using anchor bolts. The adhesive method was attempted with the geophone units in Test #1; however, the adhesive did not bond well to the pit floor. Therefore, the geophone seismograph models were coupled with mud caps for the remaining tests, which maintained good coupling at the larger distances that the geophone units were used.

The accelerometer-based seismographs were constructed with the accelerometers inside of the control box. Therefore, a steel plate was attached to the bottom of the control box so that the plate extended beyond the sides of the box (Figure 3.2). Then, the plate was attached to the quarry floor using small mechanical anchor bolts. The anchor bolts were fully threaded, which allowed for the plates to be mounted tightly to the pit floor (Figure 3.3).

Figure 3.2. Steel plate mounted to the bottom of the Mini-Seis x1 seismographs.

Figure 3.3. Mini-Seis x1 seismograph mounted to the quarry floor.

The geophones were coupled to the pit floor using mud caps and standard spike plates (Figure 3.4). They were placed in such a way that the arrow on top of the geophone was facing the charge to ensure that the vibration components were monitored correctly. Then, the geophone was draped with plastic and covered in mud. Though this method may be unconventional, the seismograms did not show decoupling, so the method was considered acceptable for coupling the seismographs at the larger monitoring distances.

Figure 3.4. Mini-Seis x2 geophone coupled to the pit floor using a mud cap.

3.5.2.3.2. <u>Velocity of detonation.</u> The velocity of detonation (VOD) was recorded for the signature hole tests in order to compare explosive performance characteristics for the range of charge diameters and identify any anomalies in the detonation process of the explosive.

The VOD was monitored using an MREL MicroTrap™ (Table 3.8 and Figure 3.5), which uses the resistance wire technique. For this technique, a two-strand wire of known resistance is placed axially down the blasthole, attached to the booster assembly. The MicroTrap™ outputs a constant current; therefore, as the explosive detonates (decreasing the length of cable/resistance), the data acquisition system monitors the drop in voltage through the cable. The MicroTrap™ can also use the VOD channel to trigger

four oscilloscope channels. These were used as part of the propagation velocity monitoring work described in the following section.

Table 3.8. MREL MicroTrap™ specifications.

Channels	VOD + 4 scope channels
Scope voltage	+/-10volts
Resolution	14 bits, 1 part in 16,384
Recording rates:	1 Hz to 2 MHz
Recording Time (@ 2 MHz rate)	2 seconds

Figure 3.5. Microtrap™ with accelerometer array.

3.5.2.3.3. <u>Propagation velocity.</u> Two methods were used to determine the propagation velocity of the vibration through the rock: multi-unit triggering of the seismographs and high sample rate accelerometers. These include multi-unit triggering of the seismographs and accelerometers monitored with the MicroTrap™.

Multi-unit triggering was done using the master/slave option of the Mini-Seis seismographs. The seismographs were connected using a signal cable that allowed the master unit to send a trigger command to the slave units so that the master and slave units triggered simultaneously. This setup enabled the vibration arrival time difference between the seismographs to be evaluated, when in turn allowed for the calculation of the propagation velocity.

The downside of the signal cable is that the sample rates of the seismographs are not high enough to calculate an exact measurement of velocity. The measurement error in the seismographs spaced close together is excessive due to the limited sample rates of the seismographs. Higher sampling of vibrations were achieved using tri-axial Micro Electro-Mechanical Systems (MEMS) accelerometer units (±3g, analog output module AXDL335, manufactured by Analog Devices, Inc.) connected through the oscilloscope channels of the MicroTrap™ (Figure 3.6). The accelerometers, which were each powered by a 3 volt wafer battery (model CR 2016), output variable voltages in response to the blast vibrations. Using a minimum sample rate of 100,000 samples per second, the MicroTrap™ produced a more precise seismic arrival time than the seismographs, and therefore, more accurate propagation velocity values than the seismograph setup. Additionally, the high sample rate also allowed the ADXL335 accelerometers to be placed very close together so that they were essentially monitoring the instantaneous propagation velocity of the vibration as opposed to the overall average propagation velocity that was monitored by the chain of seismographs. The ADXL335 accelerometers were mounted to the pit floor using a single anchor bolt.

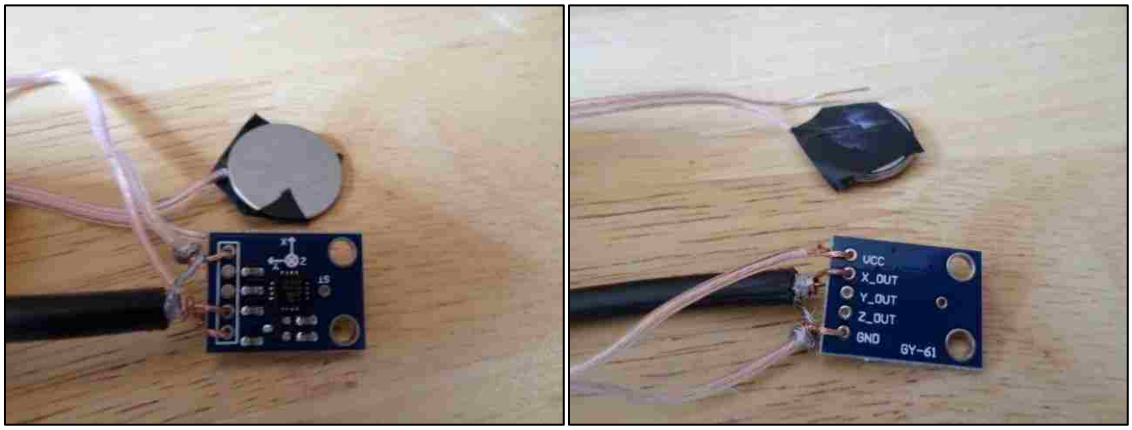

Figure 3.6. ADXL335 MEMS accelerometer.

The propagation velocity values calculated using the MEMS accelerometers were used to check the propagation velocity values that were calculated using the seismographs. The ADXL335 accelerometers were not calibrated to accurately record seismic waveform amplitudes and produced an inconsistent output signal during vibration events. Therefore, The ADXL335 accelerometers were not used as a source of any data other than vibration arrival time.

3.5.2.3.4. <u>Other factors.</u> Other factors include setup parameters and post-test observations. It was important to record the setup parameters of each experiment so the information could be revisited during the data analysis phase of the project. For example, booster information, presence of water in the blasthole, seismograph mounting procedures and issues, and seismograph sample rates were recorded.

It was also important to record all post-test observations, including the equipment status and the characteristics of the rock heave around the signature hole. For example, the altered state of the ground around the signature hole can be indicative of the level of charge confinement and, therefore, the level of energy transfer to vibrations.

3.5.3. Test Results. This section highlights the results from the signature hole tests that were conducted in the limestone quarries. The full equipment array used for those tests is shown in Figure 3.7.

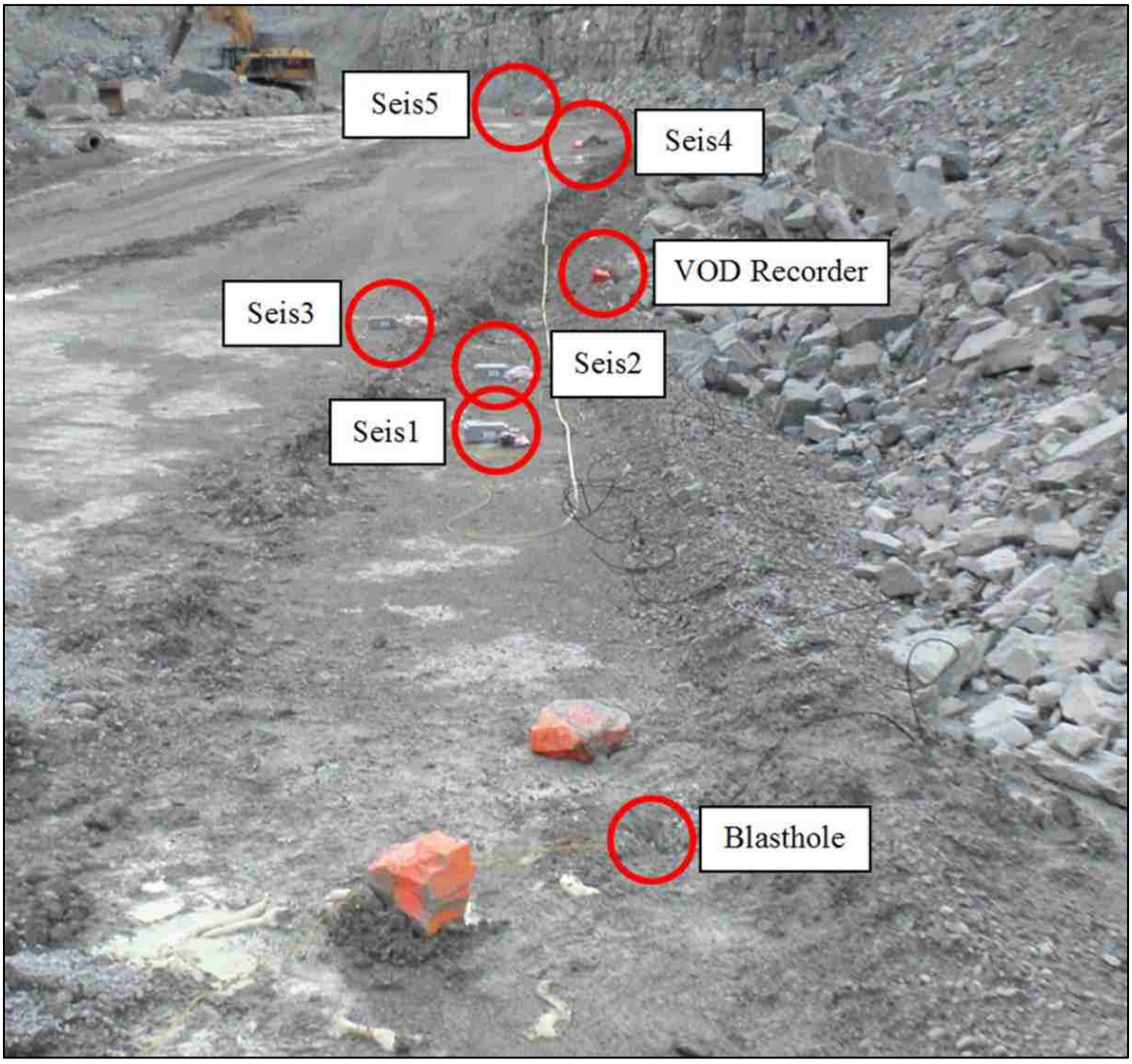

Figure 3.7. Full test array for Test 2.

The data produced for the signature hole dataset from the limestone quarry tests is given in Table 3.9 (Appendix A). Note that only the radial component values are given.

The transverse and vertical components were not evaluated; however, if required, they could be evaluated following the same procedure described in the following sections of this document. The input variables and post-test results that were recorded for each test are given in Appendix B.

Table 3.9. Data produced by seismographs from limestone quarry signature hole tests.

Test #	Date	Seis#	Distance From Blast		Charge Weight		SRSD		Radial PPV		Peak Radial Freq.	Dom. Radial Freq.	Radial Waveform Duration
			m	(ft)	kg	(lbs)	M	(I)	mmps	(ips)	Hz	Hz	s
1	9/18/2013	Seis1	14.8	(48.5)	117	(258)	1.37	(3.0)	235.7	(9.28)	21.7	13.0	0.0674
		Seis2	19.8	(65.1)	117	(258)	1.83	(4.1)	162.6	(6.40)	20.0	-	0.0854
		Seis3	27.6	(90.5)	117	(258)	2.55	(5.6)	51.8	(2.04)	18.6	14.1	0.1406
		Seis4	67.4	(221.2)	117	(258)	6.23	(13.8)	38.6	(1.52)	-	-	-
		Seis5	151.8	(498.1)	117	(258)	14.04	(31.0)	32.5	(1.28)	-	-	-
2	11/7/2013	Seis1	5.0	(16.4)	24	(53)	1.02	(2.3)	174.8	(6.88)	-	6.0	0.0918
		Seis2	7.3	(23.8)	24	(53)	1.48	(3.3)	73.2	(2.88)	-	-	0.1113
		Seis3	10.1	(33.0)	24	(53)	2.06	(4.5)	98.6	(3.88)	23.8	5.5	0.1431
		Seis4	37.1	(121.6)	24	(53)	7.58	(16.7)	12.4	(0.49)	48.7	28.5	0.1377
		Seis5	73.9	(242.4)	24	(53)	15.10	(33.4)	6.9	(0.27)	35.3	36.0	0.1689
3	12/2/2013	Seis1	4.0	(13.0)	19	(42)	0.91	(2.0)	516.1	(20.32)	-	-	-
		Seis2	6.4	(20.9)	19	(42)	1.47	(3.2)	345.4	(13.60)	-	-	-
		Seis3	8.4	(27.7)	19	(42)	1.94	(4.3)	109.7	(4.32)	48.8	26.0	0.0713
		Seis4	29.2	(95.8)	19	(42)	6.73	(14.9)	42.7	(1.68)	47.5	53.8	0.0762
		Seis5	57.7	(189.2)	19	(42)	13.28	(29.4)	23.1	(.91)	32.8	85.3	0.1030
4	7/29/2014	Seis1	14.5	(47.5)	63	(138)	1.83	(4.0)	252.0	(9.92)	25.6	-	-
		Seis2	25.4	(83.4)	63	(138)	3.21	(7.1)	93.5	(3.68)	24.9	27.0	0.0723
		Seis3	35.4	(116.3)	63	(138)	4.48	(9.9)	48.8	(1.92)	23.8	26.0	0.1147
		Seis4	64.0	(209.9)	63	(138)	8.08	(17.9)	29.0	(1.14)	44.5	25.0	0.1597
		Seis5	89.8	(294.7)	63	(138)	11.34	(25.1)	18.8	(0.74)	78.7	24.0	0.1729
		Seis6	147.9	(485.3)	63	(138)	18.68	(41.3)	10.9	(0.43)	51.2	48.0	0.2256
5	7/30/2014	Seis1	19.5	(63.9)	117	(258)	1.80	(4.0)	130.0	(5.12)	68.3	-	-
		Seis2	32.9	(108.1)	117	(258)	3.04	(6.7)	44.7	(1.76)	24.9	10.0	0.0737
		Seis3	49.6	(162.7)	117	(258)	4.58	(10.1)	34.5	(1.36)	39.3	11.0	0.0962
		Seis4	89.3	(293.0)	117	(258)	8.25	(18.2)	12.7	(0.50)	28.4	30.0	0.2431
		Seis5	122.9	(403.2)	117	(258)	11.35	(25.1)	6.6	(0.26)	35.3	33.0	0.1992
		Seis6	215.5	(706.9)	117	(258)	19.90	(44.0)	5.8	(0.23)	36.5	35.0	0.2217

The dashes in Table 3.9 are data points that were not recoverable from the seed waveforms due to either decoupling of the seismograph sensor or a poor quality seismogram. In the tests, seismographs were not always adequately coupled during the vibration event due to poor ground conditions in the pit floors. However, the peak particle velocity values for the decoupled seismographs appeared to be reasonable after evaluation using the scaled distance versus PPV plot for each test (Figure 3.8).

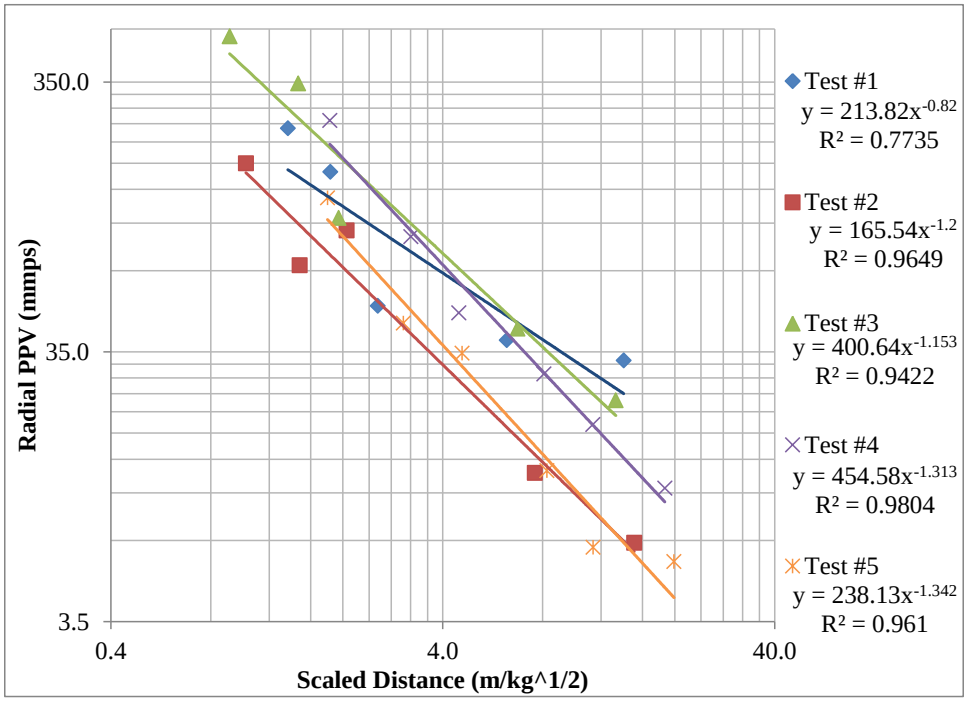

Figure 3.8. Scaled distance versus Radial PPV of limestone quarry data.

Signature hole data produced by an individual test tend to conform tightly to SRSD regression models, as evidenced by the high coefficient of determination values given in the figure. The figure does show three data points that do not conform as well as could be expected: the third Test #1 data point from the left, the second Test #2 data point

from the left, and the third Test #3 data point from the left. This could be due to slight decoupling of the sensor during the event. Additionally the adhesive mounted units that were used in Test #1 were not coupled as well as the remaining tests. However, the data points recorded at small monitoring distances appear to have decoupling, yet conform to their respective regression lines. Therefore, apparent decoupling of a seismograph during an event does not necessarily mean the peak particle velocity data is poor quality. Additionally, the near-field waveforms are typically single-spike waveforms, with the spike occurring in the first cycle of the vibration, at a point prior to any decoupling effects appearing on the seismogram. Therefore, the seismographs do not appear to be decoupled during the recording of the first peak amplitude. Thus, there is no clear reason to remove any of the PPV data points from the dataset.

Figure 3.9 gives an example of a poor seismogram. The dominant radial frequency and waveform duration were not recorded for this data point since the calculated dominant frequency is affected by the decoupling of the waveform after the first two peaks. This is the same reason the duration was not recorded. In contrast, the principal frequency, which is the frequency of the peak amplitude, could be recorded because it was assumed the principal cycle was not affected by decoupling due to the reasons described in the previous paragraph.

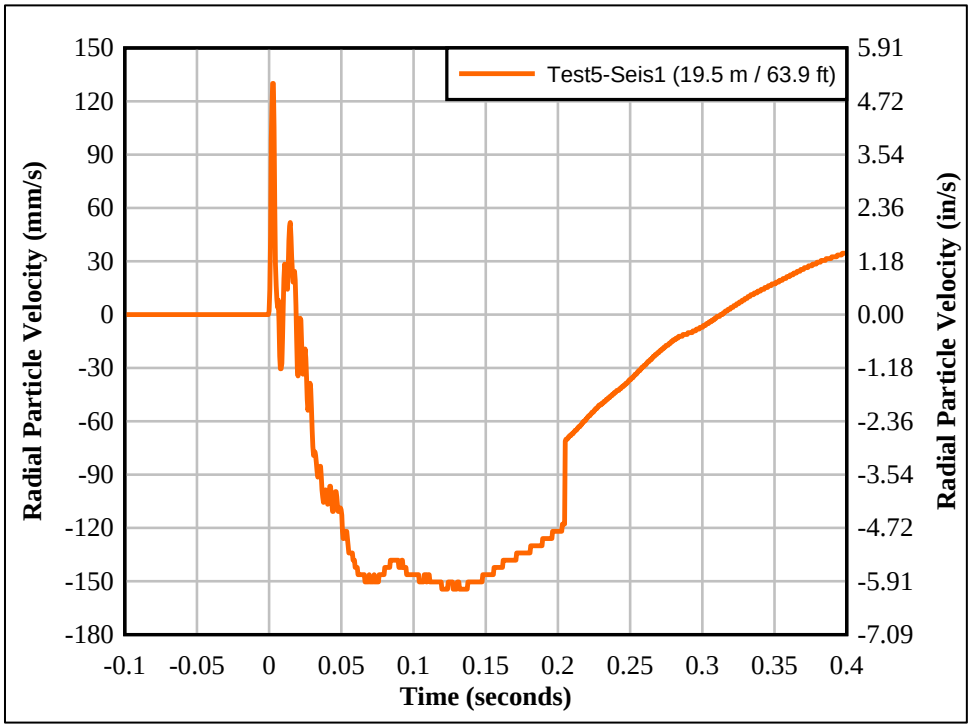

Figure 3.9. Example of radial particle velocity for seismograph showing error in waveform.

Figure 3.10 shows typical good quality waveforms produced by seismographs. Most seismograms were similar to those displayed in this figure, where all the required data was able to be extracted from the recording. The figure also displays the primary difference between near-field vibrations and far-field vibrations: the near-field waveform exhibits a single, high amplitude cycle, while the far-field waveform exhibits multiple, low amplitude cycles.

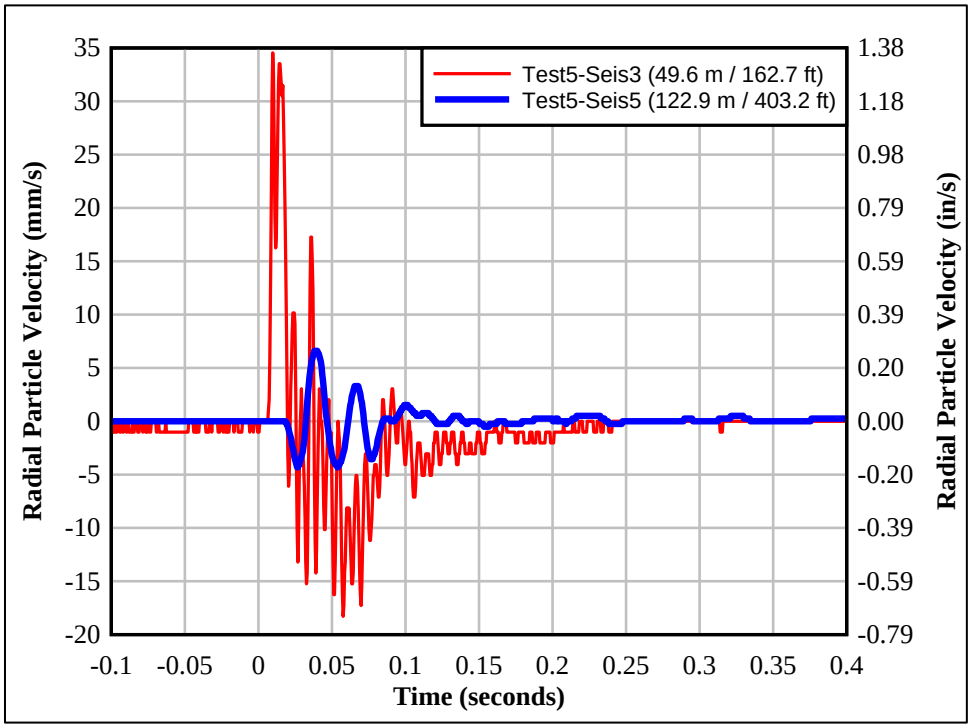

Figure 3.10. Example of radial particle velocity waveform produced by two seismographs in Test5.

The values for the propagation velocity were calculated using the master seismograph (Seis1) and the two geophone-based seismographs (Seis4 and Seis5) (Table 3.10). The ADXL335 accelerometers were used in the second and third signature hole tests to ensure the seismographs produced accurate propagation velocity data. The velocities calculated using the accelerometers confirmed that the Seis4 and Seis5 were placed far enough from Seis1 that the propagation velocity could be calculated using the seismograph data with confidence. Additionally, the propagation velocity recorded during each test was shown to have a constant value because the propagation velocity calculated using the ADXL335 accelerometers is essentially the instantaneous propagation velocity in the near-field, and the ADXL335-produced propagation velocity matched well with the seismograph-produced propagation velocity.

Table 3.10. Radial component propagation velocity values for limestone quarry tests.

Test #	Distance from Charge						Time of Arrival		Radial Propagation Velocity					
	Seis1		Seis4		Seis5		Seis4	Seis5	Seis4		Seis5		Average	
	m	(ft)	m	(ft)	m	(ft)	ms	ms	m/s	(ft/s)	m/s	(ft/s)	m/s	(ft/s)
1	14.8	(48.5)	67.4	(221.2)	149.1	(489.1)	7.8	24.4	6,700	22,000	5,500	18,000	**6,100**	**20,000**
2	5.0	(16.4)	37.1	(121.6)	73.9	(242.4)	8.3	15.1	4,000	13,000	4,600	15,000	**4,300**	**14,000**
3	4.0	(13.0)	29.2	(95.8)	57.7	(189.2)	5.9	12.7	4,300	14,000	4,300	14,000	**4,300**	**14,000**
4	14.5	(47.5)	64.0	(209.9)	89.8	(294.7)	10.7	16.1	4,600	15,000	4,600	15,000	**4,600**	**15,000**
5	19.5	(63.9)	89.3	(293.0)	122.9	(403.2)	15.6	22.0	4,600	15,000	4,600	15,000	**4,600**	**15,000**

*Seis1 arrival time is zero.

Additional information that was of interest for the tests included the propagation velocity, velocity of detonation, and the heave of the rock. The propagation velocity, VOD, and heave were used to evaluate each signature hole test and adjust the subsequent tests if need be to ensure the tests provided the required data. The data was not used in the statistical analyses described in the next section because similar data were not recorded for the other three data sources.

The average propagation velocity values ranged from 4,300 to 6,100 m/s (14,000 to 20,000 ft/s), although four of the five tests were within the 4,300 to 4,600 m/s (14,000 to 15,000 ft/s) range. The wide range of propagation velocity values is a consequence of the seismographs' low sample rates.

The VOD was monitored for all tests; however, the VOD equipment did not trigger during Test #4 and Test #5 and is not reported herein. The VOD monitored for Test #1 in the 127 mm (5 inch) diameter blasthole was 5,940 m/s (19,500 ft/s). In Test #2, the 79 mm (3-1/8 inch) diameter blasthole had two detonation velocities, which was most likely caused by improper loading. The test had an initial VOD (VOD1) of 5,420 m/s (17,800 ft/s) and then detonated at 4,570 m/s (15,000 ft/s) (VOD2). In Test #3, the 79 mm (3-1/8 inch) diameter charge had a VOD of 5,100 m/s (16,750 ft/s) (Table 3.11).

In summary, all measured values were near to the value listed on the technical specification sheet for PowerNel 1500™.

Table 3.11. Detonation velocity measurements for limestone quarry tests.

Test #	Hole Diameter		VOD1		VOD2	
	mm	(inch)	m/s	(ft/s)	m/s	(ft/s)
1	127	(5.0)	5,940	(19,500)		
2	79	(3.1)	5,430	(17,800)	4,570	(15,000)
3	79	(3.1)	5,110	(16,750)		

*Emulsion rated at 5,800 to 6,100 m/s (19,000 to 20,000 ft/s) in 171 mm (6.75 inch) blasthole.

Table 3.11 shows that the smaller diameters do have a slightly lower detonation velocity. This difference is most likely insignificant. For instance, in the larger hole, the explosive detonated at a rate of 0.17 ms/meter (0.051 ms/ft). The smaller hole detonated at a rate of 0.18 to 0.22 ms/meter (0.056 to 0.067 ms/ft). For a 10 meter (33 ft) long charge at either diameter, the detonation duration is approximately 2 milliseconds. If the resultant vibration from that charge has a dominant frequency of 15 Hz (66 millisecond period), the detonation duration is only 3% of the period, which is a minor percentage. Therefore, the slight difference in VOD between the blasthole diameters most likely does not affect the resulting elastic blast vibration.

The final parameter that was evaluated was the rock heave. The first two tests showed slight heave, while the final two tests showed zero heave with only surface fractures. The third test was only lightly stemmed and therefore produced major heave. The valuation of rock heave primarily showed the importance of stemming length in the confinement of the explosive.

4. SIGNATURE HOLE DATA REGRESSION ANALYSIS

4.1. INTRODUCTION

This section is the first of two focal sections of this document. It provides a statistical overview of the signature hole data, the sources of which were described in the previous section. The section then follows with a description of the multiple regression analyses of the dataset with a focus on the relative effect of the variables on amplitude, frequency, and duration of the seed waveforms.

4.2. SIGNIFICANCE OF STUDY

This study is significant as it provides insight into blast-induced vibrations from a unique statistical perspective. The unique use of signature hole data from multiple sites allows for an assessment of a wide variation in geology, as well as major variations in monitoring distance and charge weight, charge geometry, and charge density. The wide ranges of values for each variable most likely could not have been achieved by using signature hole data from a single site.

Charge weight is a function of charge geometry and charge density, assuming no outside influences, such as voids. Therefore, one difficulty of this study is identifying whether the charge weight is a primary variable or if charge geometry or density are primary variables. The regression analysis helps to solve this problem.

In the past, the industry has assumed that vibrations could not be compared from site to site because of the geologic influences on vibration attenuation. In most cases, this is a reasonable assumption because geologic parameters such as rock characteristics,

bedding planes, fractures, and discontinuities have a significant effect on vibration propagation, even within a specific site. However, the multiple regression analysis can be used to compare data from multiple sites because geology can be included as an variable.

4.3. SIGNATURE WAVEFORM DATASET

The complete signature hole dataset includes 105 sets of signature hole test data (Appendix C). The data was compiled from a range of sources, as described in the previous section. These represent a variety of regions and mine types including:

- Operator controlled surface gold mine tests from the western United States
- Explosive supplier controlled surface gold mine tests from the western United States
- Operator controlled surface coal mine tests in Central Appalachia
- Limestone quarry tests in Kentucky

The range of sources produced data of varying ranges of quality. This is not to say the data is unreliable. It only means that some of the data is more tightly controlled and provides more information than other data due to the intended purpose of each dataset. The signature waveform dataset is a sample population of signature hole-produced vibrations that are affected by a number of variables, including:

- geology,
- scaled distance,
- charge geometry, and
- charge density.

Other factors also influence the vibration characteristics but were not included in this study due to the lack of available information on them for the entire dataset. These factors include velocity of detonation, propagation velocity, heave, specific characteristics of geology, and other influencing variables not typically documented during signature hole tests. As it is, the signature hole dataset represents a wide range of values for each variable, making multiple regression analysis an applicable method of evaluation.

4.3.1. Geology. The signature hole dataset represents a wide range of geology. The gold operator and coal operator monitored in a variety of locations on and off the mine site. The varying geological units, topsoil, and topography influenced the data for these two sources. In contrast, the gold-supplier and limestone quarry datasets were recorded in mine pits with uniform geology in order to minimize the effect of geology on the vibrations. Therefore, the data from the gold-supplier and limestone quarry tests are less affected by geologic variability than the other two sources. Overall, the data is evenly distributed by source, and therefore, by geologic influence (Figure 4.1).

4.3.2. Monitoring Distance. Each set of data, apart from the coal-operator data, was recorded at similar ranges of distance from the charge (Figure 4.2). The coal-operator signature hole data were recorded at the largest monitoring distances because the vibrations were monitored off the mine site, while the limestone quarry tests produced data at the smallest monitoring distances since the vibrations were recorded in the quarry pit.

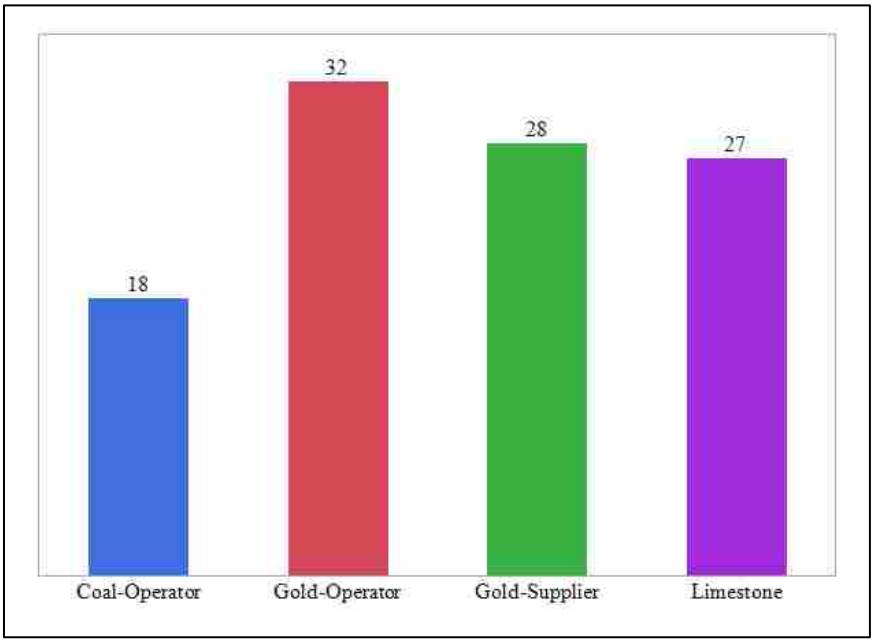

Figure 4.1. Number of signature hole seed waveforms by source.

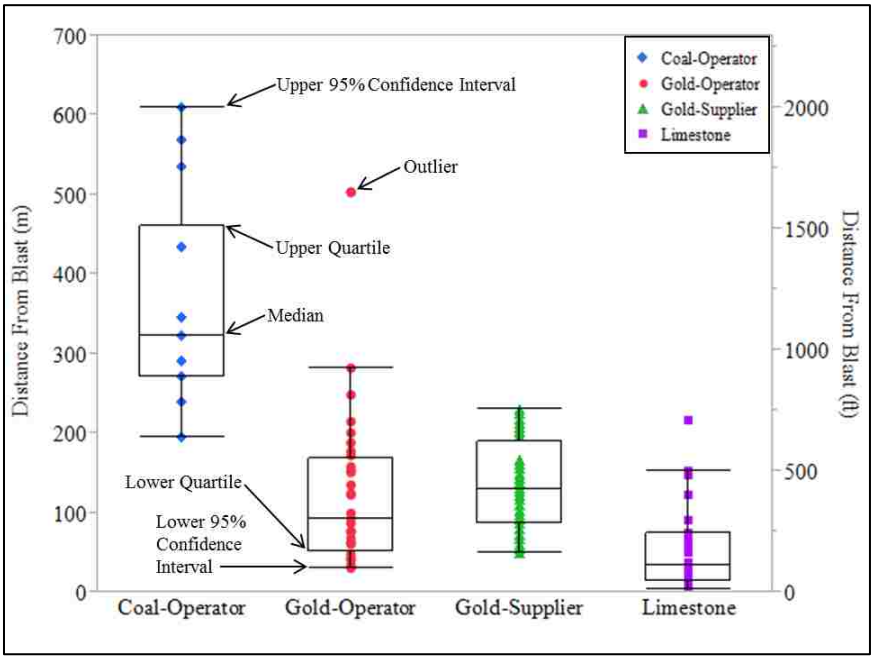

Figure 4.2. Distance from charge to monitoring point by source with box-and-whisker plots.

4.3.3. Charge Weight. The charge weight values vary between data sources (Figure 4.3). The limestone quarry typically has lower charge weights than the other three sources, due to the smaller hole diameters used in the limestone quarry tests. The gold-operator tests have the greatest variance in charge weight, while the gold-supplier data has the smallest variance. Overall, the full dataset has a wide range of charge weights, which is optimal for the regression analysis.

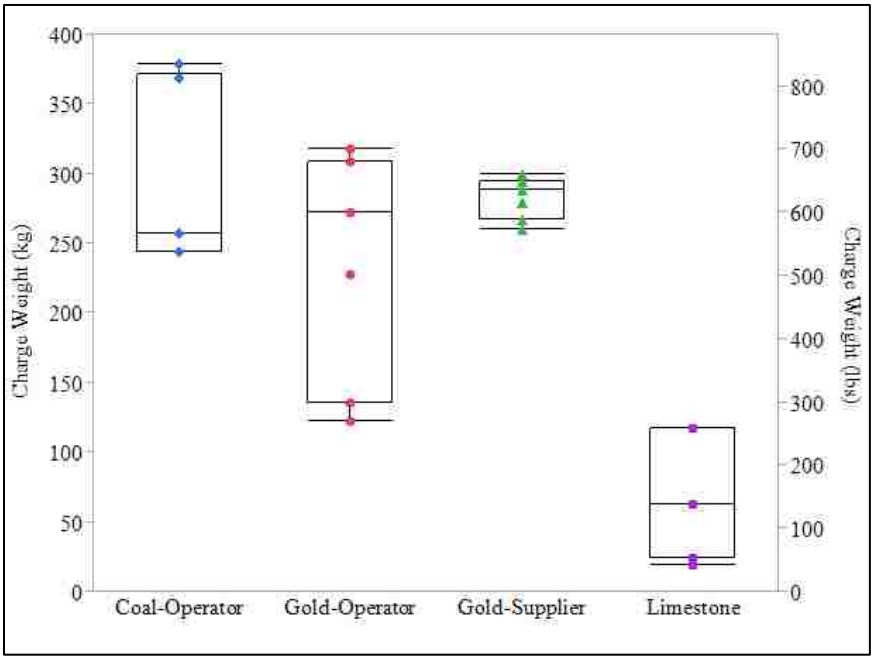

Figure 4.3. Charge weight by source with box-and-whisker plots.

4.3.4. Scaled Distance. The variability of scaled distance by source is similar to that of both the monitoring distance and the charge weight since scaled distance is directly related to both of these variables (Figure 4.4).

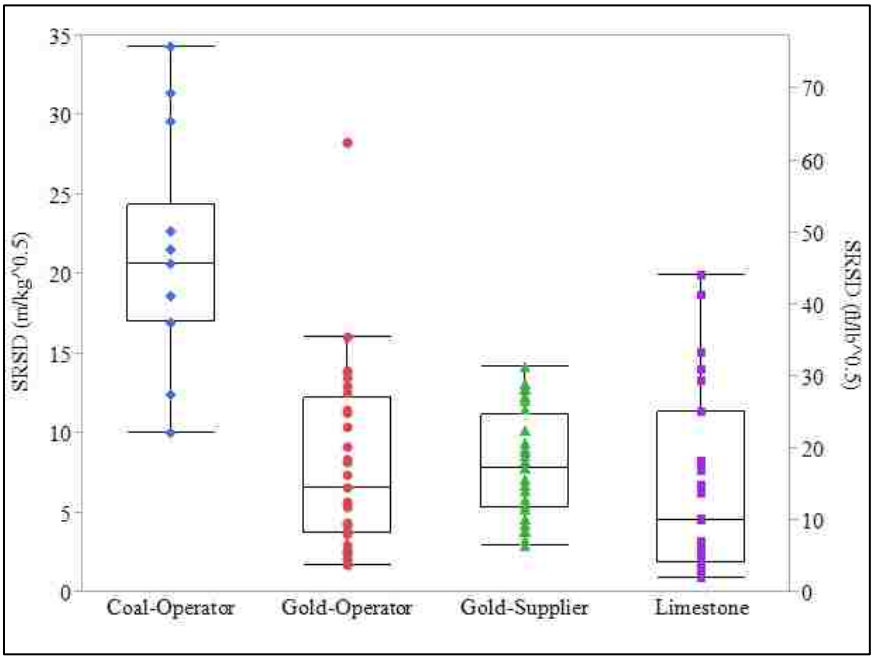

Figure 4.4. Scaled distance by source with box-and-whisker plots.

4.3.5. Charge Diameter. The charge diameter is a focal point of the regression analysis. The represented diameters range from 79 to 251 mm (3-1/8 to 9-7/8 inches). The intermediate charge diameter values are 127, 140, 172, 200, and 222 mm (5, 5.5, 6-3/4, 7-7/8, and 8-3/4 inches). The charge diameter values do not vary much by source (Figure 4.5). However, each source did provide data at a variety of distances from the charge, which is beneficial (Figure 4.6).

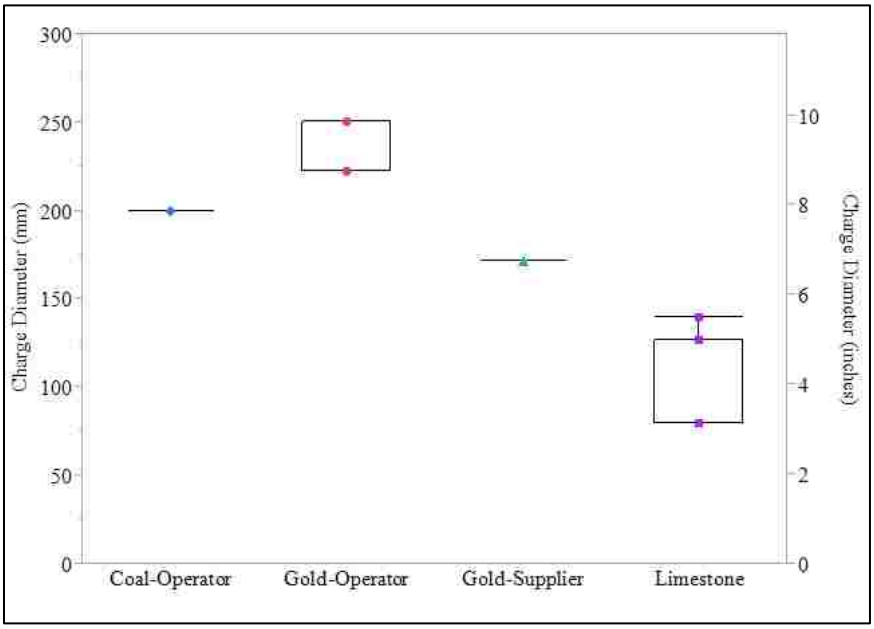

Figure 4.5. Charge (hole) diameter by source with box-and-whisker plot.

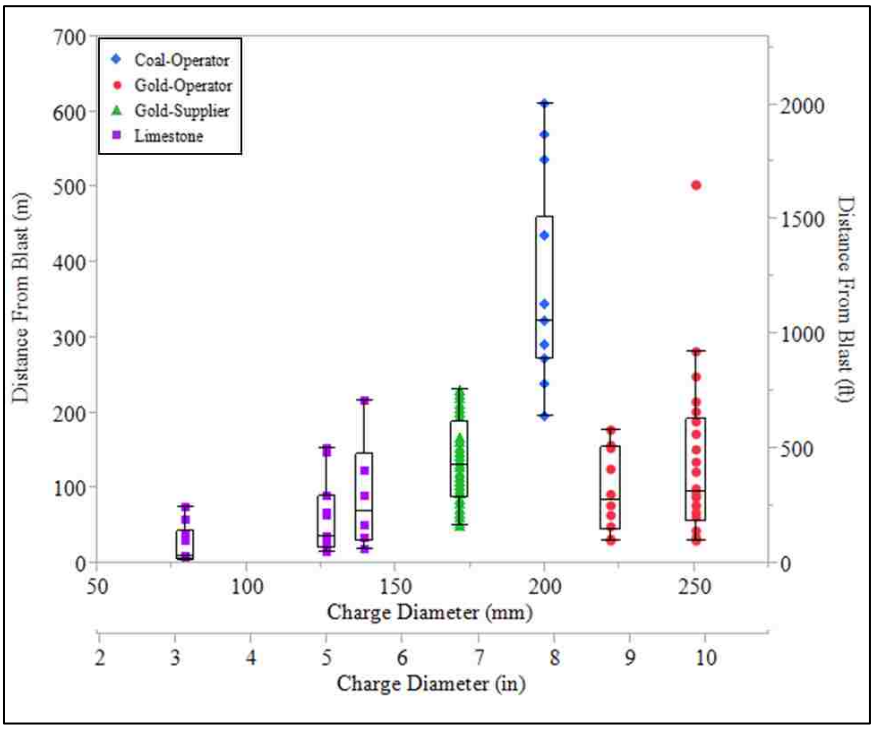

Figure 4.6. Distance from charge to monitoring point by charge diameter with box-and-whisker plots.

4.3.6. Charge Length. The charge length is a function of hole depth and stemming length. In the case of the gold mine-operator tests, it was also a function of the length of a decking plug used at the bottom of the blasthole. This plug left a 1.1 m (3.5 ft) gap of air at the bottom of the blast hole, in order to protect the bench floor and decrease explosive consumption. The air deck length was only used to calculate charge length and weight. This additional variable was not used with any of the other signature hole test sources and therefore was not included in the regression analysis. Figure 4.7 illustrates the charge length values by source and distance. The figure shows that the limestone quarry and gold-operator test data were produced with similar charge lengths at the lower range of represented charge lengths, and the coal-operator and gold-supplier represent the higher range of charge length values.

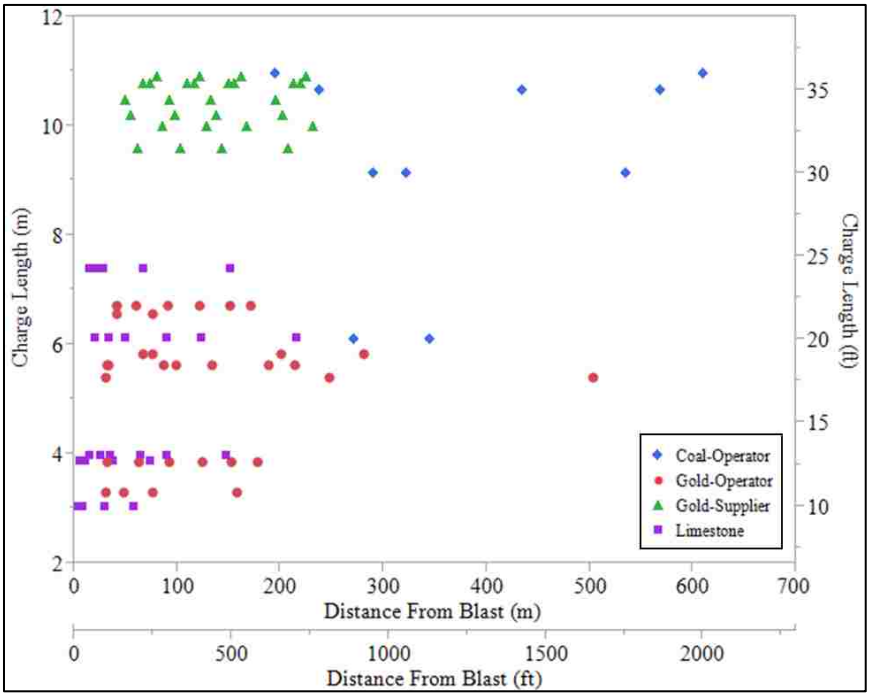

Figure 4.7. Charge length by distance from the charge to the monitoring point. Box-and-whisker plots not used due to wide range of hole depth values.

4.3.7. Hole Depth. The hole depths represented by the signature hole dataset are indicative of the working face heights at each site. Figure 4.8 gives the hole depth versus monitoring distance values for each data source. The hole depth was not used in the regression analyses since it is accounted for by charge length and stemming length.

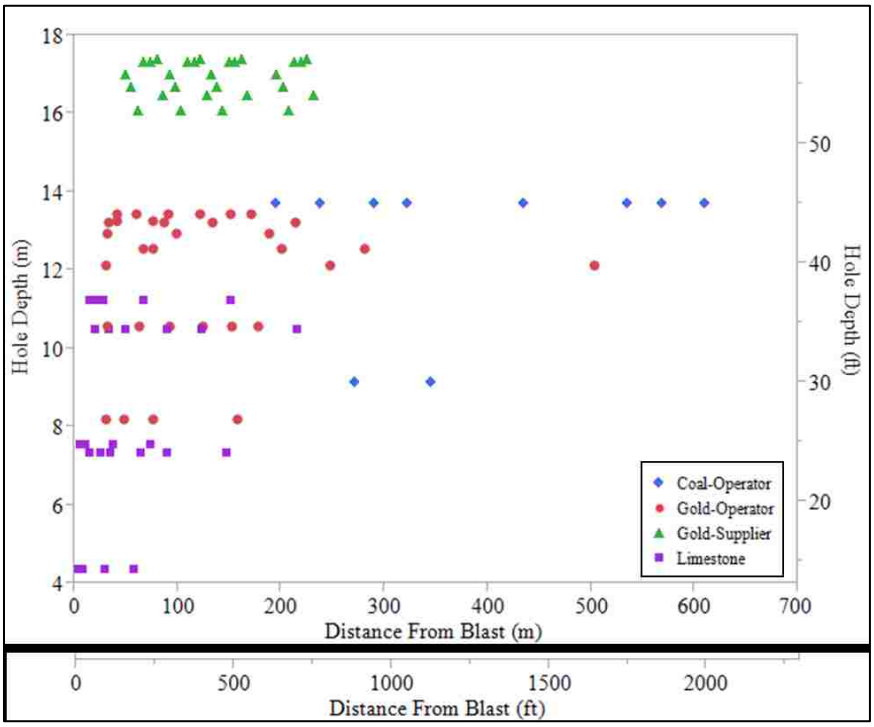

Figure 4.8. Hole depth by distance from the charge to the monitoring point. Box-and-whisker plots not used due to wide range of hole depth values.

4.3.8. Stemming Length. Stemming length is typically a function of hole diameter, which means it is also related to the working face height. The stemming length to diameter ratio (m/m or ft/ft) ranged from 14:1 to 46:1 with an average value of 29:1. Other than the coal-operator data, the signature hole data were produced by fully confined shots; therefore, the stemming length is indicative of the level of confinement of

the charge for the other three datasets. Figure 4.9 illustrates the stemming length by source. The gold-supplier tests have a constant stemming length, while the other three sources have multiple stemming length values.

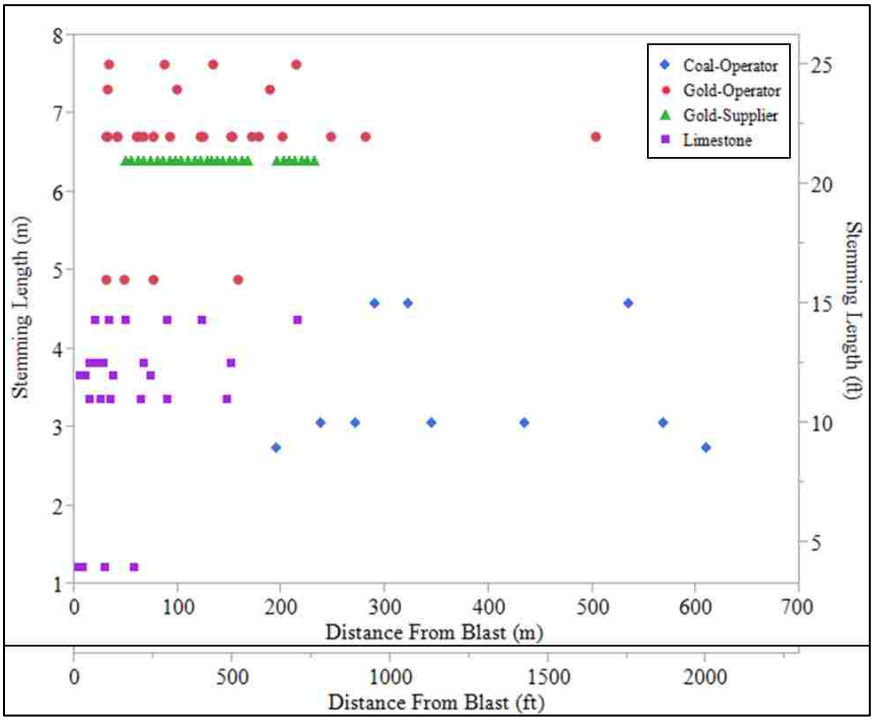

Figure 4.9. Stemming length by distance from the charge to the monitoring point. Box-and-whisker plots not used due to wide range of hole depth values.

4.3.9. Explosive Density. The explosive density ranges from 0.8 g/cc for ANFO to 1.34 g/cc for a 60/40 ANFO/emulsion blend. These are theoretical densities, as the in-hole densities were not measured during any of the tests. There are various other blends and straight emulsion explosives that are also represented by the signature hole dataset (Figure 4.10). The limestone quarry data have a constant charge density, and the gold-

supplier tests have a small variance in density. The coal-operator data and gold-operator data have the widest range of charge densities.

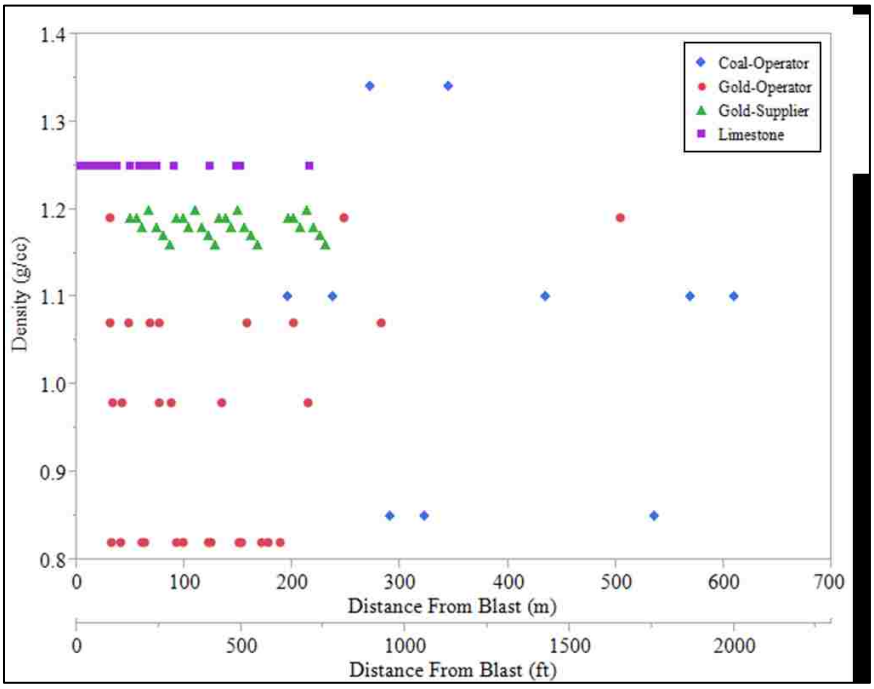

Figure 4.10. Charge density by distance from the charge to the monitoring point. Box-and-whisker plots not used due to wide range of hole depth values.

A value such as the absolute weight strength (cal/g) would have been preferred to indicate available explosive energy. However, specific explosive performance characteristics were not available for each test; therefore, the explosive characteristic chosen for use in the signature hole dataset regression analysis was the explosive density. Explosive density correlates well with theoretical bulk strength (cal/cc), as illustrated by Figure 4.11. Therefore, the use of explosive density to approximate available explosive energy per unit weight is appropriate.

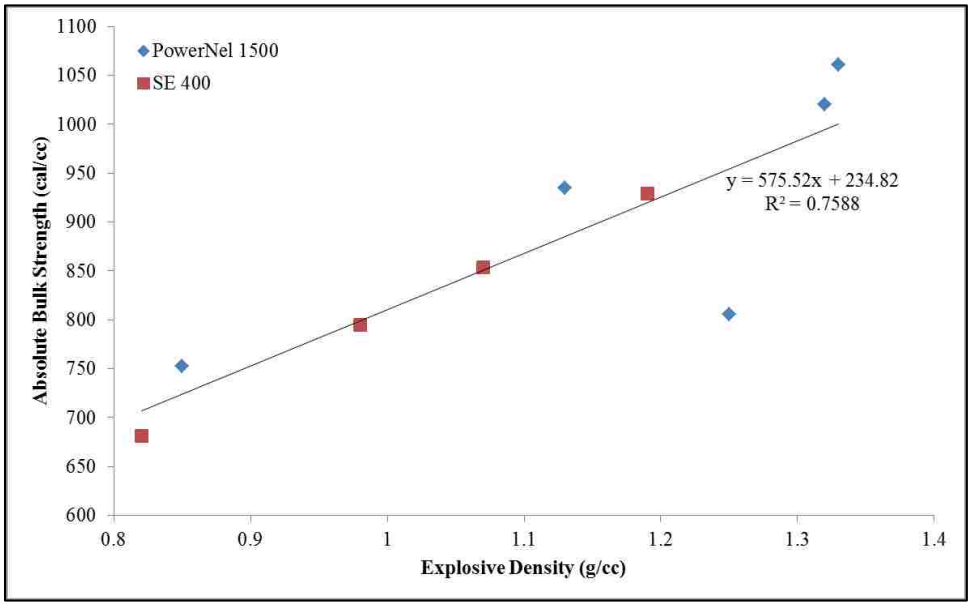

Figure 4.11. Absolute bulk strength/explosive density relationship for SE 400 Series used in the gold-operator tests and PowerNel 1500 blends used in the coal-operator tests and limestone quarry tests (regression line generated using all data points).

4.4. STATISTICAL EVALUATION

This section details the process and results of the multiple regression analysis. Multiple regression analysis is used to evaluate the relative effect of the signature hole test variables on the three important features of a blast vibration: amplitude, frequency, and duration. The amplitude, frequency, and duration of the seed waveforms are evaluated separately to identify if there are any statistically significant effects of charge geometry on vibration attenuation. The multiple regression process is described in Section 4.4.1.3.

4.4.1. Amplitude. The first of the three features evaluated with the multiple regression analysis is the peak vibration amplitude. For this study, the relative effect of the variables on the amplitude is assessed using radial peak particle velocity amplitude values. As discussed in the literature review, the blasting industry primarily focuses on

particle velocity values as opposed to the acceleration or displacement values, and the radial component was chosen since it is the predominant component in the near-field. However, if required, this analysis could be repeated using any of the other two component waveforms or the vector sum waveform.

This section discusses weaknesses of the square root scaled distance (SRSD) versus peak particle velocity (PPV) plot, which is the method currently used by the blasting industry for evaluating vibration amplitudes. It then describes the multiple regression process used to evaluate the signature hole dataset and discusses the results of the regression process.

4.4.1.1. SRSD versus PPV plot. A typical blast data analysis includes a plot of square root scaled distance against peak particle velocity (Figure 4.12). The scaled distance versus PPV relationship is typically plotted on a log-log chart and includes a power-type trendline of the form shown in Equation 6. It can also include a 95% confidence interval plot of the trendline (dashed lines in Figure 4.12). In this case, the power regression equation produced for the SRSD versus radial PPV component is:

$$PPV\ \left[\frac{mm}{s}\right] = 329.89 * \left(SRSD\ \left[\frac{m}{kg^{\frac{1}{2}}}\right]\right)^{-1.531} \tag{24}$$

$$PPV\ \left[\frac{in}{s}\right] = 43.746 * \left(SRSD\ \left[\frac{ft}{lb^{\frac{1}{2}}}\right]\right)^{-1.531} \tag{25}$$

The regression process also calculates a coefficient of determination (R^2), which indicates how well the data fit the model. An adjusted R^2 ($\overline{R}^2$) can also be calculated. The adjusted R^2 value is used in this study because it accounts for spurious increases in the R^2 value by adjusting for the number of predictors. For the plot shown in Figure 4.12, the $\overline{R}^2$ value is 0.80.

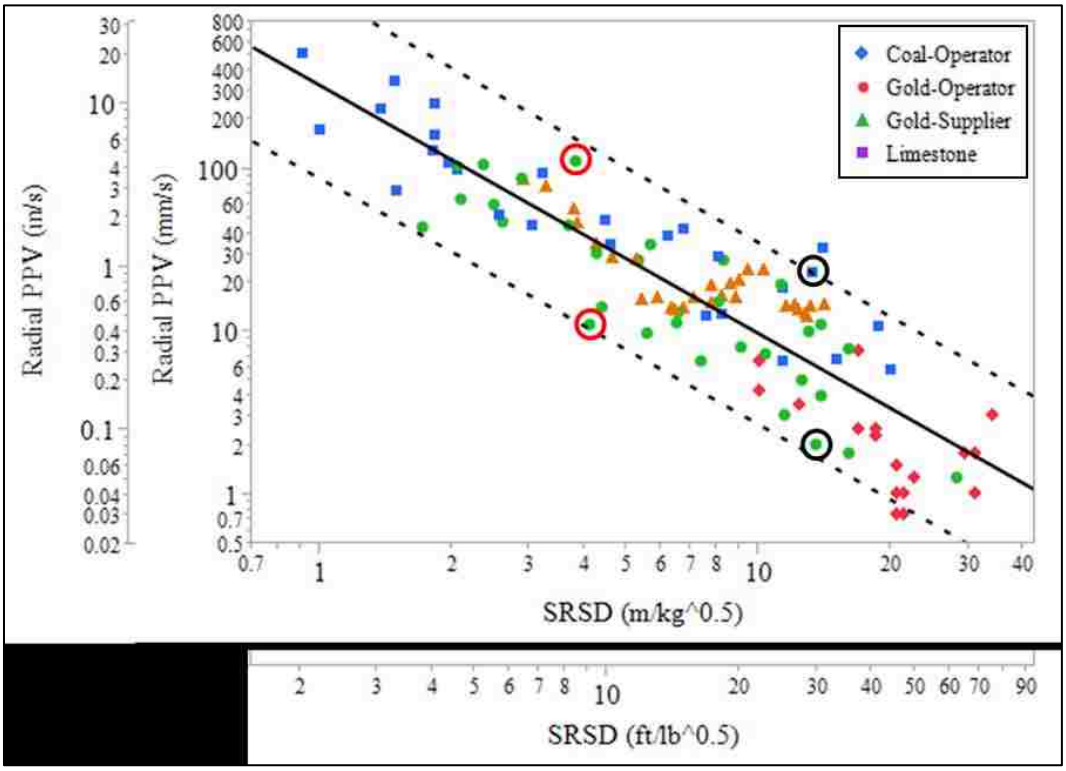

Figure 4.12. Regression plot of signature hole dataset with SRSD versus radial PPV.

Notice the high variability in the data. There is decent correlation between the scaled distance and the PPV; however, due to the nature of the power-type trendline and log-log graph, the range of PPV values within the 95% confidence interval varies at different scaled distances. For instance, the confidence interval is relatively small between the two black circled points at a SRSD of approximately 13.6 m/kg$^{1/2}$ (30 ft/lb$^{1/2}$) with a range from 2 to 23 millimeters per second (0.08 to 0.91 inches per second). In contrast, the confidence interval is relatively large between the two red circled points at a SRSD of approximately 4.5 m/kg$^{1/2}$ (10 ft/lb$^{1/2}$) with a range from 10 to 112 millimeters per second (0.40 to 4.40 inches per second). There is a major difference in the range of PPV values that are expected at each scaled distance. The wide confidence interval is especially significant at small scaled distances. Therefore, the predictive

equation (Equations 24 and 25) is much less precise at small scaled distances in the nonlinear vibration attenuation range.

The issues with the predictive equation become evident when the relationship is plotted with linear axis scaling (Figure 4.13). Linear axis scaling shows that peak particle velocity attenuation is essentially linear at scaled distances greater than 13.5 m/kg$^{1/2}$ (30 ft/lb$^{1/2}$). Therefore, at scaled distances greater than 13.5 m/kg$^{1/2}$ (30 ft/lb$^{1/2}$), the power-relationship represents the data well, but the regression could just be plotted with a linear equation and still have similar adjusted R-squared value.

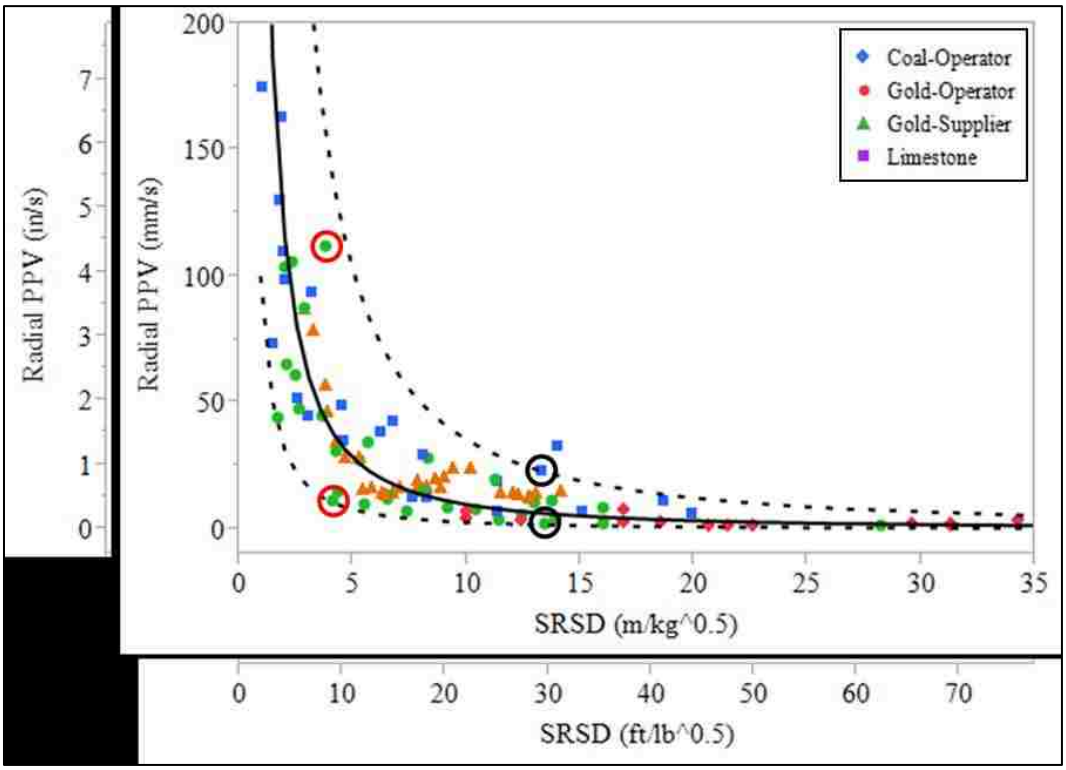

Figure 4.13. SRSD versus Radial PPV with linear axis scaling.

As the scaled distance becomes smaller, the vibration behaves nonlinearly. This is especially true as the scaled distance becomes less than 4.5 m/kg$^{1/2}$ (10 ft/lb$^{1/2}$). Figure 4.13 illustrates a major issue with the power-relationship when the vibration attenuation is nonlinear at small scaled distances. As it is typically used in the blasting industry, the regression line is used to predict PPV values to ensure the PPV of a blast vibration does not have a chance of exceeding a maximum allowable limit. As the power trend approaches zero scaled distance, extremely minor changes in scaled distance result in extremely major ranges for the predicted PPV values. For example, the red circles show how great the confidence interval is for vibrations as scaled distance is reduced to approximately 4.5 m/kg$^{1/2}$ (10 ft/lb$^{1/2}$). This is a telling example of how little the regression of scaled distance versus particle velocity can be trusted as the distances become small. Small scaled distances especially become an issue with construction blasting, which frequently occurs near structures, or mine production blasting where highwall stability is a concern.

The above example shows that the SRSD versus PPV plots are not optimum for studying the influence of individual variables on vibration attenuation, especially at near-field distances. The variability of the method is too great at small scaled distances. A preferable method of evaluating the signature hole dataset is using multiple regression analysis, which can be used to assess the relative effect of each variable and identify only those variables that have a statistically significant effect on the blast vibration.

4.4.1.2. Qualitative evaluation. The first obstacle of this dataset is comparing signature hole data from varying sites and test parameters. The primary variable that changes from site to site is geology. Therefore, the data may be comparable between

multiple sites if the effect of geology can be normalized or the data that is affected by geology can be removed from the analysis. The second option, if viable, requires the impact of geology to be statistically immaterial to the remaining data.

The following procedure was developed with the second option in mind to identify any data points that may be statistically unaffected by geology. First, the driving factor of vibration attenuation is the distance of the monitoring point from the charge. The distance is a continuous variable; therefore, it is impossible to compare multiple data at identical distances from the charge. However, if the distances are arbitrarily rounded to the nearest 30.5 m (100 ft), the distances become discrete and data can be compared at each discrete value.

With the discrete values substituted as the monitoring distance, any influencing variable can be plotted against any response variable at each discrete distance. The precision of each relationship is a function of the variance of the recorded distance from the rounded distance; however, the rounded distance analysis is sufficient to see patterns in the data.

Figure 4.14 shows the correlation between charge diameter and radial PPV by distance rounded to the nearest 30.5 m (100 ft). The same analysis can be done by rounding the distance to a different value, such as every 10 m (32.1 ft); however, the small number of data points at each rounded 10 m distance does not give a high enough confidence in the analysis. Note that the distances greater than 198 meters (650 feet) were combined into one plot due to the lack of data points at greater monitoring distances.

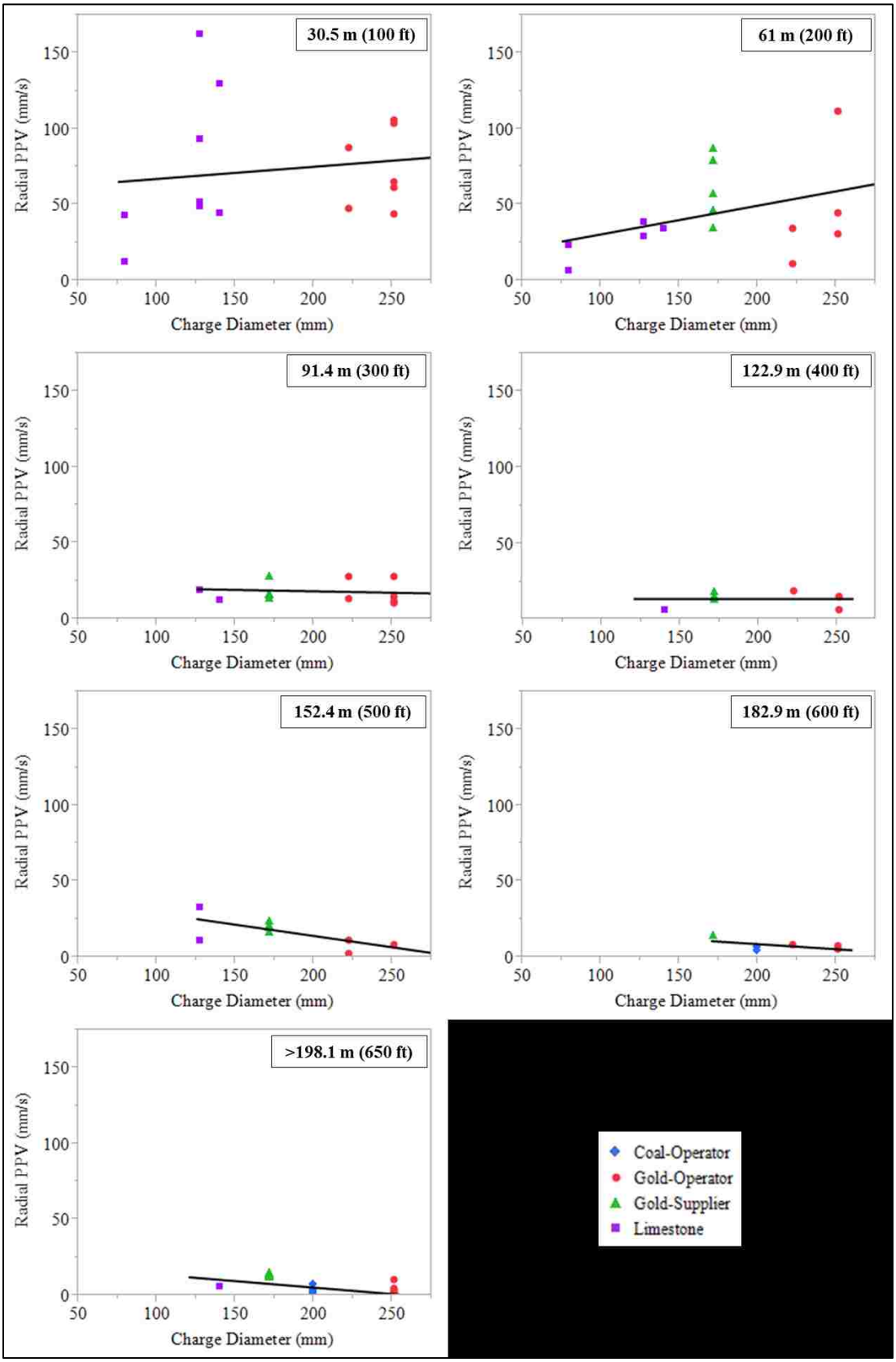

Figure 4.14. Charge diameter versus radial PPV by rounded distance.

Note that Figure 4.14 is for qualitative analysis only; therefore, the linear regression lines are provided to aid in the analysis but the coefficient of determination is not included. Figure 4.14 illustrates a possible trend in the near field holes at distances less than 76 m (250 ft) where the larger charge diameters produce higher PPVs than the smaller charge diameters. However, at distances between 76 m and 137 m (250 ft and 450 ft) there is no correlation. At distances beyond 137 m (450 ft), the correlation reverses and the smaller charge diameters have higher particle velocity than the larger charge diameters. The image shows that the high PPV amplitudes in the near-field may not be as affected by geology as the PPV amplitudes are in the far-field. It is also interesting that 76 m (250 ft) is also the distance where the vibrations begin to behave linearly as opposed to the nonlinear behavior exhibited near the blasthole (Figure 4.15). Note that the coal-operator data are nonexistent at rounded distances of 182.9 m (600 ft) or less. Therefore, the near-field analyses are unaffected by the unconfined charges of the coal-operator tests.

The relationship between most of the remaining variables and the PPV within 76 m (250 ft) of the charge is similar to the relationship between the charge diameter and the PPV: as charge weight, charge diameter, charge length, and stemming length increase, the PPV increases (Appendix D). This relationship is expected for two reasons: (a) charge weight, which is related to charge diameter and charge length, is proportional to the vibration amplitude and (b) longer stemming length provides confinement, which directs more of the explosive energy to vibration energy. The density does not have a noticeable relationship with vibration amplitude within 76 m (250 ft).

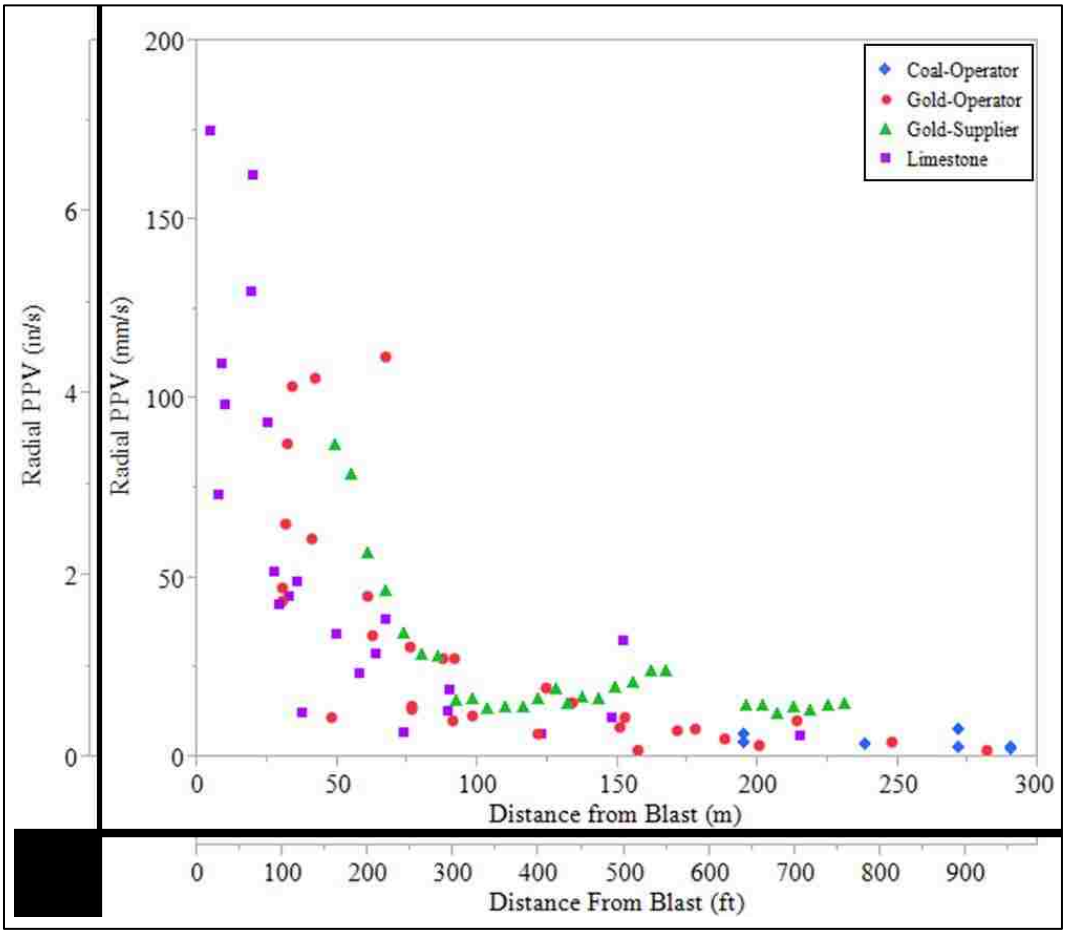

Figure 4.15. Radial PPV plotted against distance between the charge and monitoring point.

At distances beyond 76 m (250 ft), there does not appear to be a relationship between any of the variables and PPV. This could be due to the linear amplitude attenuation at these distances and increasing effect of geology as the distance increases.

From the qualitative analysis, it appears that the non-geology variables have a noticeable effect on vibration amplitudes in the near-field distances, which shall be defined as distances less than 76 m (250 ft), or the distance at which the vibration amplitude attenuation begins to behave linearly (Figure 4.15). This value agrees with

Siskind et al. (1989), who identified the distance where geology begins to effect vibrations as 91.4 m (300 ft).

The data appears to reverse the correlation at the rounded distance of 91.4 m (300 ft), which supports the assumption that the geology begins to have an effect (or more than a minor effect) on vibration attenuation at monitoring distances greater than 76 meters (250 feet). Therefore, all tests with monitoring distances greater than 76 meters are assumed to be affected by geology, and further study on the relationship of the variables to the radial PPV is limited to tests that were monitored at 76 meters or less from the charge. This distance is not significant to most mining operations; however, mining operations concerned for highwall stability, mining operations near private structures, and construction blasting operations near private structures may find this knowledge useful.

4.4.1.3. Multiple regression of amplitude. Multiple regression was used to model the data recorded within 76 m (250 ft) of the charge and determine which factors had the strongest effect on the peak particle velocity data. Thirty-eight data points were recorded within that distance. Those 38 data points are considered to be affected solely by monitoring distance and charge specific variables. The multiple regression model for prediction of PPV included the following parameters as variables:

- Distance from Blast: The original distance measurement from the charge to the monitoring point is used as opposed to the rounded distance. A logarithm transformation was applied to the distance to account for the nonlinearity of the relationship between the distance and the PPV.

- Charge Weight: Charge weight is equal to the truck-weighed charge weight if available. Otherwise, charge weight is the theoretical charge weight calculated from charge geometry and explosive density.
- Charge Diameter: The diameter of the drill bit used to drill the blasthole.
- Charge Cross-Sectional Area: Charge cross-sectional area is dependent on the charge diameter; it is proportional to the square of the charge diameter. The charge cross-sectional area is included in order to see if the charge cross-sectional area has better correlation with the vibration data than the charge diameter; however, the multiple regression analyses should show the dependence of the cross-sectional area on diameter. Typically, the charge diameter is a primary means used to describe a charge in the blasting industry. In spite of this, the cross-sectional area of the charge may be the more important descriptor of the charge because the cross-sectional area of the charge detonates simultaneously while the length of the charge detonates over a period of time. This is one reason why the charge geometry variables may have an effect on vibration attenuation.
- Stemming Length: Stemming length is the length of inert material placed in the blasthole above the charge to provide confinement to the explosive. For this dataset, it is assumed that all stemming material provides identical confinement.
- Charge Length: Charge length is the length of the explosive charge, which is calculated by subtracting stemming length from hole depth. In cases where truck measured explosive weight is used, the charge length is

back-calculated using charge weight and the other charge geometry variables.

- Density: Density is used to describe the type of explosive used in each test.

The hole depth was not included as a variable since charge length and stemming length account for hole depth and are assumed to have a greater effect, if any, than hole depth.

The multiple regression process used in this study was used to systematically remove variables that had little statistical influence on the regression model. To this end, the statistics software, JMP® 11 Statistical Discovery Software from SAS was used to analyze the input data and output an initial model that included all the input variables. The software can calculate the p-value for each of the variables, which is used to quantify the statistical significance of each variable to the fit of the regression model. Lower p-values equate to more statistically significant results than higher p-values. Therefore, the variable with the highest p-value can be removed from the model, and the model can be recomputed. This process is repeated until the adjusted R-squared value for the model begins to significantly decrease, meaning the model is becoming significantly less accurate. At that point, the remaining variables are considered to have a statistically significant effect on the fit of the model. In summary, the final regression model gives a similar $\bar{R}^2$ value as that given by the original model but only consists of the statistically significant variables.

The first run of the regression model using the parameters listed above gives a $\bar{R}^2$ of 0.60 using the 38 near-field observations (Table 4.1 and Appendix E). The variable

with the least effect on the model is the charge length; therefore, the charge length was removed from the model prior to the second run. Each successive run was completed in a similar manner until the final run, which produced only statistically significant p-values. The $\bar{R}^2$ value of the final tests, Test Run V, is 0.59. Model V has a similar $\bar{R}^2$ value to Model I but only includes the significant variables: the log of the distance from the charge, the charge weight, and the stemming length.

Table 4.1. Multiple regression runs and results for PPV (near-field).

Test Run	**Variable Removed**	**R^2 Adj. after Regenerating Model**
I	N/A	0.60
II	Charge Length (m)	0.60
III	Explosive Density (g/cc)	0.59
IV	Charge Cross-Sectional Area (sq. m)	0.58
V	Charge Diameter (mm)	0.59

Remaining Variable: Log (Distance from the Blast (m))
Charge Weight (kg), Stemming Length (m)

The final model correlates well with the scaled distance equation; therefore, the final model supports the weighting of distance with the charge weight, as is done in the scaled distance equation. Stemming, the least significant of the three significant variables, is a factor that indicates the confinement of the blast for the fully confined charges in the near-field dataset. Therefore, stemming is relatable to the amount of energy that manifests as seismic vibrations. Increased stemming equates to higher PPV, whereas less stemming equates to lower PPV. It is apparent that the geometric factors of the explosive charge do not statistically influence the PPV.

Note that the multiple regression model was reevaluated with geology as a factor, and geology was the first variable removed, further indicating that the geology was statistically insignificant to this dataset in the near-field.

4.4.1.4. Charge weight per unit length. A comparison of the fit of data using total charge weight versus PPV and charge weight per unit length versus PPV shows that the total charge weight has better correlation with the PPV than the charge weight per unit length. For instance, the $\bar{R}^2$ between charge weight and PPV is 0.38 at 200 rounded feet, while the $\bar{R}^2$ between charge weight per unit length and PPV at the same rounded distance is only 0.13.

It is understandable that the charge weight has a better correlation than the charge weight per unit length. For example, assume an explosive column detonates at a velocity of 4,600 meters per second (15,000 feet per second). For a 9 m (30 ft) powder column, the full charge will detonate in 2 milliseconds. The signature hole dataset has a principal frequency range of 4.7 Hz to 78.7 Hz. This equates to peak particle velocity periods that range from 13 milliseconds to 213 milliseconds. When comparing the detonation velocity to the period, the entire explosive column will detonate in 1% to 15% of the time of one cycle of the peak particle velocity. Thus, the entire explosive column contributes energy to the PPV, as opposed to only a fraction of the explosive column. At higher frequencies, where the period reaches unity with the detonation time, the charge per unit length will most likely have more of a noticeable effect. The effect of the charge per unit length most likely becomes noticeable close enough to the blasthole that the ground undergoes shock, which is outside of the scope of this document.

4.4.1.5. Summary. This section highlights a number of drawbacks with the scaled distance versus PPV equation, including the high variability of data and the imprecise values produced by the scaled distance equation in the non-linear attenuation range. The evaluation showed that geology appears to have a limited effect on vibration attenuation during non-linear vibration attenuation.

The qualitative evaluation of the data demonstrated that the geology has little or no effect on the PPV amplitude within approximately 76 meters (250 feet) of the blasthole. Therefore, the data within 76 meters was assessed by assuming the only variables affecting vibration attenuation within that distance are the distance from the charge to the monitoring point and the charge-specific factors.

The multiple regression analysis showed that the variables that have a statistically significant influence on vibration amplitude within 76 meters of the blasthole are the distance from the charge, the charge weight, and the stemming length. The analysis also showed that the SRSD versus PPV plots should only be used on data produced from charges with similar charge confinement. The easiest way to improve upon the use of the SRSD versus PPV plots is to plot results from charges with varying confinements separately. However, plotting SRSD versus PPV at various confinements does not account for the lack of accuracy of the scaled distance model in the near-field. This issue shows that the SRSD versus PPV method requires improvement.

Finally, regression analysis also showed that the charge weight per unit length does not affect elastic vibrations. This point contradicts studies that predict vibration amplitude using charge weight per unit length as opposed to the total charge weight.

4.4.2. Frequency. Frequency, the second feature of a blast vibration, can also be evaluated using multiple regression analysis. For this study, the same methodology used in the previous section is applied to both principal frequency and dominant frequency. As discussed in the literature review, the principal frequency is the frequency associated with the peak amplitude of the vibration and is calculated using the half cycle estimate, and the dominant frequency is the most repeated frequency in a vibration and is found using a FFT analysis.

The principal frequency and dominant frequency are important to blast vibration analysis. The principal frequency dictates the length of time a cycle of the blast vibration impacts the monitoring point. Therefore, the principal frequency of a particle velocity waveform dictates the acceleration and displacement of that cycle. The dominant frequency, which has been assumed to be indicative of the harmonic structural frequency of rock (Crum et al., 1992; Yang et al., 2009), could affect structures if it is near the structural resonant frequency.

The principal frequency was plotted against the dominant frequency for each seed waveform in the signature hole dataset to identify any relationship between the two frequencies (Figure 4.16). The principal frequency and dominant frequency for each value correlate relatively linearly through all ranges of frequency. Therefore, higher principal frequencies typically equate to higher dominant frequencies.

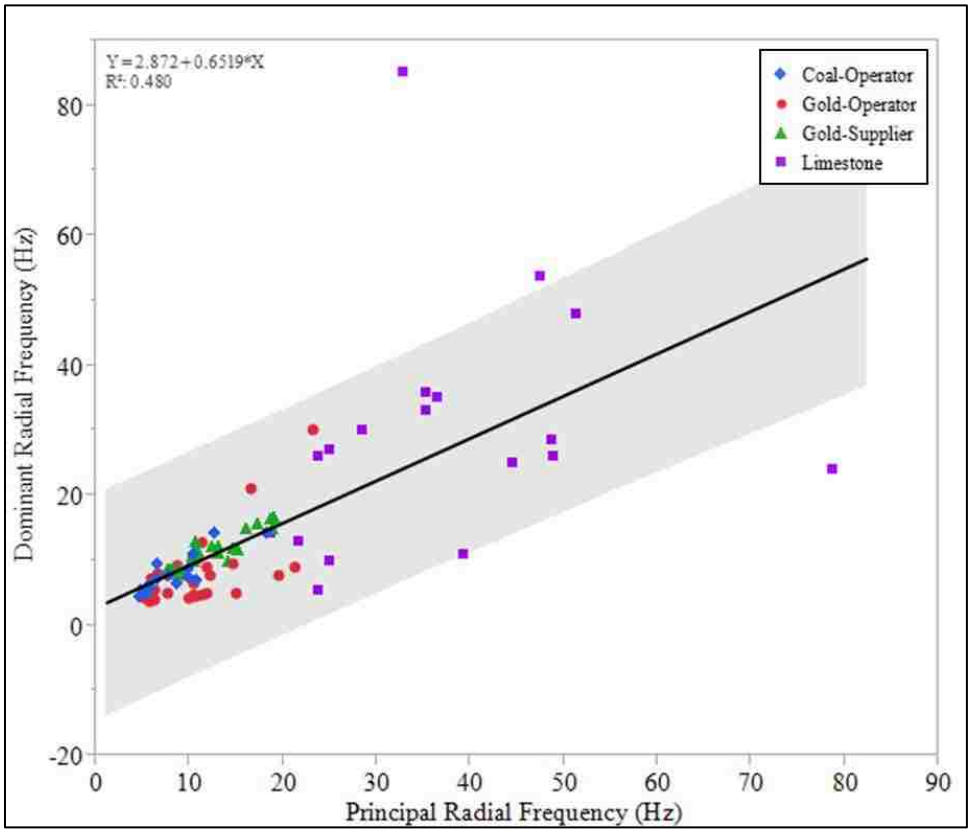

Figure 4.16. Principal frequency plotted against dominant frequency with regression and 95% confidence interval shown.

4.4.2.1. SRSD versus frequency plot. The square root scaled distance equation can be plotted against the frequency values in a similar way that it can be plotted against the PPV. However, theoretically, the frequency must also be scaled by the charge weight (Ambraseys & Hendron, 1968). Ambraseys and Hendron (1968) show from Buckingham's π theorem, that the frequency should be scaled by the cube root of the charge weight. Figure 4.17 gives the SRSD versus scaled principal frequency for the signature hole dataset using square root scaling. The plot includes 99 data points. There is no discernable relationship between the scaled distance and the scaled principal

frequency except for somewhat displaying groupings by source. Therefore, the scaled distance plot is not useful.

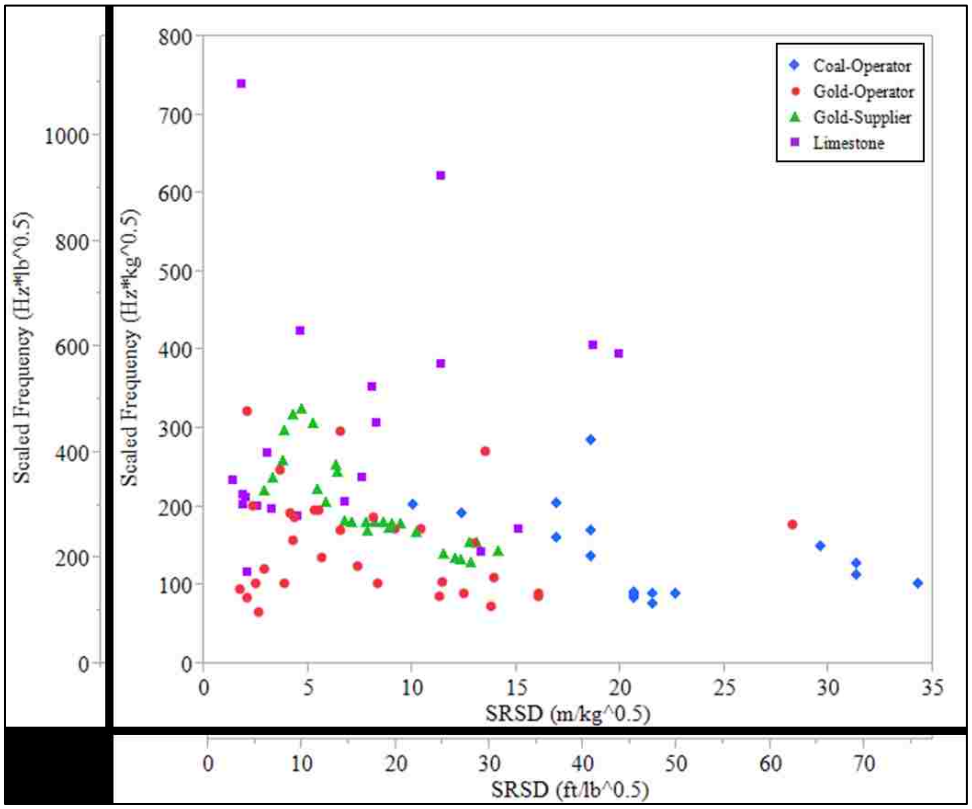

Figure 4.17. Principal frequency plotted against square root scaled distance (99 data points).

4.4.2.2. Qualitative evaluation. Each variable can be plotted against the principal frequency at discrete rounded distances, as was done for PPV in the previous section. For example, the relationship between charge diameter and the principal frequency at distances rounded to the nearest 30.5 m (100 ft) is shown in Figure 4.18.

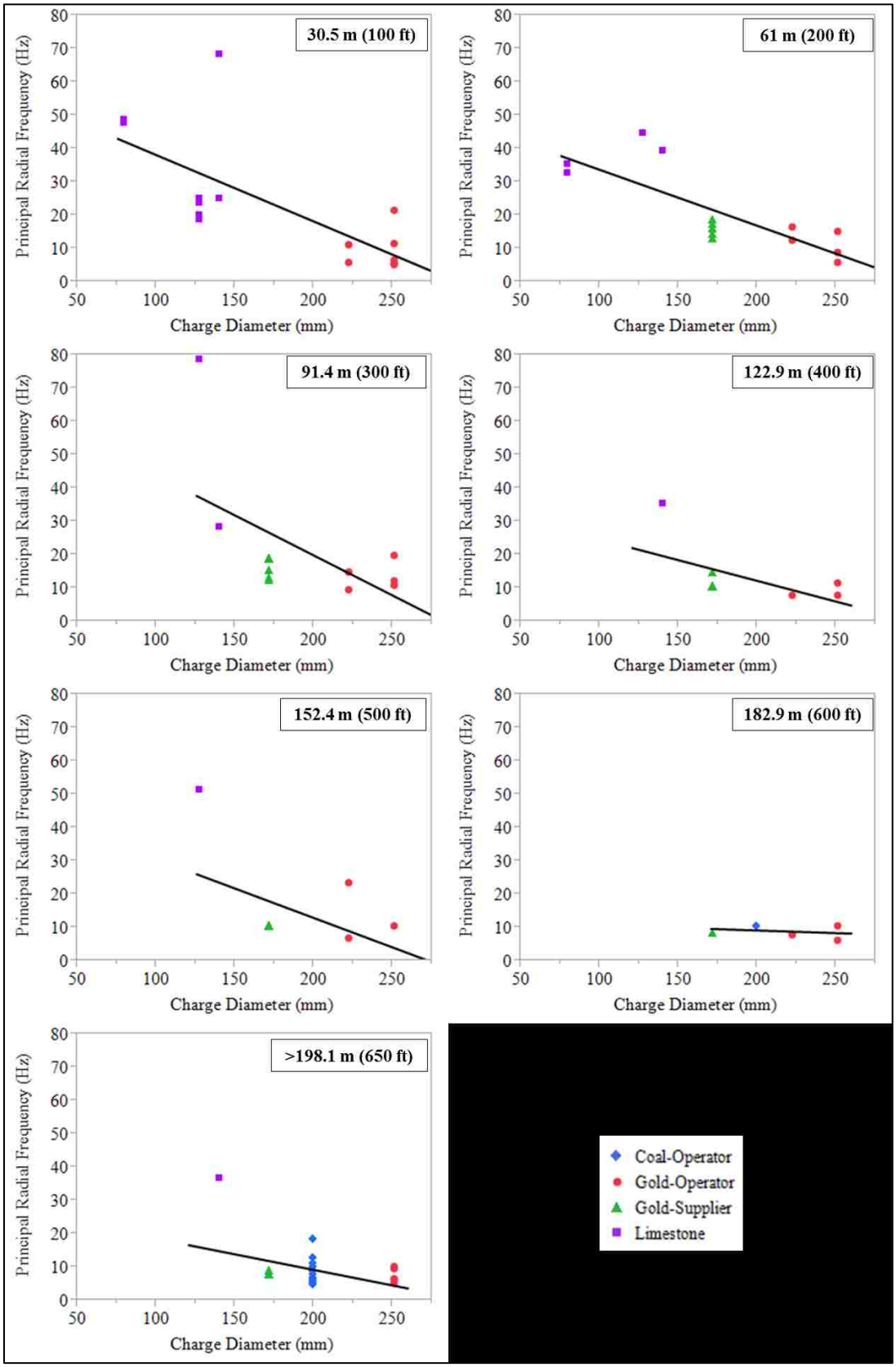

Figure 4.18. Charge diameter versus principal frequency by rounded distance.

Figure 4.18 shows that the charge diameter appears to have a relatively consistent effect on frequency regardless of distance: larger charge diameters, or charge cross-sectional areas, create lower principal frequencies. This could be due to the cross-sectional area of the charge controlling the energy release of the explosive during the detonation process, thereby controlling the output frequency. However, the geology and charge diameter are related in the signature hole dataset; therefore, this relationship could be more of a function of geology than charge diameter.

Figures similar to Figure 4.18 were also generated to compare the principal frequency against each of the remaining variables (Appendix D). The strongest relationship is between stemming and frequency, where increased stemming is equivalent to lower frequencies. Charge weight and density also have a similar relationship with frequency; however, their relationship is not as strong. The charge length does not have a discernable relationship with principal frequency. These same figures were plotted to evaluate the relationship between each variable and the dominant frequency of the waveform (Appendix D). Similar correlations are apparent.

The previous section proposed that geology begins to have a noticeable effect on vibration amplitude attenuation at distances greater than 76 m (250 ft), meaning the effect of the remaining factors begins to be less significant at distances greater than 76 m. Therefore, the effect of the variables on frequency was compared using two regression analyses: one for all data, regardless of monitoring distance, and the second for only data recorded within 76 m of the charge.

4.4.2.3. Multiple regression of frequency. The principal and dominant frequencies of a blast wave may be influenced by any of the variables: geology,

monitoring distance from the blast, charge weight, charge diameter, charge cross-sectional area, charge length, stemming length, or density. Geology was included in the analysis as a nominal variable, meaning the values are applied as sets of indicator columns. This allows the geology to be included in the multiple regression process.

The first regression analysis focused on the principal frequency of the full dataset. The total number of principal frequency observations is 99, which is less than the total number of data points due to a few poor recordings, as discussed in the previous section. The multiple regression iterations followed the same methodology discussed in the last section to produce Table 4.2 (Appendix E). The multiple regression model has a final $\bar{R}^2$ value of 0.64 with only geology as a predictive variable for principal frequency.

Table 4.2. Multiple regression runs and results for principal frequency (entire dataset).

Test Run	**Variable Removed**	**R^2 Adj. after Regenerating Model**
I	N/A	0.66
II	Log (distance from Blast (m))	0.67
III	Charge Cross-Sectional Area (sq. m)	0.67
IV	Charge Diameter (mm)	0.67
V	Stemming Length (m)	0.66
VI	Charge Weight (kg)	0.65
VII	Explosive Density (g/cc)	0.65
VIII	Charge Length (m)	0.64

Remaining Variable: Geology

The multiple regression analysis over the dominant frequency dataset produced Table 4.3 (Appendix E). The total number of observations of dominant frequency is 96. The multiple regression model of the dominant frequency has a final $\bar{R}^2$ value of 0.59

with stemming length, geology and log of distance as statistically significant variables. The stemming length describes the degree of confinement for the fully confined signature holes; therefore, this analysis shows that confinement is a driving factor of dominant frequency. This is most likely due to high confinement causing a greater percentage of explosive energy to be directed into the rock as vibrations, thereby putting more energy into the rock, which increases the period of the cycles of the blast vibration. Geologic factors are known to affect frequencies; therefore, it is not surprising that the regression analysis concluded that geology is also significant. Distance is most likely a significant variable due to the fact that geology has a varying effect on frequency at varying distances.

Table 4.3. Multiple regression runs and results for dominant frequency (entire dataset).

Test Run	Variable Removed	R^2 Adj. after Regenerating Model
I	N/A	0.64
II	Charge Diameter (mm)	0.64
III	Charge Cross-Sectional Area (sq. m)	0.64
IV	Charge Weight (kg)	0.63
V	Charge Length (m)	0.62
VI	Explosive Density (g/cc)	0.59

Remaining Variables: Stemming Length (m), Geology, Log (Distance from Blast (m))

The multiple regression analysis was also conducted on data that were recorded within 76 m (250 ft) of the charge, where the PPV values of the dataset did not appear to be significantly affected by geology (Table 4.4 and Table 4.5). In this case, geology is

simply removed from the regression analysis. The multiple regression analyses included 33 principal frequency and 31 dominant frequency observations within the limiting distance. Although the results are valid, it would be preferable for the sample size to be larger.

Table 4.4. Multiple regression runs and results for principal frequency (near-field).

Test Run	Variable Removed	R^2 Adj. after Regenerating Model
I	N/A	0.46
II	Log (distance from Blast (m))	0.48
III	Stemming Length (m)	0.50
IV	Hole Diameter (mm)	0.51
V	Explosive Density (g/cc)	0.52
VI	Charge Weight (kg)	0.53
VII	Charge Length (m)	0.50

Remaining Variable: Charge Cross-Sectional Area (sq. m.)

Table 4.5. Multiple regression runs and results for dominant frequency (near-field).

Test Run	Variable Removed	R^2 Adj. after Regenerating Model
I	N/A	0.73
II	Charge Cross-Sectional Area (sq. m)	0.74
III	Charge Length (m)	0.72
IV	Charge Diameter (mm)	0.71
V	Charge Weight (kg)	0.71
VI	Explosive Density (g/cc)	0.70

Remaining Variables: Log (Distance from the Blast (m)),
Stemming Length (m)

The results of the multiple regression analysis in the near-field show that the principal frequency is related to the charge cross-sectional area and the dominant frequency is related to the log of the distance from the charge to the monitoring point and the stemming length.

The results of the principal frequency regression analysis highlight one issue with the signature hole dataset: the drillhole diameters and therefore charge diameters and cross-sectional areas are related to the data source and, therefore geology. Figure 4.19 illustrates this relationship. The gold-operator data have the largest charge diameter values, while the limestone quarry data have the lowest charge diameter values. A regression analysis between the geology and the near-field principal frequency shows that the geology/near-field principal frequency relationship has a $\bar{R}^2$ value of 0.53, which is higher than the value produced by the near-field multiple regression analysis without geology (Table 4.4). Most likely, geology is actually the statistically significant variable that affects the near-field principal frequency due to its ability to filter out frequencies from passing blast vibrations. This evaluation requires additional research as there is insufficient evidence to quantitatively determine which of the two variables is significant. However, the model that uses geology is a better predictor; therefore, from this point on, geology is assumed to be the statistically significant variable and charge cross-sectional area is assumed to be insignificant.

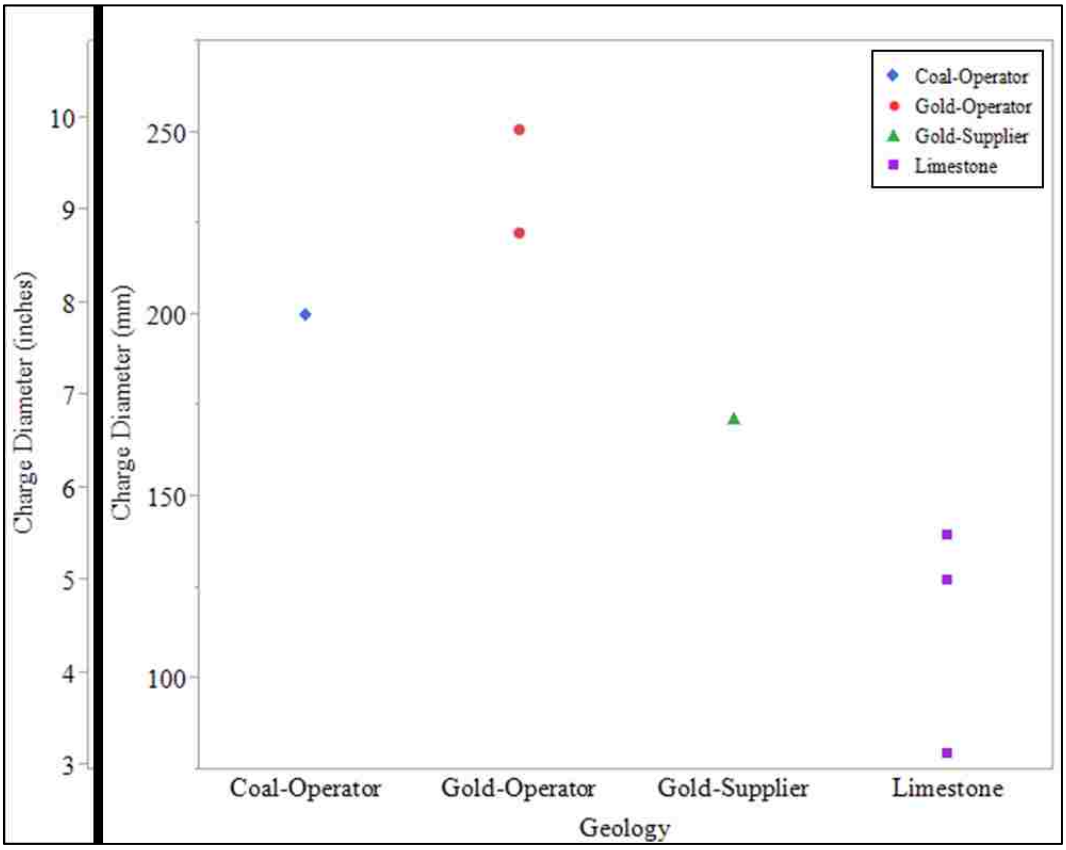

Figure 4.19. Relationship between charge diameter/cross-sectional area and data source/geology.

The dominant frequency is affected by the distance from the charge and the length of stemming. The frequency most likely attenuates noticeably as distance increases during the nonlinear, near-field attenuation phase before the geology begins to affect the frequency. The length of stemming provides confinement, which is proportional to the explosive energy that manifests as vibration energy, as described previously. The near-field model was recalculated using geology as a variable to check the results of original near-field, dominant frequency model. Geology was shown to be an insignificant variable in the near-field model check, which supports the conclusions derived from the near-field, dominant frequency multiple regression model.

4.4.2.4. Summary. In summary, the multiple regression analyses described in this section show that the frequency is statistically affected by the stemming length, geology, and monitoring distance at most standard monitoring distances. In the near-field range, the same variables affect both the principal frequencies and dominant frequencies.

The principal frequency is affected by geology over the full dataset and in the near-field because the geology acts as a filter for the vibrations. The adjusted R-squared value for the near-field principal frequency model is low though; therefore, increasing the size of the principal frequency dataset could produce a better model.

The dominant frequency is affected by stemming length, geology, and distance for the full dataset; however, in the near-field range, the dominant frequencies are only significantly affected by the stemming length and the distance. The vibrations are filtered by the ground, which is why geology is a major variable over the full dataset; however, in the near-field, the ground has not influenced the vibration as much as the distance has, most likely due to the nonlinearity of the vibration attenuation at distances less than 76 m (250 ft). The stemming length affects the dominant frequency due to the amount of confinement it provides the charge during the detonation process. Higher confinements force more explosive energy into the rock which increases the amplitude and duration of each vibration cycle; therefore, increased stemming relates to longer dominant periods or lower dominant frequencies.

4.4.3. Duration. The third feature of blast vibrations that was studied using multiple regression analysis is the blast vibration duration. The duration of each seed waveform was approximated by visual inspection; therefore, there will be some inherent error in the data. Regardless, the multiple regression analysis produces useable results.

4.4.3.1. SRSD versus duration plot. Dimensionless analysis has been not developed for evaluating vibration duration because the duration was not considered a dependent variable of explosion phenomena when the scaled distance equations were developed. However, wave broadening does occur over distance due to geologic influence and timing design for multiple-charge blasts.

If the duration is plotted against the scaled distance, there is some relation, as can be seen in Figure 4.20, which was generated using 98 observations of seed waveform duration.

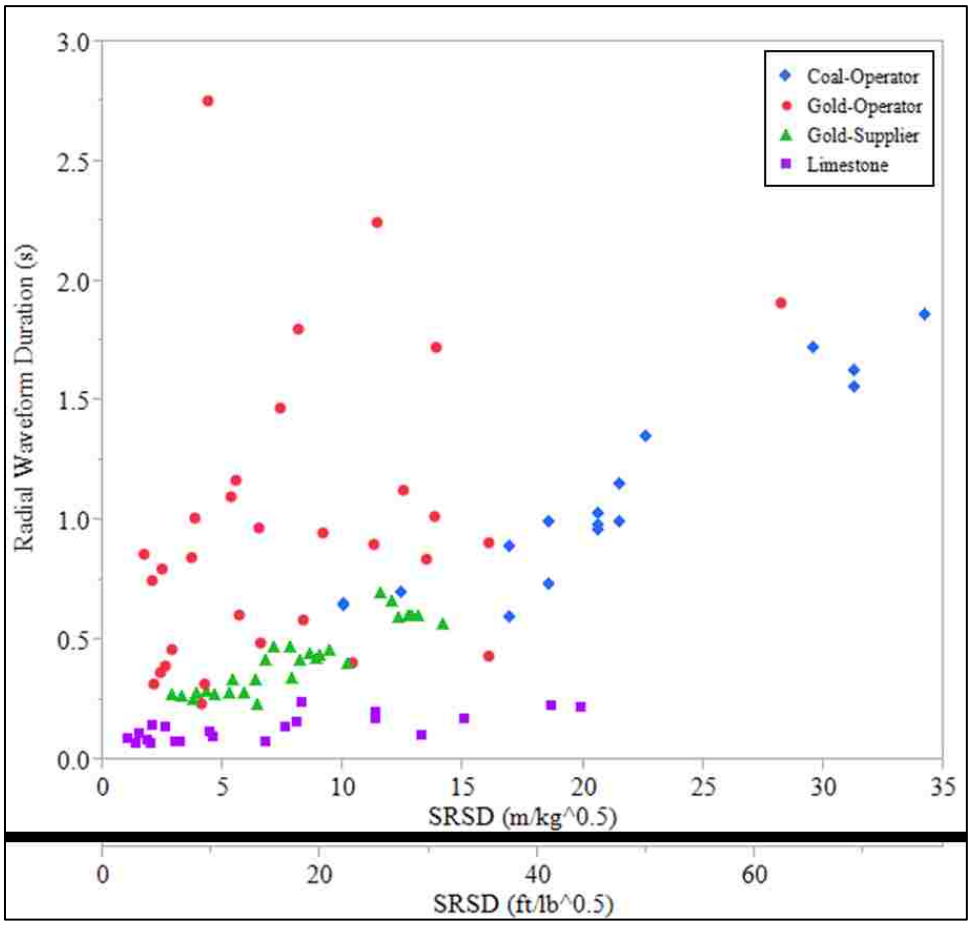

Figure 4.20. SRSD plotted against radial seed waveform duration from the full signature hole dataset.

Figure 4.20 shows a correlation between the scaled distance and the duration. The impact due to geology is readily identified by groupings of data points by source. The limestone tests produce shorter durations than the other tests at equivalent scaled distances, while the gold-operator signature hole tests produced the longest durations at equivalent scaled distances. The gold-supplier and coal-operator tests fell between the limestone and gold-operator tests along a straight trend line. In fact, each of the individual datasets, other than the gold-operator dataset, illustrate a noticeable linear relationship between the scaled distance and the waveform duration.

4.4.3.2. Qualitative evaluation. Each variable was plotted against the waveform duration at discrete rounded distances, as was done in the previous two sections (Appendix D). The relationship between the charge diameter and the radial waveform duration is shown in Figure 4.21 as an example.

The charge diameter appears to correlate for the most part with the waveform duration for the rounded distances from 30.5 m (100 ft) to 152.4 m (500 ft). At these distances, the larger charge diameters equate to longer waveform duration. The last two images show less correlation, due to the lack of data or an outlier at 182.9 m (600 ft) and the large range of distances pictured in the plot for data monitored at distances >198.1 m (650 ft).

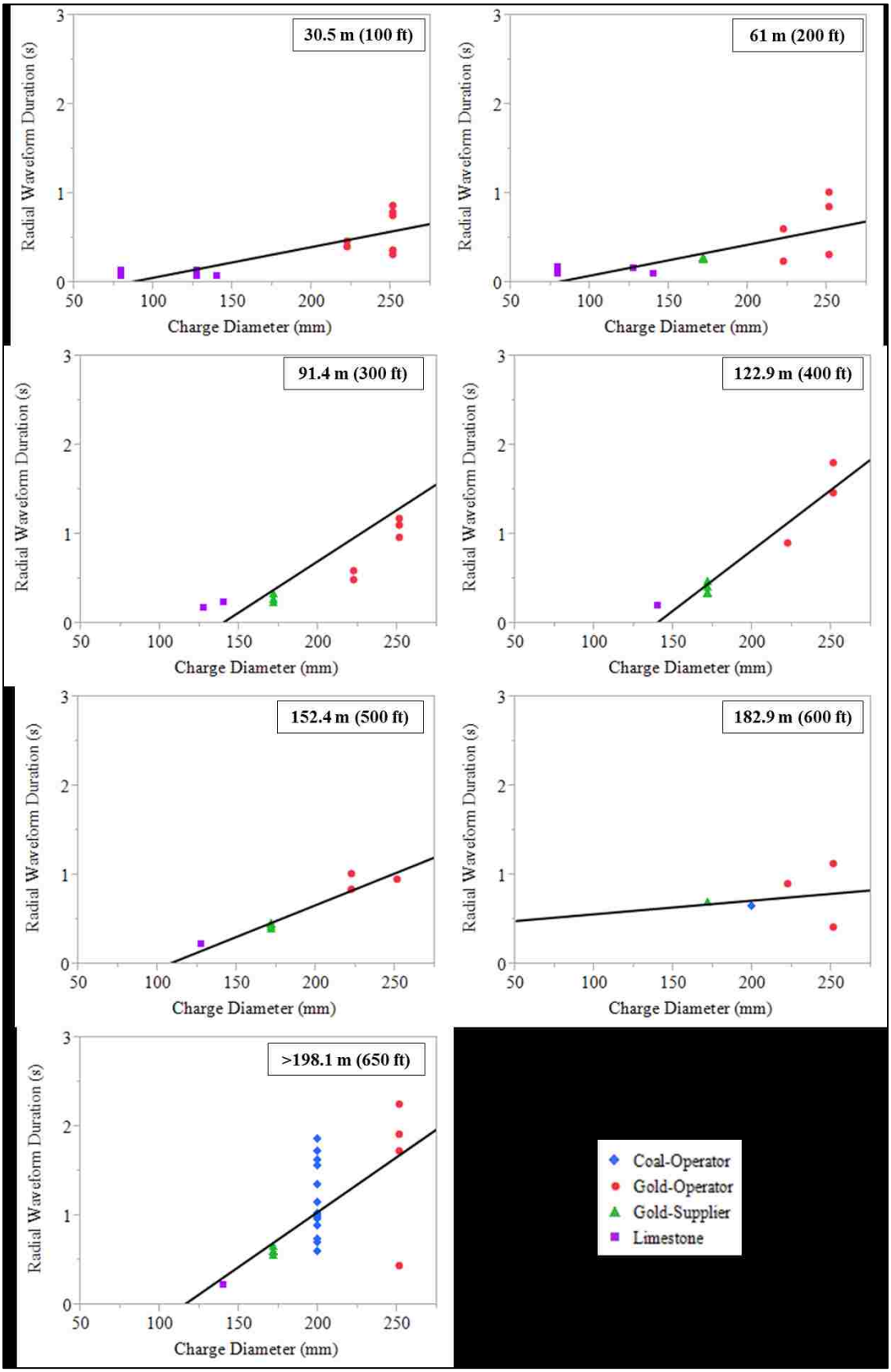

Figure 4.21. Charge diameter versus radial waveform duration by rounded distance.

The relationship between the charge cross-sectional area and the waveform duration are obviously similar to the relationship between diameter and duration. The relationship between the charge weight and the waveform duration and the stemming length and the waveform duration is similar but weaker than the relationship shown in Figure 4.21, where larger charge weights and longer stemming lengths appear to equate to longer waveform durations. The explosives density has an inverse relationship, where higher density values equate to shorter waveform durations. Charge length has little to no correlation with the waveform duration.

4.4.3.3. Multiple regression of waveform duration. The multiple regression analyses in this section are completed in two parts. The first part includes the entire dataset, while the second part includes only the data within 76 m (250 ft) of the charge assuming geology does not affect duration within 76 m of the charge.

The signature hole dataset includes 98 observations of waveform duration, 33 of which are within 76 m (250 ft) of the charge. Again, there is a smaller sample population than would be preferred in the near-field; however, the results from the analysis do appear to be reasonable.

The regression analysis of the full dataset shows that the distance from the charge to the monitoring point and the geology have the greatest statistical effect on the waveform duration (Table 4.6 and Appendix E). These results support the qualitative evaluation of Figure 4.20 which shows groupings by geology and a linear relationship within those groupings between the square root scaled distance and the radial waveform duration.

Table 4.6. Multiple regression runs and results for waveform duration (entire dataset).

Test Run	Variable Removed	R^2 Adj. after Regenerating Model
I	N/A	0.62
II	Charge Length (m)	0.63
III	Charge Cross-Sectional Area (sq. m)	0.62
IV	Explosive Density (g/cc)	0.62
V	Stemming Length (m)	0.61
VI	Charge Diameter (mm)	0.59
VII	Charge Weight (kg)	0.56

Remaining Variables: Geology,
Log (Distance from the Blast (m))

The multiple regression analysis of the data points that were recorded within 76 m (250 ft) of the charge produces a different conclusion than the regression analysis of the full dataset. In the near-field, the cross-sectional area of the charge becomes the most significant factor (Table 4.7 and Appendix E). Distance is most likely statistically insignificant to the near-field dataset since the waveform does not begin noticeably broadening at such small distances.

Table 4.7. Multiple regression runs and results for waveform duration (near-field).

Test Run	Variable Removed	R^2 Adj. after Regenerating Model
I	N/A	0.67
II	Explosive Density (g/cc)	0.68
III	Log (distance from Blast (m))	0.69
IV	Charge Length (m)	0.70
V	Charge Weight (kg)	0.70
VI	Stemming Length (m)	0.70
VII	Charge Diameter (mm)	0.68

Remaining Variable: Charge Cross-Sectional Area (sq. m.)

The statistical significance of the charge cross-sectional area brings the relationship between charge cross-sectional area and geology to light as discussed in the previous section. The perceived relationship between the charge cross-sectional area and duration could simply be due to the relationship between geology and duration. Therefore, geology was plotted against the waveform duration using the standard least squares regression model. The regression revealed that geology is a statistically significant variable with an $\bar{R}^2$ value of 0.64, which is similar to the final adjusted R-squared value given in Table 4.7. Additionally, the charge weight and charge length, together, produce an $\bar{R}^2$ value of 0.67. Therefore, there is no statistically valid method of determining which variable affects the waveform duration in the near-field without a larger sample population with a greater variance in charge diameters.

Qualitatively, the most likely factor to affect the duration in the near-field is the geology as evidenced in Figure 4.20. The limestone quarry data have the largest variety of charge diameter values, yet the tightest relationship between duration and scaled distance, while the gold-operator data is has the most variance between duration and scaled distance, yet has a smaller range of charge diameters. Therefore, it is most likely that the near-field data is statistically affected by geology as opposed to charge diameter or charge cross-sectional area.

4.5. REVIEW

This section has shown the importance of multiple regression analyses when studying a large population of signature hole data. It proved that multiple regression can

be used to evaluate and determine the statistically important variables that affect each feature of the blast vibration waveform.

4.5.1. Amplitude. The amplitude was qualitatively evaluated using the SRSD versus radial PPV plot and the rounded distance plots, then quantitatively studied using multiple regression analysis. The qualitative study showed that the data appear to become noticeably influenced by geology at distances greater than 76 m (250 ft). This distance corresponds to the transition of the vibration from nonlinear amplitude attenuation to linear amplitude attenuation. Therefore, the data within 76 m were defined as near-field data and treated as if geology does not statistically affect the data in that range. This assumption was proven to be true after a check using a multiple regression analysis that included geology.

The near-field data were evaluated using multiple regression analysis to determine the variables that have a statistically significant relationship with the radial PPV. The regression analysis showed that the radial PPV amplitudes are most affected by the distance from the charge, the charge weight, and the stemming length. These results support the scaled distance equation, which accounts for both the distance and the charge weight. The stemming length relates to confinement for the fully confined signature hole data; therefore, the confinement also has a statistically significant effect on particle velocity amplitude. Higher confinements produce higher amplitudes because greater confinement causes the explosive energy to be directed into the ground as vibrations.

4.5.2. Frequency. The principal frequency and dominant frequency were both evaluated in this section. Both qualitative and quantitative analyses were used to evaluate

frequency. The section also discusses the relationship between the charge cross-sectional area and geology for this dataset.

The principal frequency was evaluated using the entire signature hole dataset and the near-field dataset. The multiple regression analysis of the full dataset produced geology as the only statistically significant variable, while the multiple regression analysis of the near-field dataset produced either the charge cross-sectional area or geology as being the only statistically significant variable. Most likely, the near-field is affected by geology as opposed to the cross-sectional area since geology acts as a frequency filter to blast vibrations. However, the near-field dataset has too small of a variation in values of charge diameter for each source to show a difference in the effects of geology and charge diameter.

Multiple regression analysis on the dominant frequency produced stemming length, geology, and distance as the statistically significant variables for the full dataset and stemming length and distance for the near-field dataset. Geology acts as a filter for dominant frequencies over the full dataset; however, the effect of geology on the near-field dataset is less noticeable. Confinement, which is provided by stemming for the fully confined near-field tests, dictates the percentage of explosive energy that is directed into the rock. Increased stemming means a greater amount of energy is directed into the rock, which increases the period and lowers frequencies of the vibration.

4.5.3. Duration. The duration is the last of the three blast vibration features that was studied. The multiple regression analysis of the duration was completed on the full dataset and on the near-field dataset. Over the full dataset, the distance between the charge and the monitoring point and the geology are the statistically significant variables,

while in the near-field, the charge cross-sectional area appears to be the statistically significant variable. Most likely, geology is the statistically significant variable in the near-field as opposed to the charge cross-sectional area. Figure 4.20 shows how noticeable the grouping of the data is by site, meaning the geology has a major effect on the duration of the waveform. The distance is most likely not a significant variable in the near-field since there is not enough space within 76 m (250 ft) of the charge for the waveform to begin noticeably broadening.

4.5.4. Summary. In summary, the statistically significant variables that affect blast vibrations are distance from the charge to the monitoring point, charge weight, stemming length, and geology. This statement assumes that the cross-sectional area of the hole was only shown to be statistically significant due to the relationship between the charge diameter and the geology for this dataset. The dataset does not have enough variability of charge diameter at each site to show a difference between the charge diameter and geology for the tests. However, based on the literature review and practical knowledge of the blasting industry, geology is most likely the driving variable, as opposed to the charge cross-sectional area. Near the charge, where shock and fracturing occur, the charge cross-sectional area most likely does have more of an impact than it does in the elastic vibration range.

In summary, the charge geometry does not statistically affect the features of a blast waveform. The one variable produced by the statistical analysis that is of most interest is the stemming length, which gives a measure of confinement for the signature hole dataset. Longer stemming lengths produce higher PPV, lower principal and dominant frequencies, and longer durations because the confinement of the charge

directly affects the amount of explosive energy that is directed into the ground as vibrations. The results also show that energy is not just related to amplitude; it also relates to the periods of the vibration cycles. The fact that energy relates to all three features highlights another issue with the SRSD versus PPV plot: the plot only visualizes the PPV and does nothing to illustrate the frequency, which could be just as damaging, if not more, than the amplitude.

The final section of this document presents the foundation for a new method of assessing blast vibrations by evaluating vibration energy. Blast vibration energy could account for all the features of the blast vibration waveform, which could improve upon the SRSD versus PPV method.

5. BLAST-INDUCED SEISMIC ENERGY

5.1. BACKGROUND

Federal and state regulations have outlined standard methods for evaluating and proving blast vibrations are not harmful to residences and other public structures; however, these tools can be confusing and misleading. The blast vibration levels and limits defined by regulatory agencies are easily misunderstand and misinterpreted both by the public and by members of the blasting industry. In some extreme cases, individual communities take it upon themselves to set safe blasting levels without any understanding of the nature or effect of blast vibrations. In addition, the technical terminologies used by those in the industry only make blast vibration phenomena more confusing to the public.

Currently, the Z-Curve and the scaled distance versus PPV regression plots are commonly used methods of describing blasting vibrations. They are used for a number of reasons. First, the two methods are used throughout the industry since they were developed by the USBM and adopted by regulatory agencies. Second, both methods are used to produce an image, which can help visually describe the blast vibrations. Third, seismograph software includes functions for creating both of these charts, meaning users do not have to understand or know how to create the charts themselves. Finally, the majority of blast vibration models and tools use at least the scaled distance versus PPV charge as a foundation. Therefore, there are few new developments that address the root issue of the Z-Curve and scaled distance versus PPV methods.

Communities continue to grow and expand; therefore, quarrying and construction blasting operations face increasing numbers of scenarios where structures are located

near to blasts. This issue will affect other mining types as well. Near-field vibration concerns will require the blasters to be better educators of and communicators with the communities to ensure the property owners that blasting and other transient activities associated with the quarries will not harm their properties. The blasting community is in need of a tool to help illustrate to the public that blast vibrations are safe in an easily understandable way.

This section details the development, use, and issues of the Z-Curve and the scaled distance versus PPV regression methods. Then, three alternative methods are proposed that address the issues of both the Z-Curve and the scaled distance versus PPV regression methods. Note that the proposed methods are not necessarily solutions to the concerns described herein. They are, however, a foundation for the development of a new vibration evaluation method that will be sound, practical and easy to understand by both the public and blast professionals, alike.

5.2. INDUSTRY-ACCEPTED VIBRATION EVALUATION TOOLS

The two methods most commonly used to illustrate blast vibration data are the Z-Curve and the scaled distance versus PPV regression plot. These methods were both developed by federal agencies in order to estimate blast vibration characteristics for two purposes.

5.2.1. Z-Curve. The Z-Curve was developed by the USBM and first published in Report of Investigations (RI) 8507 in 1980 (Siskind, Stagg, Kopp, & Dowding, 1980). RI 8507 details a study on the effects of blast vibrations on residential structures. The Z-Curve was created from this study to quantify safe blasting levels based on frequency and

particle velocity amplitude (Figure 5.1). The Z-Curve is used to plot data against the safe limits, which were defined by the study.

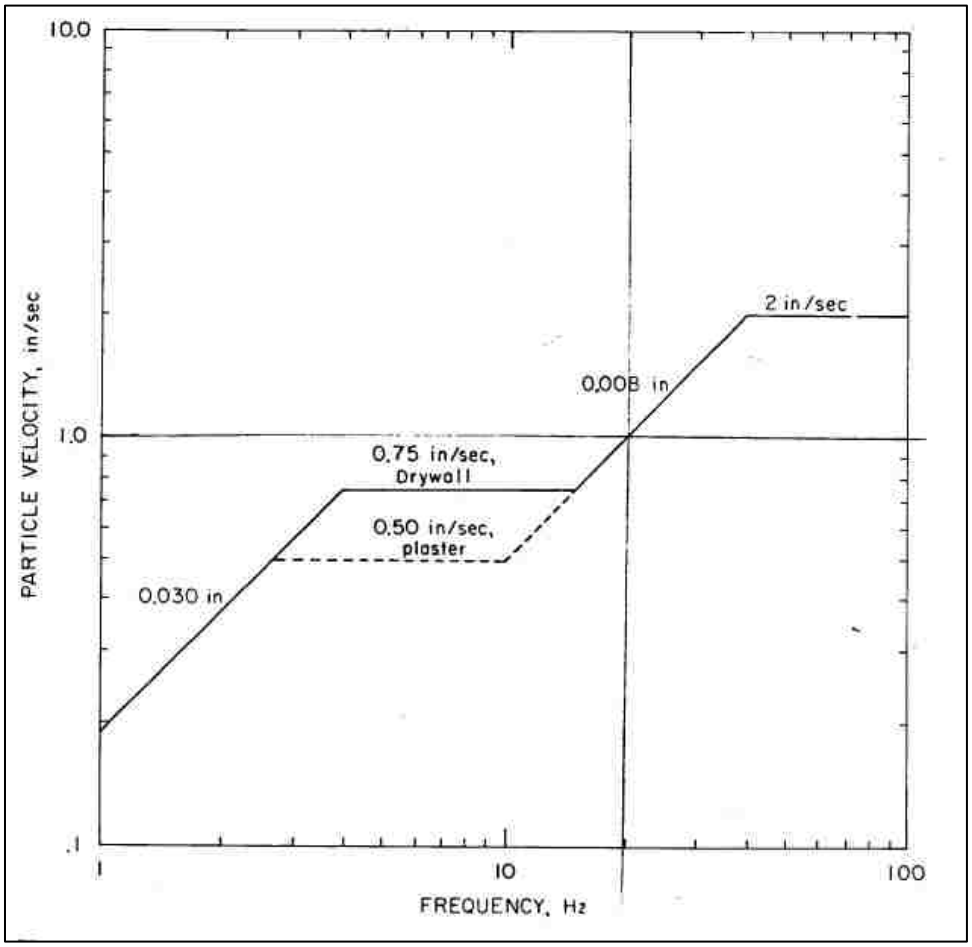

Figure 5.1. Z-Curve showing safe blast vibration levels for residential structures (source: Siskind, Stagg, Kopp, & Dowding, 1980).

The safe blasting criterion, given by Figure 5.1, has two frequency ranges: low frequency, under 40 Hz, and high frequency, greater than 40 Hz. The lower frequency data have a greater impact on residential structures; therefore, the peak velocity limits are lower in that range. The lower frequency range also includes separate limits for modern

drywall (gypsum board) and plaster around their structural resonances of 4 to 12 Hz. Above 40 Hz, the safe limit for peak particle velocity is constant at 51 mm/s (2 in/s). The Z-Curve includes constant displacement limits in the lower frequency range:

- At frequencies under 4 Hz for drywall and under 2.5 Hz for plaster, the table limits displacement to 0.76 mm (0.03 inches).
- Displacement is limited to 0.2 mm (0.008 inches) between 10 Hz and 40 Hz for plaster and approximately 12 Hz and 40 Hz for drywall.
- Particle velocity is limited to 13 mm/s (0.5 in/s) for plaster and 19 mm/s (0.75 in/s) for drywall between the displacement limit ranges for each material.

5.2.1.1. Development of the Z-Curve. The Z-Curve is the result of a probability analysis of the data collected during a series of field tests on blast vibrations and structural response by the USBM. The field tests included observations and measurements of wall, floor, and cracking response to blast vibration events. The majority of data were gathered from blast events originating from large-diameter production blasts at surface coal mines. Seventy-six houses constructed with plaster on wood lath or drywall were studied during the multi-year study. The study used a mean and variance analysis and a probability analysis of seven datasets to construct the Z-Curve.

5.2.1.1.1. Mean and variance analysis. The authors of RI 8507 used a mean and variance analysis to assess damage classification relating to displacement as a function of frequency. The overall summary of the seven datasets shows that low frequencies require greater caution than higher frequencies at equal damage probability (Figure 5.2).

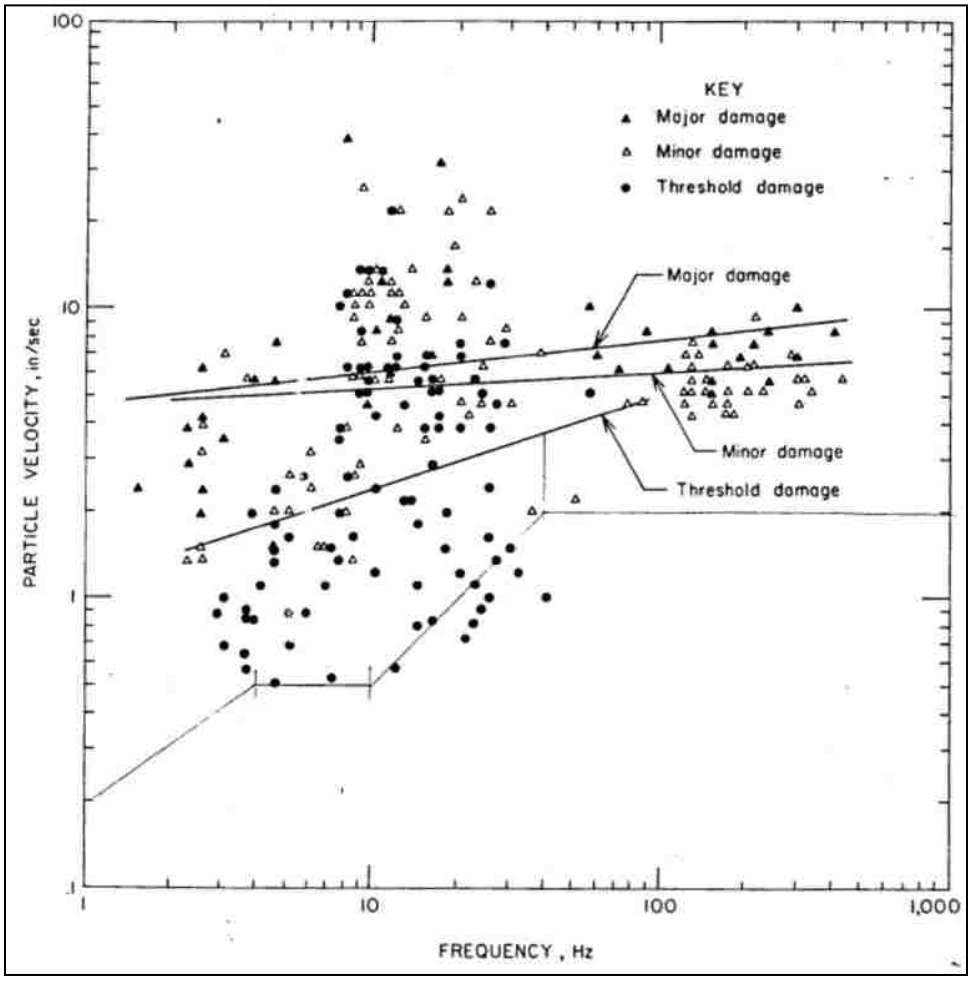

Figure 5.2. Plot of summary dataset and lower limit line used to create the Z-Curve (source: Siskind, Stagg, Kopp, & Dowding, 1980).

5.2.1.1.2. <u>Probability analysis.</u> A probability analysis was applied to the data as an alternative to the mean and variable analysis. The probability analysis resulted in plots of the relationship between particle velocity and probability of damage at each level of particle velocity (Figure 5.3). The plots show a low probability of damage (<5%) below 51 mm/sec (2 in/sec) for high frequency vibrations. Lower frequency vibrations show a low probability of damage below 13 mm/sec (0.5 in/sec). The low frequency limit was adjusted to 19 mm/sec (0.75 in/sec) for modern houses constructed using

drywall due to the conservative nature of the 13 mm/sec criterion. These numbers were used to construct the final Z-Curve for each respective frequency range. The final Z-Curve estimates the safe blast vibration levels that provide protection from blast damage in 95% of cases.

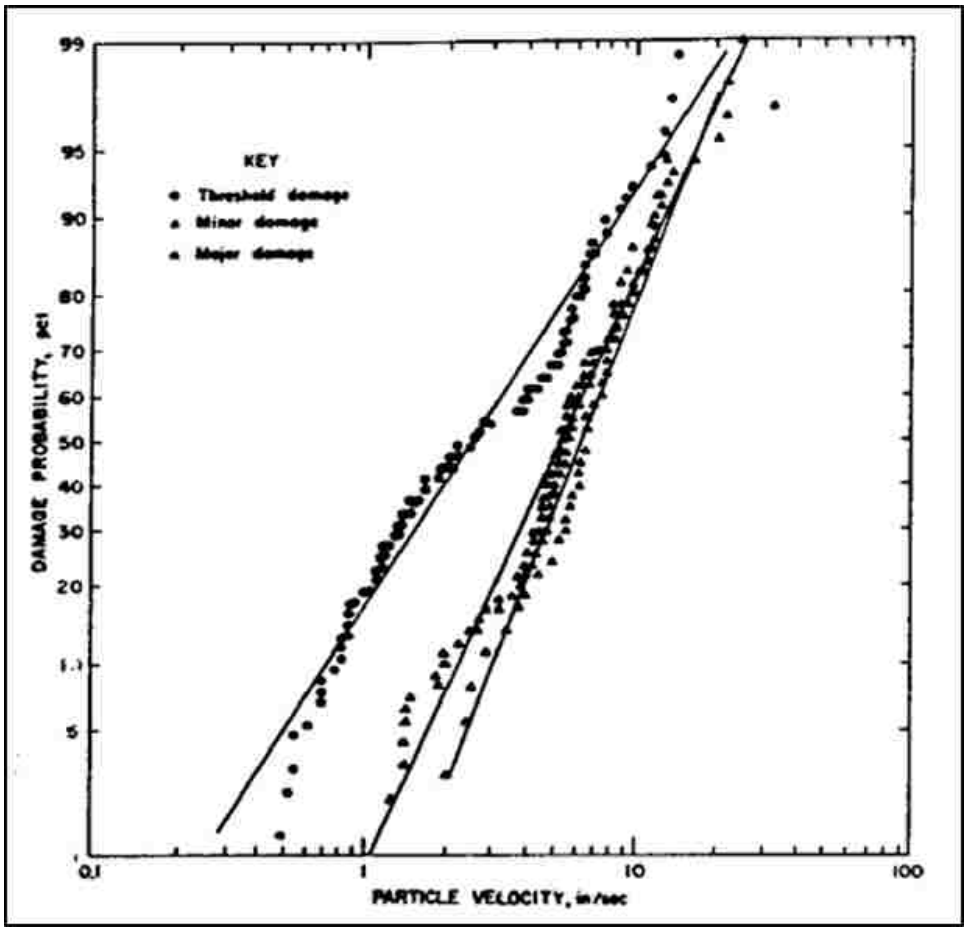

Figure 5.3. Probability plot of summary dataset used in RI 8507 (source: Siskind, Stagg, Kopp, & Dowding, 1980).

5.2.1.2. Disadvantage of the Z-Curve. The Z-Curve includes important features of blast vibrations, including the particle velocity and displacement amplitudes and the

frequency. The curve is based on structural response and blast damage data and recognizes the effect of displacement on structure response to blast vibrations by relating peak particle velocity to frequency.

RI 8507 highlights one disadvantage of the Z-Curve, in that it underestimates annoyance reactions due to differences in structural response between midwalls and corners. Midwall response is dissimilar to corner response, so that midwall response to vibrations in the 20 to 35 Hz range are relatively more annoying at the maximum safe blasting levels shown in the Z-Curve.

There are additional issues with the Z-Curve rising from its use. First, the plot is easily constructed using computer software; therefore, little thought is required to plot data on the Z-Curve. Following that it takes little understanding to construct the plot, and proper application of the plot is most likely poorly understood. For instance, RI 8507 clearly states that the upper limit of 51 mm/sec (2 in/sec) can be exceeded without damaging a structure. Additionally, the chart does not apply to brick and mortar construction, only residential construction using drywall or plaster since drywall and plaster are the first materials to have noticeable damage from blast vibrations. The document also states that 5% of blast vibrations that plot on the limit line will statistically cause damage, although, this depends on the frequency at which the vibration occurs. Therefore, the limit line on the chart is not a “black and white” safe blasting limit. Finally, the public have little understanding of particle velocity and frequency. Therefore, the table is of little practical sense to those outside of the blasting industry who have concern over blasting vibration limits. In spite of these issues, the Z-Curve is

adopted by regulatory agencies as a safe blasting guideline; therefore, it is used throughout the blasting industry.

Figure 5.4 shows an example of the Z-Curve using data from one of the signature hole tests recorded at the limestone operation. None of the points exceed the limit; therefore, a person without much knowledge of the subject would assume the blast vibrations were below damaging limits. The two points outlined in red are near, but below, the limit line. The blue point is also below both the drywall and the plaster limits in the lower frequency range. The log-log plot makes the data point outlined in blue appear to be safe; however, the blue point corresponds to a particle velocity period over four times the duration of the period of the upper right red point. Therefore, the displacement of all three points is nearly identical (approximately 0.2 mm or 0.008 inches) meaning all three of the points could be indicative of potential damage. This may not be an obvious correlation, even for experienced blasters; therefore, some relationships derived using this plot may be incorrect.

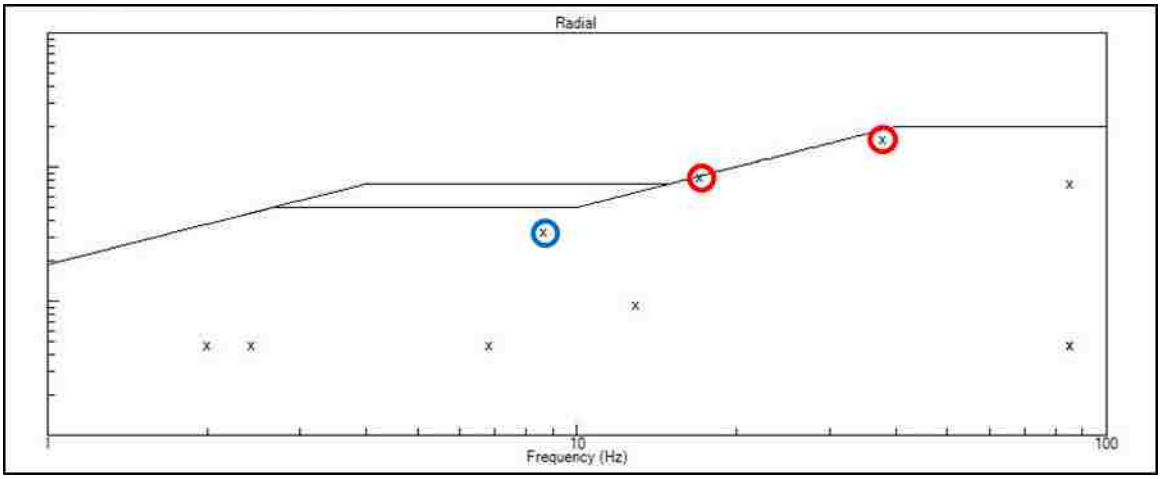

Figure 5.4. Test5-Seis3 signature hole waveform data plotted on a Z-Curve chart using seismograph software.

5.2.2. Scaled Distance versus PPV Regression. The scaled distance equation and its derivation are introduced in Section 2. This subsection focuses on issues concerning the use of the scaled distance versus PPV regression plot.

The square root scaled distance (SRSD) equation is used for surface blast vibration scaling; however, it is oversimplified and not a dimensionless or a fundamental equation of blast vibration. There are also no reviewed and published guidelines for determining whether cube root or scale root scaled distance is more appropriate, and in many cases, both equations result in similar coefficients of determination. In reality, regardless of which equation is used, scaled distance versus particle velocity plots typically have noticeable scatter; therefore, a best-fit regression line is applied to the data. The typical scatter of blast vibration data requires the 95% confidence interval of the best-fit line to be plotted in order to define the range of expected particle velocity values at a specific scaled distance. This method allows blasting engineers to be confident that vibration levels using a similar blast design will fall within the 95% confidence interval plotted using the recorded data.

The discussion in Section 4 raises another significant issue with use of the logarithmic scale with the scaled distance versus PPV plot. Logarithmic scales are used to compare a wide range of charge weights and distances; however, blasting charge weights and distances typically do not vary enough to require logarithmic scaling. Logarithmic scaling, which scales the range logarithmically so that the range compared to the mean value is comparable, hides the fact that small scaled distance values correspond to a much larger range of peak particle velocity values within the 95% confidence interval than larger scaled distances. However, on a log-log scaled distance versus PPV

plot, the 95% confidence interval appears to be equal throughout the range of scaled distance values.

Another issue with the scaled distance versus PPV plot is the lack of valuable information concerning the charge. The plot only accounts for particle velocity and does not include frequency. Withholding frequency is misleading , especially when regulatory limits for peak particle velocity are exceeded, but frequencies are within an acceptable range. In this case, the vibration as a whole may still be within acceptable, non-damaging limits.

Finally, the scaled distance versus PPV plot is typically only used at a single blast site. Operations typically only use one combination of charge geometry and blast design for a particular working face; therefore, in most cases, there is absolutely no need to scale distance with charge weight. A constant charge weight only scales the distance by a constant value, meaning it is irrelevant to include the charge weight in that scenario. Of course, removing charge weight from the equation is not feasible if regulatory procedures requiring scaled distance must be followed.

Figure 5.5 is an example of a regression analysis for Test 5 of the limestone quarry tests. The left-hand image illustrates a typical SRSD versus PPV log-log regression plot. The distance versus radial PPV for the same data is shown in the right-hand image. This comparison illustrates that the regression plots produce identical coefficients of determination ($R^2 = 0.95$), regardless of whether SRSD or distance from the charge is plotted on the x-axis.

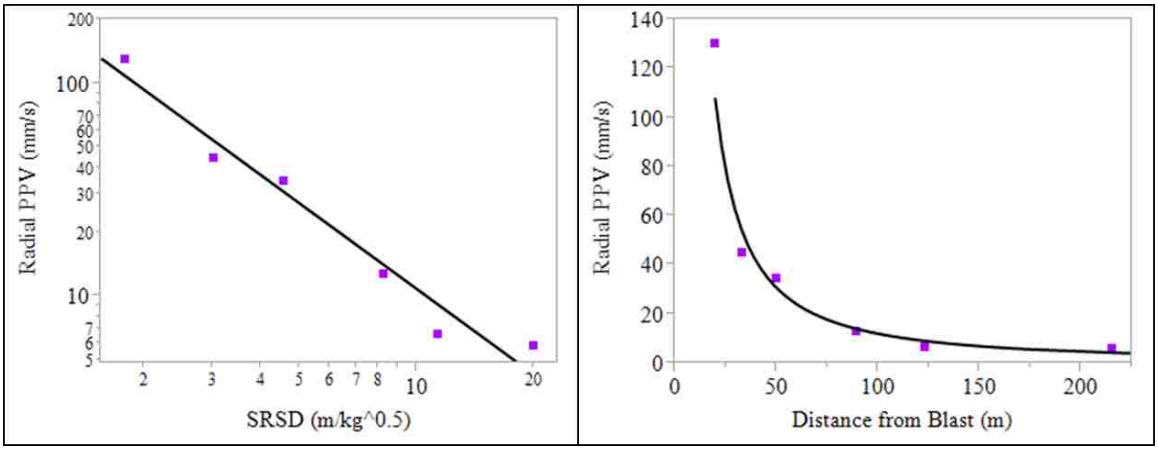

Figure 5.5. SRSD versus radial PPV and distance versus radial PPV for Test 5 of the limestone quarry tests.

Without much experience with logarithmic plots, it would be easy to think that the data fit of the line is just as accurate at low scaled distances as it is at high scaled distances. This is incorrect. The lower scaled distances in the non-linear attenuation range have residual values over 35 mm/sec residual, while the higher scaled distances in the linear attenuation range have residual values of less than 5 mm/sec residual (Figure 5.6). The Residual by X plot shown in Figure 5.6 is identical to the Residual by X plot for the distance versus PPV regression.

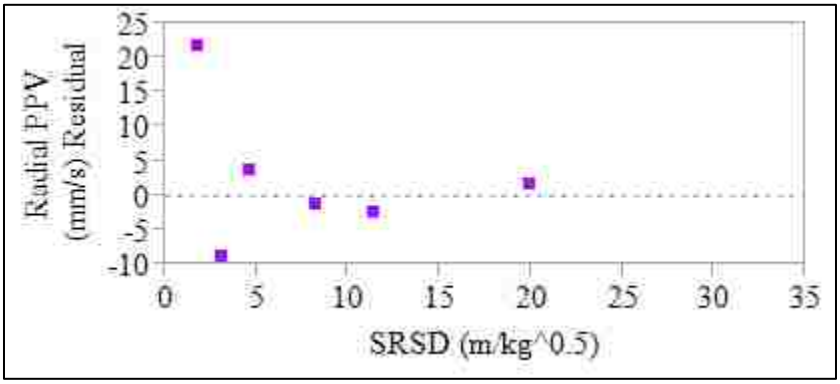

Figure 5.6. Residual by X plot for SRSD versus radial PPV of Test 5.

5.3. PROPOSED METHOD FOR EVALUATING VIBRATION ENERGY

Despite the drawbacks to both methods, the Z-Curve and the scaled distance versus PPV plot have proven to be useful in predicting blast vibration levels and limiting damage. However, the previous discussion in this document shows that there is room for improvement for these methods. The following section presents three alternative approaches to the Z-Curve and the scaled distance versus PPV plot using blast vibration energy estimations.

The energy calculations and subsequent analyses include the important aspects of the Z-Curve and SD plots, such as displacement, particle velocity, and frequency, and distance, while eliminating the drawbacks of both methods by producing values with units that are more recognizable and easily understood by the general public. Energy can also be tied into the statistically significant variables and used to classify vibrations by those variables. Three potentially feasible energy calculations, which are used to evaluate the concept of estimating blast vibration energy, are described in this section. These include Newton's Second Law of Motion, a Hugoniot equation of state, and a seismic energy equation based on energy flux.

5.3.1. Newton's Second Law of Motion. Newton's Second Law of Motion states that the net force acting upon an object, *F*, with constant mass, *m*, is equal to the product of the object's mass and acceleration, a_m:

$$F = ma_m \tag{26}$$

Equation 26 could be applied to blast vibrations as a method for approximating the force of a blast vibration since a vibrating particle can be defined by a mass and an acceleration waveform. Therefore, the equation requires two variables: mass and

acceleration. The first task in the application of this equation is determining the mass of the "particle" that is monitored by the seismograph. The particle is an arbitrary point, so the particle could be assumed to be the seismograph, the transducer in the seismograph, a unit volume of rock, or a component of a structure of interest. This section only evaluates the concept of the energy equations; therefore, the mass of the "particle" does not need to be completely accurate. For this evaluation, the particle mass is assumed to be equivalent to the mass of a unit volume of rock. The acceleration of the particle can be calculated by taking the derivative of the particle velocity waveform. The derivative of the particle velocity waveform is a function of both the frequency and the particle velocity in the calculation.

Knowing mass and acceleration, the force equation can be applied to each point of the acceleration waveform. This calculates the force of the vibration on the particle at each sample point of the waveform.

The product of force and displacement, d, is equivalent to work, W_k. Therefore, the energy of a blast vibration passing a monitoring point can be approximated by Equation 27.

$$W_k = Fd = ma_m d \tag{27}$$

The displacement waveform of the monitoring point is equivalent to the integral of the particle velocity waveform. The work equation can also include a factor for the cosine of the angle between the force and displacement if the resultant displacement is not the same direction as the applied force. This study only focuses on the radial component of the vibration; therefore, the resultant displacement is assumed to be in the same direction as the applied force, eliminating the need for the cosine of the angle.

5.3.1.1. Force equation application. The steps for calculating the energy of the blast vibration using Newton's Second Law of Motion, or the force equation, are:

1. Calculate the mass of the particle, which is assumed to be equivalent to the mass of a unit volume of rock.
2. Export the particle velocity data from the seismograph software into graphing software and calculate the derivative and the integral of the waveform. The derivative is the acceleration waveform, and the integral is the displacement waveform.
3. Multiply the particle mass by the acceleration waveform and displacement waveform value at each sample point. This results in the energy waveform.

This process can be completed using a number of methods; however, the basic approach described above was used for this analysis due to the author's familiarity with the software and the ease of calculations using the software. For this analysis, the software included Seismograph Data Analysis® by White Industrial Seismology, Microsoft Excel®, and DPlot® graphing software.

5.3.1.2. Force equation example. The following example uses the seed waveform from Test5-Seis6 of the limestone quarry tests. The ground in this test had a density of 2.6 g/cc; therefore, assuming the particle is one cubic meter of the ground, the mass of the particle was 2600 kg.

The particle velocity waveform (Figure 5.7) was recorded using a standard geophone-based seismograph placed 215.5 m (706.9 ft) from the charge. The particle

velocity waveform, although produced by a single charge, is indicative of typical waveforms that might be monitored near structures for compliance purposes.

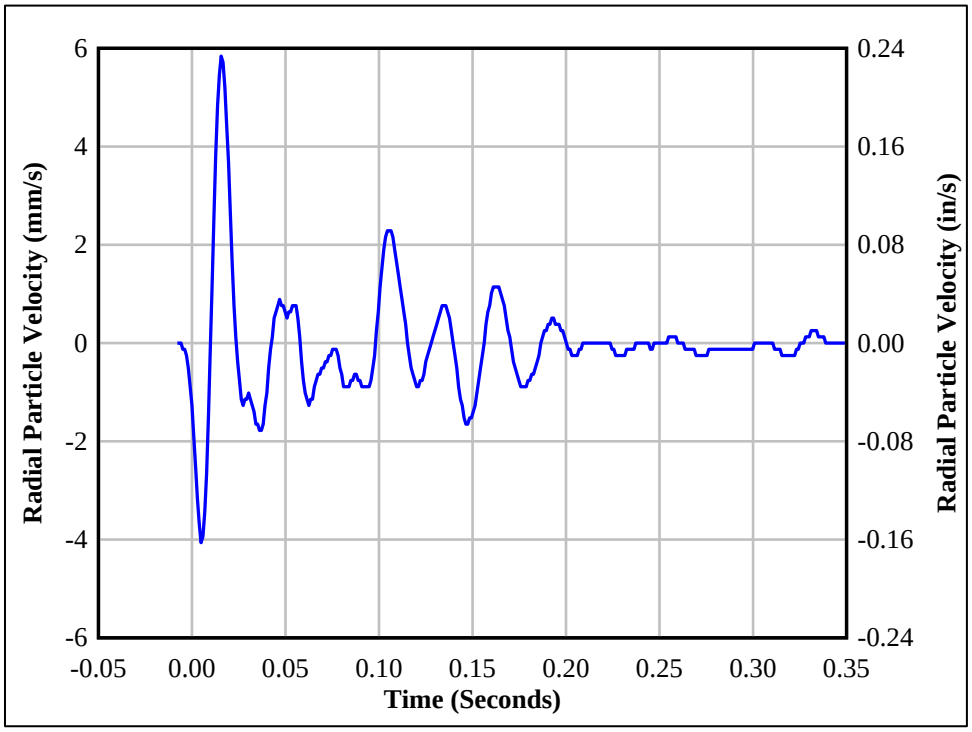

Figure 5.7. Test5-Seis6 radial particle velocity waveform.

The particle velocity waveform was imported into DPlot®, which was used to differentiate and integrate the particle velocity waveform to produce the particle acceleration and particle displacement waveforms, respectively (Figure 5.8 and Figure 5.9). The central difference method was used to differentiate the particle velocity waveform and the trapezoidal rule was used to integrate the particle velocity waveform.

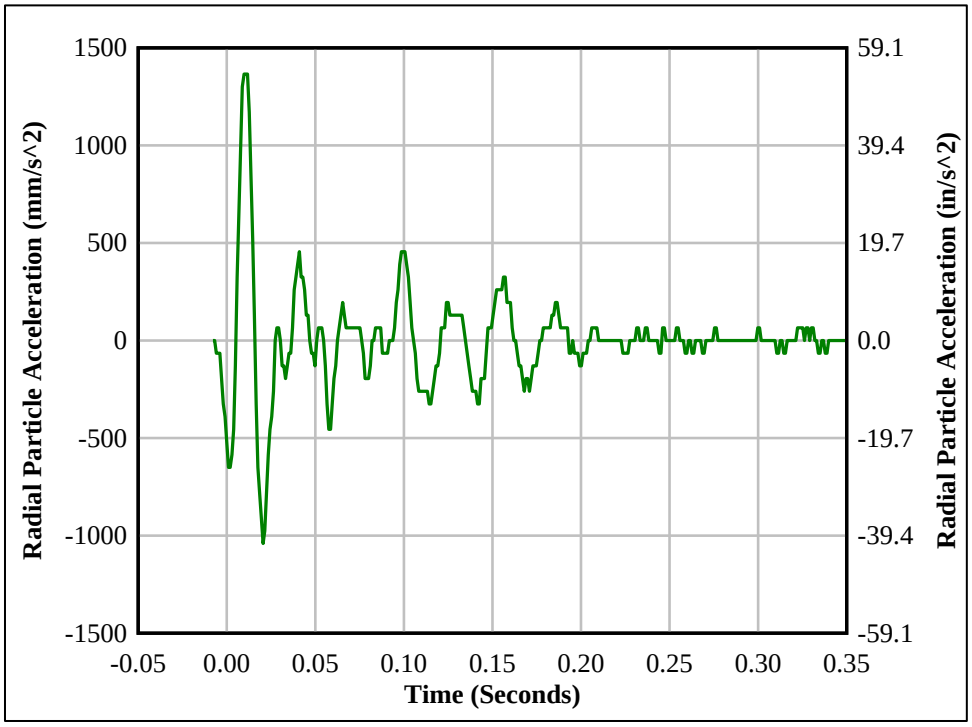

Figure 5.8. Test5-Seis6 radial particle acceleration waveform.

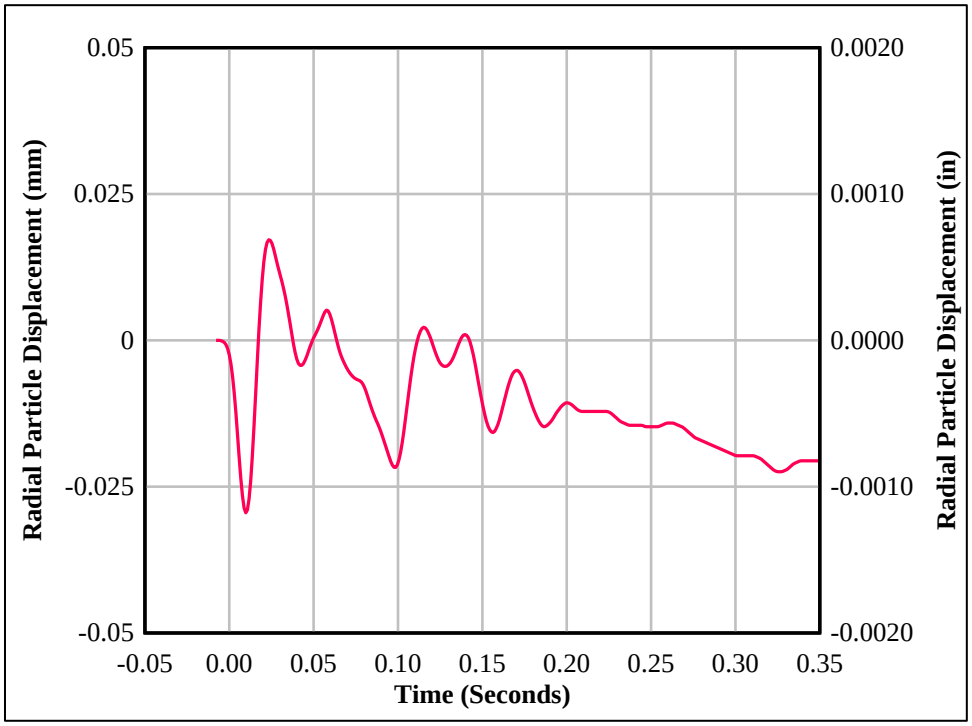

Figure 5.9. Test5-Seis6 radial particle displacement waveform.

Figure 5.9 shows that the displacement waveform deviates from zero displacement. The particle velocity waveform has more area between the negative waveform values and equilibrium than it does between the positive waveform values and equilibrium; therefore, the integration of the particle velocity waveform cannot terminate at equilibrium. The smallest displacement values should occur after a duration of 0.2 seconds when the particle velocity is essentially zero, meaning no movement. In contrast, after 0.2 seconds, the displacement values deviate from equilibrium and from the displacement waveform's maximum absolute value of displacement. Due to this complication, the integral of the particle velocity does not appear to produce the most accurate values for displacement. However, in order to continue the evaluation of the energy equations, it is assumed that the displacement waveform is accurate.

The acceleration and displacement waveforms have sample points at identical sample times. Therefore, the displacement and acceleration value at each point can be used in Equation 27, thereby calculating an energy value at each sample point, which can be used to generate an energy waveform for the event (Figure 5.10). This process produced a maximum absolute value of energy imparted to the particle equal to 0.1 J.

Figure 5.10 illustrates another issue with the force equation method. The work equation produces mostly negative values because the acceleration and displacement values are theoretically always opposite when motion is sinusoidal. In other words, while acceleration is negative, displacement is positive, and vice versa. However, the work equation considers vector quantities as opposed to scalar quantities; therefore, the negative values only indicate the direction of the energy, not that the energy itself is negative.

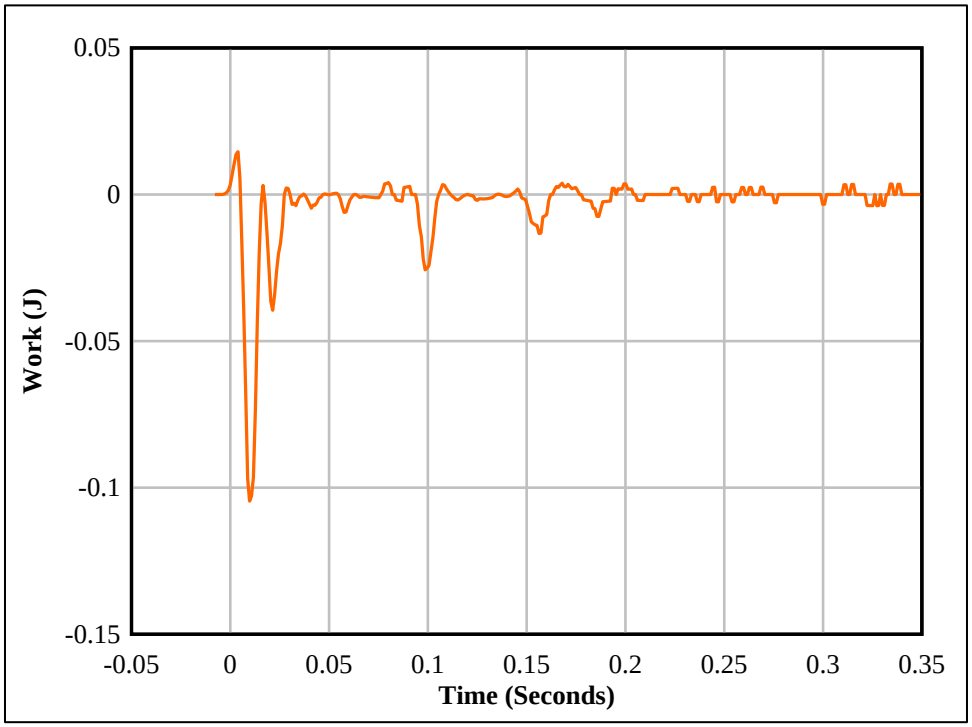

Figure 5.10. Test5-Seis6 radial particle energy waveform, calculated using work equation.

5.3.1.3. Force equation summary. This equation has multiple drawbacks. (a) The acceleration is the driving variable in this equation; therefore, it has more of an effect on the outcome than the displacement. The resulting energy waveform is similar in shape to the acceleration waveform. (b) The displacement waveform does not return to equilibrium. Displacement is a minor value though, so this did not have much effect on the shape of the energy waveform. (c) Acceleration and displacement theoretically have opposite signs due to the nature of integration and derivation of sinusoidal waveforms; therefore, the energy waveform is negative. (d) The particle and, therefore, the mass of the particle that the equation refers to are open to interpretation. (e) Additionally, without being able to monitor that the actual values of force or energy, this equation cannot be evaluated for accuracy.

5.3.2. Hugoniot Equation of State. The Hugoniot equation of state applies to the jump condition of a shock wave by relating the state of a medium immediately prior to a shock to the state of the medium immediately after the shock front passes. The Hugoniot equation of state is derived from the conservation of momentum equation (Equation 21). Equation 21 can be simplified when applying to blast vibrations because the initial pressure and particle velocity of the ground are equal to zero. The shock velocity variable in Equation 21 is substituted with the *U*-*u* Hugoniot equation of state (Equation 20) to form the following equation for final pressure, P_1:

$$P_1 = \rho_0 u_1 (C_0 + s u_1) \tag{28}$$

Equation 28 incorporates the initial material density, ρ_0, the material's particle velocity after the shock front passes, u_1, bulk sound speed, C_0, which is the y-intercept of the *U*-*u* Hugoniot plot, and *s*, which is the slope of the *U*-*u* Hugoniot. For this study, the bulk sound speed is substituted with the longitudinal seismic propagation velocity, and the particle velocity is taken from the radial particle velocity waveform recorded by the seismographs. The bulk sounds speed can be approximated by the longitudinal propagation velocity because the product of the particle velocity and *s* is negligible with respect to the magnitude of the longitudinal propagation velocity. However, for illustration, this evaluation will assume the product of *s* and the particle velocity is consequential. The dimensionless variable *s* is estimated as 1.43, from empirical shock data gathered from Solenhofen Limestone samples (Johansson & Persson, 1970). The value of *s* for Solenhofen Limestone can be applied to this study since *s* can be approximated from similar materials (Cooper, 1996). The density used in this analysis is the density of the limestone at Big Bend Quarry, which is 2.6 g/cc.

The blast-induced vibrations monitored in this study originated as shock waves; however, the initial shock generated by the blast had already attenuated to a stress wave by the time the vibration wave reached the monitoring locations. The Rankine-Hugoniot equations of state do theoretically apply to elastic vibrations that are the focus of this study (Cooper, 1996); however, this is not a common application for the equations of state. Also, since the equation is being applied to elastic vibrations, it is essentially calculating the stress in the rock as opposed to pressure.

5.3.2.1. Hugoniot equation of state application. The Hugoniot equation of state approach is similar to the approach using the Second Law of Motion in that both equations produce a value with recognizable units and can be applied to the entire vibration waveform. However, in this application, this equation produces stress, as opposed to force, which can be used to calculate energy with a known surface area and displacement. The following steps were used to calculate the energy of the blast vibration using the Hugoniot equation of state.

1. Determine the density of the ground at the monitoring point.
2. Estimate the value for *s*.
3. Calculate the propagation velocity of the blast vibration.
4. Export the particle velocity data from the seismograph software into graphing software.
5. Calculate the stress at each sample point using Equation 28.
6. Calculate the energy using the stress values, the area over which the stress is distributed, and the displacement. This results in the energy waveform.

5.3.2.2. Hugoniot equation of state example. The constant values for density (2.6 g/cc), propagation velocity (4.27 km/s), and *s* (1.43) are applied to Equation 28 as follows:

$$P_1[GPa] = 2.6\left[\frac{g}{cc}\right] * u_1\left[\frac{km}{s}\right] * \left(4.27\left[\frac{km}{s}\right] + 1.43 * u_1[\frac{km}{s}]\right) \quad (29)$$

Using the data from Test5-Seis6, the peak radial particle velocity is 5.8 mm/s (0.23 in/s). Using Equation 29, the peak stress produced at the monitoring point is 65 kPa (9.4 psi). The results of the calculation on the full waveform is shown in Figure 5.11.

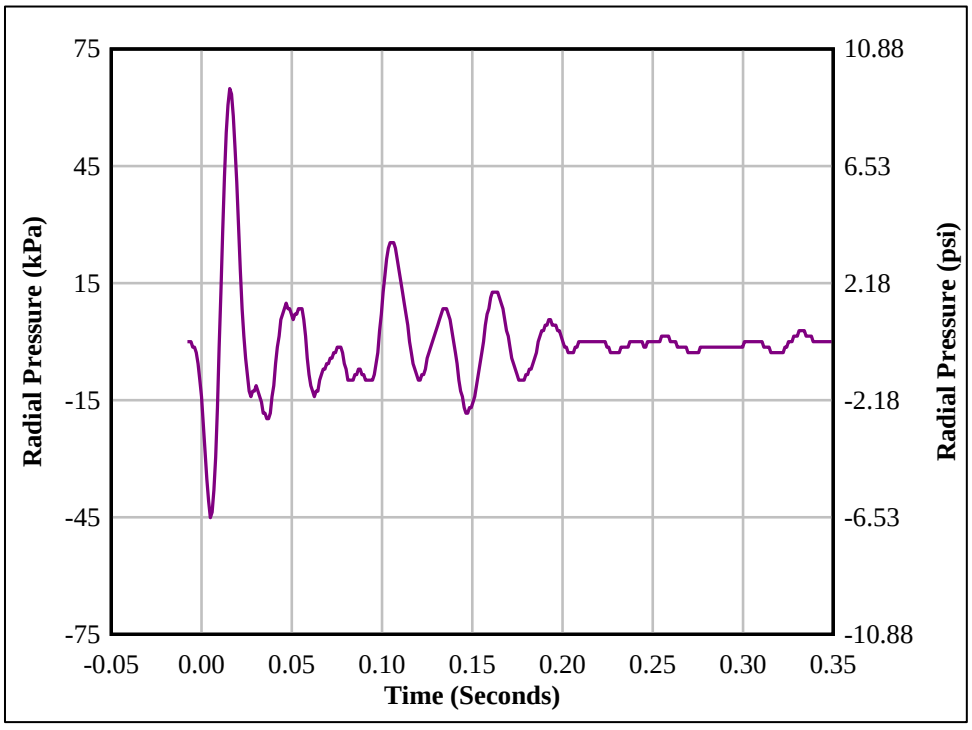

Figure 5.11. Stress-time waveform calculated using the Hugoniot equation of state.

The stress can be converted to work by multiplying stress by the area of the particle over which the stress is distributed, A_R, and by the displacement, d (Equation 30).

$$W[J] = P_1[Pa] * A_R[m^2] * d[m] \quad (30)$$

In this case, the particle is assumed to be a unit area of the ground, although the proper object with which to represent the particle to use is up for debate. The unit surface area over which the stress is distributed is assumed to be one square meter of ground in order to keep the evaluation consistent with the force equation evaluation. If the Hugoniot equation of state method is further developed, the proper object and surface area would need to be defined. The displacement for this equation is once again assumed to be the radial particle displacement, as given in Figure 5.9.

Using Equation 30, the waveform for work that is produced by the Hugoniot equation of state can be plotted (Figure 5.12). The Hugoniot equation of state method produced a maximum absolute value of 1.1 J, which is larger than the value produced by the force equation method by a factor of ten.

5.3.2.3. Hugoniot equation summary. Using the Hugoniot equation gives rise to a number of thoughts. (a) The equation results in values for work that are essentially zero. This is due to the equation calculating work on a particle that has a net displacement of zero. (b) Another point of interest, and not necessarily a drawback, for the Hugoniot equation of state is that any changes in the rock density, particle velocity, or propagation velocity have a directly proportional effect on the resulting stress. The value for *s* is essentially a non-factor in the equation due to the insignificant value of the particle velocity with respect to the propagation velocity. Therefore, the equation could be written as $P_1=\rho_0 u_1 C_0$, where density and propagation velocity are constant. Therefore,

this simplification shows that the shape of the stress waveform calculated by the Hugoniot equation of state is identical to the shape of the particle velocity waveform.

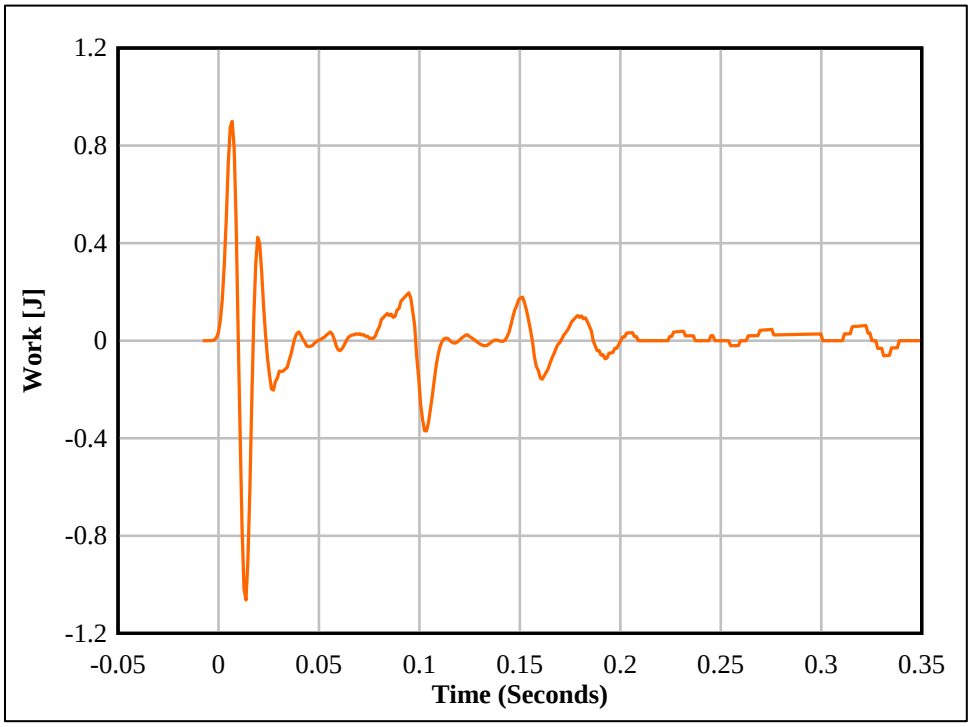

Figure 5.12. Test5-Seis6 radial particle energy waveform, calculated using Hugoniot equation of state.

The resulting energy waveform's shape is also similar to the particle velocity waveform, although it is affected by varying values of the displacement waveform. (c) Finally, unlike the energy waveform calculated using the force equation, the energy waveform calculated by the Hugoniot equation of state is positive and negative since the equation is a function of the particle velocity and displacement, as opposed to the acceleration and displacement.

5.3.3. Seismic Energy Equation. The seismic energy equation was derived in an attempt to calculate the total energy passing a spherical surface at radius, *D*, from the charge. The equation is a function of the radial distance from the charge, *D*, the rock density, ρ, radial propagation velocity, C_R, and radial particle velocity, PV_R, as shown by Equation 17, which is repeated here (Sanchidrián, et al., 2007):

$$E_{SR} = -4\pi D^2 \rho c_R \int_0^\infty PV_R^2 dt$$

The derivation of the seismic energy equation includes three equations, which are shown here as described by Sanchidrián, et al. (2007). The first equation is the calculation to determine the total power across the spherical surface, *P*, assuming constant flux, Φ:

$$P = 4\pi D^2 \Phi \tag{31}$$

The energy flux is a function of Lame's constants, λ and μ, which are parameters that relate stress to strain, and the radial particle velocity:

$$\Phi = \left[(\lambda + 2\mu)\frac{dPV_R}{dD} + 2\lambda\frac{PV_R}{D}\right] PV_R \tag{32}$$

Equation 33 estimates the strain, ε, which is the derivative of the radial particle velocity with respect to distance. The strain can be approximated as the ratio of the radial particle velocity to the radial propagation velocity, c_R as shown in Equation 18:

$$\frac{dPV_R}{dD} = \varepsilon_R = -\frac{PV_R}{c_R} \tag{33}$$

Energy is equivalent to the integral of power with respect to time; therefore, the energy can be approximated by integrating Equation 31 with respect to time, *t*:

$$E_{SR} = \int_0^\infty 4\pi D^2 \Phi \, dt \tag{34}$$

Substituting Equations 32 and 33 into Equation 34, the following equation is produced:

$$E_{SR} = -\int_0^{\infty} 4\pi D^2 \left[(\lambda + 2\mu)\frac{PV_R^2}{c_R} + 2\lambda\frac{PV_R^2}{c_R}\right] dt \quad (35)$$

The second summand within the integral of Equation 35 is equivalent to zero; therefore, it can be ignored with little error. The equation can be further simplified by substituting in the following relationship, which equates the radial propagation velocity to Lame's constants and the rock density, ρ:

$$c_R^2 = \frac{\lambda+2\mu}{\rho} \quad (36)$$

The final form of the equation is as follows (Equation 17):

$$E_{SR} = -4\pi D^2 \rho c_R \int_0^{\infty} PV_R^2 dt$$

This equation is essentially the function of the surface area of a sphere ($4\pi D^2$), the strain induced by the blast vibration, ε, the density of the rock, ρ, and the radial particle velocity (PV_R) and radial propagation velocity (c_R) of the blast vibration.

The seismic energy equation has further been adjusted to account for two issues noted prior to its application for this project.

1. By including $4\pi D^2$, Sanchidrian's equation assumes the vibration wave propagates spherically. This is an incorrect assumption for two reasons. (a) The charge is not located in a continuous medium. It is near the ground surface so the vibration only propagates in the shape of a half-sphere. (b) The seismic energy equation evaluates body waves, but this study is evaluating waves traveling on the surface. The wave propagation characteristics differ between body waves and waves that travel along the

surface because the surface waves do not propagate in a simple spherical manner. The seismic energy equation is only being applied to evaluate the energy of the vibration at the monitoring point; therefore, the spherical portion of the seismic energy equation is replaced by the surface area, A_R, over which the energy from the vibration is distributed. As in the Hugoniot equation of state methodology, the particle's surface area is assumed to be equivalent to one square meter of ground.

2. The equation given by Sanchidrián is negative to account for the energy leaving the control volume. For the purposes of this study, the total energy is calculated from the vibration recorded at a single point. There is no reason to include the negative sign.

In summary, the final equation used to calculate the seismic energy is:

$$E_{SR} = A_R \rho c_R \int_0^\infty PV_R^2 dt \tag{37}$$

5.3.3.1. Seismic energy equation application. The following points describe the steps used to apply the seismic energy equation to a seed waveform:

1. Determine the density of the rock mass and value used for the surface area of the particle.
2. Calculate the propagation velocity of the blast vibration.
3. Export the particle velocity data from the seismograph software into graphing software.
4. Calculate the square of each data point of the vibration waveform.
5. Integrate the squared particle velocity waveform over time.
6. Export the integrated data back into the tabulating software.

7. Calculate seismic energy at each sample point by multiplying the integral of the squared particle velocity with the rock density, radial vibration propagation velocity, and the surface area of the particle. This results in the energy waveform.

5.3.3.2. Seismic energy equation example. The following example demonstrates the use of the seismic energy equation using the data from Test5-Seis6. The particle velocity waveform is first squared to produce the values for PV_R^2 (Figure 5.13). The squared radial particle velocity values are then integrated over time to produce the waveform shown in Figure 5.14.

The integral of the PV_R^2 waveform gives the accumulative value of energy passing the point rather than the instantaneous energy value. The values trend positive and accumulate due to the integral. The positive and negative values of the particle velocity waveform could be squared and integrated separately to produce a positive and negative waveform; however, there is no good reason to justify the separation of the positive and negative values at this point.

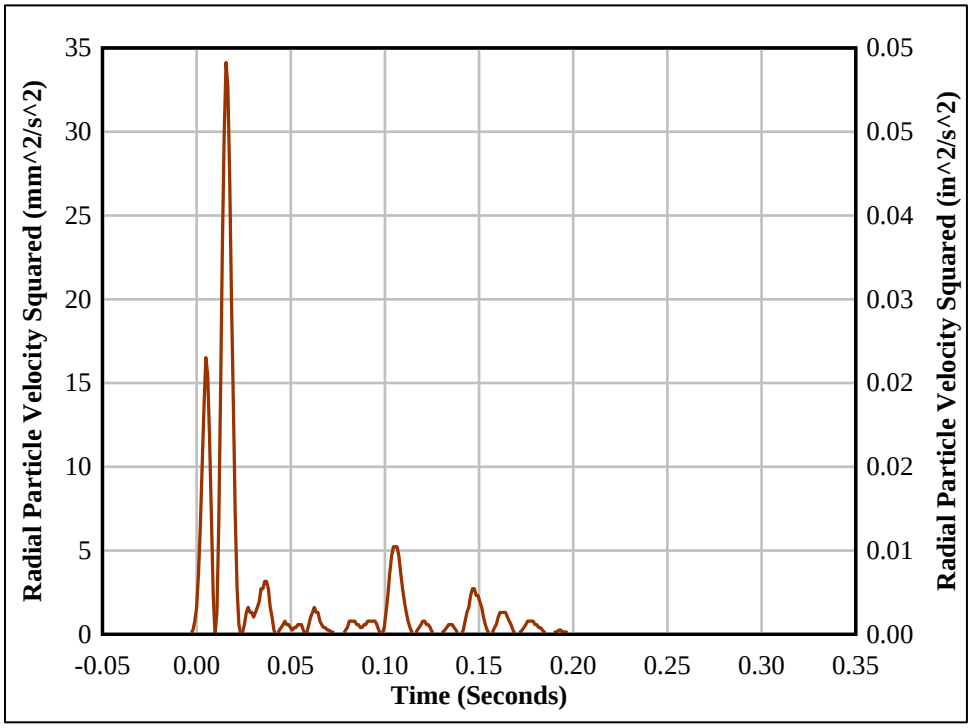

Figure 5.13. Test5-Seis6 squared radial particle velocity waveform.

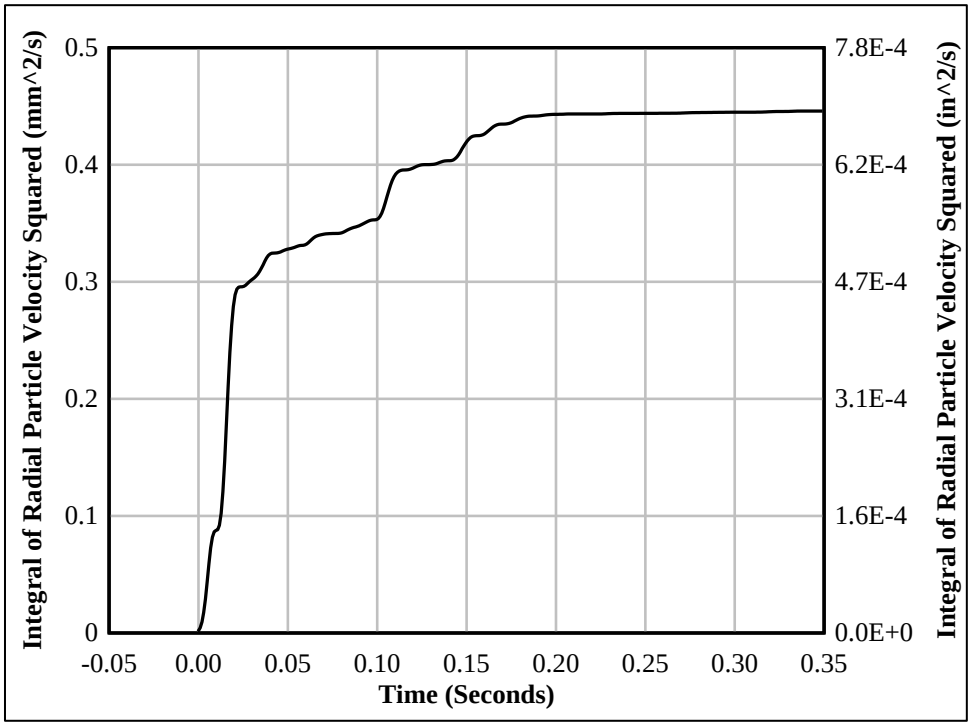

Figure 5.14. Integral of Test5-Seis6 squared radial particle velocity waveform.

The values calculated using the integral function can be multiplied against the rock density, radial vibration propagation velocity, and contact area of the particle to complete the seismic energy calculation, as follows:

$$E_{SR} = A_R[m^2] * \rho \left[\frac{kg}{m^3}\right] * c_R \left[\frac{m}{s}\right] * \int_0^\infty v_R^2 dt \left[\frac{mm^2}{s}\right] * 10^{-6} \quad (38)$$

For Test5-Seis6, A_R is 1 m^2 (10.76 ft^2), ρ is 2600 kg/m^3 (163 lb/ft^3), and c_R is 4,270 m/s (14,000 ft/s). The results from the calculation are shown in Figure 5.15, which gives a total seismic energy value of 4.9 Joules over the 0.35 second duration. The greatest energy occurs during the first 0.02 seconds of duration and is equivalent to 3.3 J. Further evaluation of the relationship between the energy waveform and the particle velocity waveform reveals that the first peak cycle in the particle velocity waveform equals 1.0 J of energy, while the second cycle equals 2.3 J (Figure 5.16). The benefit of the accumulative plot is that it accounts for the total energy over the duration of the waveform.

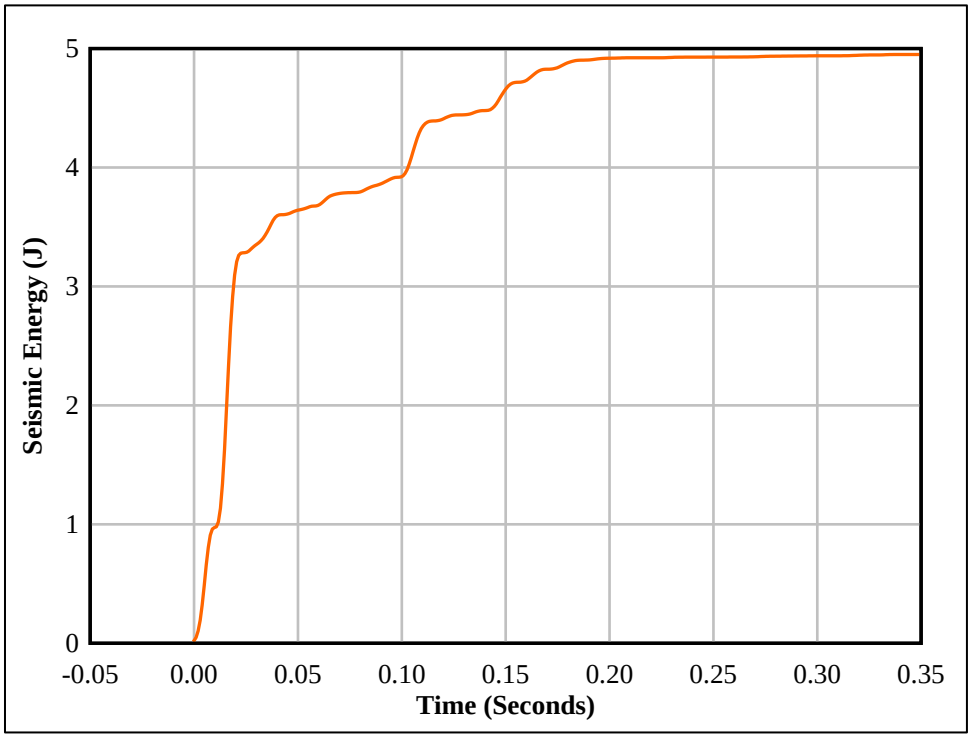

Figure 5.15. Test5-Seis6 radial particle energy waveform, calculated using seismic energy equation.

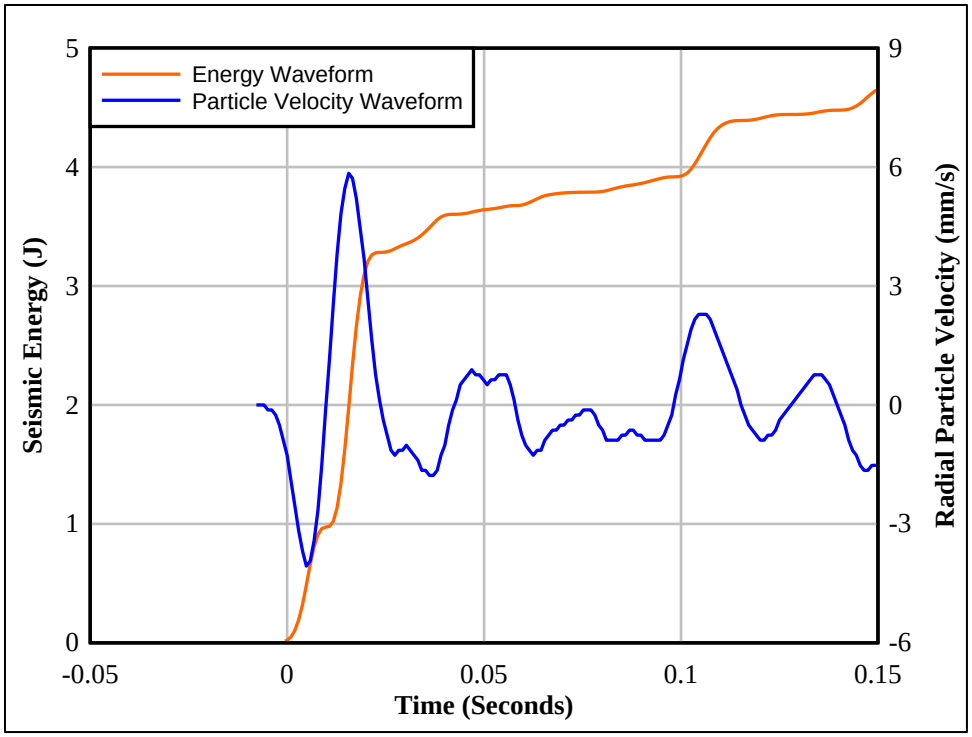

Figure 5.16. Seismic energy compared to radial particle velocity for Test5-Seis6.

5.3.3.1. Seismic energy equation summary. The process described in this section illustrates two issues with the original seismic energy equation and then adjusts for them. (a) The original seismic energy equation assumed the control surface was a full sphere; however, this is an overestimate since ground vibration propagates half-spherically in the ground. (b) The equation also theoretically calculates energy leaving a control surface; therefore, the use of the negative sign is not required in this analysis.

Of the three equations described in this section, the seismic energy equation is the only equation that accounts for the duration of the blast vibration waveform. It does so by calculating the accumulative energy passing the monitoring point over time due to the integration of the squared particle velocity waveform. Therefore, the final energy plot produced by the seismic energy equation is dissimilar in shape compared to the plots developed using the previous two energy methods.

The use of the integral of the particle velocity waveform continues to be a potential issue with these calculations. The seismic energy equation is completely dependent on the waveform produced by the integral; therefore, if the integral calculates incorrect values, the results of the calculations are directly affected.

5.4. SUMMARY

This section described a number of drawbacks of the Z-Curve and the PPV versus scaled distance plot. In an effort to lay a foundation for a new method that addresses these drawbacks, this section also presented three methods that could be used to calculate the vibration energy. Examples of each method are also presented. Though the methods have various drawbacks, as discussed, the section gave the initial framework for a more

comprehensive method of evaluating blast vibration energy and potential structural effects. Additional work is required to produce and prove a method of calculating blast vibration energy and accurately define the energy relationship of blast vibrations.

The first method that was presented is the calculation of energy using Newton's Second Law, or the force equation. This equation is used to calculate the work of the radial component of the vibration by incorporating the mass of the particle, radial acceleration waveform, and radial displacement waveform. The acceleration waveform is the significant variable in this equation, although the displacement values cause the energy waveform to trend negative since displacement theoretically has opposite sign conventions than the acceleration. The maximum absolute value of the energy estimated by this equation was 0.1 J for the Test5-Seis6 seed waveform.

The second method presented was the Hugoniot equation of state, which relates stress to the rock density, radial particle velocity, radial propagation velocity, and the unitless value *s*, which was shown to be insignificant to the equation when applied to elastic vibration waveforms. The stress values produced by the equation are used to calculate the vibration energy by including two additional factors: the surface area over which the stress is distributed and the displacement. The density, surface area, and propagation velocity are constant; therefore, the two variables in the equation are the particle velocity and the displacement. However, the particle velocity is the driving variable in this calculation. The maximum absolute value of the energy calculated by this equation for the Test5-Seis6 seed waveform was 1.1 J.

The seismic energy equation is the final method for calculating vibration energy that was presented. The seismic energy equation was altered for this study to address two

features of the equation that do not apply to this application. The altered equation relates the vibration energy to the surface area of the particle over which the vibration is distributed, the rock density, the propagation velocity, and the integral of the square of the particle velocity with respect to time. Therefore, the final energy waveform is driven by the values produced by the integral of the square of the particle velocity, which is the only variable in the equation. The total value of the energy calculated by this equation for the Test5-Seis6 seed waveform was 4.9 Joules. This energy value is the greatest value produced by the three methods, although it is an accumulative energy value, as opposed to the values produced by the first two methods, which are instantaneous energy values. Finally, in addition to the energy equation being a function of the amplitude and frequency of the particle velocity waveform, the seismic energy method also accounts for the duration of the waveform.

In summary, there is no proven method for calculating the vibration energy since actual energy values are not known and could not be directly measured. Additionally, there is a drawback to all three methods, in that the integral of the particle velocity trends away from equilibrium. This value should trend back to zero since the monitoring location is not displaced from equilibrium. Finally, it appears that the force method is acceleration-driven, the Hugoniot equation of state method is velocity driven, and the seismic energy equation can be said to be displacement driven since it is driven by the integral of the squared particle velocity waveform over time. Therefore, each method is driven by a different kinematic value. The first step to identifying the best energy calculation method could be by determining the kinematic value that is most significant to the seismic energy. Based on Equation 12, energy is theoretically proportional to the

square of the maximum particle displacement. Therefore, the seismic energy equation is theoretically the most applicable equation of the three energy calculation methods.

This section proves that modern computers and software can be used to easily approximate vibration energy using a number of different methods. These methods are not intended to replace the Z-Curve method or the SRSD versus PPV method. However, they do provide a simple means of using a typical seismogram to evaluate blast vibrations using the important vibration features, whereas current methods do not include all of the vibration features and factors in one method.

The energy of a vibration wave could be compared between different blasthole configurations. It could also be directly related to total available charge energy, compared with the distance from the charge, and evaluated to determine confinement effects or geologic effects. Therefore, a proper seismic energy equation could improve on the commonly used methods of the Z-Curve and scaled distance versus PPV plot by including all of the important aspects of a blast wave and variables that affect a blast wave.

Another potential outcome of using energy is the ability to plot monitoring distance versus energy values from an array of sample points at a specific time value, assuming each sample is triggered simultaneously. An energy versus distance plot for a specific time during the vibration event could provide a depiction of the energy profile of a blast wave. In other words, the shape of the vibration wave could be plotted. This type of plot is difficult to construct due to the long duration of a blast vibration. A large number of seismographs would need to be chained together over a large distance to accurately depict the waveshape.

Future work on this topic includes the determination of the part of the energy waveform that is of most interest between the accumulative energy or peak energy. Additionally, the effects that a multiple-charge blast has on the energy calculations could also be determined. Finally, the power, or energy rate, could be important to determining the effects of blast vibrations on structures.

Calculating the energy or power of a blast vibration does not only allow for the inclusion of the important features of a blast vibration and variables that affect a blast wave. Energy and power are terms with units that are more easily understood by the general public. Therefore, a plot of energy over time, although similar in shape to the acceleration, particle velocity or displacement waveforms, is also more easily understood by the general public.

6. CONCLUSIONS

6.1. OVERVIEW

This study identified a major shortcoming in the current blasting industry: a current tool or model does not exist that evaluates all of the important blast vibration features and variables that affect blast vibrations. The first primary contribution of this study is the application of multiple regression analyses to a signature hole dataset compiled from multiple sources to determine the statistically significant variables that contribute to variations in blast vibrations. The second primary contribution of the study is the comparison of energy equations that are applied to vibration traces in order to approximate the vibration energy passing a monitoring point. Most of the contributions of this study may not be significant to the majority of mining operations that are only concerned with far-field vibrations; however, mining operations concerned with highwall stability and/or nearby structures or construction and demolition blasting operations near structures will find the results and conclusions of this study valuable.

This document is divided into three primary units. The first of these units was the literature review, which provided a background of blast vibration characteristics and features, variables that affect vibrations to varying degrees, and methods currently used in the blasting industry to evaluate vibrations. The second unit was a combination of a signature hole vibration data collection phase and statistical evaluation phase of the dataset. The collection of signature hole data included a compilation of data from various sources, including field tests designed for this specific project. The statistical evaluation phase included a number of multiple regression analyses on the dataset to determine the

statistically significant variables that affect vibration amplitude, frequency and duration. The final unit focused on blast-induced seismic energy calculations. Three methods were presented. Details of each method, sample calculations, and the results and drawbacks of each method were discussed.

This section summarizes and discusses the conclusions of each of the three primary units. Finally, the section also provides a summary of novel contributions from this research and recommendations for future work based on this study.

6.2. LITERATURE REVIEW

The literature review of this work presented the important features of blast-induced vibrations, variables that affect blast vibrations, and methods currently used to evaluate blast vibrations.

The blasting industry and regulations are overly dependent on outdated methods of vibration characterization. These methods are primarily the Z-Curve and scaled distance versus PPV plots. These tools are used with highly variable data to produce images that are difficult for many, especially the public, to understand. In some cases, analyses with these tools are not practically sound.

With respect to the scaled distances versus PPV plots, the data is plotted with logarithmic axis scaling. As discussed, the depiction of low scaled distances, where vibrations are nonlinear, is especially misleading due to the high variability of the nonlinear attenuation of the blast vibration in the near-field.

The literature review also identified issues with standard blasting seismographs, which do not have sample rates high enough for research applications or near-field

compliance monitoring. It is also difficult to mount standard seismographs for vibrations in the near-field. The preferred method for monitoring in that range is with accelerometers.

6.3. SIGNATURE HOLE DATA ANALYSIS

The signature hole study incorporated a signature hole dataset with data from various sources that included variables such as charge weight, monitoring distance, charge geometry, and geology. This type of compilation of signature hole data, along with the accompanying statistical dataset, has not been done before.

The analysis included a field study that produced vibration data from very near the charge and from larger monitoring distances. The field work was important in that it provided a hands-on perspective of signature hole data collection methods and practices, including experiment design, equipment selection, and data processing. One important outcome of this procedure showed that near-field propagation velocity is equivalent to far-field propagation velocity for elastic vibrations.

The dataset of signature holes included a total of 105 data points. The dataset was evaluated using regression plots at rounded distances to provide a qualitative method of evaluation and multiple regression analysis to determine the relative effect of the variables on vibration amplitude, frequency, and duration. The qualitative and quantitative analyses showed the following results for the signature hole dataset:

- Scaled distance equations can be relatively accurate in the linear amplitude attenuation range of blast vibrations; however, in the near-field where the vibration amplitudes attenuate non-linearly, this is not the case. The

variability of peak particle velocity values in the near-field makes regression modeling imprecise.

- Monitoring distances can be rounded in order to group data and assess the effects of variables at each rounded distance.
- Geology appears to affect vibration amplitudes at distances greater than 76 m (250 ft) where the vibration attenuation becomes linear. This contradicts the USBM report that stated the effects of geology occur at distances greater than 152 m (500 ft) (Siskind et al., 1985), but agrees with the USBM report that stated the effects of geology occur at distances greater than 91 m (300 ft) (Siskind et al., 1989).
- Total charge weight is more significant than charge weight per unit length to elastic blast vibrations because of the relatively minimal detonation time compared to vibration frequency.
- Table 6.1 and Table 6.2 provide the results from the multiple regression analyses. The tables summarize the significant and insignificant variables that affect each blast vibration features.

Table 6.1. Summary of statistically significant variables.

	PPV	**Principal Frequency**	**Dominant Frequency**	**Duration**
Full Dataset	N/A	Geology	Stemming Length Geology Log(Distance)	Geology Log(Distance)
Near-Field	Log(Distance) Charge Weight Stemming Length	Geology	Log(Distance) Stemming Length	Geology

Table 6.2. Summary of statistically insignificant variables.

	PPV	Principal Frequency	Dominant Frequency	Duration
Full Dataset	N/A	Log(Distance) Charge Weight Charge Diameter Stemming Length Charge Length Density	Charge Weight Charge Diameter Charge Length Density	Charge Weight Charge Diameter Stemming Length Charge Length Density
Near-Field	Geology Charge Diameter Charge Length Density	Log(Distance) Charge Weight Charge Diameter Stemming Length Charge Length Density	Geology Charge Weight Charge Diameter Charge Length Density	Log(Distance) Charge Weight Charge Diameter Stemming Length Charge Length Density

- Overall, signature hole vibrations are affected by monitoring distance, geology, charge weight, and confinement, assuming stemming indicates confinement for the fully confined charges.
- This evaluation showed that the charge diameter and geology of each data point is related; therefore, any analysis that produced charge diameter or charge cross-sectional area as statistically significant was most likely signifying that the geology was actually the significant variable. A larger dataset with a greater range of charge diameters from each source is required to confirm this assumption.
- Charge diameter and charge length do not affect elastic vibrations at the distances that were monitored; therefore, the effect of the charge geometry variables on blast vibrations is statistically insignificant. However, charge geometry does affect vibrations in the shock region around the blasthole where the shock front is similar to or significantly smaller in duration than

the charge length and detonation duration. There is most likely a transition area where the elastic vibrations are affected by charge diameter and charge length; however, the signature hole dataset cannot be used to define the transition area due to the lack of data in that transition area.

6.4. BLAST-INDUCED SEISMIC ENERGY METHOD

This study lays the foundation for improving on the Z-Curve and the scaled distance versus PPV plots. It is possible to use a vibration waveform produced by a standard blast vibration seismograph in calculations designed to estimate the energy of the vibration. However, the accuracy of these calculations remains to be seen. Three methods and examples of each method are presented. The examples show that:

- The force equation is most affected by particle acceleration and trends negative. The value produced by this equation was the lowest of the values produced by the three equations.
- The Hugoniot equation of state was most affected by the particle velocity and calculates stress, which is converted to energy. The value produced by this equation was the median value of the values produced by the three equations.
- The seismic energy equation was most affected by the integral of the squared particle velocity, which means it is displacement driven. The value produced by this equation was the largest of the values produced by the three equations.

- Amplitude, frequency, and duration can be included in an energy calculation.
- The results from the equations can be compared against distance, charge weight (or more likely theoretical available charge energy), geology, and confinement since these are the statistically significant variables.
- Energy equations can also be used to generate the energy distribution of a blast vibration over distance at a specific point in time.
- Blast vibration energy can be directly related to structural strength and used to determine the effect of a vibration on a target structure.
- The blast vibration energy equations can be used to produce a plot of energy versus time, which can be easier to understand and related to by the public.

6.5. SUMMARY OF NOVEL CONTRIBUTIONS

The following points give a summary of novel contributions provided by this research study.

- Identification of shortcomings pertaining to the Z-Curve and PPV versus scaled distance plots.
- Application of multiple regression analyses to a compilation of signature hole data from more than one location.
- Conclusion that the distance from the blast, charge weight, confinement, and geology are the statistically significant variables that affect blast vibrations. However, the vibrations produced by multi-charge production

blasts will most likely not be as noticeably affected by these variables as the single charges studied in this research. These results are most important when studying vibrations at small distances from the charge.

- Too often charge confinement and geology are ignored in blast monitoring. Including these variables and identifying the effect of these variables in blast vibration evaluations should help a blasting engineer to better understand the outcome of a particular blast design.
- Blast vibration energy calculations are a relatively new field of study. The calculations can be used to approximate blast vibration energy; however, the accuracy of each of these equations is unknown.
- The vibration energy equations can combine all of the important blast vibration features into one energy waveform. The energy waveform can be evaluated using the statistically significant variables that affect blast vibrations. Therefore, once sufficiently understood, energy calculations could be used to evaluate all of the important blast vibration features and variables in one chart.

6.6. RECOMMENDATIONS FOR FUTURE WORK

The following points give recommendations for future work pertaining to the topic of this dissertation.

- Increase the sample size and background knowledge of the data sources to improve the statistical analysis and strengthen conclusions made from the statistical analysis. This is especially the case in the near-field.

- Compile a dataset where geology and charge diameter are not interrelated and regenerate a portion of the statistical analysis to conclude which variable truly has a greater effect on frequency and duration. This study assumes the geology has a greater effect due to various reasons mentioned previously.
- Determine how to best approximate particle displacement or monitor particle displacement.
- Determine a proper energy equation that can be used to accurately calculate the energy of a blast vibration.
- Develop a method to directly monitor the energy of a blast vibration.
- Identify important energy values of a blast vibration. These values could be the peak energy or sum energy value over time.
- Determine a new method for comparing energy to potential structural damage in the same way the Z-Curve does this.
- Collect data closer to the blasthole to determine the distance where the charge length or charge weight per unit length have an effect on vibrations and the total charge weight is less statistically significant.
- Develop a better method of using scaled distance in the near-field with vibration energy.

APPENDIX A

LIMESTONE QUARRY SEISMOGRAMS

Appendix A provides the seismograms that were produced by the seismograph arrays during the limestone quarry signature hole tests. Each seismogram was produced by White Industrial Seismology Seismograph Data Analysis® software and includes radial, vertical, transverse, and vector sum waveforms.

File: test1-seis1.dtb
Number: 007
Date and Time: 9/18/2013 4:37:00 PM
SN: 0018
Seismic Trigger: 0.0800 in/sec
Air Trigger: 142 dBL
Sample Rate: 2048
Duration: 4 Seconds
Pre-Trigger: 0.250 Second
Gain: 1.0x
Voltage: 6.3

Peaks and Frequencies	Graph Information
PPV Maximum: 9.28 in/sec (0.01416 sec)	Duration: -0.250 s To: 4.000 s
Radial: 9.28 in/sec @ 21.7 Hz (0.01416 sec)	Seismic Scale: 9.60 in/sec (2.40 in/sec/div)
Vertical: 8.96 in/sec @ 31.0 Hz (0.00293 sec)	Time Intervals: 0.50 sec
Transverse: 2.48 in/sec @ 2.4 Hz (0.09668 sec)	
Vector Sum: 10.8 in/sec (0.00537 sec)	
Last Calibration Date: 9/9/2008	

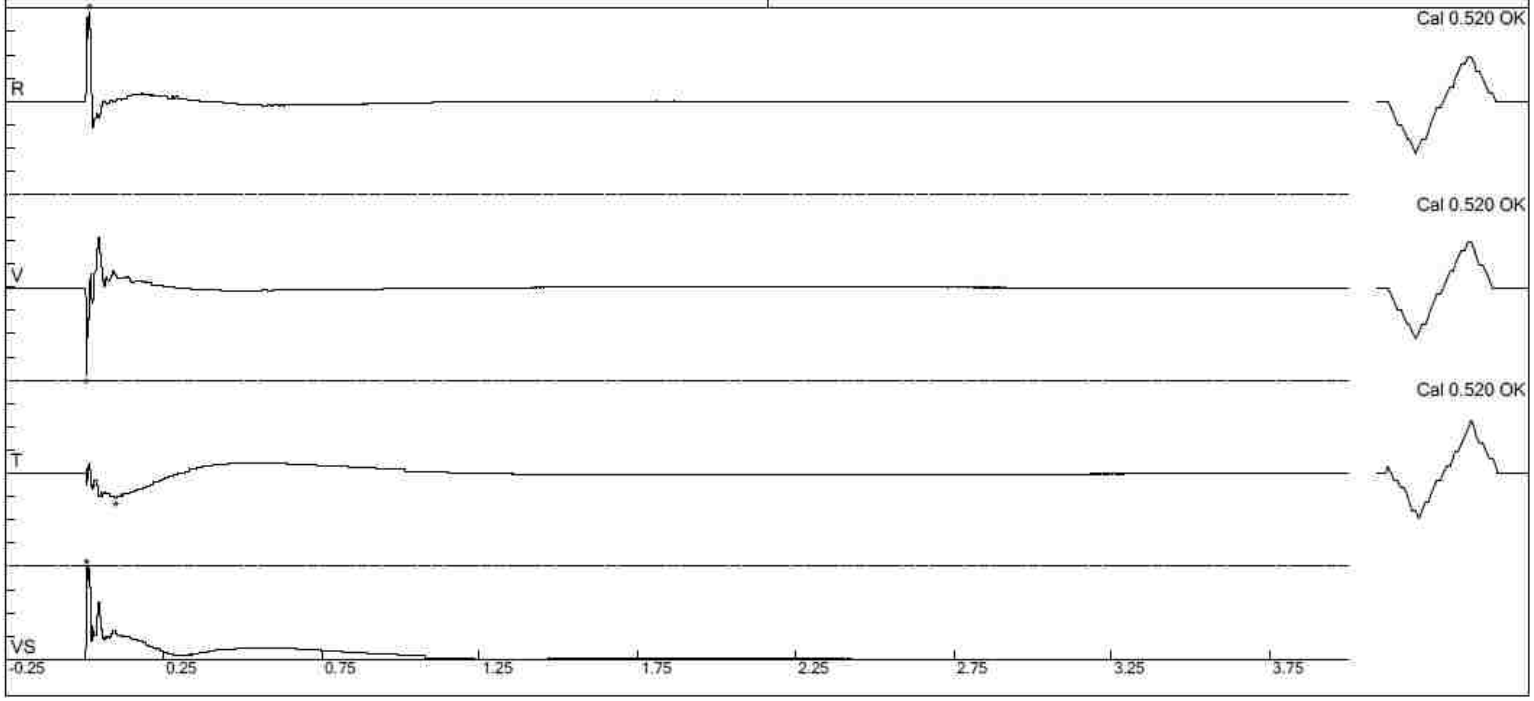

File: test1-seis2.dtb
Number: 002
Date and Time: 9/18/2013 4:25:00 PM
SN: 0017
Seismic Trigger: 0.320 in/sec
Air Trigger: 142 dBL
Sample Rate: 2048
Duration: 4 Seconds
Pre-Trigger: 0.250 Second
Gain: 1.0x
Voltage: 6.3

Peaks and Frequencies	Graph Information
PPV Maximum: 6.40 in/sec (0.00781 sec)	Duration: -0.250 s To: 4.000 s
Radial: 6.40 in/sec @ 20.0 Hz (0.00781 sec)	Seismic Scale: 6.80 in/sec (1.70 in/sec/div)
Vertical: 4.64 in/sec @ 30.1 Hz (0.00586 sec)	Time Intervals: 0.50 sec
Transverse: 1.84 in/sec @ 3.0 Hz (0.06543 sec)	
Vector Sum: 6.87 in/sec (0.00781 sec)	
Last Calibration Date: 9/9/2008	

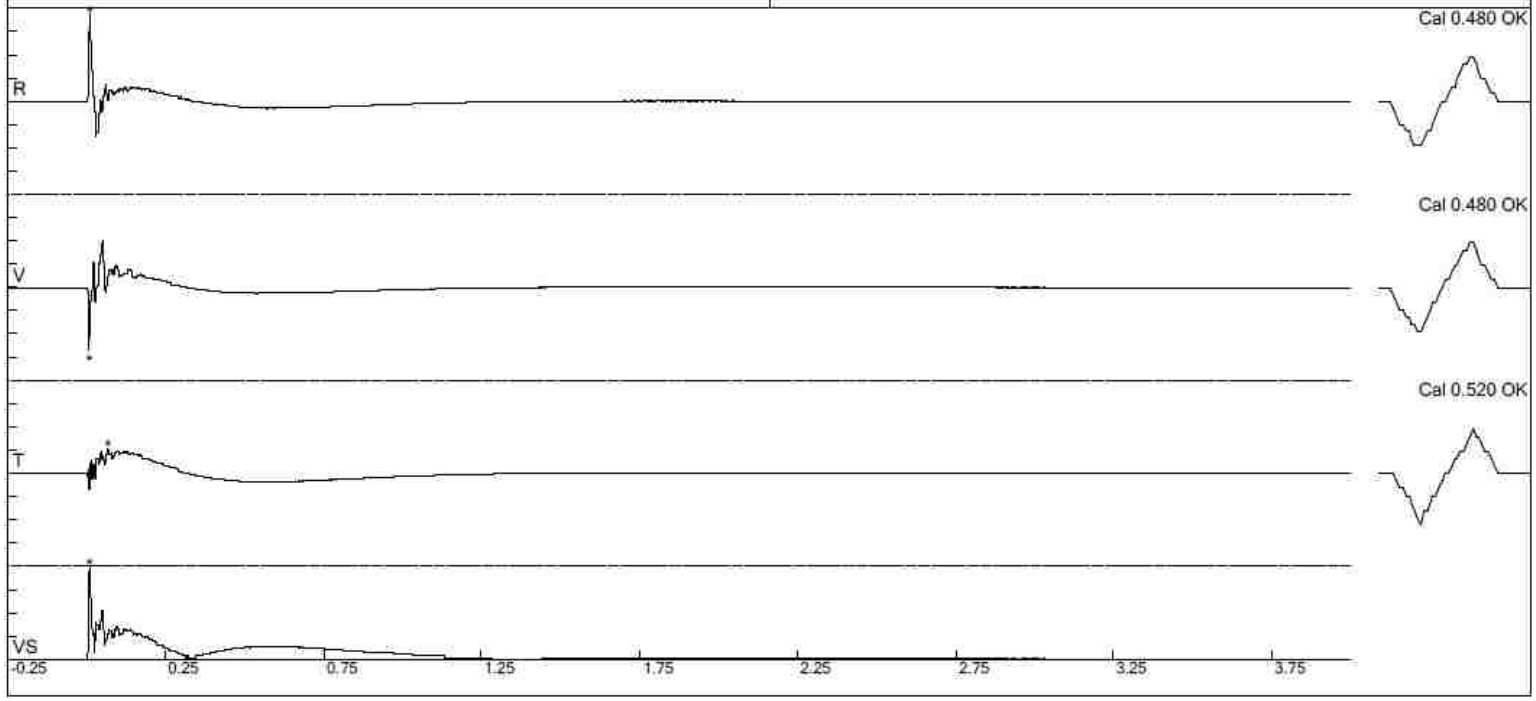

File: test1-seis3.dtb
Number: 004
Date and Time: 7/11/1998 6:47:00 AM
SN: 0016
Seismic Trigger: 0.0800 in/sec
Air Trigger: 142 dBL
Sample Rate: 2048
Duration: 4 Seconds
Pre-Trigger: 0.250 Second
Gain: 1.0x
Voltage: 6.3

Peaks and Frequencies	Graph Information
PPV Maximum: 4.32 in/sec (0.03613 sec)	Duration: -0.250 s To: 4.000 s
Radial: 2.04 in/sec @ 18.6 Hz (0.01514 sec)	Seismic Scale: 4.40 in/sec (1.10 in/sec/div)
Vertical: 4.32 in/sec @ 32.0 Hz (0.03613 sec)	Time Intervals: 0.50 sec
Transverse: 1.12 in/sec @ 20.0 Hz (0.07568 sec)	
Vector Sum: 4.71 in/sec (0.03613 sec)	
Last Calibration Date: 9/9/2008	

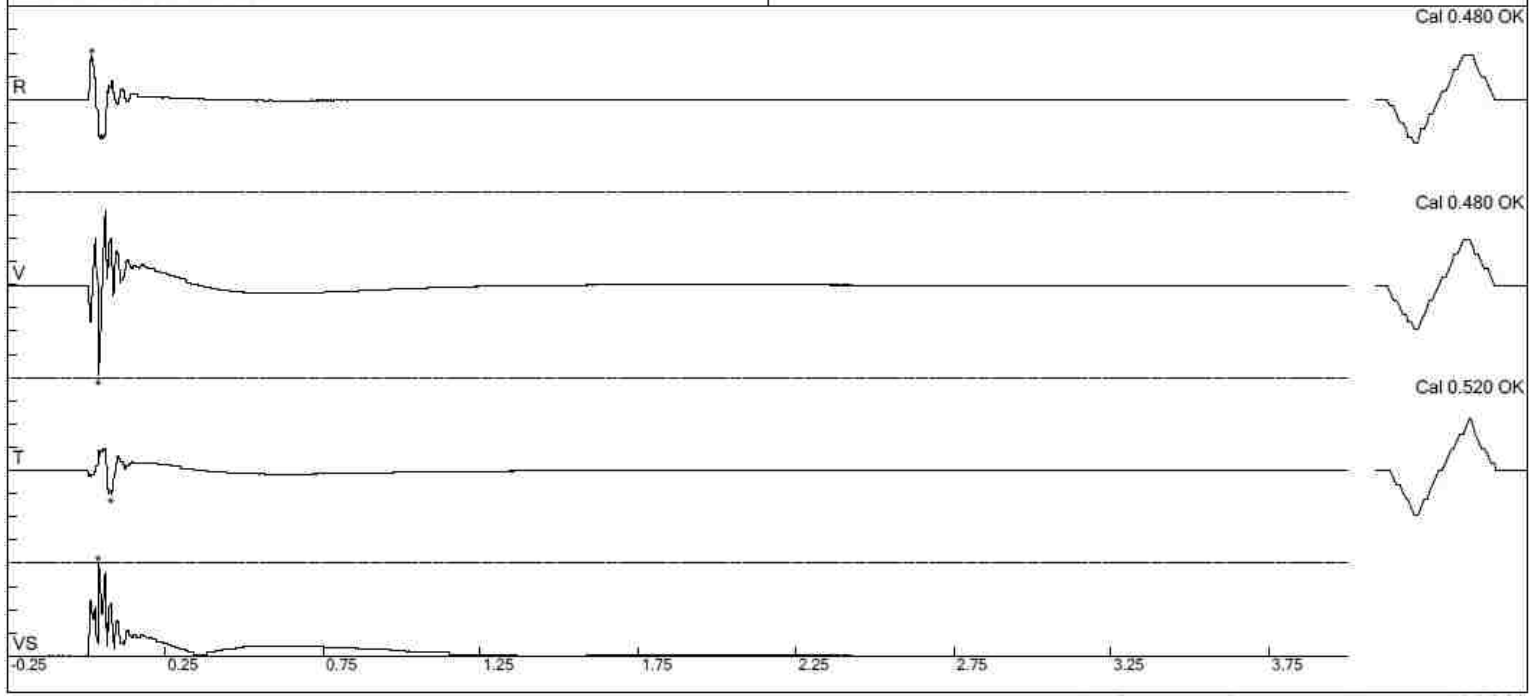

File: test1-seis4.dtb
Number: 006
Date and Time: 9/18/2013 4:32:00 PM
SN: 0492
Seismic Trigger: 0.0400 in/sec
Air Trigger: 142 dBL
Sample Rate: 2048
Duration: 4 Seconds
Pre-Trigger: 0.250 Second
Gain: 2.0x
Voltage: 6.3

Peaks and Frequencies	Graph Information
PPV Maximum: 1.52 in/sec (0.02197 sec)	Duration: -0.250 s To: 4.000 s
Radial: 1.52 in/sec @ 30.1 Hz (0.02197 sec)	Seismic Scale: 1.60 in/sec (0.400 in/sec/div)
Vertical: 1.36 in/sec @ 64.0 Hz (0.01709 sec)	Time Intervals: 0.50 sec
Transverse: 0.620 in/sec @ 93.0 Hz (0.01660 sec)	
Vector Sum: 1.53 in/sec (0.02246 sec)	
Last Calibration Date: 5/27/2010	

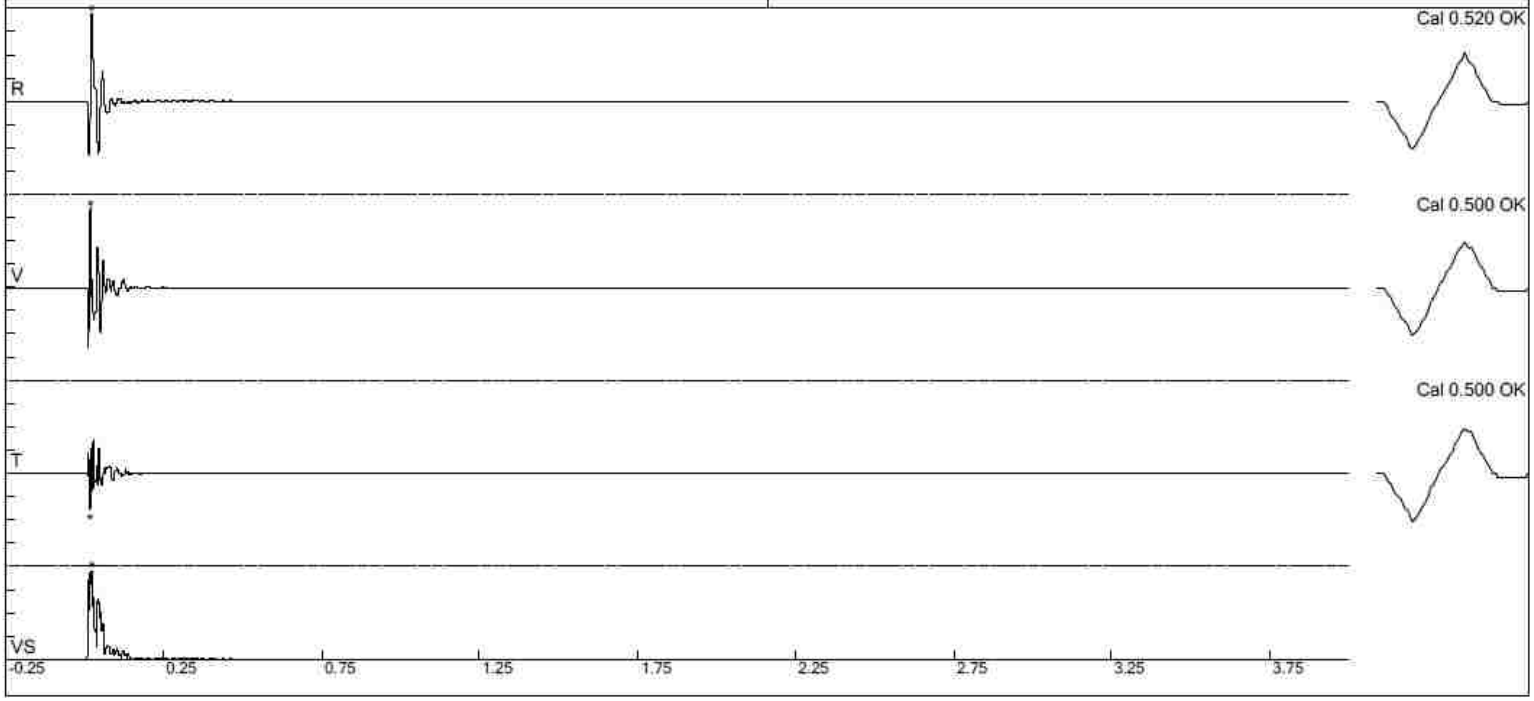

File: test1-seis5.dtb
Number: 014
Date and Time: 9/18/2013 4:39:00 PM
SN: 0180
Seismic Trigger: 0.0200 in/sec
Air Trigger: 142 dBL
Sample Rate: 2048
Duration: 4 Seconds
Pre-Trigger: 0.250 Second
Gain: 2.0x
Voltage: 6.3

Peaks and Frequencies	Graph Information
PPV Maximum: 1.28 in/sec (0.02783 sec)	Duration: -0.250 s To: 4.000 s
Radial: 1.28 in/sec @ 60.2 Hz (0.02783 sec)	Seismic Scale: 1.40 in/sec (0.350 in/sec/div)
Vertical: 0.380 in/sec @ 51.2 Hz (0.05078 sec)	Time Intervals: 0.50 sec
Transverse: 0.650 in/sec @ 33.0 Hz (0.05420 sec)	
Vector Sum: 1.36 in/sec (0.02783 sec)	
Last Calibration Date: 5/27/2010	

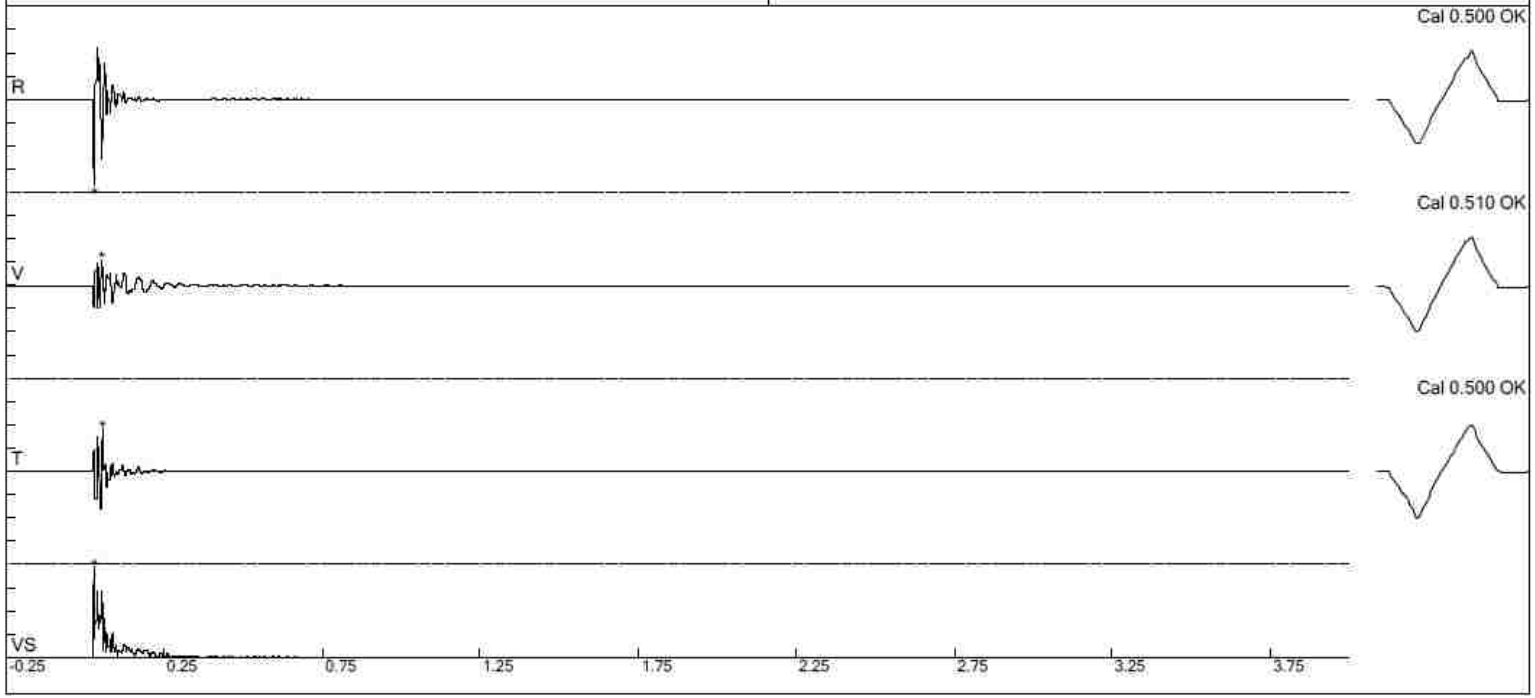

File: test2-seis1.dtb
Number: 010
Date and Time: 11/7/2013 5:21:00 PM
SN: 0018
Seismic Trigger: 0.0800 in/sec
Air Trigger: 142 dBL
Sample Rate: 2048
Duration: 4 Seconds
Pre-Trigger: 0.250 Second
Gain: 1.0x
Voltage: 6.4

Peaks and Frequencies	Graph Information
PPV Maximum: 14.9 in/sec (0.10449 sec)	Duration: -0.250 s To: 4.000 s
Radial: 6.88 in/sec @ 7.9 Hz (0.00439 sec)	Seismic Scale: 15.2 in/sec (3.80 in/sec/div)
Vertical: 14.9 in/sec @ 3.1 Hz (0.10449 sec)	Time Intervals: 0.50 sec
Transverse: 3.36 in/sec @ 3.0 Hz (0.04102 sec)	
Vector Sum: 15.1 in/sec (0.10449 sec)	
Last Calibration Date: 9/9/2008	

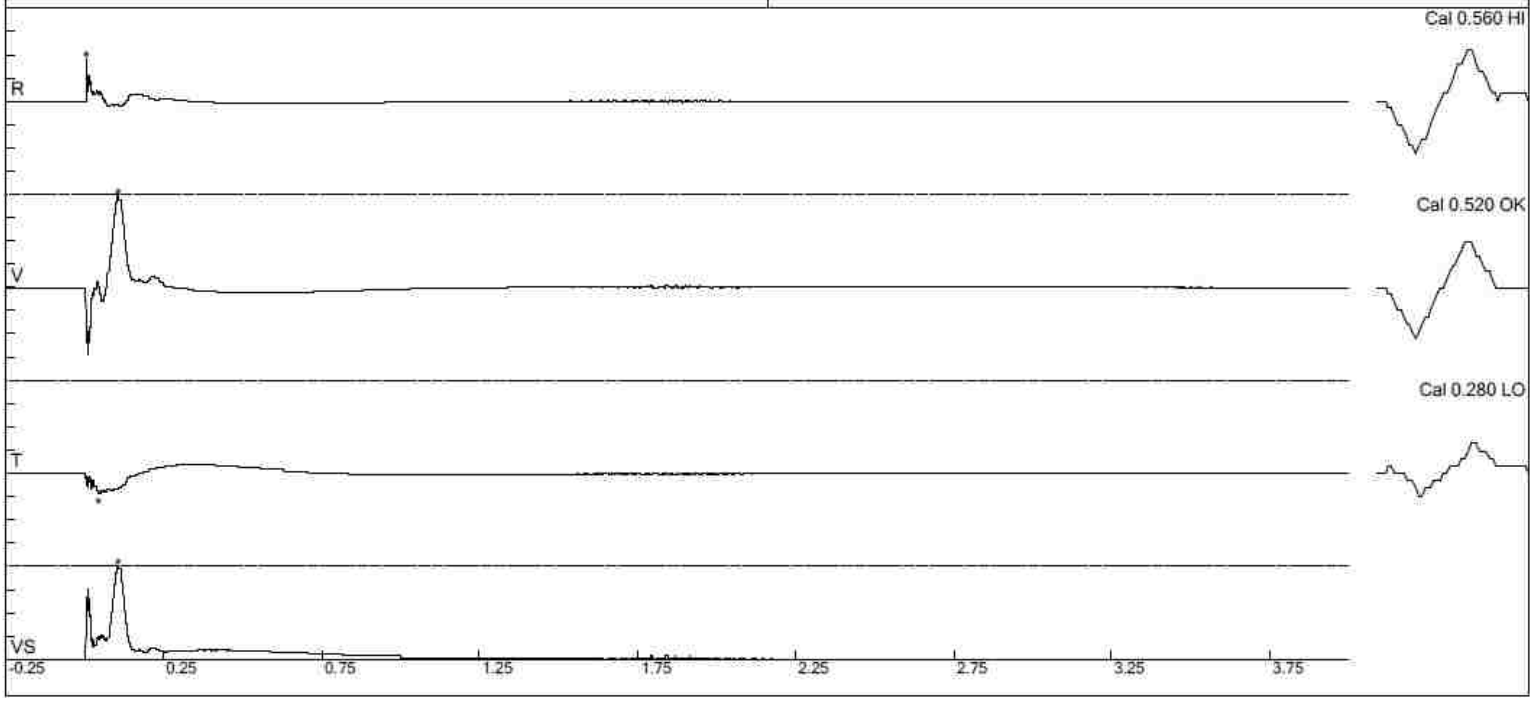

File: test2-seis2.dtb
Number: 004
Date and Time: 11/7/2013 5:07:00 PM
SN: 0017
Seismic Trigger: 0.320 in/sec
Air Trigger: 142 dBL
Sample Rate: 2048
Duration: 4 Seconds
Pre-Trigger: 0.250 Second
Gain: 1.0x
Voltage: 5.3

Peaks and Frequencies	Graph Information
PPV Maximum: 5.44 in/sec (0.00342 sec)	Duration: -0.250 s To: 4.000 s
Radial: 2.88 in/sec @ 3.7 Hz (0.00684 sec)	Seismic Scale: 5.60 in/sec (1.40 in/sec/div)
Vertical: 5.44 in/sec @ 19.6 Hz (0.00342 sec)	Time Intervals: 0.50 sec
Transverse: 0.960 in/sec @ 146.2 Hz (0.00488 sec)	
Vector Sum: 5.83 in/sec (0.00391 sec)	
Last Calibration Date: 9/9/2008	

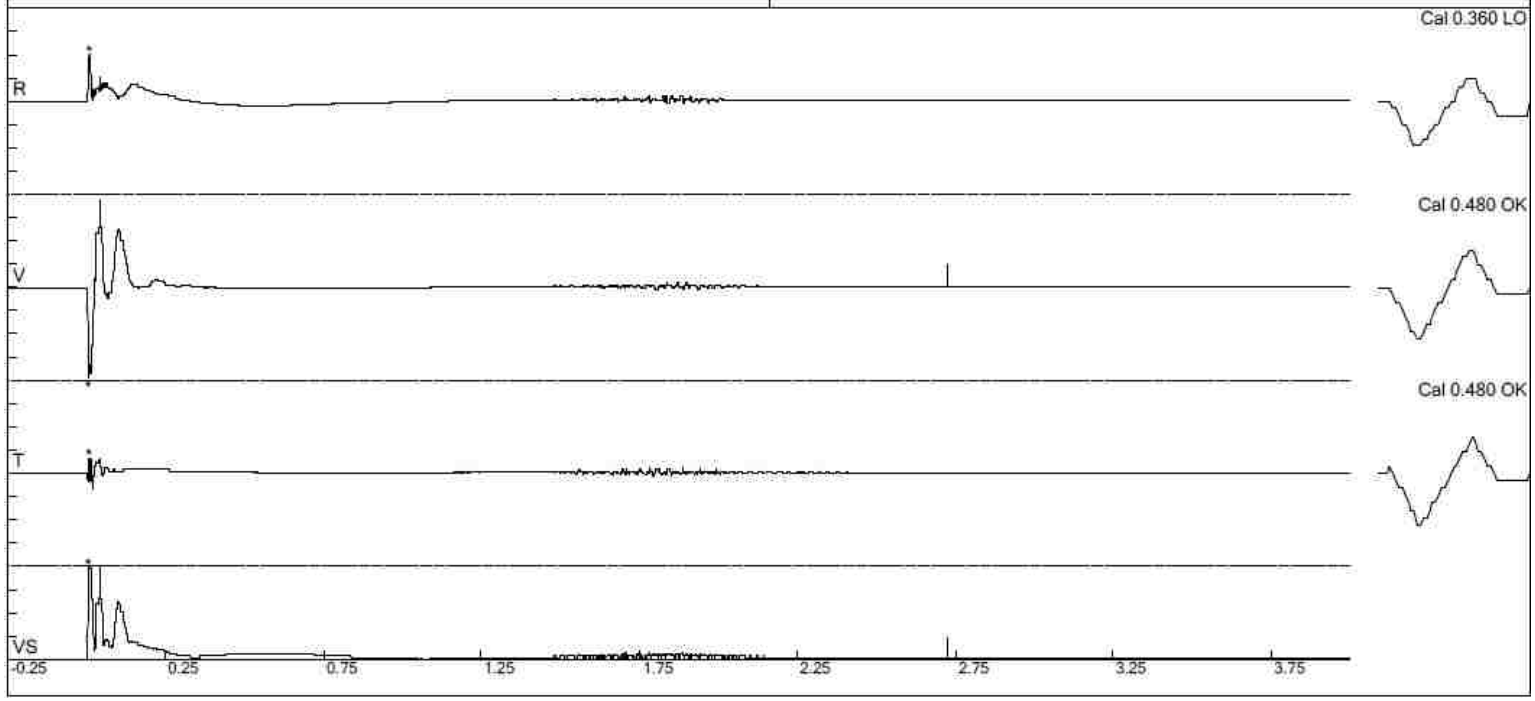

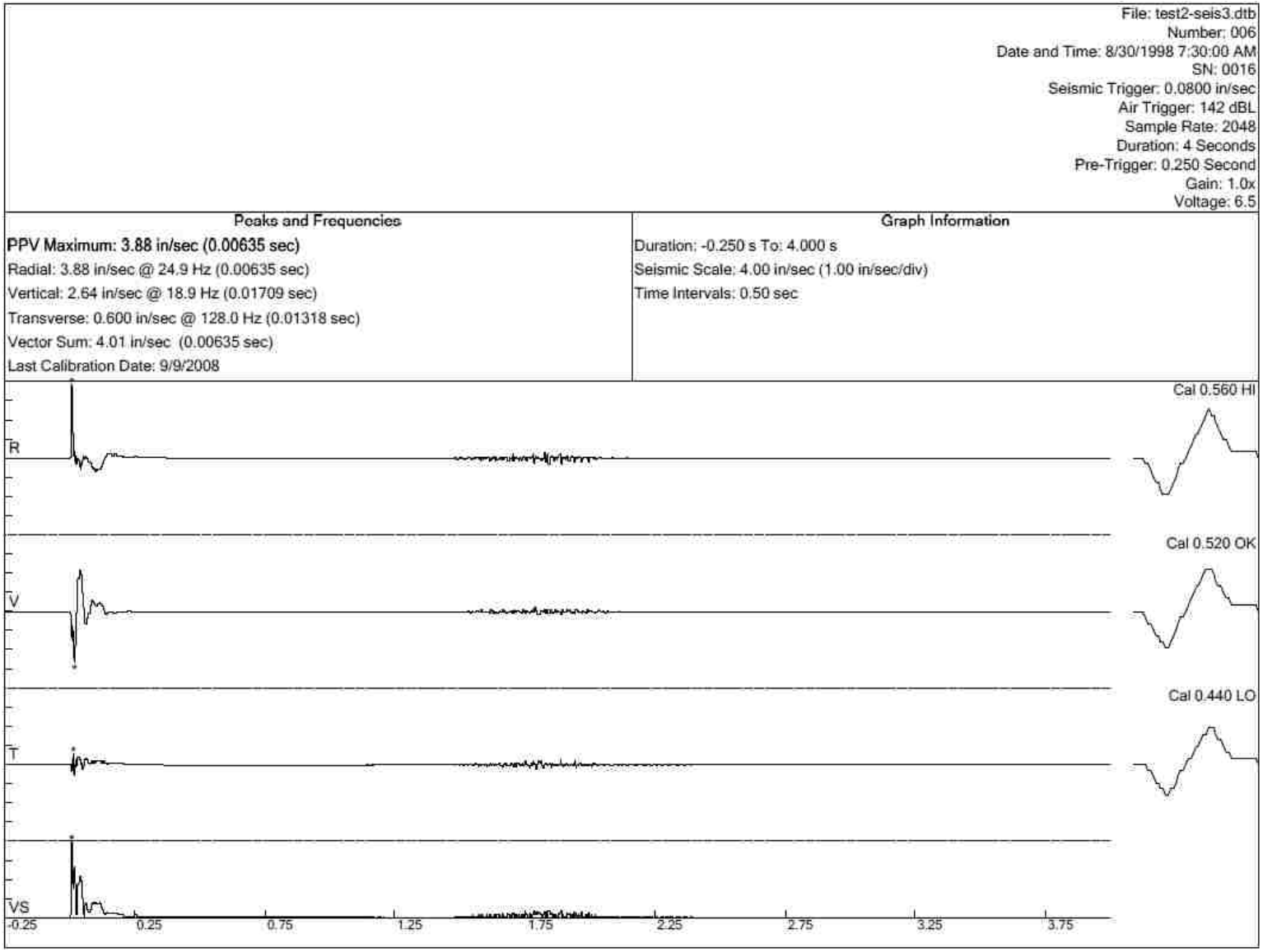
File: test2-seis3.dtb
Number: 006
Date and Time: 8/30/1998 7:30:00 AM
SN: 0016
Seismic Trigger: 0.0800 in/sec
Air Trigger: 142 dBL
Sample Rate: 2048
Duration: 4 Seconds
Pre-Trigger: 0.250 Second
Gain: 1.0x
Voltage: 6.5
Peaks and Frequencies
PPV Maximum: 3.88 in/sec (0.00635 sec)
Radial: 3.88 in/sec @ 24.9 Hz (0.00635 sec)
Vertical: 2.64 in/sec @ 18.9 Hz (0.01709 sec)
Transverse: 0.600 in/sec @ 128.0 Hz (0.01318 sec)
Vector Sum: 4.01 in/sec (0.00635 sec)
Last Calibration Date: 9/9/2008
Graph Information
Duration: -0.250 s To: 4.000 s
Seismic Scale: 4.00 in/sec (1.00 in/sec/div)
Time Intervals: 0.50 sec
Cal 0.560 HI
R
Cal 0.520 OK
V
Cal 0.440 LO
T
VS
-0.25
0.25
0.75
1.25
1.75
2.25
2.75
3.25
3.75

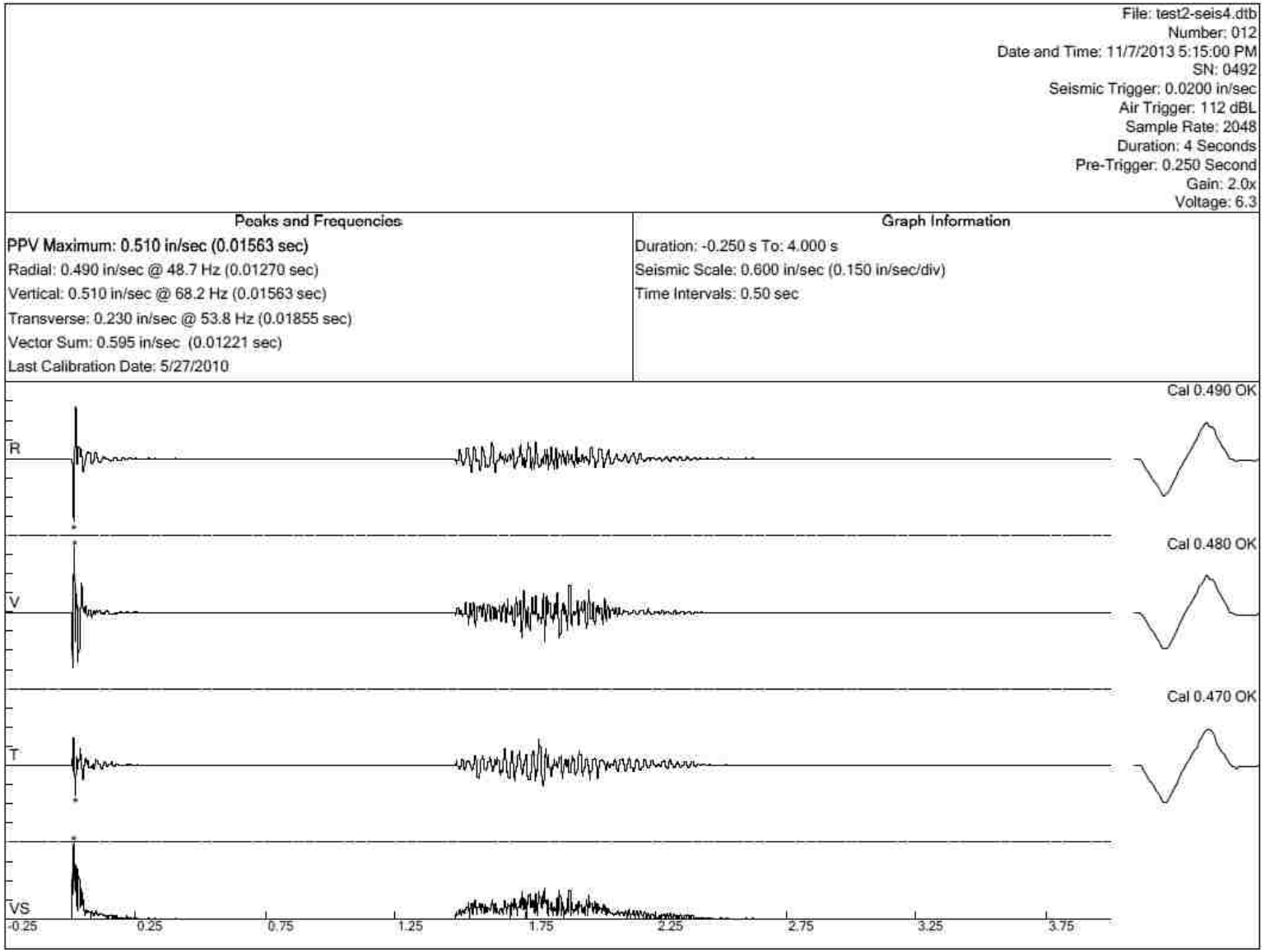
File: test2-seis4.dtb
Number: 012
Date and Time: 11/7/2013 5:15:00 PM
SN: 0492
Seismic Trigger: 0.0200 in/sec
Air Trigger: 112 dBL
Sample Rate: 2048
Duration: 4 Seconds
Pre-Trigger: 0.250 Second
Gain: 2.0x
Voltage: 6.3
Peaks and Frequencies
PPV Maximum: 0.510 in/sec (0.01563 sec)
Radial: 0.490 in/sec @ 48.7 Hz (0.01270 sec)
Vertical: 0.510 in/sec @ 68.2 Hz (0.01563 sec)
Transverse: 0.230 in/sec @ 53.8 Hz (0.01855 sec)
Vector Sum: 0.595 in/sec (0.01221 sec)
Last Calibration Date: 5/27/2010
Graph Information
Duration: -0.250 s To: 4.000 s
Seismic Scale: 0.600 in/sec (0.150 in/sec/div)
Time Intervals: 0.50 sec
Cal 0.490 OK
R
Cal 0.480 OK
V
Cal 0.470 OK
T
VS
-0.25
0.25
0.75
1.25
1.75
2.25
2.75
3.25
3.75

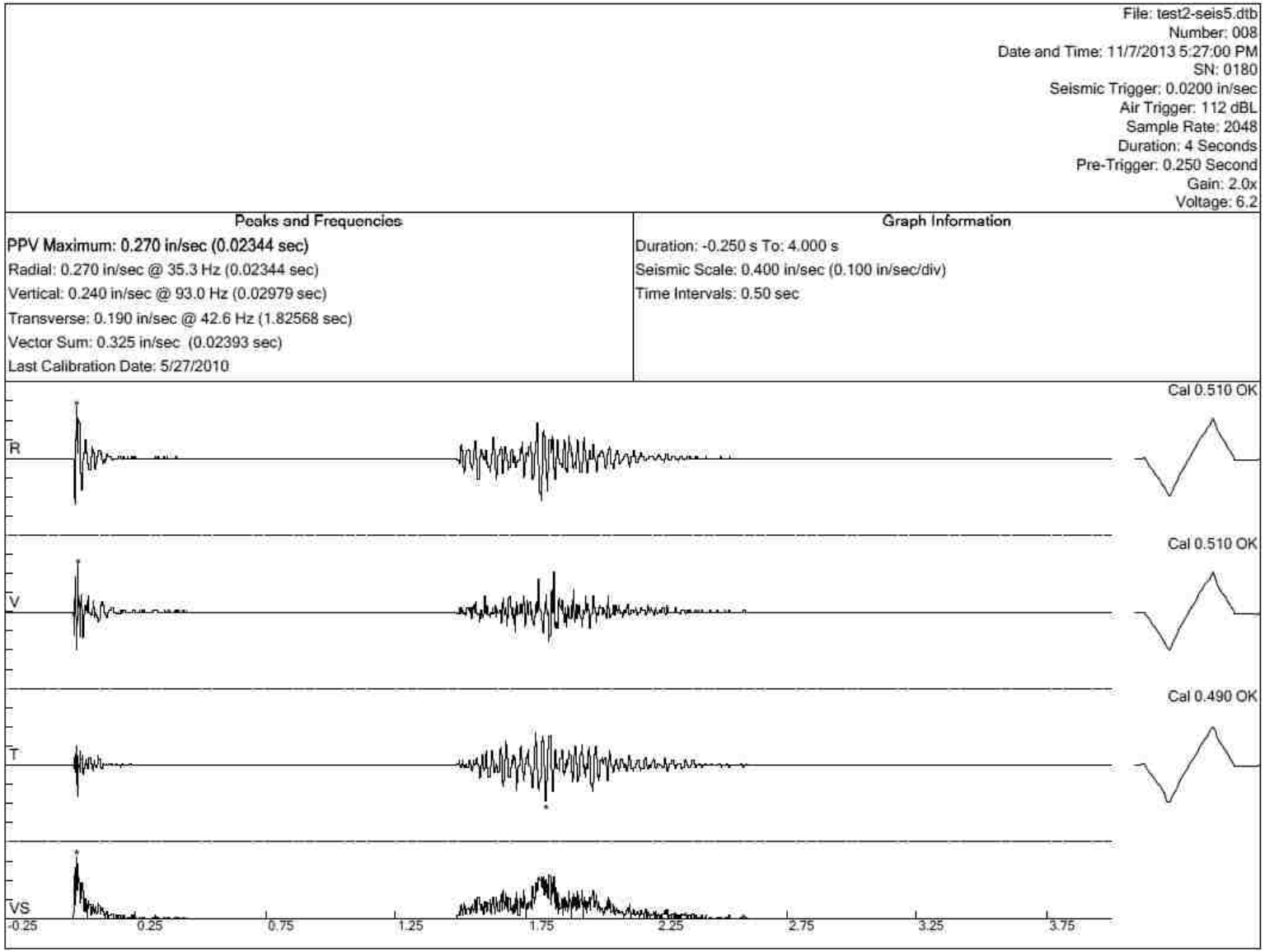
File: test2-seis5.dtb
Number: 008
Date and Time: 11/7/2013 5:27:00 PM
SN: 0180
Seismic Trigger: 0.0200 in/sec
Air Trigger: 112 dBL
Sample Rate: 2048
Duration: 4 Seconds
Pre-Trigger: 0.250 Second
Gain: 2.0x
Voltage: 6.2
Peaks and Frequencies
PPV Maximum: 0.270 in/sec (0.02344 sec)
Radial: 0.270 in/sec @ 35.3 Hz (0.02344 sec)
Vertical: 0.240 in/sec @ 93.0 Hz (0.02979 sec)
Transverse: 0.190 in/sec @ 42.6 Hz (1.82568 sec)
Vector Sum: 0.325 in/sec (0.02393 sec)
Last Calibration Date: 5/27/2010
Graph Information
Duration: -0.250 s To: 4.000 s
Seismic Scale: 0.400 in/sec (0.100 in/sec/div)
Time Intervals: 0.50 sec
Cal 0.510 OK
R
Cal 0.510 OK
V
Cal 0.490 OK
T
VS
-0.25
0.25
0.75
1.25
1.75
2.25
2.75
3.25
3.75

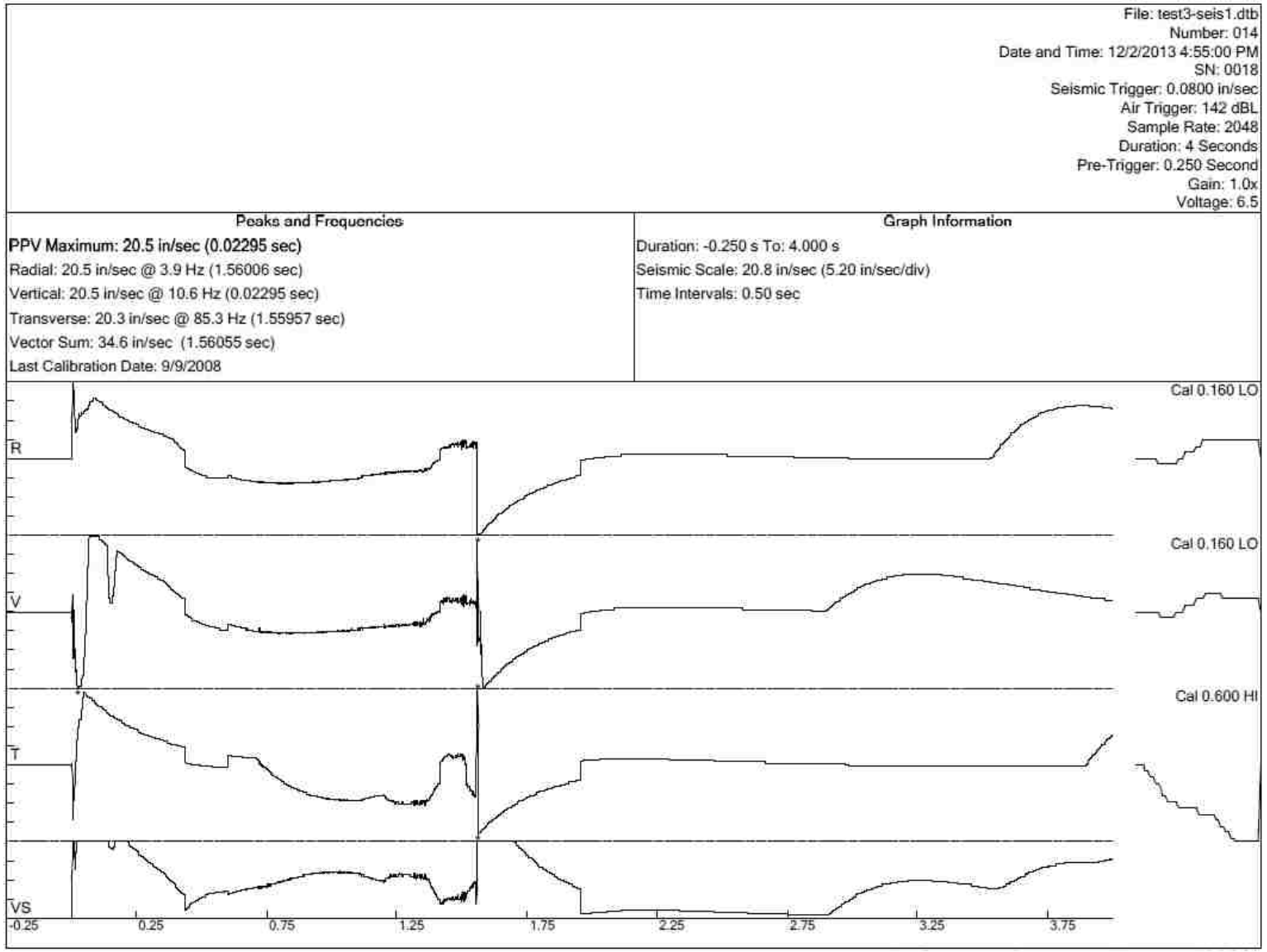
File: test3-seis1.dtb
Number: 014
Date and Time: 12/2/2013 4:55:00 PM
SN: 0018
Seismic Trigger: 0.0800 in/sec
Air Trigger: 142 dBL
Sample Rate: 2048
Duration: 4 Seconds
Pre-Trigger: 0.250 Second
Gain: 1.0x
Voltage: 6.5
Peaks and Frequencies
PPV Maximum: 20.5 in/sec (0.02295 sec)
Radial: 20.5 in/sec @ 3.9 Hz (1.56006 sec)
Vertical: 20.5 in/sec @ 10.6 Hz (0.02295 sec)
Transverse: 20.3 in/sec @ 85.3 Hz (1.55957 sec)
Vector Sum: 34.6 in/sec (1.56055 sec)
Last Calibration Date: 9/9/2008
Graph Information
Duration: -0.250 s To: 4.000 s
Seismic Scale: 20.8 in/sec (5.20 in/sec/div)
Time Intervals: 0.50 sec
Cal 0.160 LO
R
Cal 0.160 LO
V
Cal 0.600 HI
T
VS
-0.25
0.25
0.75
1.25
1.75
2.25
2.75
3.25
3.75

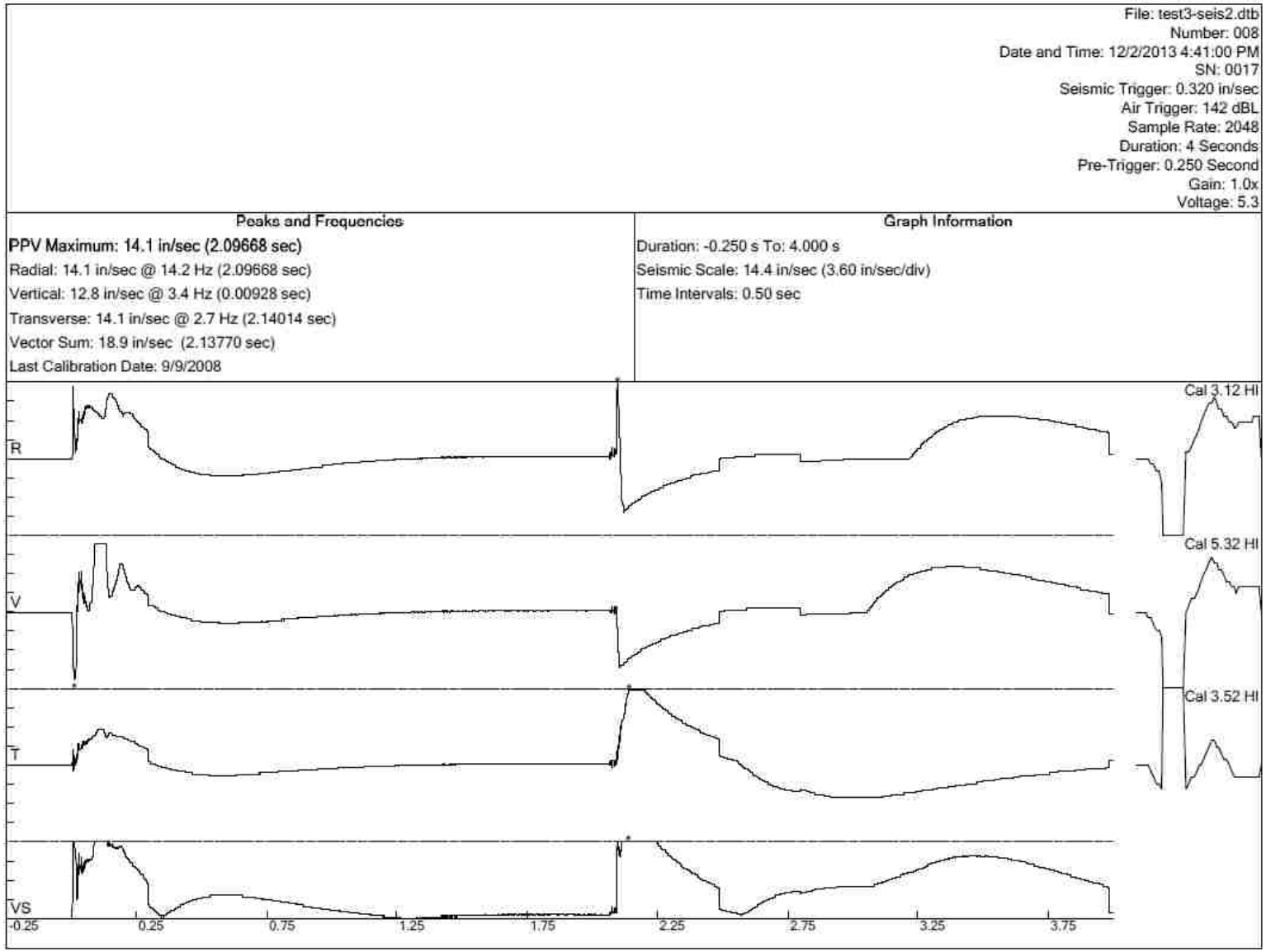
File: test3-seis2.dtb
Number: 008
Date and Time: 12/2/2013 4:41:00 PM
SN: 0017
Seismic Trigger: 0.320 in/sec
Air Trigger: 142 dBL
Sample Rate: 2048
Duration: 4 Seconds
Pre-Trigger: 0.250 Second
Gain: 1.0x
Voltage: 5.3
Peaks and Frequencies
PPV Maximum: 14.1 in/sec (2.09668 sec)
Radial: 14.1 in/sec @ 14.2 Hz (2.09668 sec)
Vertical: 12.8 in/sec @ 3.4 Hz (0.00928 sec)
Transverse: 14.1 in/sec @ 2.7 Hz (2.14014 sec)
Vector Sum: 18.9 in/sec (2.13770 sec)
Last Calibration Date: 9/9/2008
Graph Information
Duration: -0.250 s To: 4.000 s
Seismic Scale: 14.4 in/sec (3.60 in/sec/div)
Time Intervals: 0.50 sec
Cal 3.12 HI
Cal 5.32 HI
Cal 3.52 HI
R
V
T
VS
-0.25
0.25
0.75
1.25
1.75
2.25
2.75
3.25
3.75

File: test3-seis3.dtb
Number: 010
Date and Time: 9/24/1998 7:03:00 AM
SN: 0016
Seismic Trigger: 0.0800 in/sec
Air Trigger: 142 dBL
Sample Rate: 2048
Duration: 4 Seconds
Pre-Trigger: 0.250 Second
Gain: 1.0x
Voltage: 6.4

Peaks and Frequencies	Graph Information
PPV Maximum: 5.28 in/sec (0.01221 sec)	Duration: -0.250 s To: 4.000 s
Radial: 4.32 in/sec @ 53.8 Hz (0.00586 sec)	Seismic Scale: 5.60 in/sec (1.40 in/sec/div)
Vertical: 5.28 in/sec @ 32.0 Hz (0.01221 sec)	Time Intervals: 0.50 sec
Transverse: 1.12 in/sec @ 39.3 Hz (0.01221 sec)	
Vector Sum: 5.51 in/sec (0.01221 sec)	
Last Calibration Date: 9/9/2008	

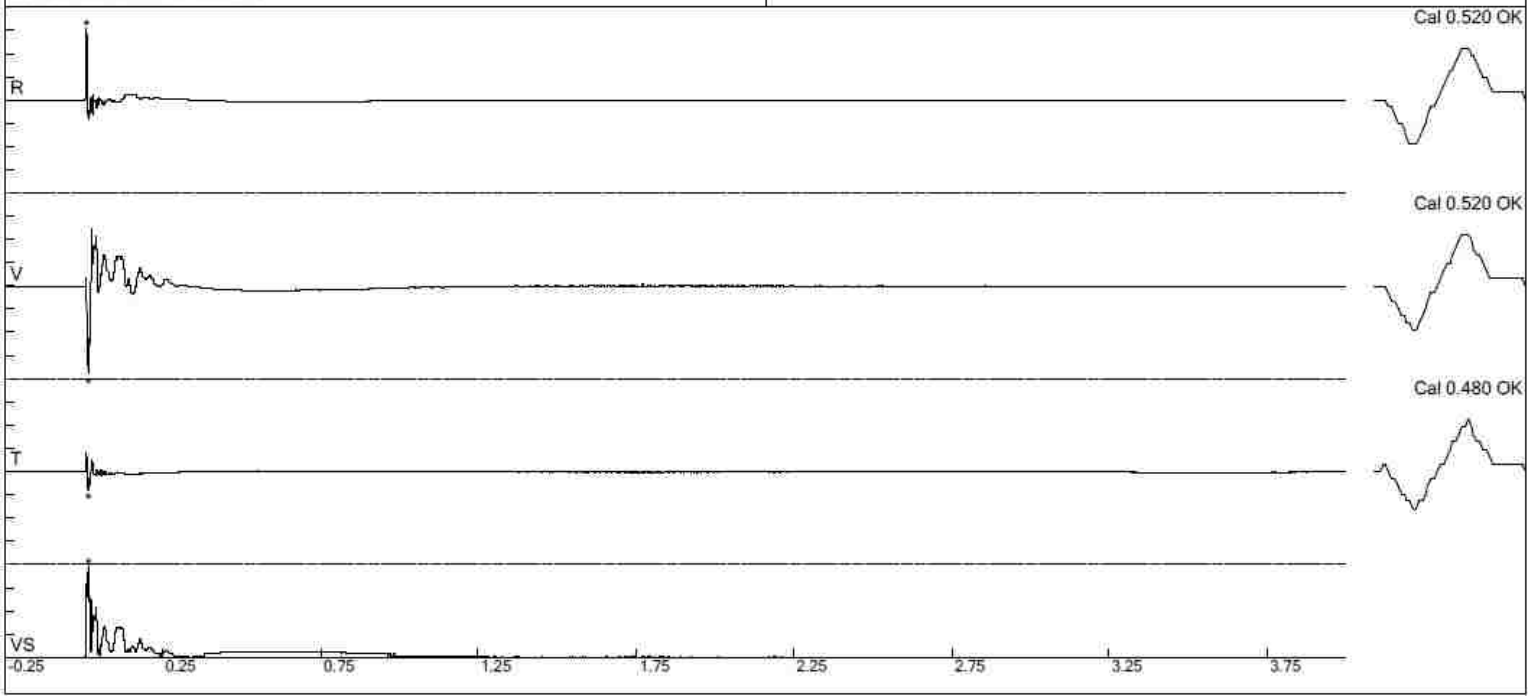

File: test3-seis4.dtb
Number: 010
Date and Time: 12/2/2013 4:50:00 PM
SN: 0492
Seismic Trigger: 0.0200 in/sec
Air Trigger: 112 dBL
Sample Rate: 2048
Duration: 3 Seconds
Pre-Trigger: 0.250 Second
Gain: 2.0x
Voltage: 6.3

Peaks and Frequencies	Graph Information
PPV Maximum: 1.68 in/sec (0.00928 sec)	Duration: -0.250 s To: 3.000 s
Radial: 1.68 in/sec @ 53.8 Hz (0.00928 sec)	Seismic Scale: 1.80 in/sec (0.450 in/sec/div)
Vertical: 1.18 in/sec @ 113.7 Hz (0.01367 sec)	Time Intervals: 0.50 sec
Transverse: 0.660 in/sec @ 68.2 Hz (0.01709 sec)	
Vector Sum: 2.09 in/sec (0.00928 sec)	
Last Calibration Date: 5/27/2010	

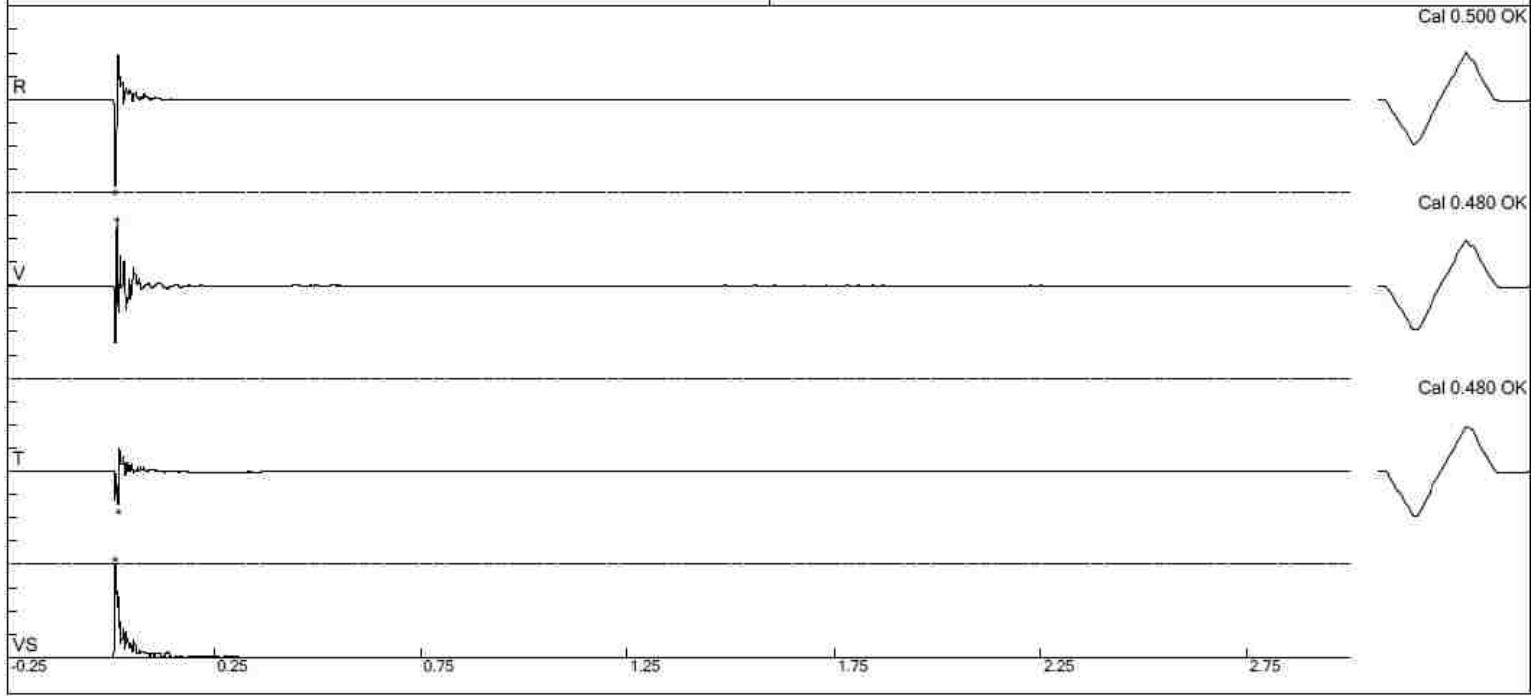

File: test3-seis5.dtb
Number: 048
Date and Time: 12/2/2013 4:59:00 PM
SN: 0180
Seismic Trigger: 0.0200 in/sec
Air Trigger: 112 dBL
Sample Rate: 2048
Duration: 3 Seconds
Pre-Trigger: 0.250 Second
Gain: 2.0x
Voltage: 6.1

Peaks and Frequencies	Graph Information
PPV Maximum: 0.910 in/sec (0.01514 sec)	Duration: -0.250 s To: 3.000 s
Radial: 0.910 in/sec @ 85.3 Hz (0.01514 sec)	Seismic Scale: 1.00 in/sec (0.250 in/sec/div)
Vertical: 0.440 in/sec @ 128.0 Hz (0.01465 sec)	Time Intervals: 0.50 sec
Transverse: 0.370 in/sec @ 64.0 Hz (0.01709 sec)	
Vector Sum: 0.990 in/sec (0.01514 sec)	
Last Calibration Date: 5/27/2010	

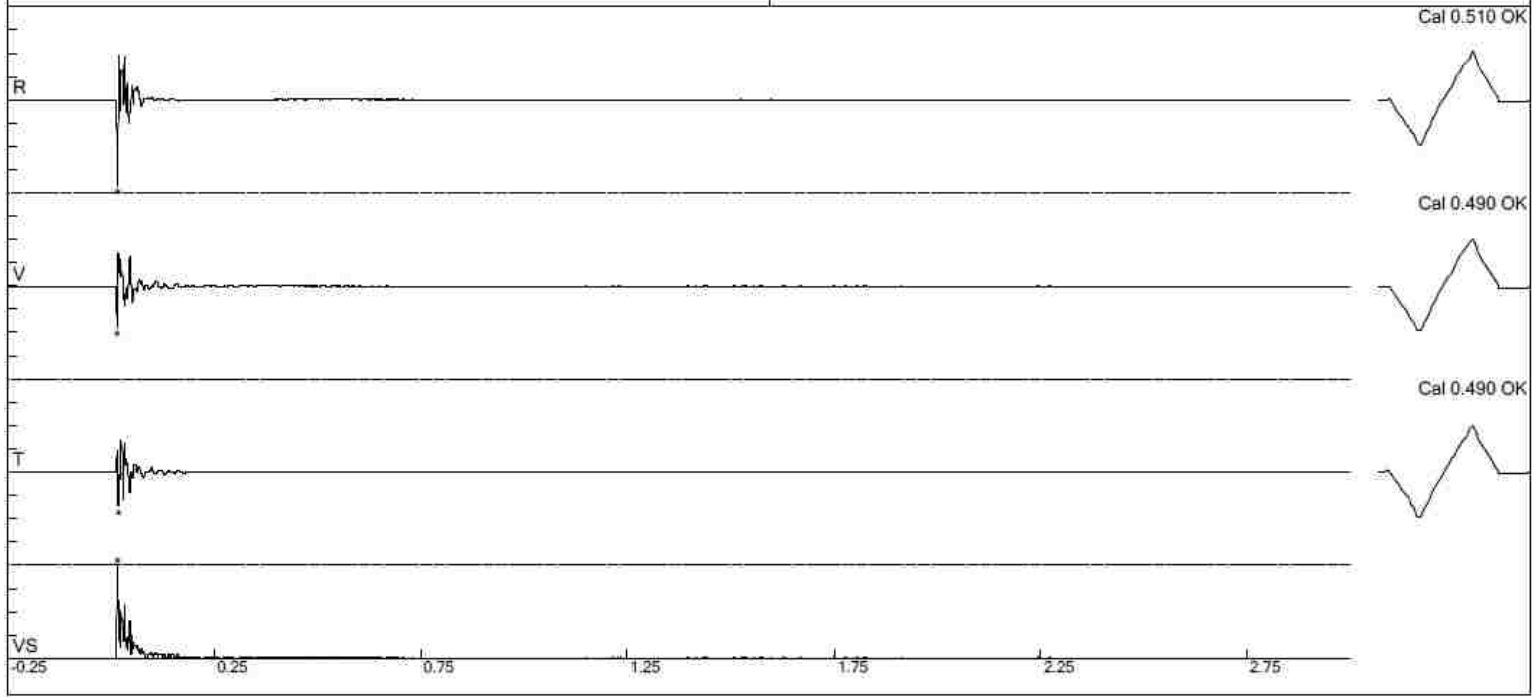

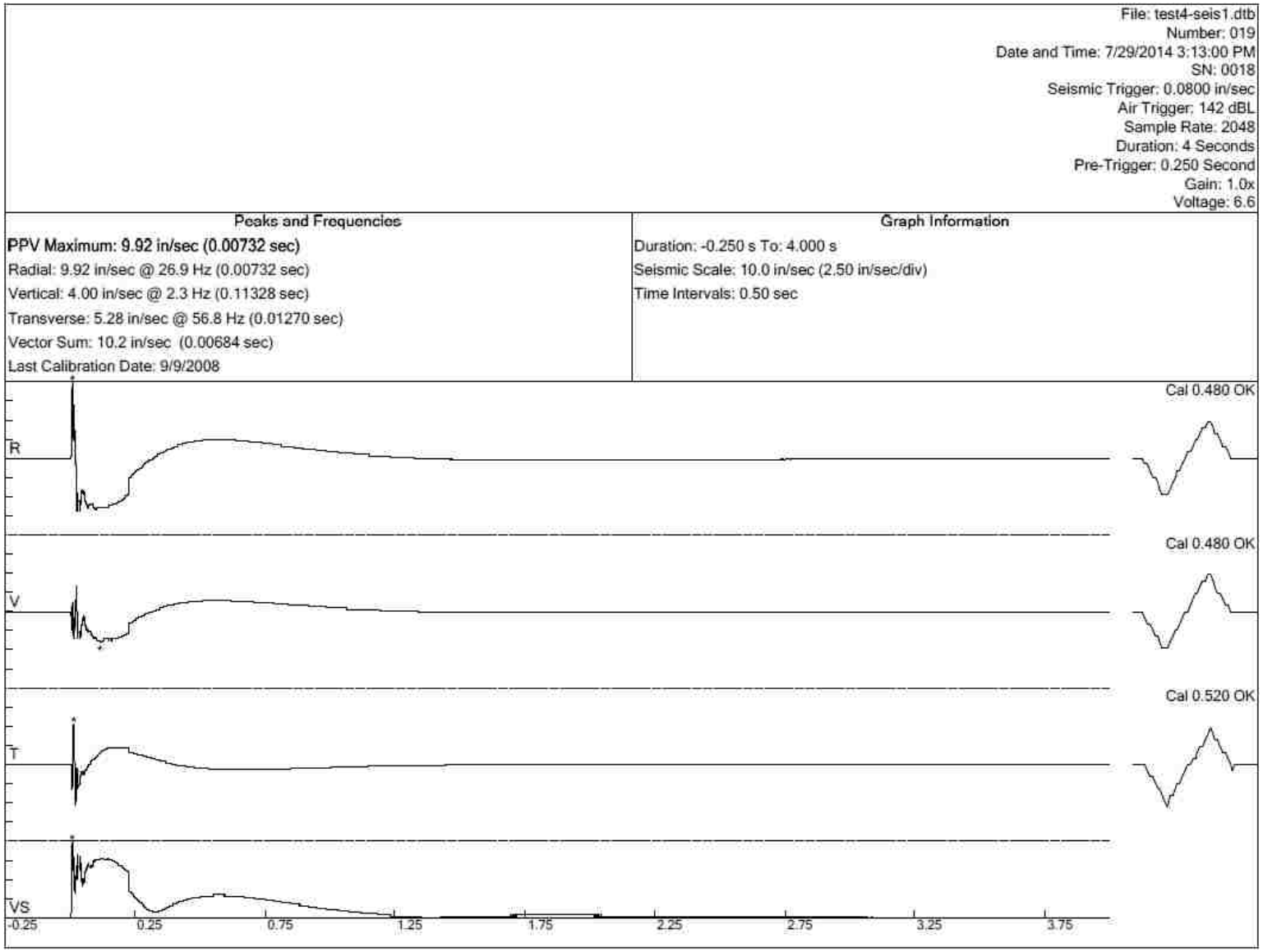
File: test4-seis1.dtb
Number: 019
Date and Time: 7/29/2014 3:13:00 PM
SN: 0018
Seismic Trigger: 0.0800 in/sec
Air Trigger: 142 dBL
Sample Rate: 2048
Duration: 4 Seconds
Pre-Trigger: 0.250 Second
Gain: 1.0x
Voltage: 6.6
Peaks and Frequencies
PPV Maximum: 9.92 in/sec (0.00732 sec)
Radial: 9.92 in/sec @ 26.9 Hz (0.00732 sec)
Vertical: 4.00 in/sec @ 2.3 Hz (0.11328 sec)
Transverse: 5.28 in/sec @ 56.8 Hz (0.01270 sec)
Vector Sum: 10.2 in/sec (0.00684 sec)
Last Calibration Date: 9/9/2008
Graph Information
Duration: -0.250 s To: 4.000 s
Seismic Scale: 10.0 in/sec (2.50 in/sec/div)
Time Intervals: 0.50 sec
Cal 0.480 OK
R
Cal 0.480 OK
V
Cal 0.520 OK
T
VS
-0.25
0.25
0.75
1.25
1.75
2.25
2.75
3.25
3.75

File: test4-seis2.dtb
Number: 015
Date and Time: 7/29/2014 2:54:00 PM
SN: 0017
Seismic Trigger: 0.320 in/sec
Air Trigger: 142 dBL
Sample Rate: 2048
Duration: 4 Seconds
Pre-Trigger: 0.250 Second
Gain: 1.0x
Voltage: 5.3

Peaks and Frequencies	Graph Information
PPV Maximum: 3.68 in/sec (0.01221 sec)	Duration: -0.250 s To: 4.000 s
Radial: 3.68 in/sec @ 24.9 Hz (0.01221 sec)	Seismic Scale: 4.00 in/sec (1.00 in/sec/div)
Vertical: 1.44 in/sec @ 68.2 Hz (0.02930 sec)	Time Intervals: 0.50 sec
Transverse: 1.64 in/sec @ 46.5 Hz (0.01514 sec)	
Vector Sum: 4.03 in/sec (0.01465 sec)	
Last Calibration Date: 9/9/2008	

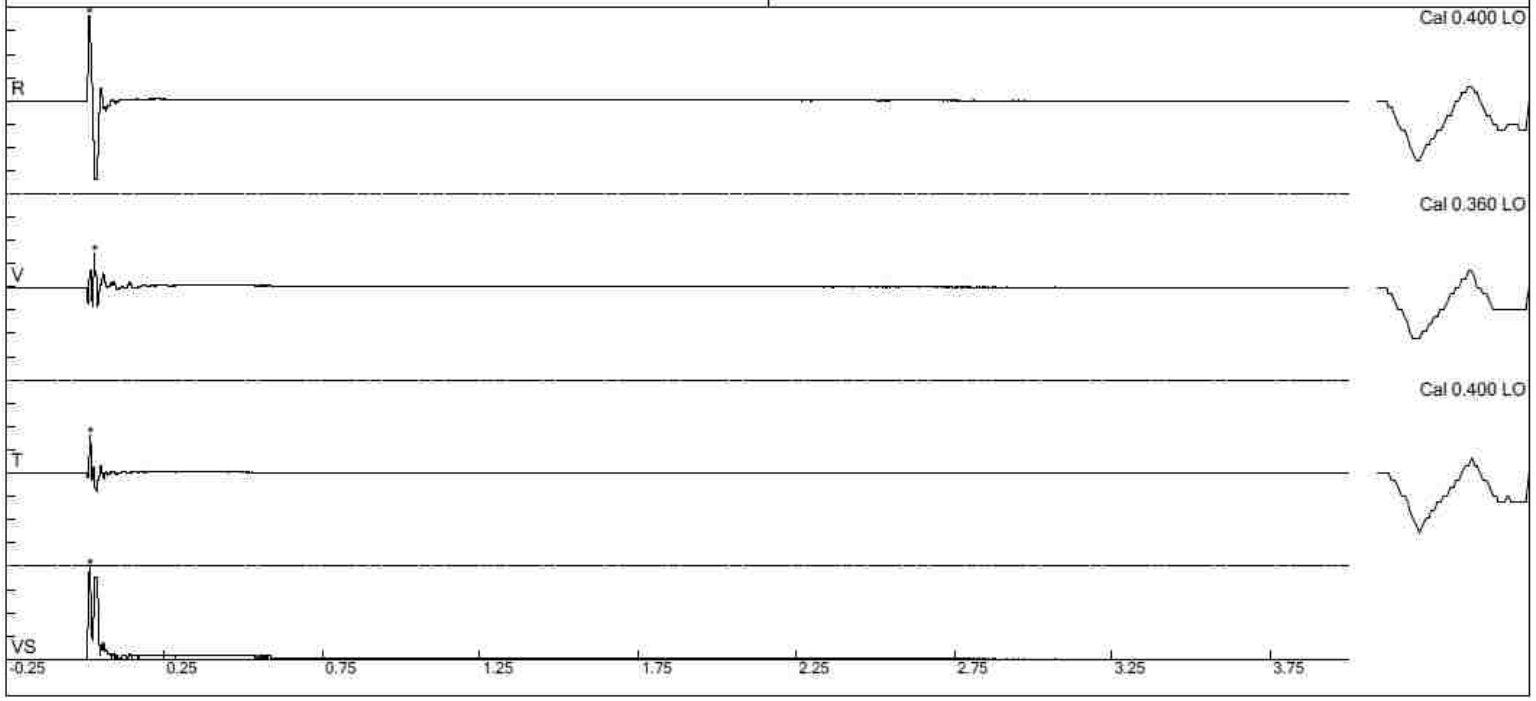

File: test4-seis3.dtb
Number: 012
Date and Time: 5/21/1999 5:17:00 AM
SN: 0016
Seismic Trigger: 0.0800 in/sec
Air Trigger: 142 dBL
Sample Rate: 2048
Duration: 4 Seconds
Pre-Trigger: 0.250 Second
Gain: 1.0x
Voltage: 6.5

Peaks and Frequencies	Graph Information
PPV Maximum: 1.92 in/sec (0.01416 sec)	Duration: -0.250 s To: 4.000 s
Radial: 1.92 in/sec @ 23.8 Hz (0.01416 sec)	Seismic Scale: 2.00 in/sec (0.500 in/sec/div)
Vertical: 0.680 in/sec @ 60.2 Hz (0.04150 sec)	Time Intervals: 0.50 sec
Transverse: 0.840 in/sec @ 64.0 Hz (0.01855 sec)	
Vector Sum: 1.96 in/sec (0.01563 sec)	
Last Calibration Date: 9/9/2008	

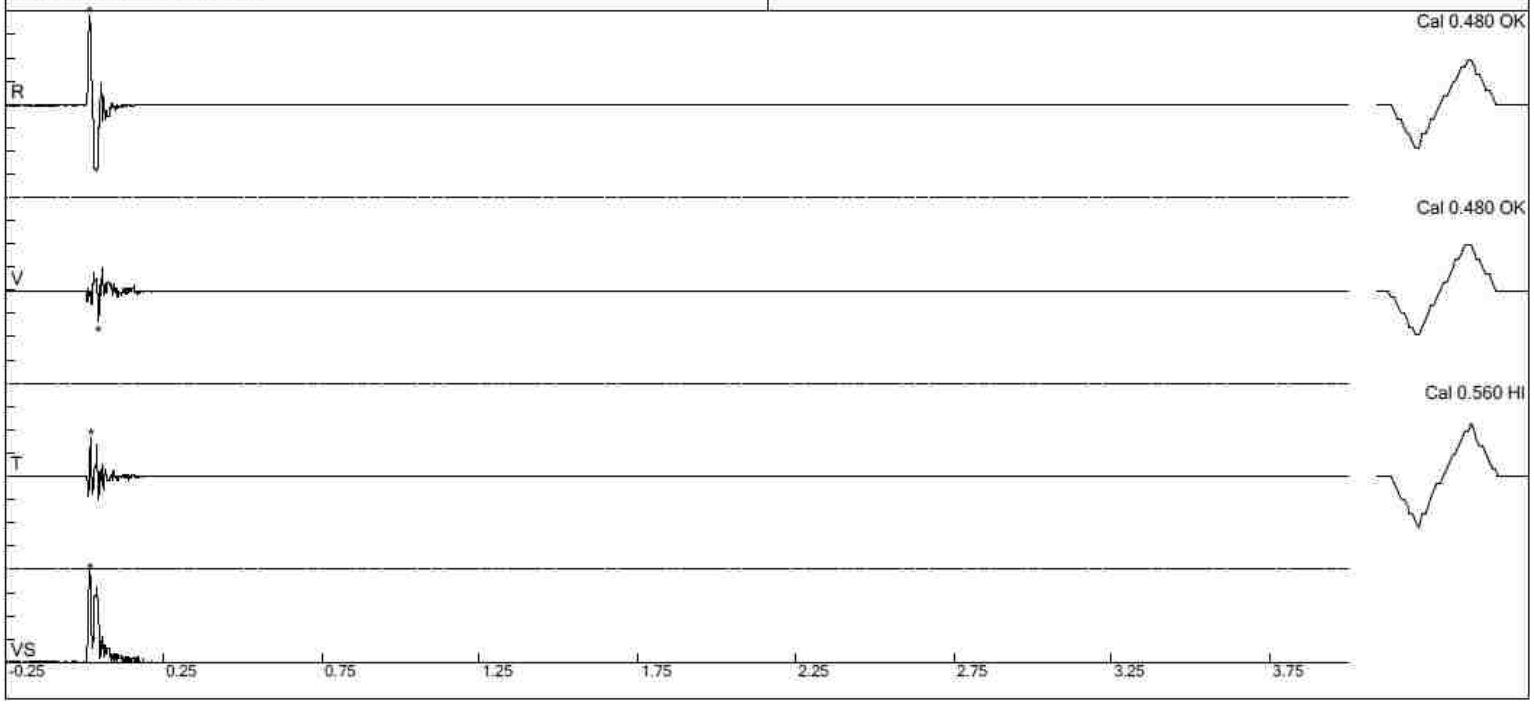

File: test4-seis4.dtb
Number: 016
Date and Time: 7/29/2014 3:07:00 PM
SN: 0492
Seismic Trigger: 0.0200 in/sec
Air Trigger: 112 dBL
Sample Rate: 2048
Duration: 3 Seconds
Pre-Trigger: 0.250 Second
Gain: 2.0x
Voltage: 6.7

Peaks and Frequencies	Graph Information
PPV Maximum: 1.14 in/sec (0.01709 sec)	Duration: -0.250 s To: 3.000 s
Radial: 1.14 in/sec @ 44.5 Hz (0.01709 sec)	Seismic Scale: 1.20 in/sec (0.300 in/sec/div)
Vertical: 0.490 in/sec @ 102.4 Hz (0.02783 sec)	Time Intervals: 0.50 sec
Transverse: 0.570 in/sec @ 53.8 Hz (0.02539 sec)	
Vector Sum: 1.17 in/sec (0.01709 sec)	
Last Calibration Date: 5/27/2010	

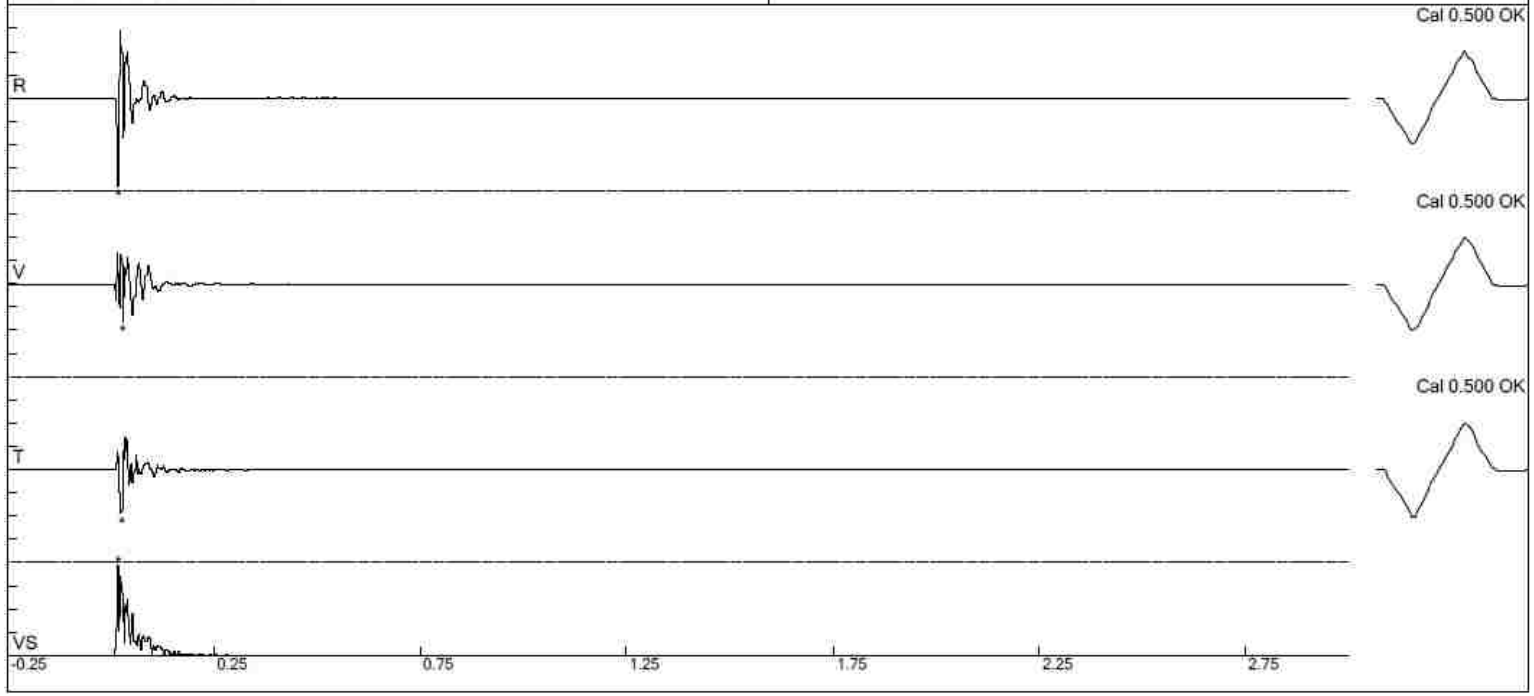

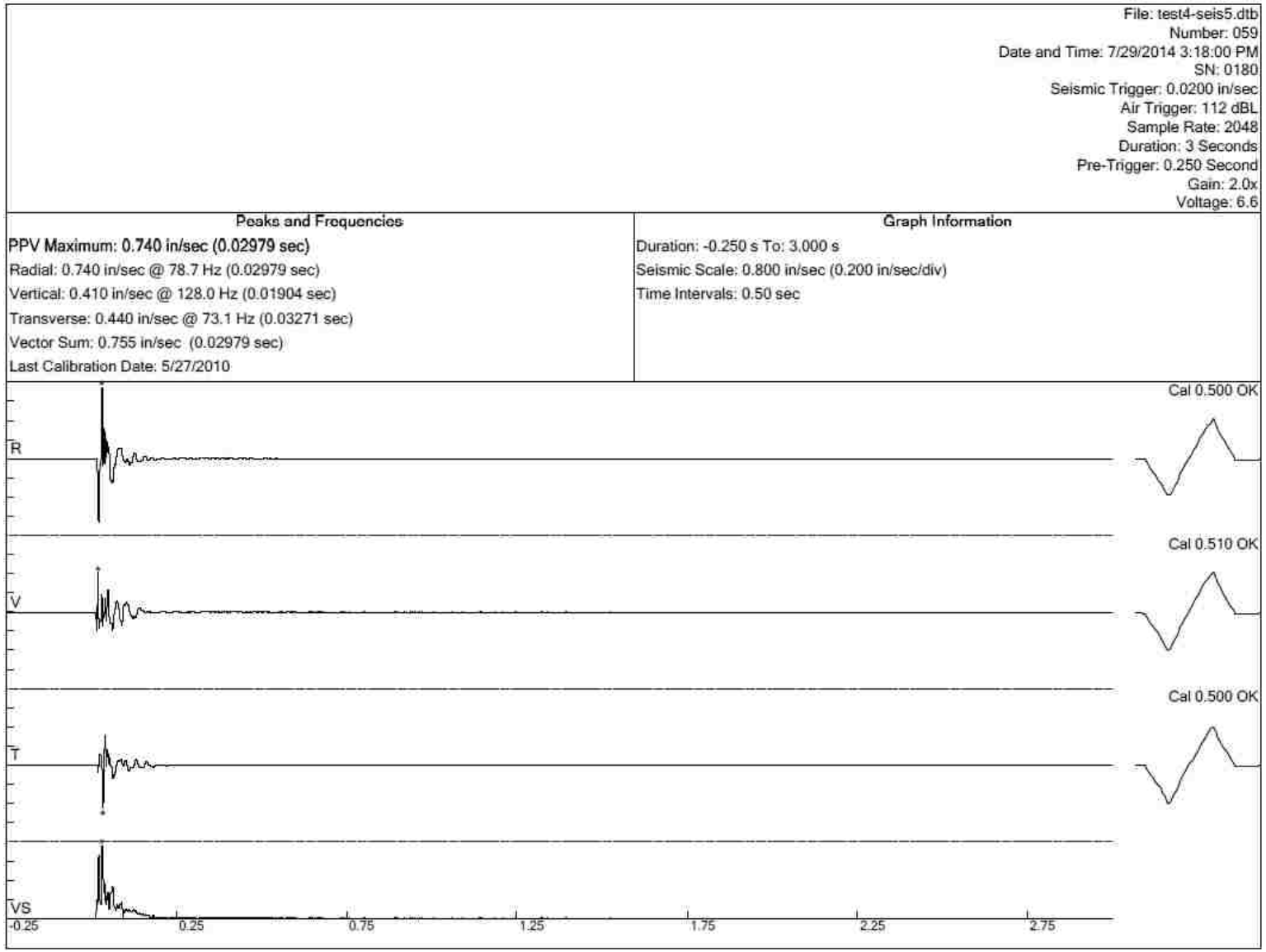
File: test4-seis5.dtb
Number: 059
Date and Time: 7/29/2014 3:18:00 PM
SN: 0180
Seismic Trigger: 0.0200 in/sec
Air Trigger: 112 dBL
Sample Rate: 2048
Duration: 3 Seconds
Pre-Trigger: 0.250 Second
Gain: 2.0x
Voltage: 6.6
Peaks and Frequencies
PPV Maximum: 0.740 in/sec (0.02979 sec)
Radial: 0.740 in/sec @ 78.7 Hz (0.02979 sec)
Vertical: 0.410 in/sec @ 128.0 Hz (0.01904 sec)
Transverse: 0.440 in/sec @ 73.1 Hz (0.03271 sec)
Vector Sum: 0.755 in/sec (0.02979 sec)
Last Calibration Date: 5/27/2010
Graph Information
Duration: -0.250 s To: 3.000 s
Seismic Scale: 0.800 in/sec (0.200 in/sec/div)
Time Intervals: 0.50 sec
Cal 0.500 OK
R
Cal 0.510 OK
V
Cal 0.500 OK
T
VS
-0.25
0.25
0.75
1.25
1.75
2.25
2.75

File: test4-seis6.dtb
Number: 022
Date and Time: 4/21/2001 12:44:00 AM
SN: 3857
Seismic Trigger: 0.0400 in/sec
Air Trigger: 142 dBL
Sample Rate: 1024
Duration: 4 Seconds
Pre-Trigger: 0.5 Second
Gain: 2.0x
Voltage: 6.4

Peaks and Frequencies	Graph Information
PPV Maximum: 0.430 in/sec (0.0137 sec)	Duration: -0.500 s To: 4.000 s
Radial: 0.430 in/sec @ 51.2 Hz (0.0137 sec)	Seismic Scale: 0.600 in/sec (0.150 in/sec/div)
Vertical: 0.270 in/sec @ 85.3 Hz (0.0068 sec)	Time Intervals: 0.50 sec
Transverse: 0.360 in/sec @ 64.0 Hz (0.0254 sec)	
Vector Sum: 0.455 in/sec (0.0137 sec)	
Last Calibration Date: 6/1/2010	

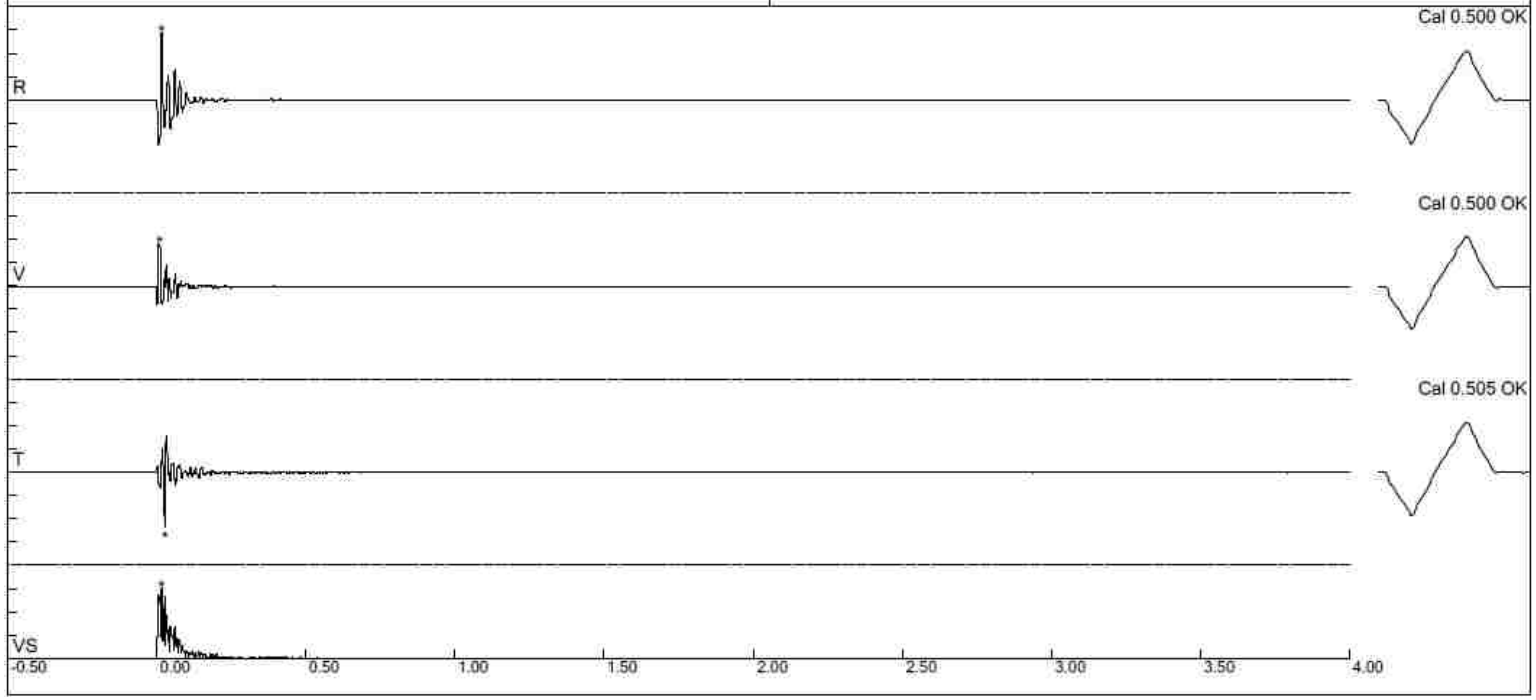

File: test5-seis1.dtb
Number: 020
Date and Time: 7/30/2014 11:57:00 AM
SN: 0018
Seismic Trigger: 0.0800 in/sec
Air Trigger: 142 dBL
Sample Rate: 2048
Duration: 4 Seconds
Pre-Trigger: 0.250 Second
Gain: 1.0x
Voltage: 6.6

Peaks and Frequencies	Graph Information
PPV Maximum: 8.80 in/sec (0.00488 sec)	Duration: -0.250 s To: 4.000 s
Radial: 6.08 in/sec @ 2.2 Hz (0.11963 sec)	Seismic Scale: 9.20 in/sec (2.30 in/sec/div)
Vertical: 8.80 in/sec @ 46.5 Hz (0.00488 sec)	Time Intervals: 0.50 sec
Transverse: 4.96 in/sec @ 3.7 Hz (0.12891 sec)	
Vector Sum: 9.04 in/sec (0.12891 sec)	
Last Calibration Date: 9/9/2008	

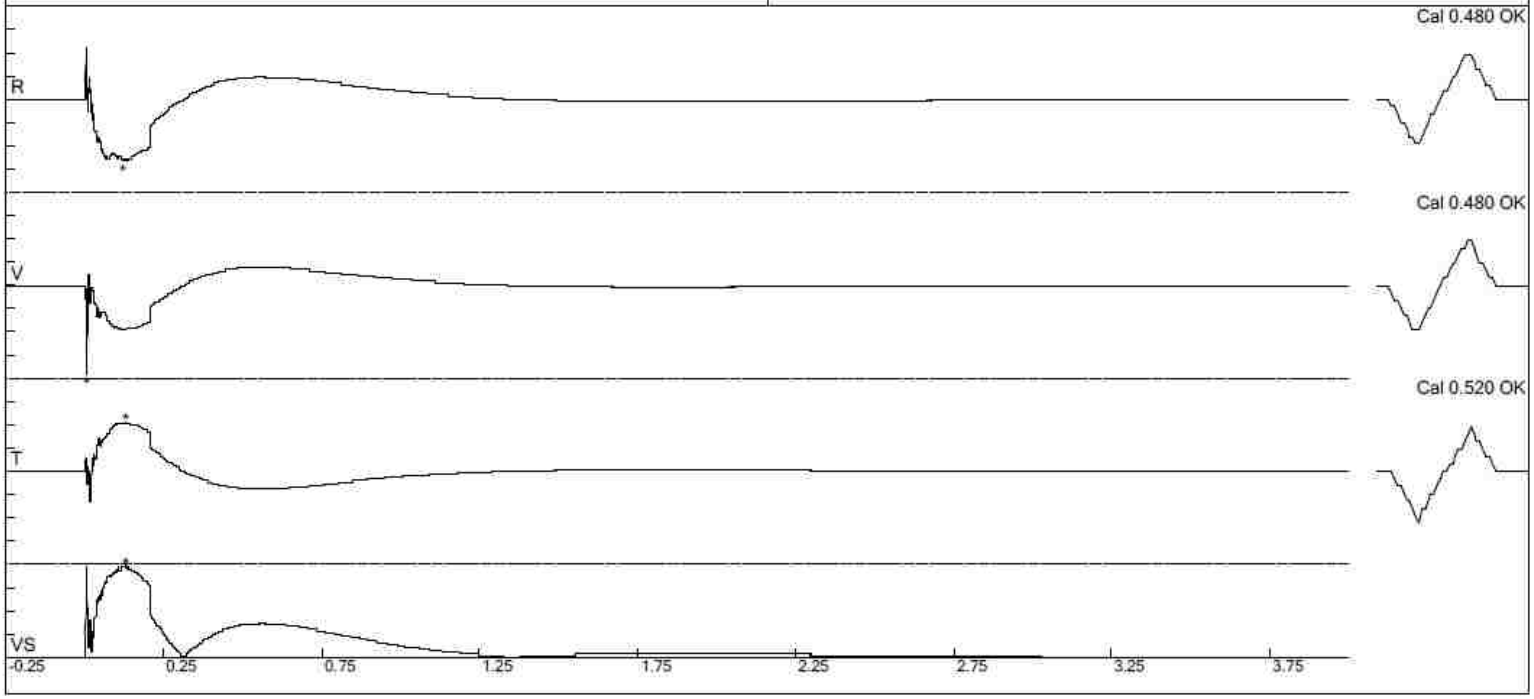

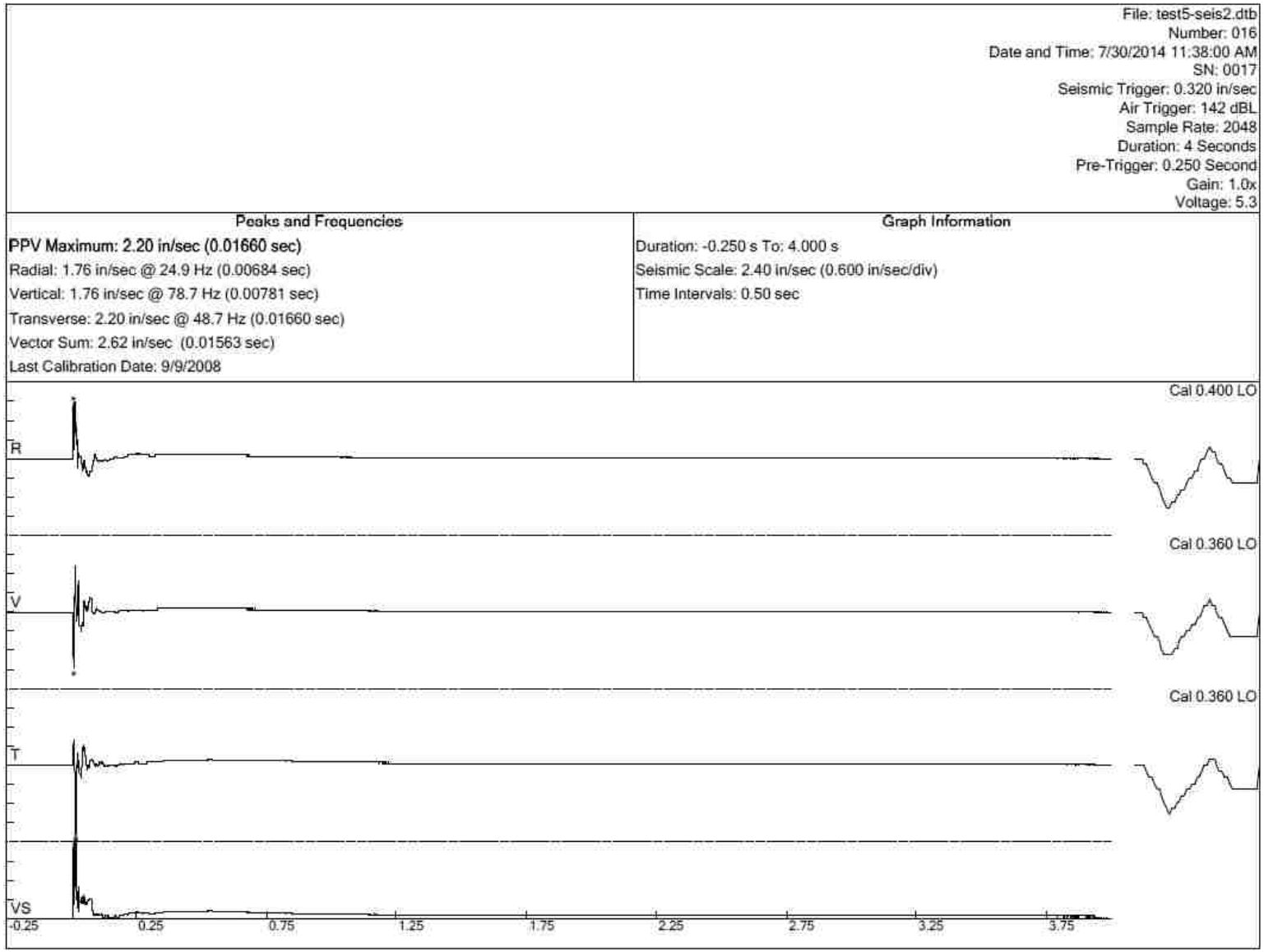
File: test5-seis2.dtb
Number: 016
Date and Time: 7/30/2014 11:38:00 AM
SN: 0017
Seismic Trigger: 0.320 in/sec
Air Trigger: 142 dBL
Sample Rate: 2048
Duration: 4 Seconds
Pre-Trigger: 0.250 Second
Gain: 1.0x
Voltage: 5.3
Peaks and Frequencies
PPV Maximum: 2.20 in/sec (0.01660 sec)
Radial: 1.76 in/sec @ 24.9 Hz (0.00684 sec)
Vertical: 1.76 in/sec @ 78.7 Hz (0.00781 sec)
Transverse: 2.20 in/sec @ 48.7 Hz (0.01660 sec)
Vector Sum: 2.62 in/sec (0.01563 sec)
Last Calibration Date: 9/9/2008
Graph Information
Duration: -0.250 s To: 4.000 s
Seismic Scale: 2.40 in/sec (0.600 in/sec/div)
Time Intervals: 0.50 sec
Cal 0.400 LO
R
Cal 0.360 LO
V
Cal 0.360 LO
T
VS
-0.25
0.25
0.75
1.25
1.75
2.25
2.75
3.25
3.75

File: test5-seis3.dtb
Number: 013
Date and Time: 5/22/1999 2:02:00 AM
SN: 0016
Seismic Trigger: 0.0800 in/sec
Air Trigger: 142 dBL
Sample Rate: 2048
Duration: 4 Seconds
Pre-Trigger: 0.250 Second
Gain: 1.0x
Voltage: 6.5

Peaks and Frequencies	Graph Information
PPV Maximum: 1.56 in/sec (0.01807 sec)	Duration: -0.250 s To: 4.000 s
Radial: 1.36 in/sec @ 39.3 Hz (0.00977 sec)	Seismic Scale: 1.60 in/sec (0.400 in/sec/div)
Vertical: 1.56 in/sec @ 60.2 Hz (0.01807 sec)	Time Intervals: 0.50 sec
Transverse: 1.00 in/sec @ 113.7 Hz (0.02979 sec)	
Vector Sum: 1.81 in/sec (0.01758 sec)	
Last Calibration Date: 9/9/2008	

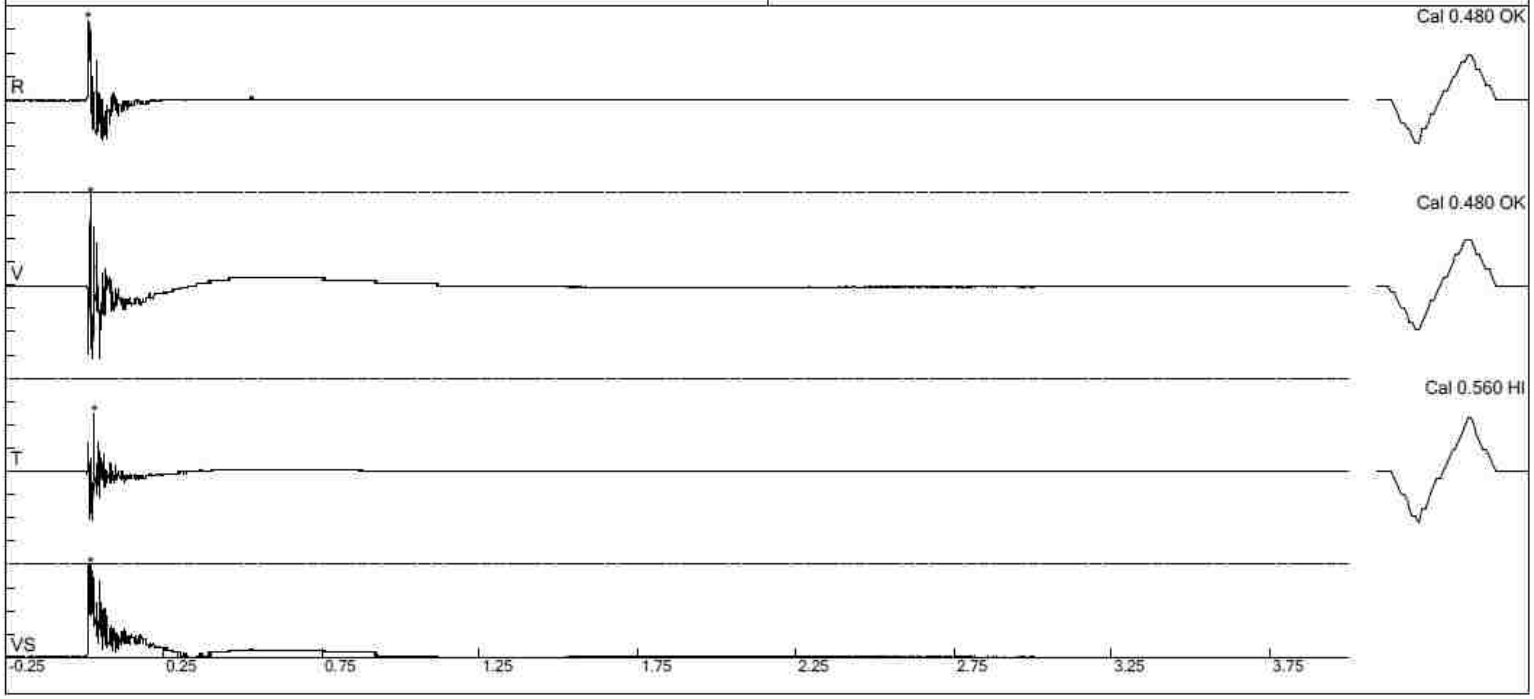

File: test5-seis4.dtb
Number: 017
Date and Time: 7/30/2014 11:51:00 AM
SN: 0492
Seismic Trigger: 0.0200 in/sec
Air Trigger: 112 dBL
Sample Rate: 2048
Duration: 3 Seconds
Pre-Trigger: 0.250 Second
Gain: 2.0x
Voltage: 6.6

Peaks and Frequencies	Graph Information
PPV Maximum: 0.500 in/sec (0.04395 sec)	Duration: -0.250 s To: 3.000 s
Radial: 0.500 in/sec @ 28.4 Hz (0.04395 sec)	Seismic Scale: 0.600 in/sec (0.150 in/sec/div)
Vertical: 0.410 in/sec @ 31.0 Hz (0.07031 sec)	Time Intervals: 0.50 sec
Transverse: 0.420 in/sec @ 27.6 Hz (0.09863 sec)	
Vector Sum: 0.585 in/sec (0.04541 sec)	
Last Calibration Date: 5/27/2010	

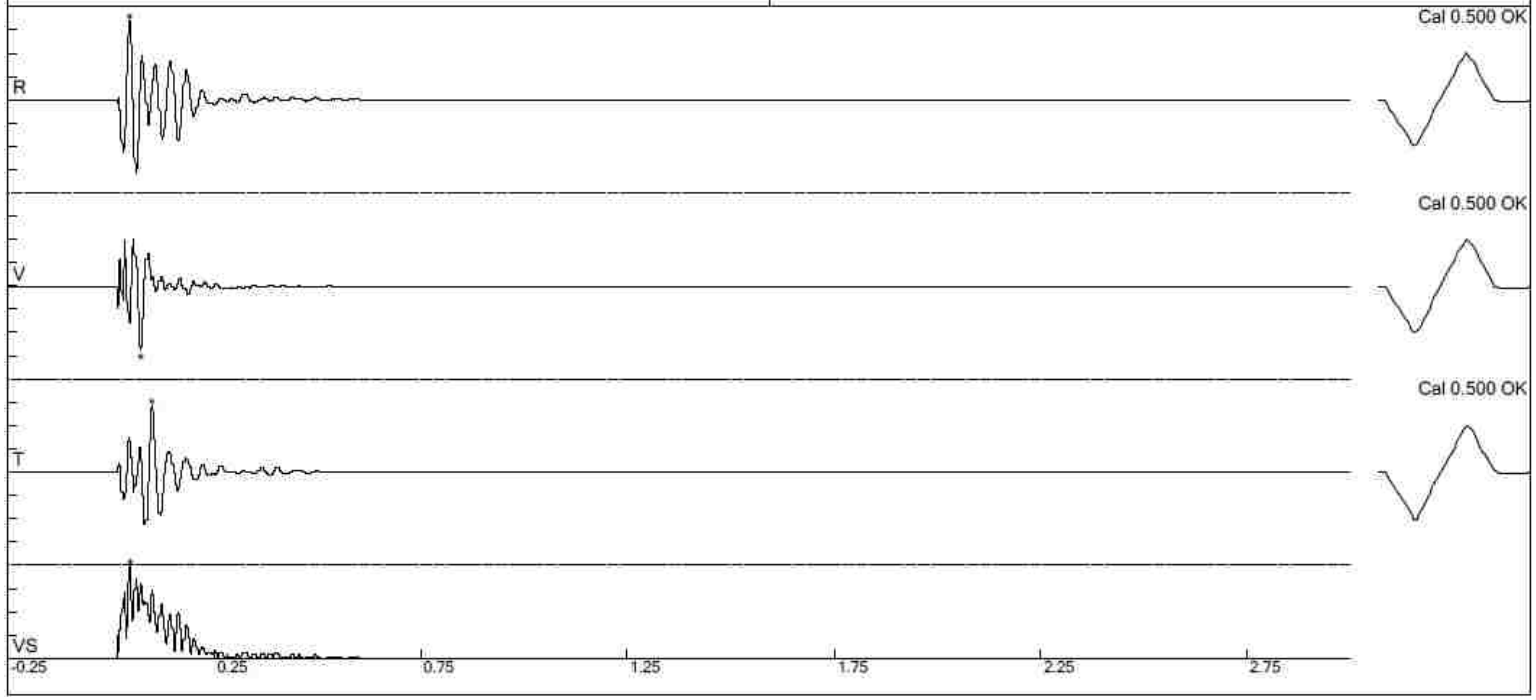

File: test5-seis5.dtb
Number: 060
Date and Time: 7/30/2014 12:02:00 PM
SN: 0180
Seismic Trigger: 0.0200 in/sec
Air Trigger: 112 dBL
Sample Rate: 2048
Duration: 3 Seconds
Pre-Trigger: 0.250 Second
Gain: 2.0x
Voltage: 6.5

Peaks and Frequencies	Graph Information
PPV Maximum: 0.260 in/sec (0.03809 sec)	Duration: -0.250 s To: 3.000 s
Radial: 0.260 in/sec @ 35.3 Hz (0.03809 sec)	Seismic Scale: 0.400 in/sec (0.100 in/sec/div)
Vertical: 0.200 in/sec @ 48.7 Hz (0.04688 sec)	Time Intervals: 0.50 sec
Transverse: 0.120 in/sec @ 36.5 Hz (0.05273 sec)	
Vector Sum: 0.320 in/sec (0.03809 sec)	
Last Calibration Date: 5/27/2010	

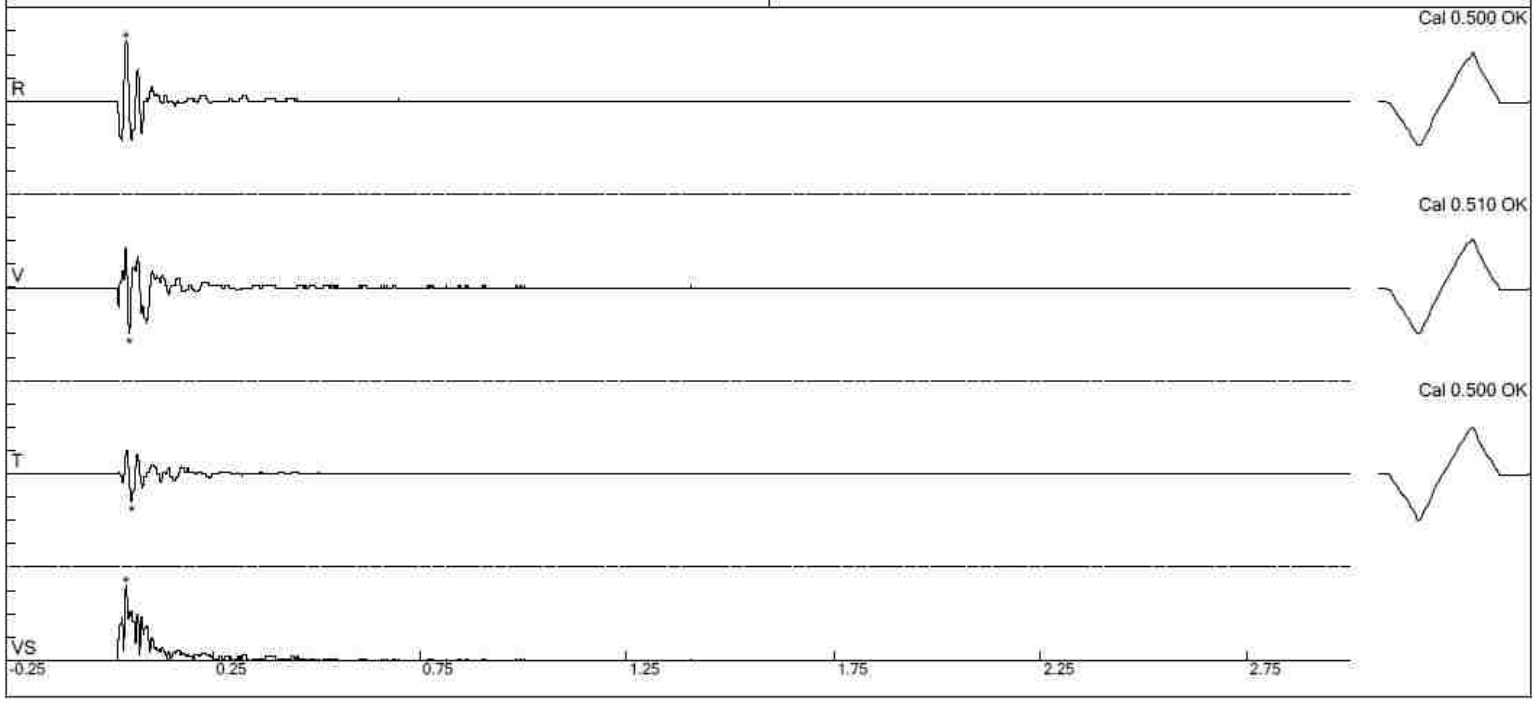

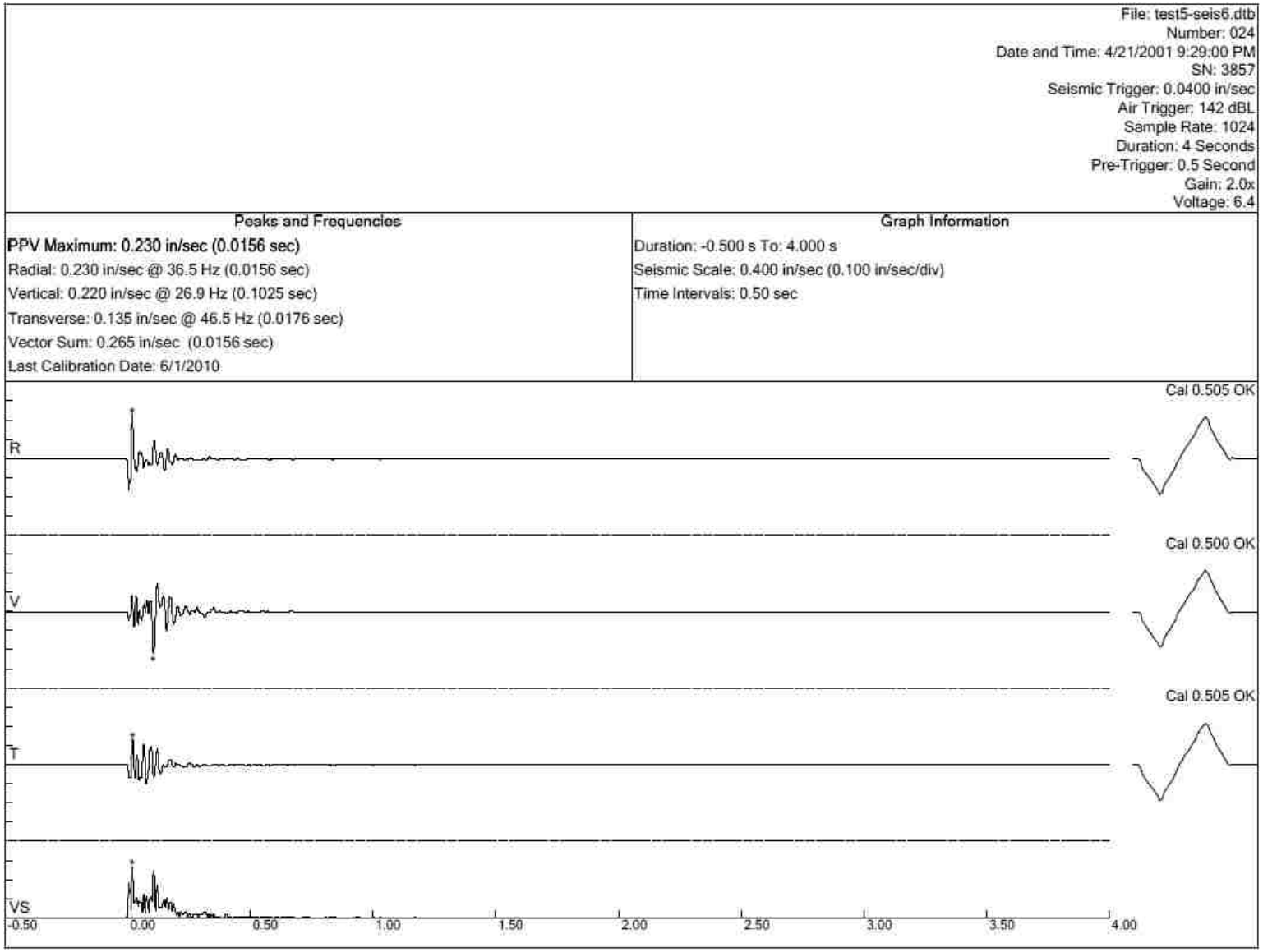
File: test5-seis6.dtb
Number: 024
Date and Time: 4/21/2001 9:29:00 PM
SN: 3857
Seismic Trigger: 0.0400 in/sec
Air Trigger: 142 dBL
Sample Rate: 1024
Duration: 4 Seconds
Pre-Trigger: 0.5 Second
Gain: 2.0x
Voltage: 6.4
Peaks and Frequencies
PPV Maximum: 0.230 in/sec (0.0156 sec)
Radial: 0.230 in/sec @ 36.5 Hz (0.0156 sec)
Vertical: 0.220 in/sec @ 26.9 Hz (0.1025 sec)
Transverse: 0.135 in/sec @ 46.5 Hz (0.0176 sec)
Vector Sum: 0.265 in/sec (0.0156 sec)
Last Calibration Date: 6/1/2010
Graph Information
Duration: -0.500 s To: 4.000 s
Seismic Scale: 0.400 in/sec (0.100 in/sec/div)
Time Intervals: 0.50 sec
Cal 0.505 OK
R
Cal 0.500 OK
V
Cal 0.505 OK
T
VS
-0.50
0.00
0.50
1.00
1.50
2.00
2.50
3.00
3.50
4.00

APPENDIX B

LIMESTONE QUARRY FIELD LOGS

Appendix B provides the field notes that were taken during the limestone quarry signature hole tests. Each sheet includes information pertaining to the explosive charge and blasthole, test array setup, post-test observations and photo (if available), and weather.

Test Number	1 - Butler Quarry
Date	9/18/2013
Weather	Cloudy with minor precipitati
Time	Afternoon

Post test observations:
Bulk heave approx. 9' radius
Fractures up to 32-35' radius

Hole Depth (ft)	36' 9"
Hole Diameter (in)	5"
Stemming Height (ft)	12.5'
Stemming Type	Crushed stone (1/4")
Explosive Type	Emulsion
Explosive Density (g/cc)	1.25
Booster Info	1 pound booster, bottom prim
Water in hole?	Yes

VOD Cable Length (ft)	42'
VOD Cable (ohm/ft)	3.29 ohms/ft

	Seis 1 (trigger)	Seis 2	Seis 3	Seis 4	Seis 5
Distance From Charge (ft)	48.5'	65.1'	90.5'	156.1' from Seis 1	267.9' from Seis 4
Mounting Method	Anchor bolt	Anchor bolt	Duct tape / epoxy	Duct tape / epoxy	Duct tape / epoxy
Sample Rate (Hz)	2048	2048	2048	2048	2048
Sample Length (sec)	4	4	4	4	4
Sample Range (in/sec)	20	20	20	10	10
Trigger level (in/sec)	0.08	0.32	0.08	0.02	0.02

Test Number	2 - Butler Quarry
Date	11/7/2013
Weather	Partly cloudy, 49 degrees
Time	Afternoon

Post test observations:
Minimal to no heave

Hole Depth (ft)	24' 8"
Hole Diameter (in)	3-1/8"
Stemming Height (ft)	12
Stemming Type	Crushed stone (1/4")
Explosive Type	Emulsion
Explosive Density (g/cc)	1.25
Booster Info	1 pound booster, bottom primed
Water in hole?	Yes

VOD Cable Length (ft)	43'
VOD Cable (ohm/ft)	3.29 ohms/ft

	Seis 1 (trigger)	Seis 2	Seis 3	Seis 4	Seis 5
Distance From Charge (ft)	16.4'	23.8'	33.0'	121.6'	242.4'
Mounting Method	Anchor bolt	Anchor bolt	Anchor bolt	Spikes / mud cap	Spikes / mud cap
Sample Rate (Hz)	2048	2048	2048	2048	2048
Sample Length (sec)	4	4	4	4	4
Sample Range (in/sec)	20	20	20	5	5
Trigger level (in/sec)	0.08	0.32	0.08	0.02	0.02

	Acc. 1	Acc. 2	Acc. 3	Acc. 4
Distance From Charge (ft)	14.55'	4' 3/16" from Acc. 1	31.03'	4' 1/4" from Acc. 3
Mounting Method	Anchor bolt	Anchor bolt	Anchor bolt	Anchor bolt
Sample Rate	100k	100k	100k	100k
Voltage Range	+/- 5 v	+/- 5 v	+/- 5 v	+/- 5 v
Seis ID Paired With	Seis 1		Seis 2	

Test Number	3 - Butler Quarry
Date	12/2/2013
Weather	Mostly Cloudy
Time	Afternoon

Post test observations:
Stemming too short, shot cratered

Hole Depth (ft)	14' 3/12"
Hole Diameter (in)	3-1/8"
Stemming Height (ft)	4' 4"
Stemming Type	Crushed stone (1/4")
Explosive Type	Emulsion
Explosive Density (g/cc)	1.25
Booster Info	1 pound booster, bottom primed
Water in hole?	No - top loaded

VOD Cable Length (ft)	40'
VOD Cable (ohm/ft)	3.29 ohms/ft

	Seis 1 (trigger)	Seis 2	Seis 3	Seis 4	Seis 5
Distance From Charge (ft)	13.02'	20.88'	27.74'	95.8'	189.2'
Mounting Method	Anchor bolt	Anchor bolt	Anchor bolt	Spikes / mud cap	Spikes / mud cap
Sample Rate (Hz)	2048	2048	2048	2048	2048
Sample Length (sec)	4	4	4	4	4
Sample Range (in/sec)	20	20	20	5	5
Trigger level (in/sec)	0.08	0.32	0.08	0.02	0.02

	Acc. 1	Acc. 2	Acc. 3	Acc. 4
Distance From Charge (ft)	11.06'	4' 1" from Acc. 1	25.73'	3' 10-5/16" from Acc. 3
Mounting Method	Anchor bolt	Anchor bolt	Anchor bolt	Anchor bolt
Sample Rate	500k	500k	500k	500k
Voltage Range	+/- 5 v	+/- 5 v	+/- 5 v	+/- 5 v
Seis ID Paired With	Seis 1		Seis 2	

Test Number	4 - Butler Quarry
Date	7/29/2014
Weather	Partly cloudy
Time	Afternoon

Post test observations:
Muck pile approx. 36' diameter
No photos taken

Hole Depth (ft)	24'
Hole Diameter (in)	5"
Stemming Height (ft)	11'
Stemming Type	Crushed stone (1/4")
Explosive Type	Emulsion
Explosive Density (g/cc)	1.25
Booster Info	1 pound booster, bottom primed
Water in hole?	Yes

VOD Cable Length (ft)	40'
VOD Cable (ohm/ft)	3.29 ohms/ft

	Seis 1 (trigger)	Seis 2	Seis 3	Seis 4	Seis 5	Seis 6
Distance From Charge (ft)	47.5'	35.9' from Seis 1	32.9' from Seis 2	93.6' from Seis 3	84.8' from Seis 4	190.6' from Seis 5
Mounting Method	Anchor bolt	Anchor bolt	Anchor bolt	Spikes / mud cap	Spikes / mud cap	Spikes / mud cap
Sample Rate (Hz)	2048	2048	2048	2048	2048	1024
Sample Length (sec)	4	4	4	3	3	4
Sample Range (in/sec)	20	20	20	5	5	2.5
Trigger level (in/sec)	0.08	0.32	0.08	0.02	0.02	0.04

Test Number	5 - Big Bend Quarry
Date	7/30/2014
Weather	Partly cloudy
Time	12:30 PM

Post test observations:
No heave
Radial fractures 60-70' diameter
No photos taken

Hole Depth (ft)	34' 5"
Hole Diameter (in)	5.5"
Stemming Height (ft)	14' 4"
Stemming Type	Crushed stone (1/4")
Explosive Type	Emulsion
Explosive Density (g/cc)	1.25
Booster Info	1 pound booster, bottom primed
Water in hole?	No

VOD Cable Length (ft)	40'
VOD Cable (ohm/ft)	3.29 ohms/ft

	Seis 1 (trigger)	Seis 2	Seis 3	Seis 4	Seis 5	Seis 6
Distance From Charge (ft)	63' 11"	44' 2" from Seis 1	54' 7" from Seis 2	130' 4" from Seis 3	110' 7" from Seis 4	303' 9" from Seis 5
Mounting Method	Anchor bolt	Anchor bolt	Anchor bolt	Spikes / mud cap	Spikes / mud cap	Spikes / mud cap
Sample Rate (Hz)	2048	2048	2048	2048	2048	1024
Sample Length (sec)	4	4	4	3	3	4
Sample Range (in/sec)	20	20	20	5	5	2.5
Trigger level (in/sec)	0.08	0.32	0.08	0.02	0.02	0.04

APPENDIX C

SIGNATURE HOLE DATASET

Appendix C provides the test matrices for the signature hole dataset for both metric and U.S. Customary Units. The test matrices are further separated by data source. Each matrix includes the monitoring distance, charge information, and radial component seed waveform features for each test. This dataset was used to conduct the multiple regression analyses described in Section 4.

Geology	Distance From Blast (ft)	Rounded Distance From Blast (ft)	Hole Diameter (inches)	Hole Area (sq. ft.)	Hole Depth (ft)	Stemming (ft)	Power Deck (ft)	Charge Length (ft)	Density (g/cc)	Charge Weight (lbs)	Weight per Unit Length (lbs/ft)	SRSD (ft/lb^0.5)	Radial PPV (ips)	Principal Radial Frequency (Hz)	Dominant Radial Frequency (Hz)	Waveform Duration (s)
Gold-Operator	111.2	100	9.875	0.532	43.448	25.0	3.0	18.45	0.98	600.0	32.5	4.5	4.08	5.10	5.13	0.7500
Gold-Operator	287.3	300	9.875	0.532	43.448	25.0	3.0	18.45	0.98	600.0	32.5	11.7	1.08	11.90	9.00	1.0967
Gold-Operator	439.1	400	9.875	0.532	43.448	25.0	3.0	18.45	0.98	600.0	32.5	17.9	0.60	11.30	4.63	1.8018
Gold-Operator	701.9	700	9.875	0.532	43.448	25.0	3.0	18.45	0.98	600.0	32.5	28.7	0.40	9.30	---	---
Gold-Operator	221.4	200	9.875	0.532	41.149	22.0	3.5	19.15	1.07	680.0	35.5	8.5	4.40	5.80	3.63	1.0098
Gold-Operator	252.3	300	9.875	0.532	41.149	22.0	3.5	19.15	1.07	680.0	35.5	9.7	0.56	10.60	4.50	2.7539
Gold-Operator	658.7	700	9.875	0.532	41.149	22.0	3.5	19.15	1.07	680.0	35.5	25.3	0.12	5.90	3.88	2.2461
Gold-Operator	924.3	900	9.875	0.532	41.149	22.0	3.5	19.15	1.07	680.0	35.5	35.4	0.07	5.10	4.38	0.4346
Gold-Operator	100.3	100	9.875	0.532	39.724	22.0	3.5	17.72	1.19	700.0	39.5	3.8	1.72	5.30	4.25	0.8613
Gold-Operator	812.8	800	9.875	0.532	39.724	22.0	3.5	17.72	1.19	700.0	39.5	30.7	0.16	6.20	4.00	1.7207
Gold-Operator	1652.1	1,700	9.875	0.532	39.724	22.0	3.5	17.72	1.19	700.0	39.5	62.4	0.05	10.00	4.25	1.9063
Gold-Operator	105.3	100	8.750	0.418	34.636	22.0	0.0	12.64	0.82	270.0	21.4	6.4	3.44	10.90	10.13	0.4590
Gold-Operator	206.0	200	8.750	0.418	34.636	22.0	0.0	12.64	0.82	270.0	21.4	12.5	1.34	12.20	7.75	0.6016
Gold-Operator	301.6	300	8.750	0.418	34.636	22.0	0.0	12.64	0.82	270.0	21.4	18.4	1.09	9.30	7.75	0.5830
Gold-Operator	409.1	400	8.750	0.418	34.636	22.0	0.0	12.64	0.82	270.0	21.4	24.9	0.76	7.80	7.88	0.8962
Gold-Operator	501.3	500	8.750	0.418	34.636	22.0	0.0	12.64	0.82	270.0	21.4	30.5	0.44	6.60	7.88	1.0156
Gold-Operator	583.1	600	8.750	0.418	34.636	22.0	0.0	12.64	0.82	270.0	21.4	35.5	0.31	7.70	7.63	0.9053
Gold-Operator	135.3	100	9.875	0.532	44.047	22.0	0.0	22.05	0.82	600.0	27.2	5.5	2.40	6.20	5.50	0.7930
Gold-Operator	198.8	200	9.875	0.532	44.047	22.0	0.0	22.05	0.82	600.0	27.2	8.1	1.76	15.00	4.88	0.8438
Gold-Operator	299.9	300	9.875	0.532	44.047	22.0	0.0	22.05	0.82	600.0	27.2	12.2	0.39	11.90	5.00	1.1689
Gold-Operator	400.4	400	9.875	0.532	44.047	22.0	0.0	22.05	0.82	600.0	27.2	16.3	0.26	7.60	4.88	1.4678
Gold-Operator	495.5	500	9.875	0.532	44.047	22.0	0.0	22.05	0.82	600.0	27.2	20.2	0.32	10.40	4.75	0.9482
Gold-Operator	562.0	600	9.875	0.532	44.047	22.0	0.0	22.05	0.82	600.0	27.2	22.9	0.29	10.40	6.38	0.4072
Gold-Operator	100.2	100	8.750	0.418	26.760	16.0	0.0	10.76	1.07	300.0	27.9	5.8	1.86	5.60	5.25	0.3945
Gold-Operator	158.5	200	8.750	0.418	26.760	16.0	0.0	10.76	1.07	300.0	27.9	9.2	0.44	16.50	21.00	0.2324
Gold-Operator	251.0	300	8.750	0.418	26.760	16.0	0.0	10.76	1.07	300.0	27.9	14.5	0.52	14.60	9.38	0.4844
Gold-Operator	516.0	500	8.750	0.418	26.760	16.0	0.0	10.76	1.07	300.0	27.9	29.8	0.08	23.20	30.13	0.8369
Gold-Operator	103.6	100	9.875	0.532	42.446	24.0	0.0	18.45	0.82	502.0	27.2	4.6	2.56	21.30	8.88	0.3145
Gold-Operator	323.2	300	9.875	0.532	42.446	24.0	0.0	18.45	0.82	502.0	27.2	14.4	0.45	19.60	7.75	0.9668
Gold-Operator	618.4	600	9.875	0.532	42.446	24.0	0.0	18.45	0.82	502.0	27.2	27.6	0.20	6.00	7.13	1.1290
Gold-Operator	248.8	200	9.875	0.532	43.522	22.0	0.0	21.52	0.98	700.0	32.5	9.4	1.20	8.80	9.31	0.3174
Gold-Operator	137.7	100	9.875	0.532	43.522	22.0	0.0	21.52	0.98	700.0	32.5	5.2	4.16	11.30	12.69	0.3662

Geology	Distance From Blast (ft)	Rounded Distance From Blast (ft)	Hole Diameter (inches)	Hole Area (sq. ft.)	Hole Depth (ft)	Stemming (ft)	Power Deck (ft)	Charge Length (ft)	Density (g/cc)	Charge Weight (lbs)	Weight per Unit Length (lbs/ft)	SRSD (ft/lb^0.5)	Radial PPV (ips)	Principal Radial Frequency (Hz)	Dominant Radial Frequency (Hz)	Waveform Duration (s)
Gold-Supplier	282.1	300	6.750	0.249	54.133	21.3	0.0	32.81	1.16	589.3	18.0	11.6	1.11	18.80	15.00	0.2810
Gold-Supplier	419.9	400	6.750	0.249	54.133	21.3	0.0	32.81	1.16	589.3	18.0	17.3	0.76	10.40	10.00	0.3460
Gold-Supplier	547.9	500	6.750	0.249	54.133	21.3	0.0	32.81	1.16	589.3	18.0	22.6	0.96	10.30	10.83	0.4047
Gold-Supplier	757.9	800	6.750	0.249	54.133	21.3	0.0	32.81	1.16	589.3	18.0	31.2	0.59	8.90	7.86	0.5674
Gold-Supplier	262.5	300	6.750	0.249	57.086	21.3	0.0	35.76	1.17	649.7	18.2	10.3	1.13	19.00	16.66	0.2737
Gold-Supplier	400.3	400	6.750	0.249	57.086	21.3	0.0	35.76	1.17	649.7	18.2	15.7	0.65	10.60	10.63	0.4713
Gold-Supplier	531.5	500	6.750	0.249	57.086	21.3	0.0	35.76	1.17	649.7	18.2	20.9	0.95	10.40	11.43	0.4601
Gold-Supplier	738.2	700	6.750	0.249	57.086	21.3	0.0	35.76	1.17	649.7	18.2	29.0	0.57	9.10	8.57	0.6070
Gold-Supplier	241.1	200	6.750	0.249	56.758	21.3	0.0	35.43	1.18	650.1	18.3	9.5	1.37	18.60	16.43	0.2895
Gold-Supplier	380.6	400	6.750	0.249	56.758	21.3	0.0	35.43	1.18	650.1	18.3	14.9	0.56	10.70	11.66	0.4182
Gold-Supplier	509.8	500	6.750	0.249	56.758	21.3	0.0	35.43	1.18	650.1	18.3	20.0	0.83	10.50	11.43	0.4412
Gold-Supplier	718.5	700	6.750	0.249	56.758	21.3	0.0	35.43	1.18	650.1	18.3	28.2	0.52	9.10	8.58	0.6017
Gold-Supplier	219.8	200	6.750	0.249	56.758	21.3	0.0	35.43	1.20	660.7	18.6	8.6	1.84	17.20	15.62	0.2837
Gold-Supplier	359.6	400	6.750	0.249	56.758	21.3	0.0	35.43	1.20	660.7	18.6	14.0	0.56	14.70	11.87	0.3363
Gold-Supplier	489.8	500	6.750	0.249	56.758	21.3	0.0	35.43	1.20	660.7	18.6	19.1	0.78	10.50	11.25	0.4446
Gold-Supplier	698.8	700	6.750	0.249	56.758	21.3	0.0	35.43	1.20	660.7	18.6	27.2	0.55	7.70	8.57	0.6000
Gold-Supplier	200.1	200	6.750	0.249	52.821	21.3	0.0	31.50	1.18	574.1	18.2	8.4	2.26	16.10	15.00	0.2572
Gold-Supplier	339.9	300	6.750	0.249	52.821	21.3	0.0	31.50	1.18	574.1	18.2	14.2	0.54	15.20	11.67	0.2359
Gold-Supplier	470.5	500	6.750	0.249	52.821	21.3	0.0	31.50	1.18	574.1	18.2	19.6	0.65	10.80	11.67	0.4276
Gold-Supplier	679.8	700	6.750	0.249	52.821	21.3	0.0	31.50	1.18	574.1	18.2	28.4	0.49	8.00	8.57	0.6012
Gold-Supplier	180.4	200	6.750	0.249	54.789	21.3	0.0	33.46	1.19	616.2	18.4	7.3	3.12	14.20	10.00	0.2663
Gold-Supplier	321.5	300	6.750	0.249	54.789	21.3	0.0	33.46	1.19	616.2	18.4	13.0	0.65	12.40	12.14	0.2801
Gold-Supplier	451.4	500	6.750	0.249	54.789	21.3	0.0	33.46	1.19	616.2	18.4	18.2	0.67	10.80	11.43	0.4219
Gold-Supplier	660.8	700	6.750	0.249	54.789	21.3	0.0	33.46	1.19	616.2	18.4	26.6	0.58	8.10	8.57	0.6659
Gold-Supplier	161.7	200	6.750	0.249	55.774	21.3	0.0	34.45	1.19	637.1	18.5	6.4	3.44	13.00	11.15	0.2762
Gold-Supplier	302.8	300	6.750	0.249	55.774	21.3	0.0	34.45	1.19	637.1	18.5	12.0	0.63	13.10	12.17	0.3372
Gold-Supplier	433.1	400	6.750	0.249	55.774	21.3	0.0	34.45	1.19	637.1	18.5	17.2	0.60	10.70	13.02	0.4719
Gold-Supplier	643.0	600	6.750	0.249	55.774	21.3	0.0	34.45	1.19	637.1	18.5	25.5	0.57	8.30	8.48	0.7010

Geology	Distance From Blast (ft)	Rounded Distance From Blast (ft)	Hole Diameter (inches)	Hole Area (sq. ft.)	Hole Depth (ft)	Stemming (ft)	Power Deck (ft)	Charge Length (ft)	Density (g/cc)	Charge Weight (lbs)	Weight per Unit Length (lbs/ft)	SRSD (ft/lb^0.5)	Radial PPV (ips)	Principal Radial Frequency (Hz)	Dominant Radial Frequency (Hz)	Waveform Duration (s)
Coal-Operator	1058.5	1,100	7.875	0.338	45.000	15.0	0.0	30.00	0.85	538.2	17.9	45.6	0.06	5.90	5.85	0.9619
Coal-Operator	1058.5	1,100	7.875	0.338	45.000	15.0	0.0	30.00	0.85	538.2	17.9	45.6	0.04	5.60	6.00	1.0283
Coal-Operator	1058.5	1,100	7.875	0.338	45.000	15.0	0.0	30.00	0.85	538.2	17.9	45.6	0.03	5.40	5.39	0.9849
Coal-Operator	1756.6	1,800	7.875	0.338	45.000	15.0	0.0	30.00	0.85	538.2	17.9	75.7	0.12	6.60	7.14	1.8627
Coal-Operator	954.4	1,000	7.875	0.338	45.000	15.0	0.0	30.00	0.85	538.2	17.9	41.1	0.09	8.80	6.43	0.7374
Coal-Operator	954.4	1,000	7.875	0.338	45.000	15.0	0.0	30.00	0.85	538.2	17.9	41.1	0.10	10.90	6.93	0.9968
Coal-Operator	954.4	1,000	7.875	0.338	45.000	15.0	0.0	30.00	0.85	538.2	17.9	41.1	0.10	18.30	14.18	0.7330
Coal-Operator	891.6	900	7.875	0.338	30.000	10.0	0.0	20.00	1.34	565.7	28.3	37.5	0.10	10.00	7.50	0.8917
Coal-Operator	891.6	900	7.875	0.338	30.000	10.0	0.0	20.00	1.34	565.7	28.3	37.5	0.30	12.80	14.30	0.5995
Coal-Operator	1132.5	1,100	7.875	0.338	30.000	10.0	0.0	20.00	1.34	565.7	28.3	47.6	0.03	5.60	5.00	1.1556
Coal-Operator	1132.5	1,100	7.875	0.338	30.000	10.0	0.0	20.00	1.34	565.7	28.3	47.6	0.04	4.80	5.30	0.9977
Coal-Operator	2002.0	2,000	7.875	0.338	45.000	9.0	0.0	36.00	1.10	835.8	23.2	69.2	0.04	6.60	9.38	1.5565
Coal-Operator	2002.0	2,000	7.875	0.338	45.000	9.0	0.0	36.00	1.10	835.8	23.2	69.2	0.07	5.80	5.89	1.6264
Coal-Operator	641.4	600	7.875	0.338	45.000	9.0	0.0	36.00	1.10	835.8	23.2	22.2	0.17	10.40	10.78	0.6460
Coal-Operator	641.4	600	7.875	0.338	45.000	9.0	0.0	36.00	1.10	835.8	23.2	22.2	0.26	10.40	10.84	0.6540
Coal-Operator	1427.1	1,400	7.875	0.338	45.000	10.0	0.0	35.00	1.10	812.6	23.2	50.1	0.05	4.70	4.45	1.3541
Coal-Operator	782.1	800	7.875	0.338	45.000	10.0	0.0	35.00	1.10	812.6	23.2	27.4	0.14	10.00	8.67	0.6987
Coal-Operator	1867.0	1,900	7.875	0.338	45.000	10.0	0.0	35.00	1.10	812.6	23.2	65.5	0.07	7.80	7.60	1.7249

Geology	Distance From Blast (ft)	Rounded Distance From Blast (ft)	Hole Diameter (inches)	Hole Area (sq. ft.)	Hole Depth (ft)	Stemming (ft)	Power Deck (ft)	Charge Length (ft)	Density (g/cc)	Charge Weight (lbs)	Weight per Unit Length (lbs/ft)	SRSD (ft/lb^0.5)	Radial PPV (ips)	Principal Radial Frequency (Hz)	Dominant Radial Frequency (Hz)	Waveform Duration (s)
LS Quarry	48.5	0	5	0.136	36.750	12.5	0.0	24.25	1.25	257.9	10.6	3.0	9.28	21.70	13.00	0.0674
LS Quarry	65.1	100	5	0.136	36.750	12.5	0.0	24.25	1.25	257.9	10.6	4.1	6.40	20.00	---	0.0854
LS Quarry	90.5	100	5	0.136	36.750	12.5	0.0	24.25	1.25	257.9	10.6	5.6	2.04	18.60	14.13	0.1406
LS Quarry	221.2	200	5	0.136	36.750	12.5	0.0	24.25	1.25	257.9	10.6	13.8	1.52	---	---	---
LS Quarry	498.1	500	5	0.136	36.750	12.5	0.0	24.25	1.25	257.9	10.6	31.0	1.28	---	---	---
LS Quarry	16.4	0	3.125	0.053	24.700	12.0	0.0	12.70	1.25	52.8	4.2	2.3	6.88	---	6.00	0.0918
LS Quarry	23.8	0	3.125	0.053	24.700	12.0	0.0	12.70	1.25	52.8	4.2	3.3	2.88	---	---	0.1113
LS Quarry	33.0	0	3.125	0.053	24.700	12.0	0.0	12.70	1.25	52.8	4.2	4.5	3.88	23.80	5.50	0.1431
LS Quarry	121.6	100	3.125	0.053	24.700	12.0	0.0	12.70	1.25	52.8	4.2	16.7	0.49	48.70	28.50	0.1377
LS Quarry	242.4	200	3.125	0.053	24.700	12.0	0.0	12.70	1.25	52.8	4.2	33.4	0.27	35.30	36.00	0.1689
LS Quarry	13.0	0	3.125	0.053	14.300	4.3	0.0	10.00	1.25	41.5	4.2	2.0	20.32	---	---	---
LS Quarry	20.9	0	3.125	0.053	14.300	4.3	0.0	10.00	1.25	41.5	4.2	3.2	13.60	---	---	---
LS Quarry	27.7	0	3.125	0.053	14.300	4.3	0.0	10.00	1.25	41.5	4.2	4.3	4.32	48.80	26.00	0.0713
LS Quarry	95.8	100	3.125	0.053	14.300	4.3	0.0	10.00	1.25	41.5	4.2	14.9	1.68	47.50	53.80	0.0762
LS Quarry	189.2	200	3.125	0.053	14.300	4.3	0.0	10.00	1.25	41.5	4.2	29.4	0.91	32.75	85.30	0.1030
LS Quarry	47.5	0	5	0.136	24.000	11.0	0.0	13.00	1.25	138.3	10.6	4.0	9.92	25.60	---	---
LS Quarry	83.4	100	5	0.136	24.000	11.0	0.0	13.00	1.25	138.3	10.6	7.1	3.68	24.90	27.00	0.0723
LS Quarry	116.3	100	5	0.136	24.000	11.0	0.0	13.00	1.25	138.3	10.6	9.9	1.92	23.80	26.00	0.1147
LS Quarry	209.9	200	5	0.136	24.000	11.0	0.0	13.00	1.25	138.3	10.6	17.9	1.14	44.50	25.00	0.1597
LS Quarry	294.7	300	5	0.136	24.000	11.0	0.0	13.00	1.25	138.3	10.6	25.1	0.74	78.70	24.00	0.1729
LS Quarry	485.3	500	5	0.136	24.000	11.0	0.0	13.00	1.25	138.3	10.6	41.3	0.43	51.20	48.00	0.2256
LS Quarry	63.9	100	5.5	0.165	34.417	14.3	0.0	20.08	1.25	258.5	12.9	4.0	5.12	68.30	---	---
LS Quarry	108.1	100	5.5	0.165	34.417	14.3	0.0	20.08	1.25	258.5	12.9	6.7	1.76	24.90	10.00	0.0737
LS Quarry	162.7	200	5.5	0.165	34.417	14.3	0.0	20.08	1.25	258.5	12.9	10.1	1.36	39.30	11.00	0.0962
LS Quarry	293.0	300	5.5	0.165	34.417	14.3	0.0	20.08	1.25	258.5	12.9	18.2	0.50	28.40	30.00	0.2431
LS Quarry	403.2	400	5.5	0.165	34.417	14.3	0.0	20.08	1.25	258.5	12.9	25.1	0.26	35.30	33.00	0.1992
LS Quarry	706.9	700	5.5	0.165	34.417	14.3	0.0	20.08	1.25	258.5	12.9	44.0	0.23	36.50	35.00	0.2217

Geology	Distance From Blast (m)	Rounded Distance From Blast (m)	Hole Diameter (mm)	Hole Area (sq. m.)	Hole Depth (m)	Stemming (m)	Power Deck (m)	Charge Length (m)	Density (g/cc)	Charge Weight (kg)	Weight per Unit Length (kg/m)	SRSD (m/kg^0.5)	Radial PPV (mmps)	Principal Radial Frequency (Hz)	Dominant Radial Frequency (Hz)	Waveform Duration (s)
Gold-Operator	33.90	30.5	250.8	0.049	13.24	7.62	0.9	5.62	0.98	272.2	48.4	2.05	103.63	5.10	5.13	0.7500
Gold-Operator	87.57	91.4	250.8	0.049	13.24	7.62	0.9	5.62	0.98	272.2	48.4	5.31	27.43	11.90	9.00	1.0967
Gold-Operator	133.83	121.9	250.8	0.049	13.24	7.62	0.9	5.62	0.98	272.2	48.4	8.11	15.24	11.30	4.63	1.8018
Gold-Operator	213.93	213.4	250.8	0.049	13.24	7.62	0.9	5.62	0.98	272.2	48.4	12.97	10.16	9.30	---	---
Gold-Operator	67.49	61.0	250.8	0.049	12.54	6.71	1.1	5.84	1.07	308.4	52.8	3.84	111.76	5.80	3.63	1.0098
Gold-Operator	76.92	91.4	250.8	0.049	12.54	6.71	1.1	5.84	1.07	308.4	52.8	4.38	14.22	10.60	4.50	2.7539
Gold-Operator	200.79	213.4	250.8	0.049	12.54	6.71	1.1	5.84	1.07	308.4	52.8	11.43	3.05	5.90	3.88	2.2461
Gold-Operator	281.74	274.3	250.8	0.049	12.54	6.71	1.1	5.84	1.07	308.4	52.8	16.04	1.78	5.10	4.38	0.4346
Gold-Operator	30.57	30.5	250.8	0.049	12.11	6.71	1.1	5.40	1.19	317.5	58.8	1.72	43.69	5.30	4.25	0.8613
Gold-Operator	247.74	243.8	250.8	0.049	12.11	6.71	1.1	5.40	1.19	317.5	58.8	13.90	4.06	6.20	4.00	1.7207
Gold-Operator	503.56	518.2	250.8	0.049	12.11	6.71	1.1	5.40	1.19	317.5	58.8	28.26	1.27	10.00	4.25	1.9063
Gold-Operator	32.09	30.5	222.3	0.039	10.56	6.71	0.0	3.85	0.82	122.5	31.8	2.90	87.38	10.90	10.13	0.4590
Gold-Operator	62.80	61.0	222.3	0.039	10.56	6.71	0.0	3.85	0.82	122.5	31.8	5.67	34.04	12.20	7.75	0.6016
Gold-Operator	91.94	91.4	222.3	0.039	10.56	6.71	0.0	3.85	0.82	122.5	31.8	8.31	27.69	9.30	7.75	0.5830
Gold-Operator	124.70	121.9	222.3	0.039	10.56	6.71	0.0	3.85	0.82	122.5	31.8	11.27	19.30	7.80	7.88	0.8962
Gold-Operator	152.79	152.4	222.3	0.039	10.56	6.71	0.0	3.85	0.82	122.5	31.8	13.81	11.18	6.60	7.88	1.0156
Gold-Operator	177.72	182.9	222.3	0.039	10.56	6.71	0.0	3.85	0.82	122.5	31.8	16.06	7.87	7.70	7.63	0.9053
Gold-Operator	41.25	30.5	250.8	0.049	13.43	6.71	0.0	6.72	0.82	272.2	40.5	2.50	60.96	6.20	5.50	0.7930
Gold-Operator	60.58	61.0	250.8	0.049	13.43	6.71	0.0	6.72	0.82	272.2	40.5	3.67	44.70	15.00	4.88	0.8438
Gold-Operator	91.41	91.4	250.8	0.049	13.43	6.71	0.0	6.72	0.82	272.2	40.5	5.54	9.91	11.90	5.00	1.1689
Gold-Operator	122.05	121.9	250.8	0.049	13.43	6.71	0.0	6.72	0.82	272.2	40.5	7.40	6.60	7.60	4.88	1.4678
Gold-Operator	151.03	152.4	250.8	0.049	13.43	6.71	0.0	6.72	0.82	272.2	40.5	9.15	8.13	10.40	4.75	0.9482
Gold-Operator	171.30	182.9	250.8	0.049	13.43	6.71	0.0	6.72	0.82	272.2	40.5	10.38	7.37	10.40	6.38	0.4072
Gold-Operator	30.54	30.5	222.3	0.039	8.16	4.88	0.0	3.28	1.07	136.1	41.5	2.62	47.24	5.60	5.25	0.3945
Gold-Operator	48.31	61.0	222.3	0.039	8.16	4.88	0.0	3.28	1.07	136.1	41.5	4.14	11.18	16.50	21.00	0.2324
Gold-Operator	76.50	91.4	222.3	0.039	8.16	4.88	0.0	3.28	1.07	136.1	41.5	6.56	13.21	14.60	9.38	0.4844
Gold-Operator	157.29	152.4	222.3	0.039	8.16	4.88	0.0	3.28	1.07	136.1	41.5	13.48	2.03	23.20	30.13	0.8369
Gold-Operator	31.57	30.5	250.8	0.049	12.94	7.32	0.0	5.62	0.82	227.7	40.5	2.09	65.02	21.30	8.88	0.3145
Gold-Operator	98.52	91.4	250.8	0.049	12.94	7.32	0.0	5.62	0.82	227.7	40.5	6.53	11.43	19.60	7.75	0.9668
Gold-Operator	188.48	182.9	250.8	0.049	12.94	7.32	0.0	5.62	0.82	227.7	40.5	12.49	5.08	6.00	7.13	1.1290
Gold-Operator	75.82	61.0	250.8	0.049	13.27	6.71	0.0	6.56	0.98	317.5	48.4	4.26	30.48	8.80	9.31	0.3174
Gold-Operator	41.99	30.5	250.8	0.049	13.27	6.71	0.0	6.56	0.98	317.5	48.4	2.36	105.66	11.30	12.69	0.3662

Geology	Distance From Blast (m)	Rounded Distance From Blast (m)	Hole Diameter (mm)	Hole Area (sq. m.)	Hole Depth (m)	Stemming (m)	Power Deck (m)	Charge Length (m)	Density (g/cc)	Charge Weight (kg)	Weight per Unit Length (kg/m)	SRSD (m/kg^0.5)	Radial PPV (mmps)	Principal Radial Frequency (Hz)	Dominant Radial Frequency (Hz)	Waveform Duration (s)
Gold-Supplier	86.00	91.4	171.5	0.023	16.50	6.50	0.0	10.00	1.16	267.3	26.7	5.26	28.19	18.80	15.00	0.2810
Gold-Supplier	128.00	121.9	171.5	0.023	16.50	6.50	0.0	10.00	1.16	267.3	26.7	7.83	19.25	10.40	10.00	0.3460
Gold-Supplier	167.00	152.4	171.5	0.023	16.50	6.50	0.0	10.00	1.16	267.3	26.7	10.21	24.42	10.30	10.83	0.4047
Gold-Supplier	231.00	243.8	171.5	0.023	16.50	6.50	0.0	10.00	1.16	267.3	26.7	14.13	14.89	8.90	7.86	0.5674
Gold-Supplier	80.00	91.4	171.5	0.023	17.40	6.50	0.0	10.90	1.17	294.7	27.0	4.66	28.60	19.00	16.66	0.2737
Gold-Supplier	122.00	121.9	171.5	0.023	17.40	6.50	0.0	10.90	1.17	294.7	27.0	7.11	16.59	10.60	10.63	0.4713
Gold-Supplier	162.00	152.4	171.5	0.023	17.40	6.50	0.0	10.90	1.17	294.7	27.0	9.44	24.05	10.40	11.43	0.4601
Gold-Supplier	225.00	213.4	171.5	0.023	17.40	6.50	0.0	10.90	1.17	294.7	27.0	13.11	14.49	9.10	8.57	0.6070
Gold-Supplier	73.50	61.0	171.5	0.023	17.30	6.50	0.0	10.80	1.18	294.9	27.3	4.28	34.90	18.60	16.43	0.2895
Gold-Supplier	116.00	121.9	171.5	0.023	17.30	6.50	0.0	10.80	1.18	294.9	27.3	6.75	14.20	10.70	11.66	0.4182
Gold-Supplier	155.40	152.4	171.5	0.023	17.30	6.50	0.0	10.80	1.18	294.9	27.3	9.05	21.02	10.50	11.43	0.4412
Gold-Supplier	219.00	213.4	171.5	0.023	17.30	6.50	0.0	10.80	1.18	294.9	27.3	12.75	13.29	9.10	8.58	0.6017
Gold-Supplier	67.00	61.0	171.5	0.023	17.30	6.50	0.0	10.80	1.20	299.7	27.8	3.87	46.81	17.20	15.62	0.2837
Gold-Supplier	109.60	121.9	171.5	0.023	17.30	6.50	0.0	10.80	1.20	299.7	27.8	6.33	14.16	14.70	11.87	0.3363
Gold-Supplier	149.30	152.4	171.5	0.023	17.30	6.50	0.0	10.80	1.20	299.7	27.8	8.62	19.73	10.50	11.25	0.4446
Gold-Supplier	213.00	213.4	171.5	0.023	17.30	6.50	0.0	10.80	1.20	299.7	27.8	12.30	14.01	7.70	8.57	0.6000
Gold-Supplier	61.00	61.0	171.5	0.023	16.10	6.50	0.0	9.60	1.18	260.4	27.1	3.78	57.28	16.10	15.00	0.2572
Gold-Supplier	103.60	91.4	171.5	0.023	16.10	6.50	0.0	9.60	1.18	260.4	27.1	6.42	13.77	15.20	11.67	0.2359
Gold-Supplier	143.40	152.4	171.5	0.023	16.10	6.50	0.0	9.60	1.18	260.4	27.1	8.89	16.44	10.80	11.67	0.4276
Gold-Supplier	207.20	213.4	171.5	0.023	16.10	6.50	0.0	9.60	1.18	260.4	27.1	12.84	12.41	8.00	8.57	0.6012
Gold-Supplier	55.00	61.0	171.5	0.023	16.70	6.50	0.0	10.20	1.19	279.5	27.4	3.29	79.25	14.20	10.00	0.2663
Gold-Supplier	98.00	91.4	171.5	0.023	16.70	6.50	0.0	10.20	1.19	279.5	27.4	5.86	16.47	12.40	12.14	0.2801
Gold-Supplier	137.60	152.4	171.5	0.023	16.70	6.50	0.0	10.20	1.19	279.5	27.4	8.23	16.93	10.80	11.43	0.4219
Gold-Supplier	201.40	213.4	171.5	0.023	16.70	6.50	0.0	10.20	1.19	279.5	27.4	12.05	14.71	8.10	8.57	0.6659
Gold-Supplier	49.30	61.0	171.5	0.023	17.00	6.50	0.0	10.50	1.19	289.0	27.5	2.90	87.45	13.00	11.15	0.2762
Gold-Supplier	92.30	91.4	171.5	0.023	17.00	6.50	0.0	10.50	1.19	289.0	27.5	5.43	16.08	13.10	12.17	0.3372
Gold-Supplier	132.00	121.9	171.5	0.023	17.00	6.50	0.0	10.50	1.19	289.0	27.5	7.76	15.12	10.70	13.02	0.4719
Gold-Supplier	196.00	182.9	171.5	0.023	17.00	6.50	0.0	10.50	1.19	289.0	27.5	11.53	14.51	8.30	8.48	0.7010

Geology	Distance From Blast (m)	Rounded Distance From Blast (m)	Hole Diameter (mm)	Hole Area (sq. m.)	Hole Depth (m)	Stemming (m)	Power Deck (m)	Charge Length (m)	Density (g/cc)	Charge Weight (kg)	Weight per Unit Length (kg/m)	SRSD (m/kg^0.5)	Radial PPV (mmps)	Principal Radial Frequency (Hz)	Dominant Radial Frequency (Hz)	Waveform Duration (s)
Coal-Operator	322.64	335.3	200.0	0.031	13.72	4.57	0.0	9.14	0.85	244.1	26.7	20.65	1.52	5.90	5.85	0.9619
Coal-Operator	322.64	335.3	200.0	0.031	13.72	4.57	0.0	9.14	0.85	244.1	26.7	20.65	1.02	5.60	6.00	1.0283
Coal-Operator	322.64	335.3	200.0	0.031	13.72	4.57	0.0	9.14	0.85	244.1	26.7	20.65	0.76	5.40	5.39	0.9849
Coal-Operator	535.42	548.6	200.0	0.031	13.72	4.57	0.0	9.14	0.85	244.1	26.7	34.27	3.05	6.60	7.14	1.8627
Coal-Operator	290.92	304.8	200.0	0.031	13.72	4.57	0.0	9.14	0.85	244.1	26.7	18.62	2.16	8.80	6.43	0.7374
Coal-Operator	290.92	304.8	200.0	0.031	13.72	4.57	0.0	9.14	0.85	244.1	26.7	18.62	2.41	10.90	6.93	0.9968
Coal-Operator	290.92	304.8	200.0	0.031	13.72	4.57	0.0	9.14	0.85	244.1	26.7	18.62	2.41	18.30	14.18	0.7330
Coal-Operator	271.78	274.3	200.0	0.031	9.14	3.05	0.0	6.10	1.34	256.6	42.1	16.97	2.41	10.00	7.50	0.8917
Coal-Operator	271.78	274.3	200.0	0.031	9.14	3.05	0.0	6.10	1.34	256.6	42.1	16.97	7.49	12.80	14.30	0.5995
Coal-Operator	345.20	335.3	200.0	0.031	9.14	3.05	0.0	6.10	1.34	256.6	42.1	21.55	0.76	5.60	5.00	1.1556
Coal-Operator	345.20	335.3	200.0	0.031	9.14	3.05	0.0	6.10	1.34	256.6	42.1	21.55	0.89	4.80	5.30	0.9977
Coal-Operator	610.22	609.6	200.0	0.031	13.72	2.74	0.0	10.97	1.10	379.1	34.6	31.34	1.02	6.60	9.38	1.5565
Coal-Operator	610.22	609.6	200.0	0.031	13.72	2.74	0.0	10.97	1.10	379.1	34.6	31.34	1.65	5.80	5.89	1.6264
Coal-Operator	195.50	182.9	200.0	0.031	13.72	2.74	0.0	10.97	1.10	379.1	34.6	10.04	4.19	10.40	10.78	0.6460
Coal-Operator	195.50	182.9	200.0	0.031	13.72	2.74	0.0	10.97	1.10	379.1	34.6	10.04	6.60	10.40	10.84	0.6540
Coal-Operator	434.97	426.7	200.0	0.031	13.72	3.05	0.0	10.67	1.10	368.6	34.6	22.66	1.27	4.70	4.45	1.3541
Coal-Operator	238.39	243.8	200.0	0.031	13.72	3.05	0.0	10.67	1.10	368.6	34.6	12.42	3.56	10.00	8.67	0.6987
Coal-Operator	569.08	579.1	200.0	0.031	13.72	3.05	0.0	10.67	1.10	368.6	34.6	29.64	1.78	7.80	7.60	1.7249

Geology	Distance From Blast (m)	Rounded Distance From Blast (m)	Hole Diameter (mm)	Hole Area (sq. m.)	Hole Depth (m)	Stemming (m)	Power Deck (m)	Charge Length (m)	Density (g/cc)	Charge Weight (kg)	Weight per Unit Length (kg/m)	SRSD (m/kg^0.5)	Radial PPV (mmps)	Principal Radial Frequency (Hz)	Dominant Radial Frequency (Hz)	Waveform Duration (s)
LS Quarry	14.78	0.0	127.0	0.013	11.20	3.81	0.0	7.39	1.25	117.0	15.8	1.37	235.71	21.70	13.00	0.0674
LS Quarry	19.84	30.5	127.0	0.013	11.20	3.81	0.0	7.39	1.25	117.0	15.8	1.83	162.56	20.00	---	0.0854
LS Quarry	27.58	30.5	127.0	0.013	11.20	3.81	0.0	7.39	1.25	117.0	15.8	2.55	51.82	18.60	14.13	0.1406
LS Quarry	67.42	61.0	127.0	0.013	11.20	3.81	0.0	7.39	1.25	117.0	15.8	6.23	38.61	---	---	---
LS Quarry	151.82	152.4	127.0	0.013	11.20	3.81	0.0	7.39	1.25	117.0	15.8	14.04	32.51	---	---	---
LS Quarry	5.00	0.0	79.4	0.005	7.53	3.66	0.0	3.87	1.25	23.9	6.2	1.02	174.75	---	6.00	0.0918
LS Quarry	7.25	0.0	79.4	0.005	7.53	3.66	0.0	3.87	1.25	23.9	6.2	1.48	73.15	---	---	0.1113
LS Quarry	10.06	0.0	79.4	0.005	7.53	3.66	0.0	3.87	1.25	23.9	6.2	2.06	98.55	23.80	5.50	0.1431
LS Quarry	37.06	30.5	79.4	0.005	7.53	3.66	0.0	3.87	1.25	23.9	6.2	7.58	12.45	48.70	28.50	0.1377
LS Quarry	73.88	61.0	79.4	0.005	7.53	3.66	0.0	3.87	1.25	23.9	6.2	15.10	6.86	35.30	36.00	0.1689
LS Quarry	3.96	0.0	79.4	0.005	4.36	1.31	0.0	3.05	1.25	18.8	6.2	0.91	516.13	---	---	---
LS Quarry	6.37	0.0	79.4	0.005	4.36	1.31	0.0	3.05	1.25	18.8	6.2	1.47	345.44	---	---	---
LS Quarry	8.44	0.0	79.4	0.005	4.36	1.31	0.0	3.05	1.25	18.8	6.2	1.94	109.73	48.80	26.00	0.0713
LS Quarry	29.20	30.5	79.4	0.005	4.36	1.31	0.0	3.05	1.25	18.8	6.2	6.73	42.67	47.50	53.80	0.0762
LS Quarry	57.67	61.0	79.4	0.005	4.36	1.31	0.0	3.05	1.25	18.8	6.2	13.28	23.11	32.75	85.30	0.1030
LS Quarry	14.48	0.0	127.0	0.013	7.32	3.35	0.0	3.96	1.25	62.7	15.8	1.83	251.97	25.60	---	---
LS Quarry	25.42	30.5	127.0	0.013	7.32	3.35	0.0	3.96	1.25	62.7	15.8	3.21	93.47	24.90	27.00	0.0723
LS Quarry	35.45	30.5	127.0	0.013	7.32	3.35	0.0	3.96	1.25	62.7	15.8	4.48	48.77	23.80	26.00	0.1147
LS Quarry	63.98	61.0	127.0	0.013	7.32	3.35	0.0	3.96	1.25	62.7	15.8	8.08	28.96	44.50	25.00	0.1597
LS Quarry	89.83	91.4	127.0	0.013	7.32	3.35	0.0	3.96	1.25	62.7	15.8	11.34	18.80	78.70	24.00	0.1729
LS Quarry	147.92	152.4	127.0	0.013	7.32	3.35	0.0	3.96	1.25	62.7	15.8	18.68	10.92	51.20	48.00	0.2256
LS Quarry	19.48	30.5	139.7	0.015	10.49	4.37	0.0	6.12	1.25	117.2	19.2	1.80	130.05	68.30	---	---
LS Quarry	32.94	30.5	139.7	0.015	10.49	4.37	0.0	6.12	1.25	117.2	19.2	3.04	44.70	24.90	10.00	0.0737
LS Quarry	49.58	61.0	139.7	0.015	10.49	4.37	0.0	6.12	1.25	117.2	19.2	4.58	34.54	39.30	11.00	0.0962
LS Quarry	89.31	91.4	139.7	0.015	10.49	4.37	0.0	6.12	1.25	117.2	19.2	8.25	12.70	28.40	30.00	0.2431
LS Quarry	122.89	121.9	139.7	0.015	10.49	4.37	0.0	6.12	1.25	117.2	19.2	11.35	6.60	35.30	33.00	0.1992
LS Quarry	215.47	213.4	139.7	0.015	10.49	4.37	0.0	6.12	1.25	117.2	19.2	19.90	5.84	36.50	35.00	0.2217

APPENDIX D

ROUNDED DISTANCE CHARTS

Appendix D provides the rounded distance charts that were used to qualitatively evaluate the signature hole dataset. Each rounded distance chart compares a variable that affects blast vibration to a blast vibration feature at rounded distances of 30.5 m (100 ft) from the blast. Trendlines are included to aid in the qualitative evaluation process.

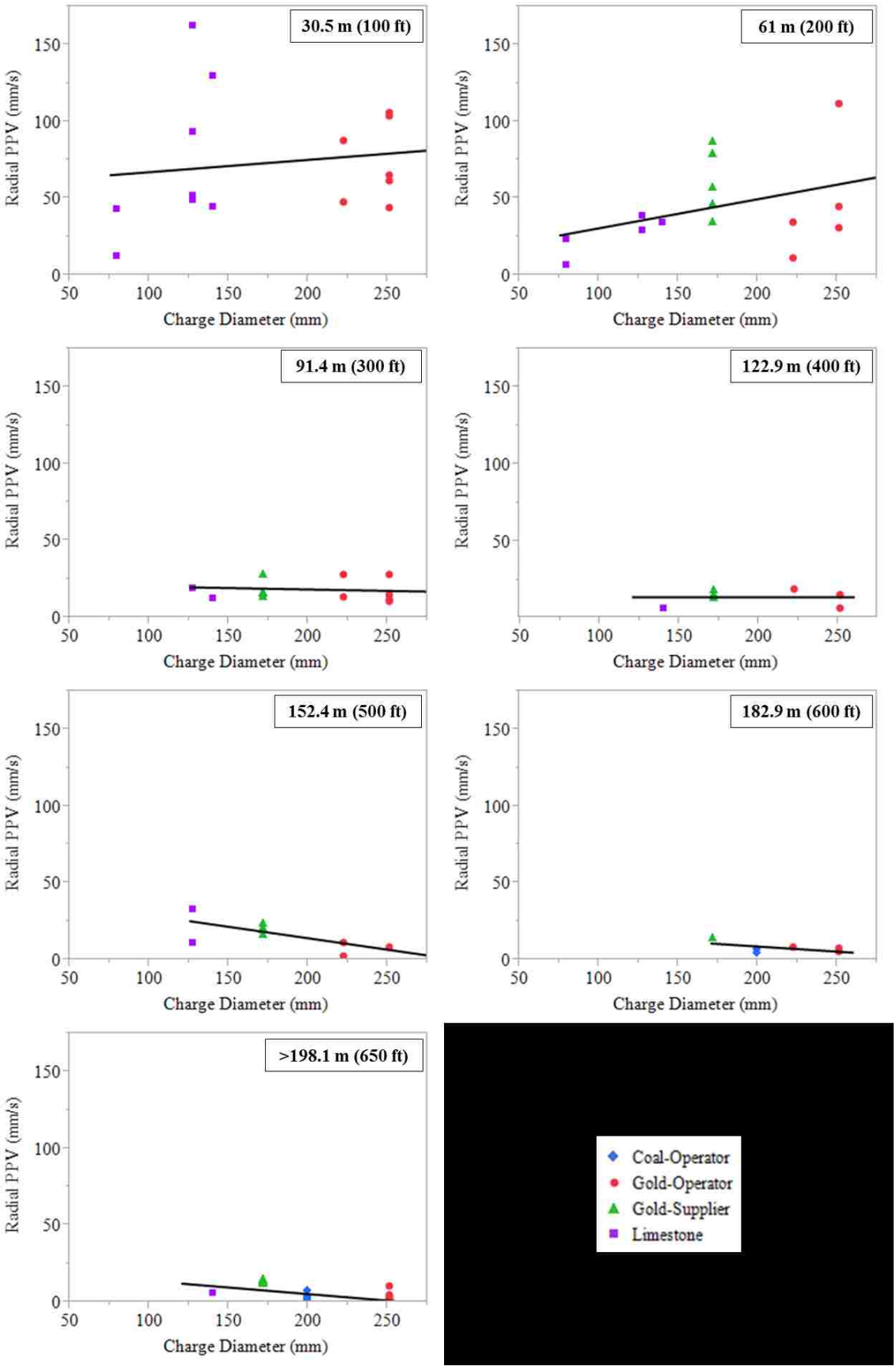
30.5 m (100 ft)
61 m (200 ft)
91.4 m (300 ft)
122.9 m (400 ft)
152.4 m (500 ft)
182.9 m (600 ft)
>198.1 m (650 ft)
Radial PPV (mm/s)
Charge Diameter (mm)
0
50
100
150
200
250
Coal-Operator
Gold-Operator
Gold-Supplier
Limestone

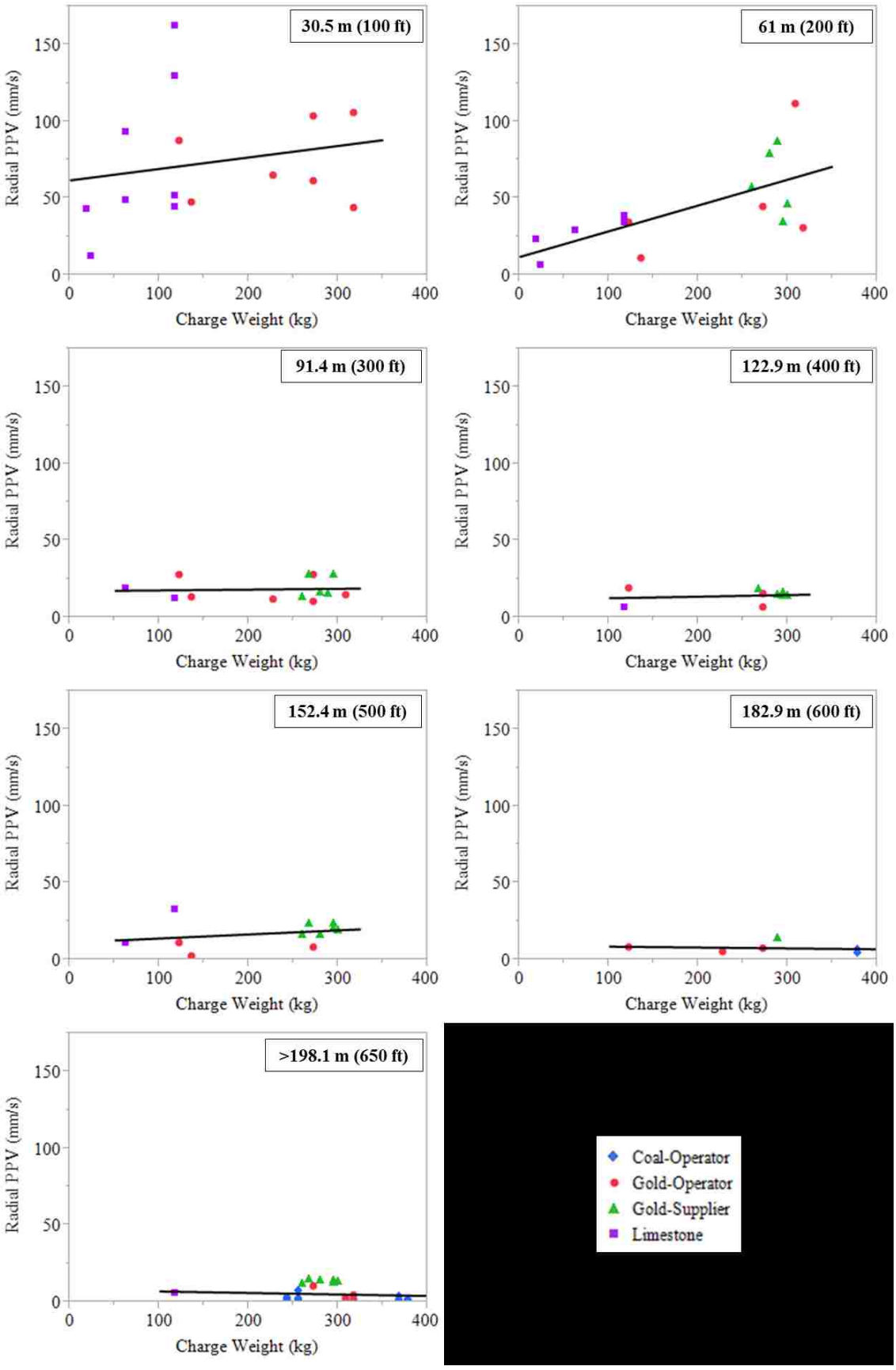
30.5 m (100 ft)
61 m (200 ft)
91.4 m (300 ft)
122.9 m (400 ft)
152.4 m (500 ft)
182.9 m (600 ft)
>198.1 m (650 ft)
Radial PPV (mm/s)
Charge Weight (kg)
0
50
100
150
200
300
400
Coal-Operator
Gold-Operator
Gold-Supplier
Limestone

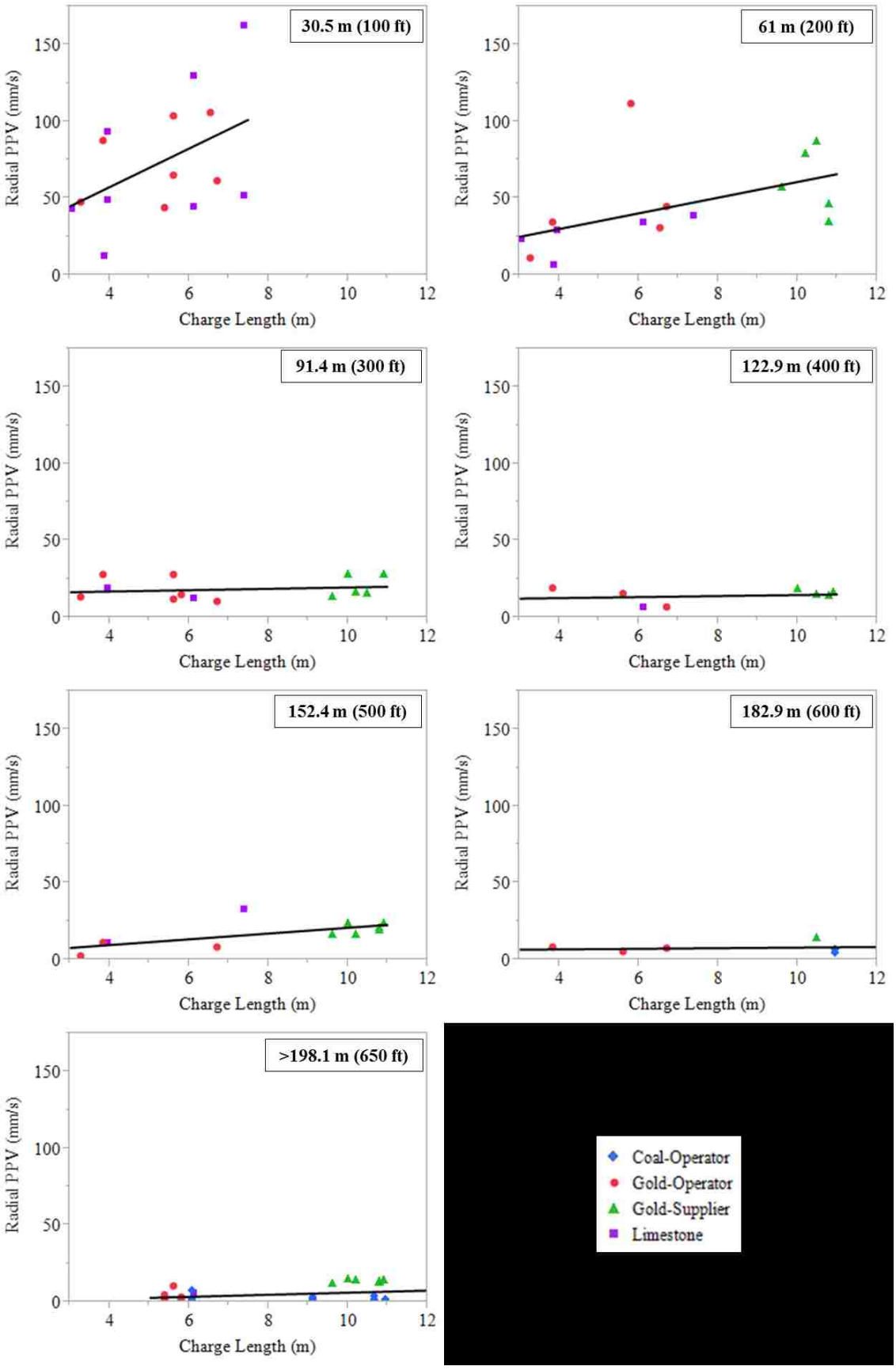
30.5 m (100 ft)
61 m (200 ft)
91.4 m (300 ft)
122.9 m (400 ft)
152.4 m (500 ft)
182.9 m (600 ft)
>198.1 m (650 ft)
Radial PPV (mm/s)
Charge Length (m)
0
50
100
150
4
6
8
10
12
Coal-Operator
Gold-Operator
Gold-Supplier
Limestone

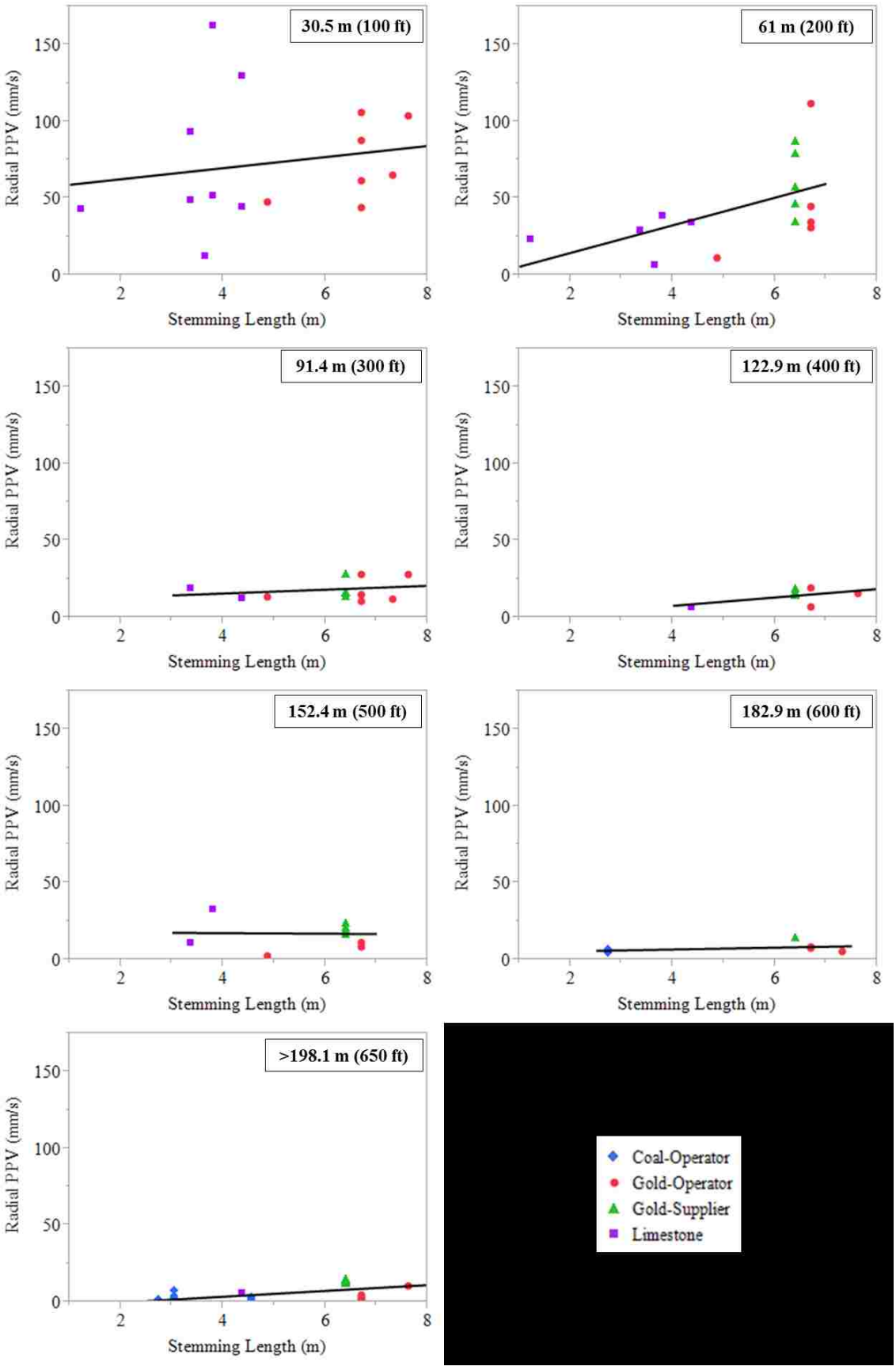
30.5 m (100 ft)
61 m (200 ft)
91.4 m (300 ft)
122.9 m (400 ft)
152.4 m (500 ft)
182.9 m (600 ft)
>198.1 m (650 ft)
Radial PPV (mm/s)
Stemming Length (m)
0
50
100
150
2
4
6
8
Coal-Operator
Gold-Operator
Gold-Supplier
Limestone

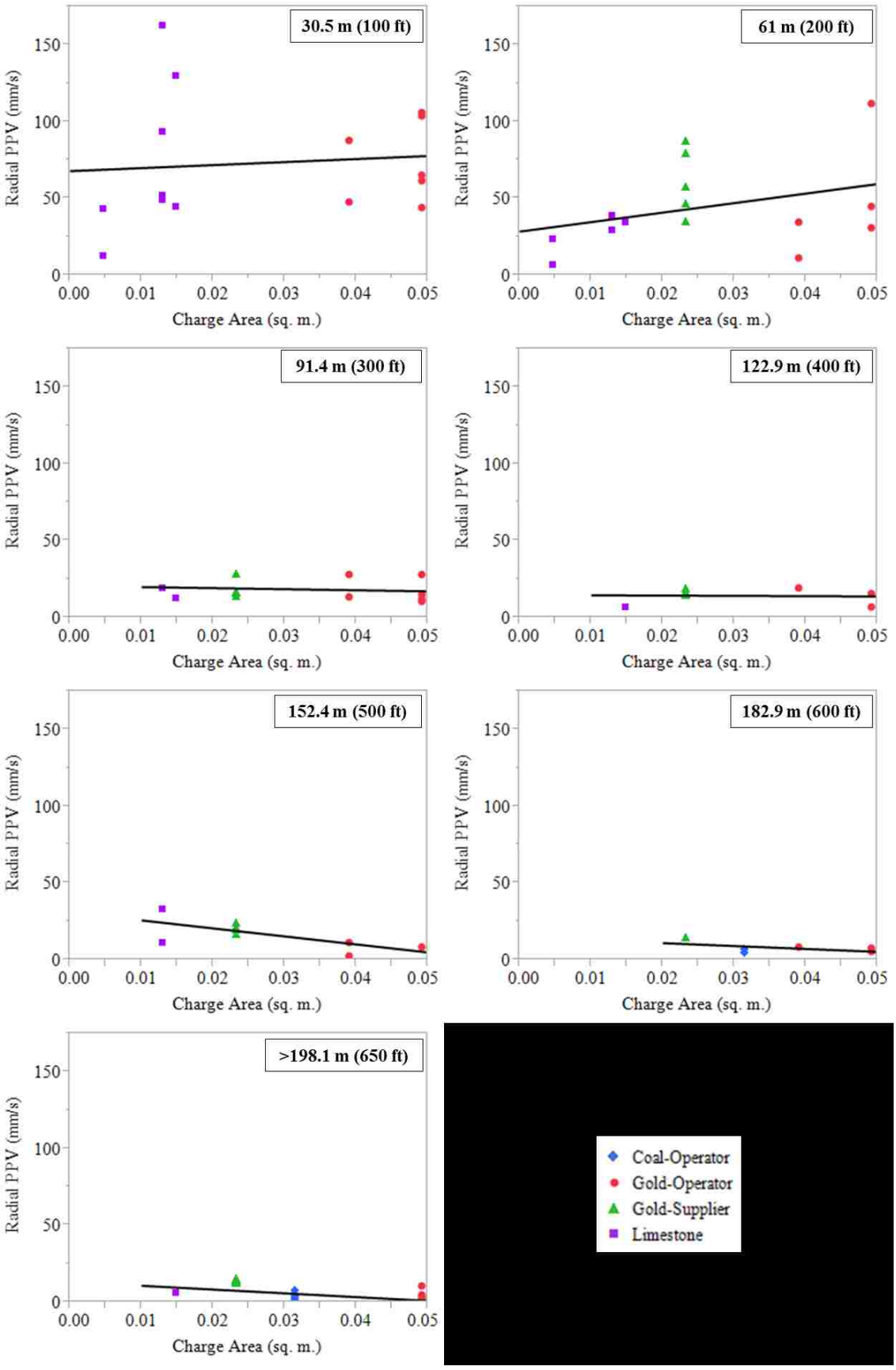
30.5 m (100 ft)
61 m (200 ft)
91.4 m (300 ft)
122.9 m (400 ft)
152.4 m (500 ft)
182.9 m (600 ft)
>198.1 m (650 ft)
Radial PPV (mm/s)
Charge Area (sq. m.)
0
50
100
150
0.00
0.01
0.02
0.03
0.04
0.05
Coal-Operator
Gold-Operator
Gold-Supplier
Limestone

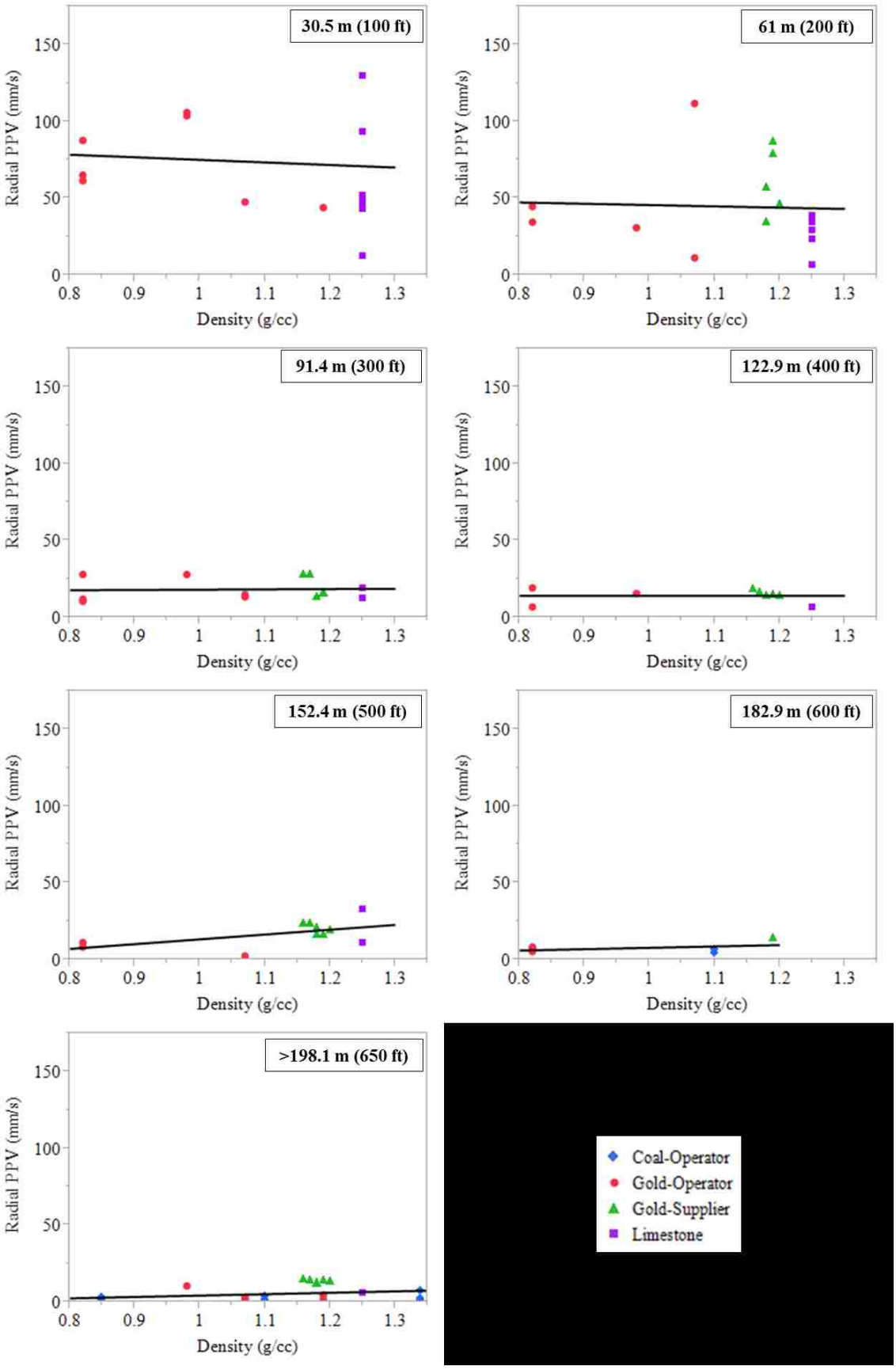
30.5 m (100 ft)
61 m (200 ft)
91.4 m (300 ft)
122.9 m (400 ft)
152.4 m (500 ft)
182.9 m (600 ft)
>198.1 m (650 ft)
Radial PPV (mm/s)
Density (g/cc)
Coal-Operator
Gold-Operator
Gold-Supplier
Limestone

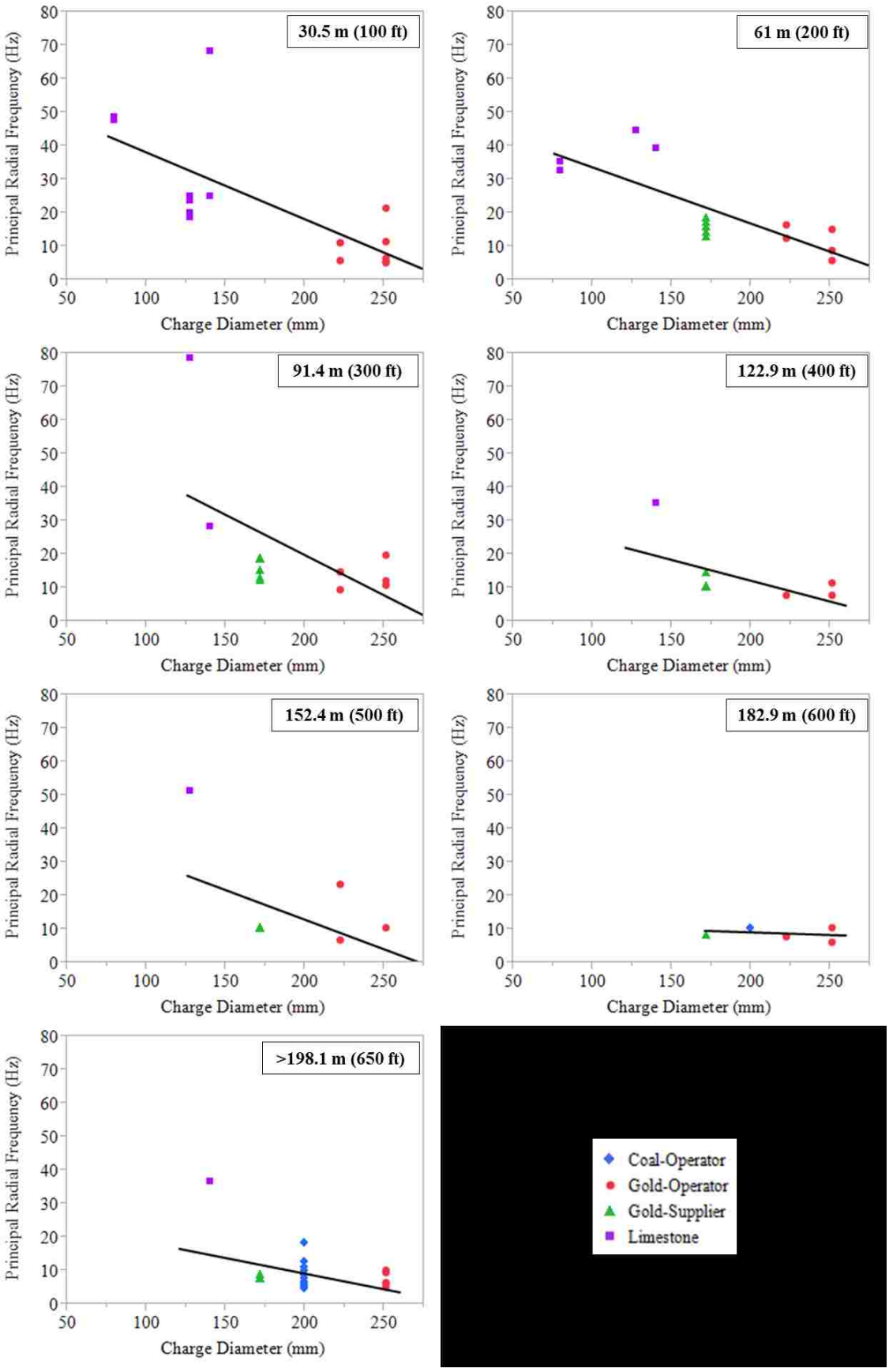
30.5 m (100 ft)
61 m (200 ft)
91.4 m (300 ft)
122.9 m (400 ft)
152.4 m (500 ft)
182.9 m (600 ft)
>198.1 m (650 ft)
Principal Radial Frequency (Hz)
Charge Diameter (mm)
Coal-Operator
Gold-Operator
Gold-Supplier
Limestone

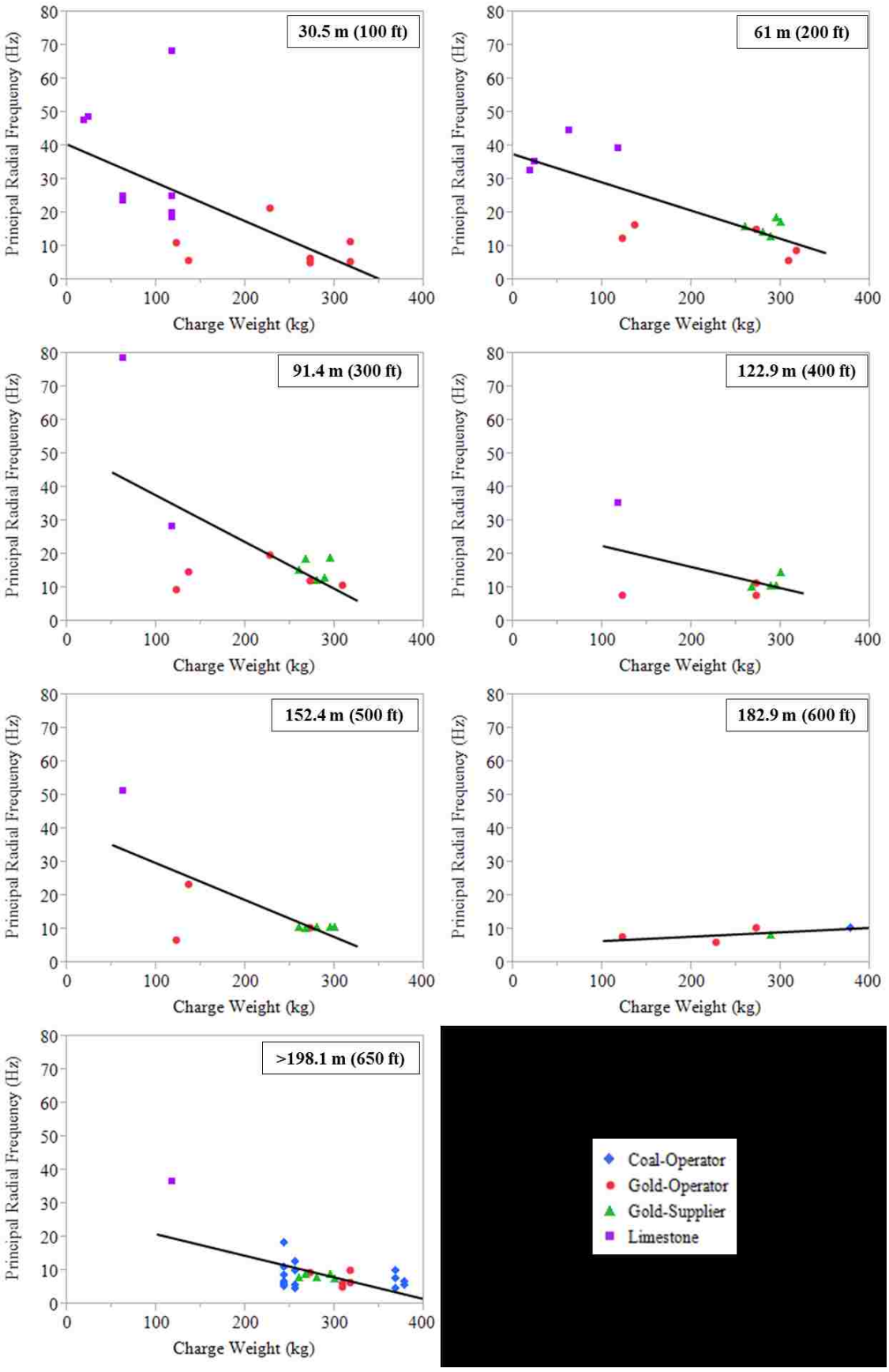
30.5 m (100 ft)
61 m (200 ft)
91.4 m (300 ft)
122.9 m (400 ft)
152.4 m (500 ft)
182.9 m (600 ft)
>198.1 m (650 ft)
Principal Radial Frequency (Hz)
Charge Weight (kg)
0
10
20
30
40
50
60
70
80
100
200
300
400
Coal-Operator
Gold-Operator
Gold-Supplier
Limestone

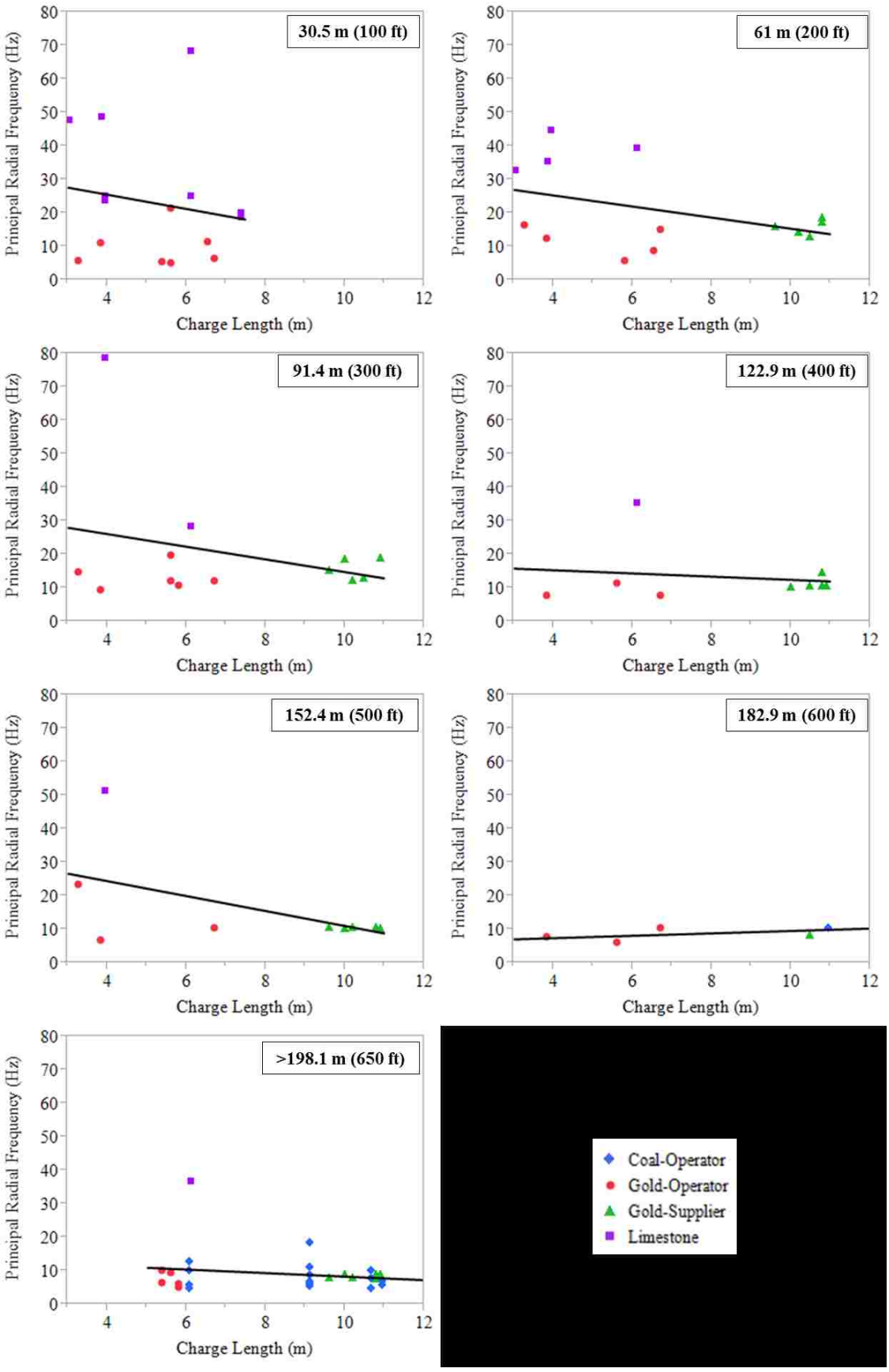
30.5 m (100 ft)
61 m (200 ft)
91.4 m (300 ft)
122.9 m (400 ft)
152.4 m (500 ft)
182.9 m (600 ft)
>198.1 m (650 ft)
Principal Radial Frequency (Hz)
Charge Length (m)
Coal-Operator
Gold-Operator
Gold-Supplier
Limestone

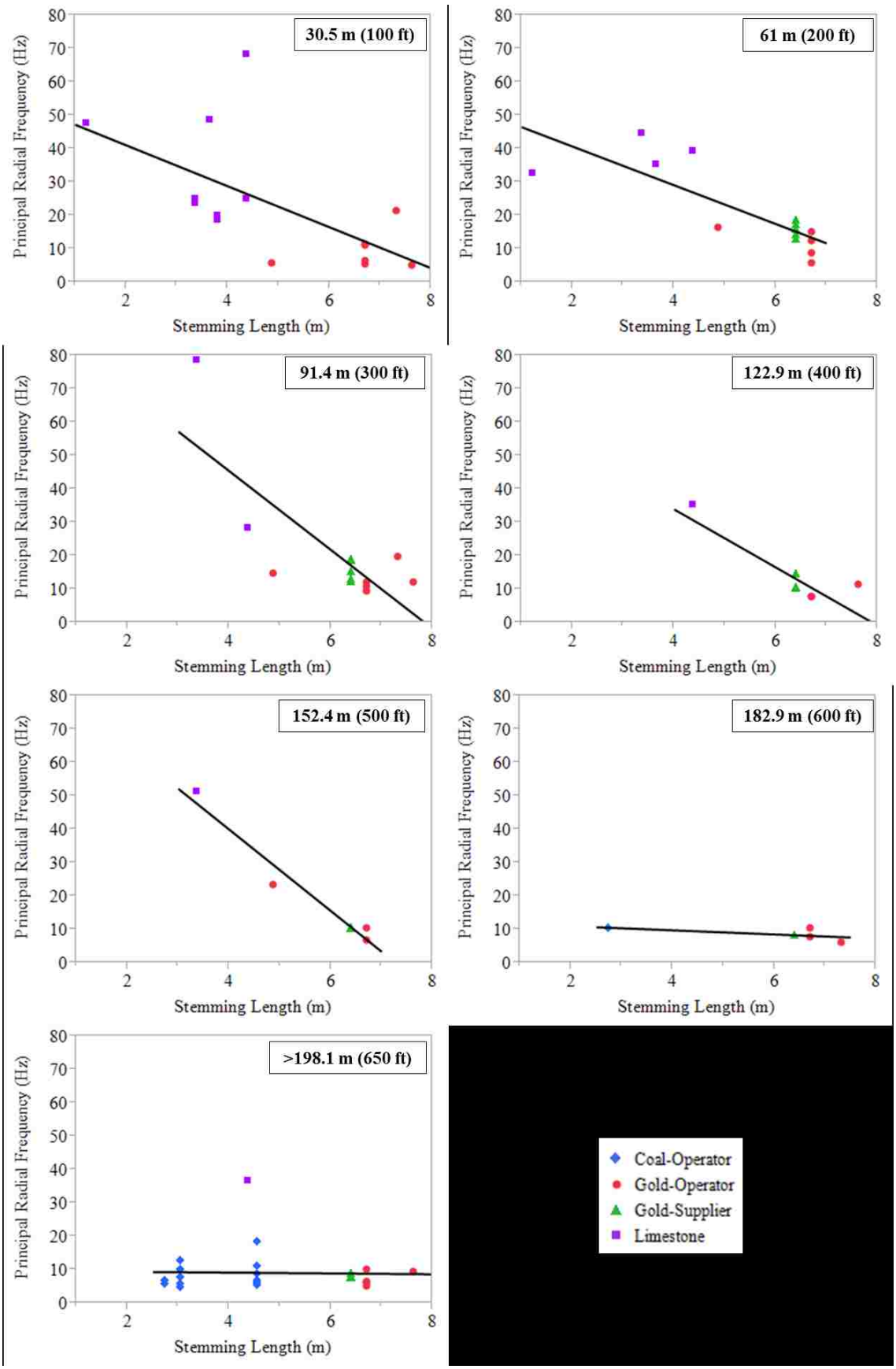
30.5 m (100 ft)
61 m (200 ft)
91.4 m (300 ft)
122.9 m (400 ft)
152.4 m (500 ft)
182.9 m (600 ft)
>198.1 m (650 ft)
Principal Radial Frequency (Hz)
Stemming Length (m)
Coal-Operator
Gold-Operator
Gold-Supplier
Limestone

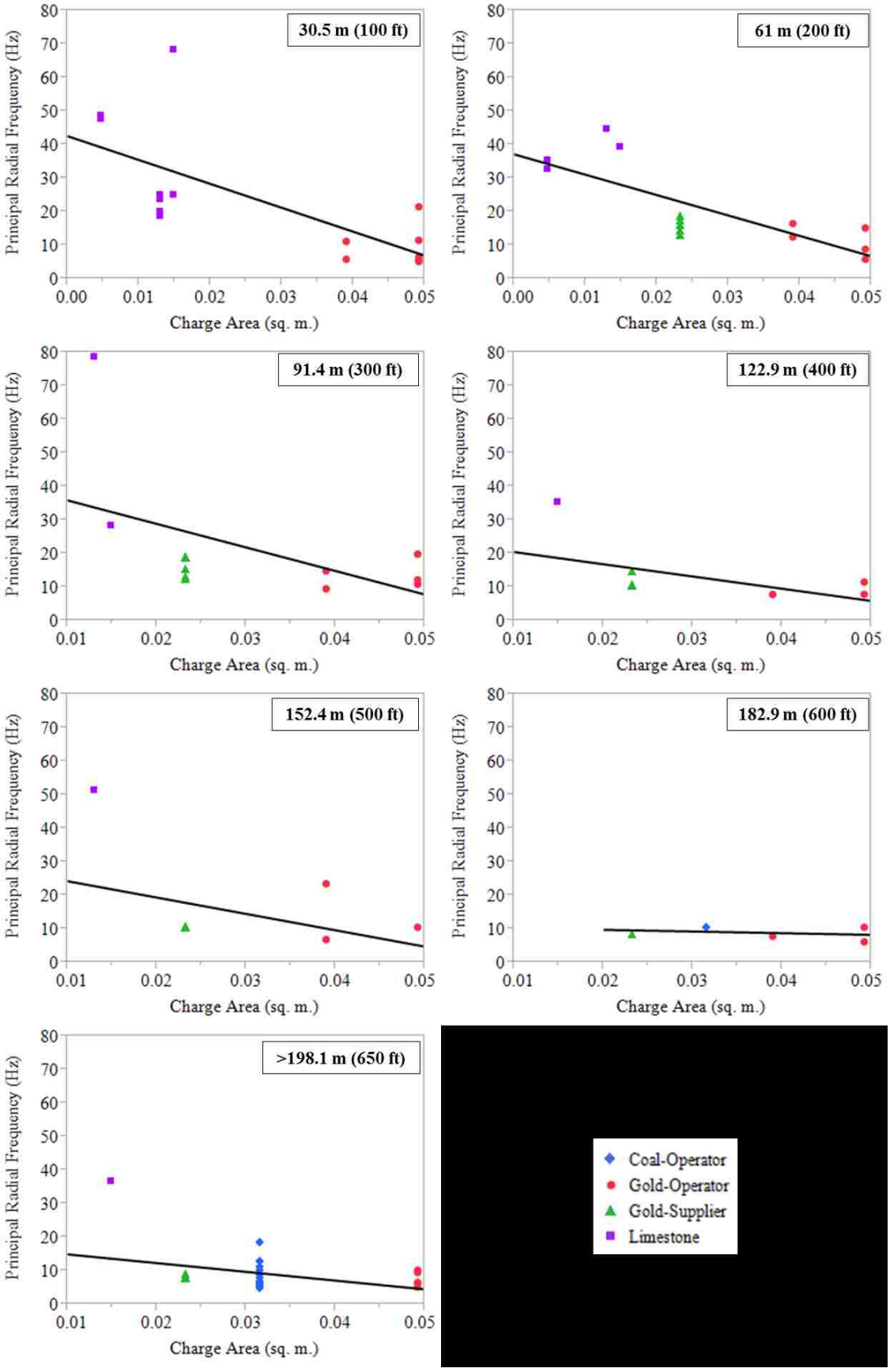
30.5 m (100 ft)
61 m (200 ft)
91.4 m (300 ft)
122.9 m (400 ft)
152.4 m (500 ft)
182.9 m (600 ft)
>198.1 m (650 ft)
Principal Radial Frequency (Hz)
Charge Area (sq. m.)
Coal-Operator
Gold-Operator
Gold-Supplier
Limestone

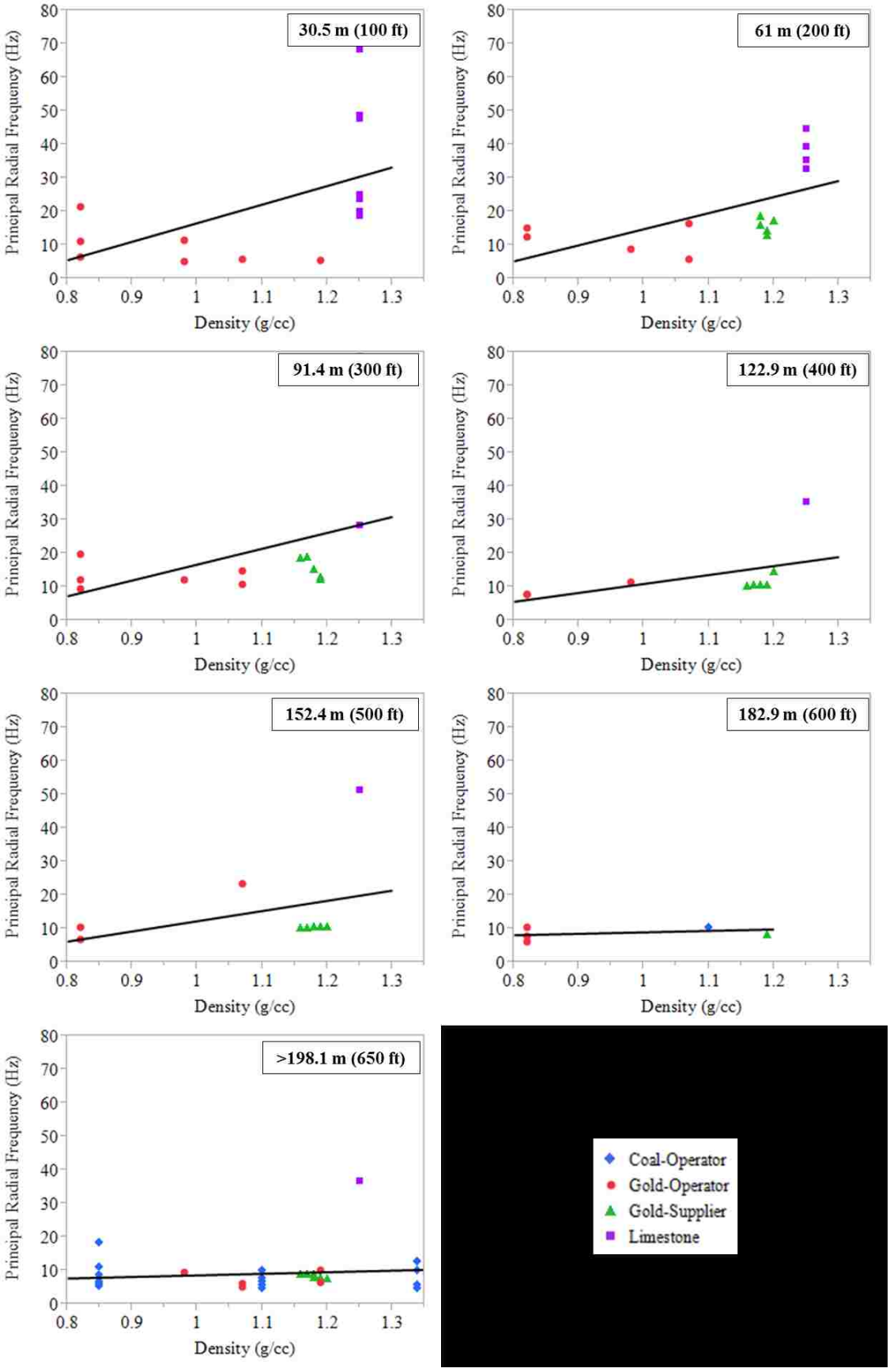
30.5 m (100 ft)
61 m (200 ft)
91.4 m (300 ft)
122.9 m (400 ft)
152.4 m (500 ft)
182.9 m (600 ft)
>198.1 m (650 ft)
Principal Radial Frequency (Hz)
Density (g/cc)
Coal-Operator
Gold-Operator
Gold-Supplier
Limestone

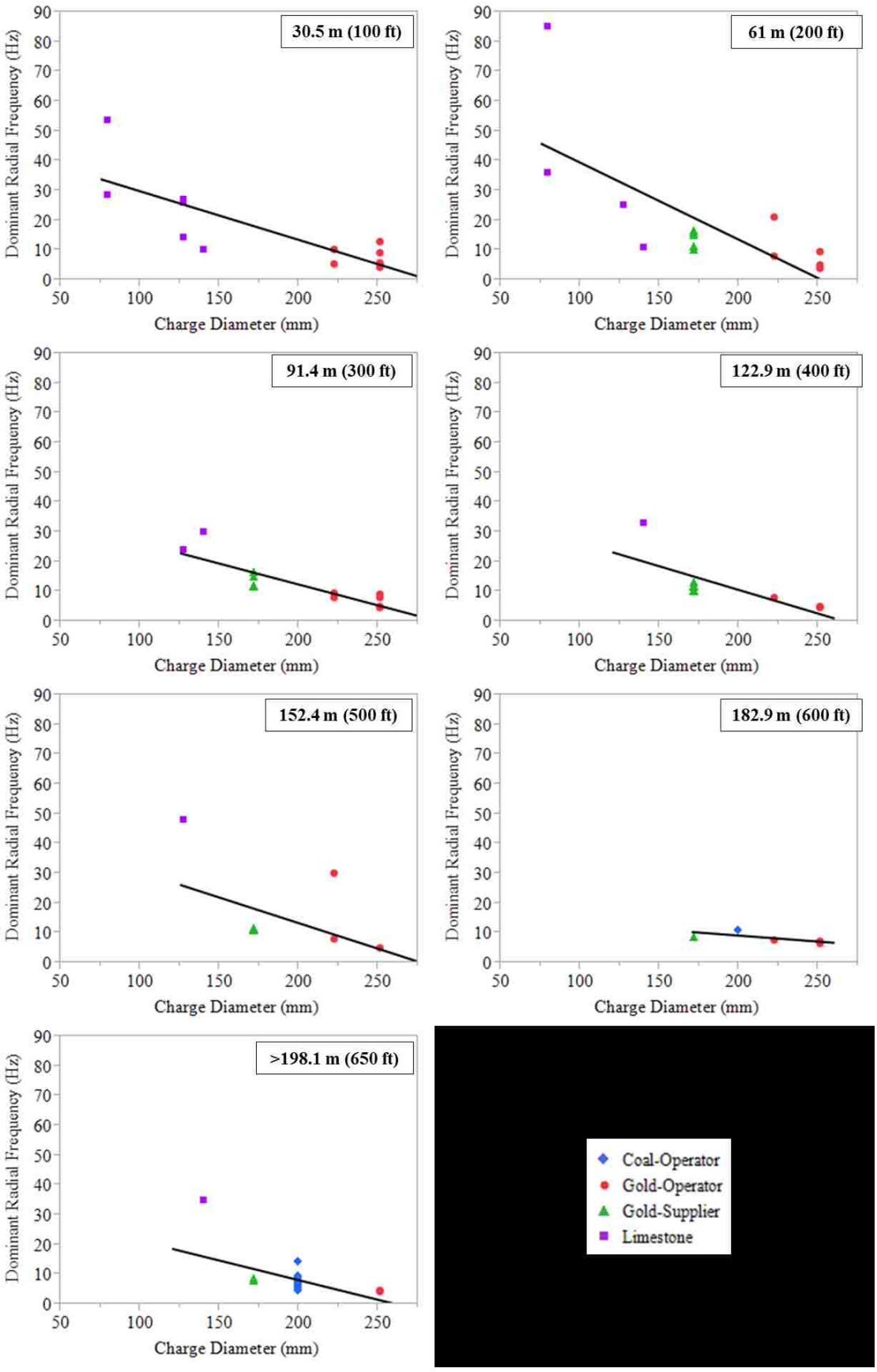
30.5 m (100 ft)
61 m (200 ft)
91.4 m (300 ft)
122.9 m (400 ft)
152.4 m (500 ft)
182.9 m (600 ft)
>198.1 m (650 ft)
Dominant Radial Frequency (Hz)
Charge Diameter (mm)
Coal-Operator
Gold-Operator
Gold-Supplier
Limestone

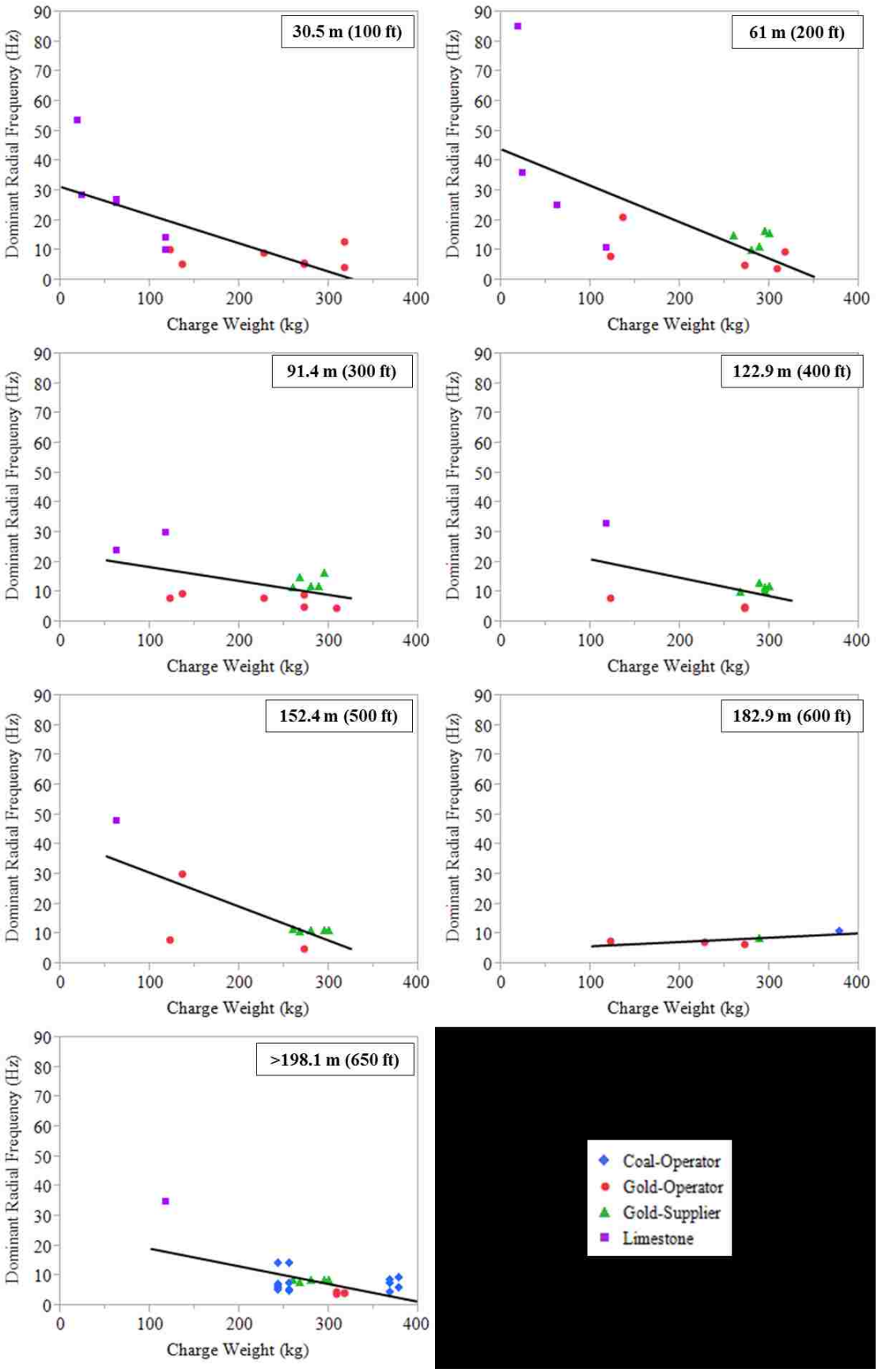
30.5 m (100 ft)
61 m (200 ft)
91.4 m (300 ft)
122.9 m (400 ft)
152.4 m (500 ft)
182.9 m (600 ft)
>198.1 m (650 ft)
Dominant Radial Frequency (Hz)
Charge Weight (kg)
Coal-Operator
Gold-Operator
Gold-Supplier
Limestone

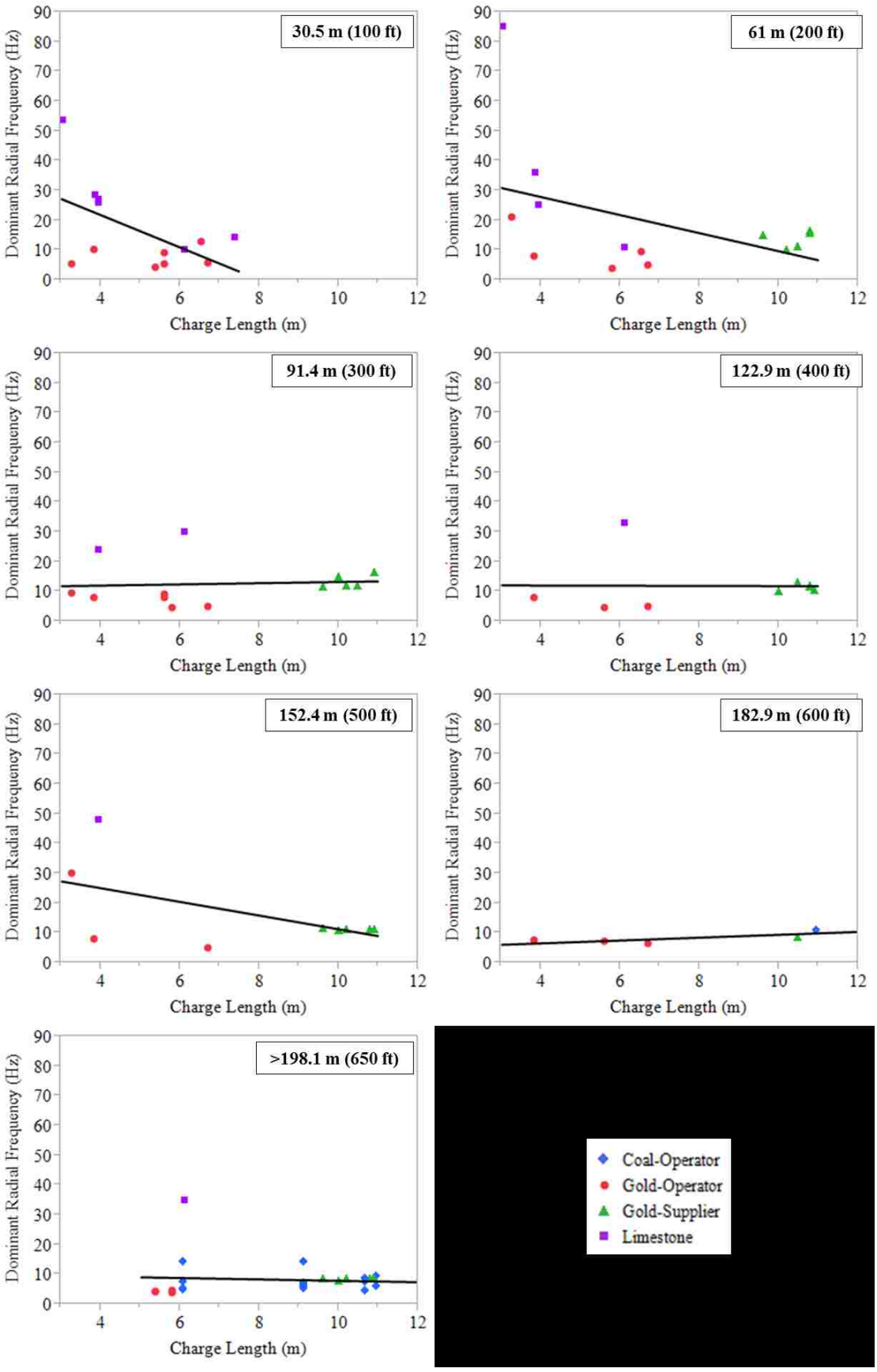
30.5 m (100 ft)
61 m (200 ft)
91.4 m (300 ft)
122.9 m (400 ft)
152.4 m (500 ft)
182.9 m (600 ft)
>198.1 m (650 ft)
Dominant Radial Frequency (Hz)
Charge Length (m)
Coal-Operator
Gold-Operator
Gold-Supplier
Limestone

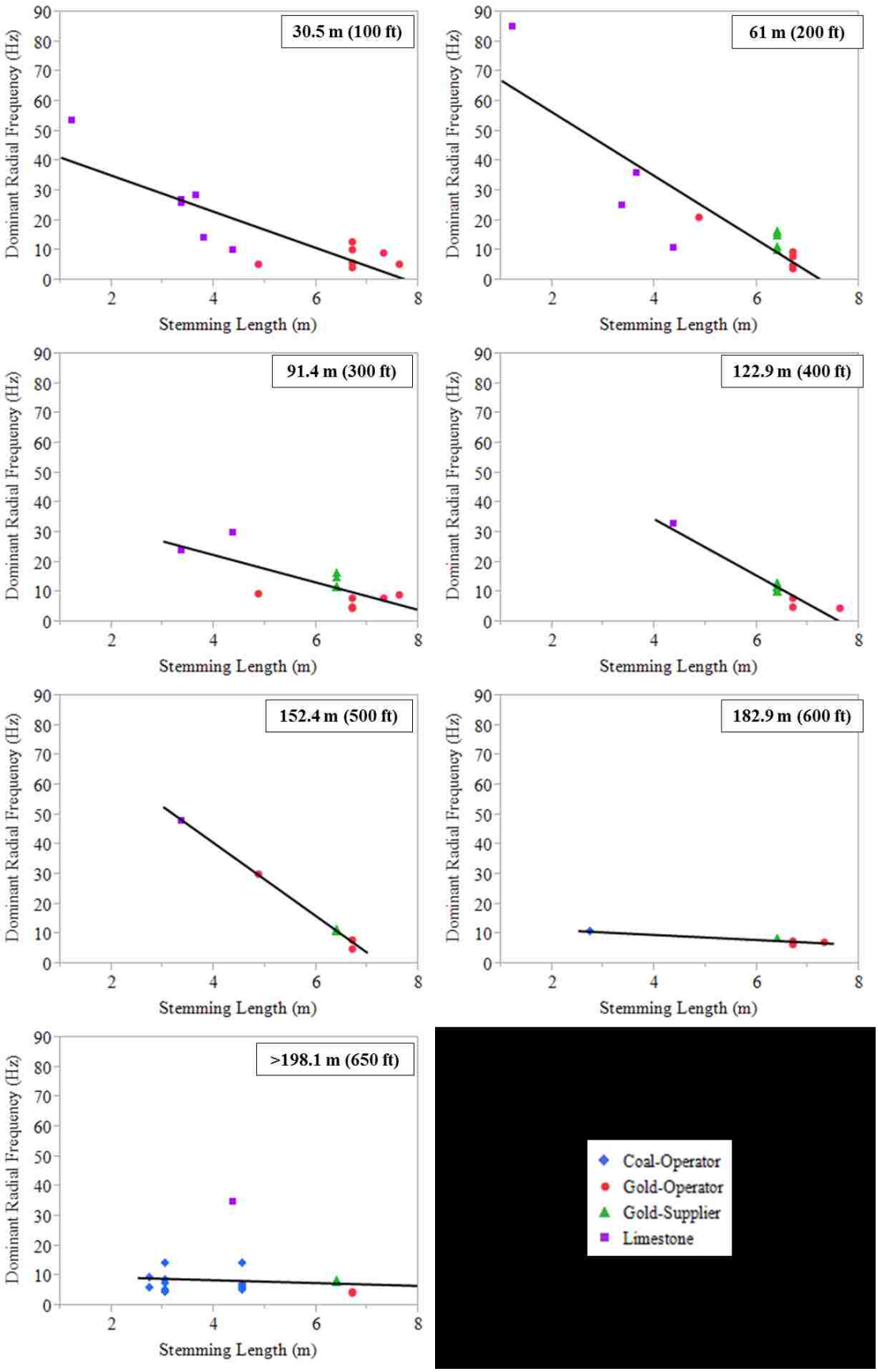
30.5 m (100 ft)
61 m (200 ft)
91.4 m (300 ft)
122.9 m (400 ft)
152.4 m (500 ft)
182.9 m (600 ft)
>198.1 m (650 ft)
Dominant Radial Frequency (Hz)
Stemming Length (m)
Coal-Operator
Gold-Operator
Gold-Supplier
Limestone

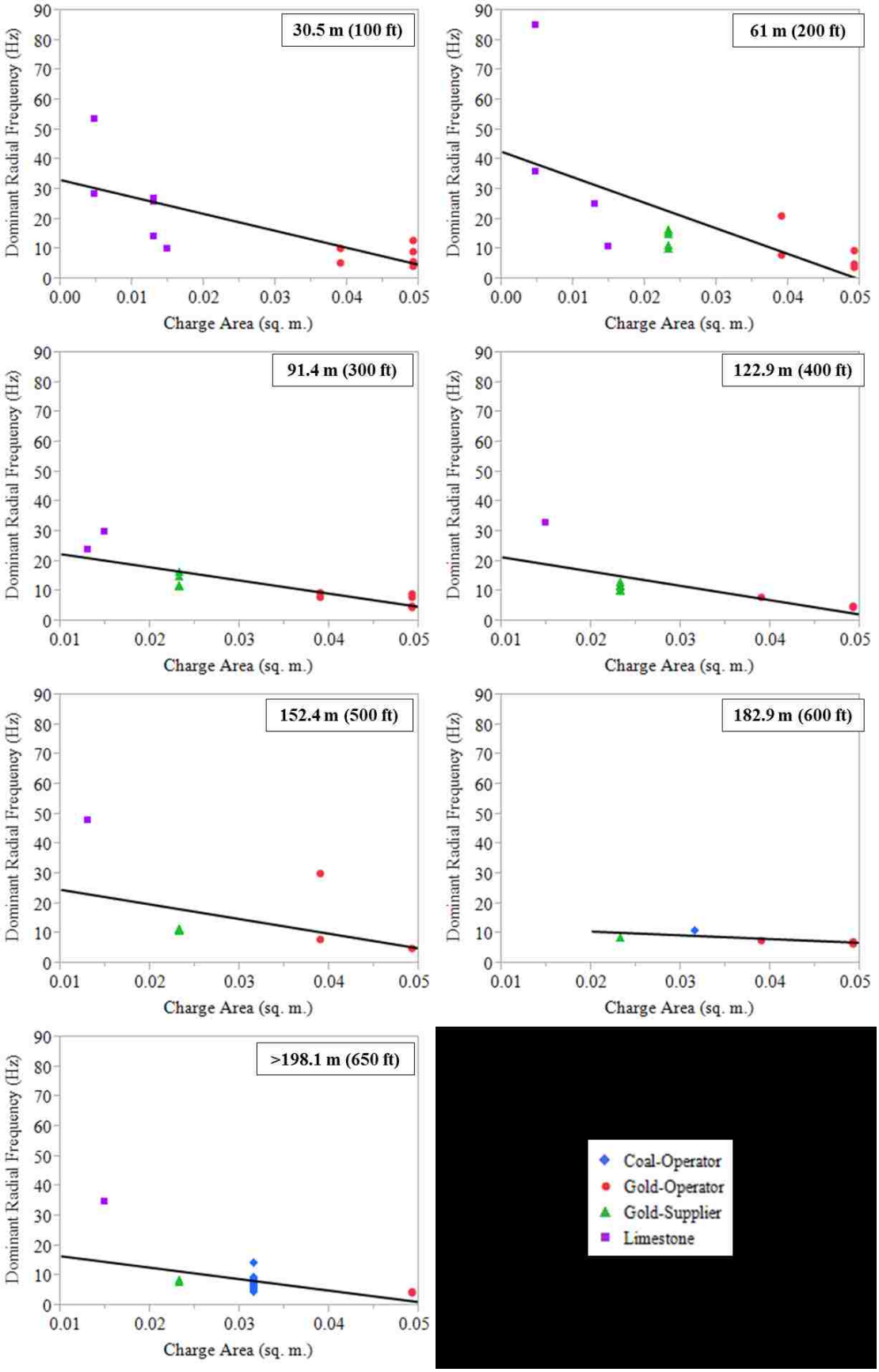
30.5 m (100 ft)
61 m (200 ft)
91.4 m (300 ft)
122.9 m (400 ft)
152.4 m (500 ft)
182.9 m (600 ft)
>198.1 m (650 ft)
Dominant Radial Frequency (Hz)
Charge Area (sq. m.)
Coal-Operator
Gold-Operator
Gold-Supplier
Limestone

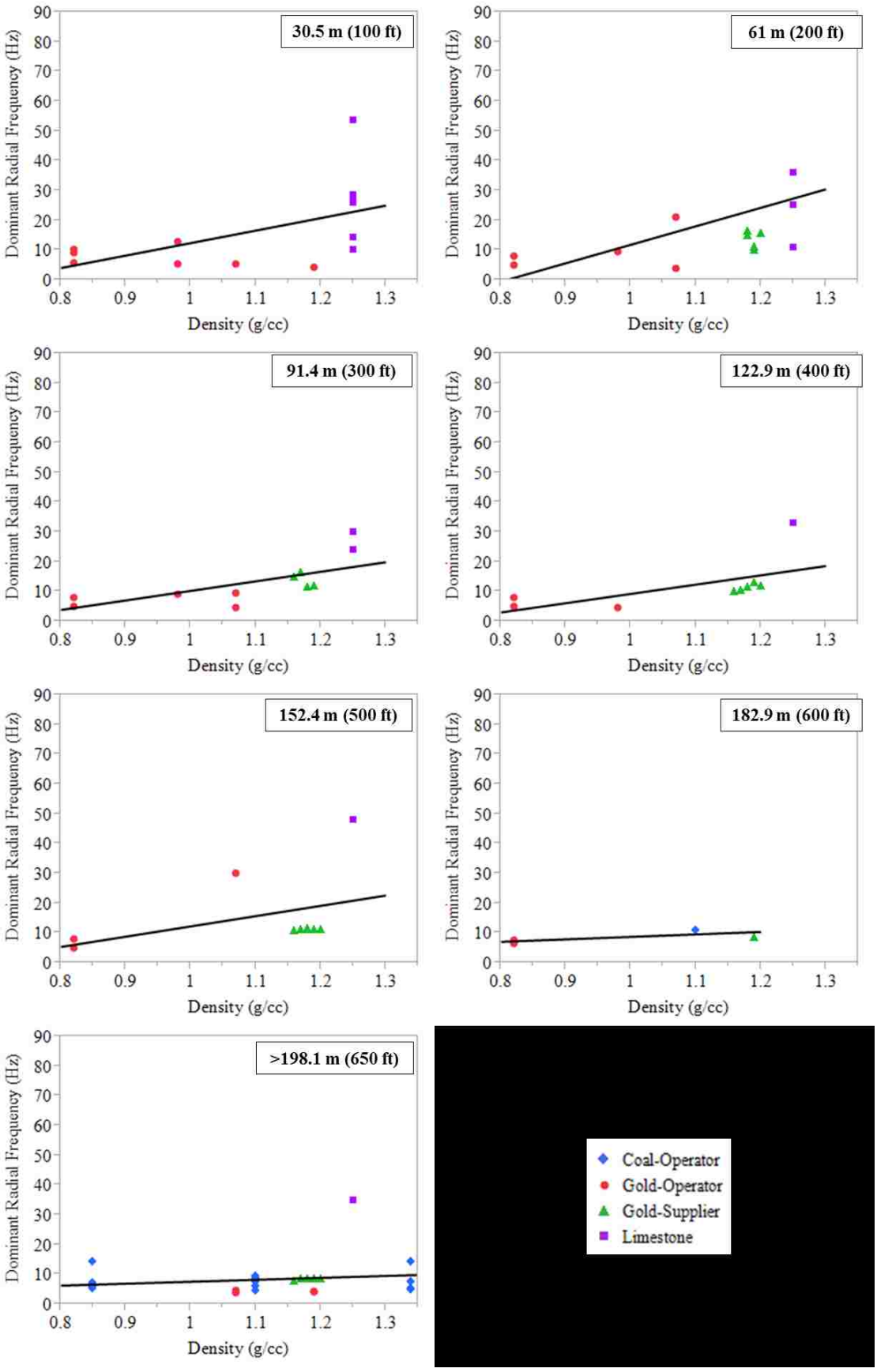
30.5 m (100 ft)
61 m (200 ft)
91.4 m (300 ft)
122.9 m (400 ft)
152.4 m (500 ft)
182.9 m (600 ft)
>198.1 m (650 ft)
Dominant Radial Frequency (Hz)
Density (g/cc)
Coal-Operator
Gold-Operator
Gold-Supplier
Limestone

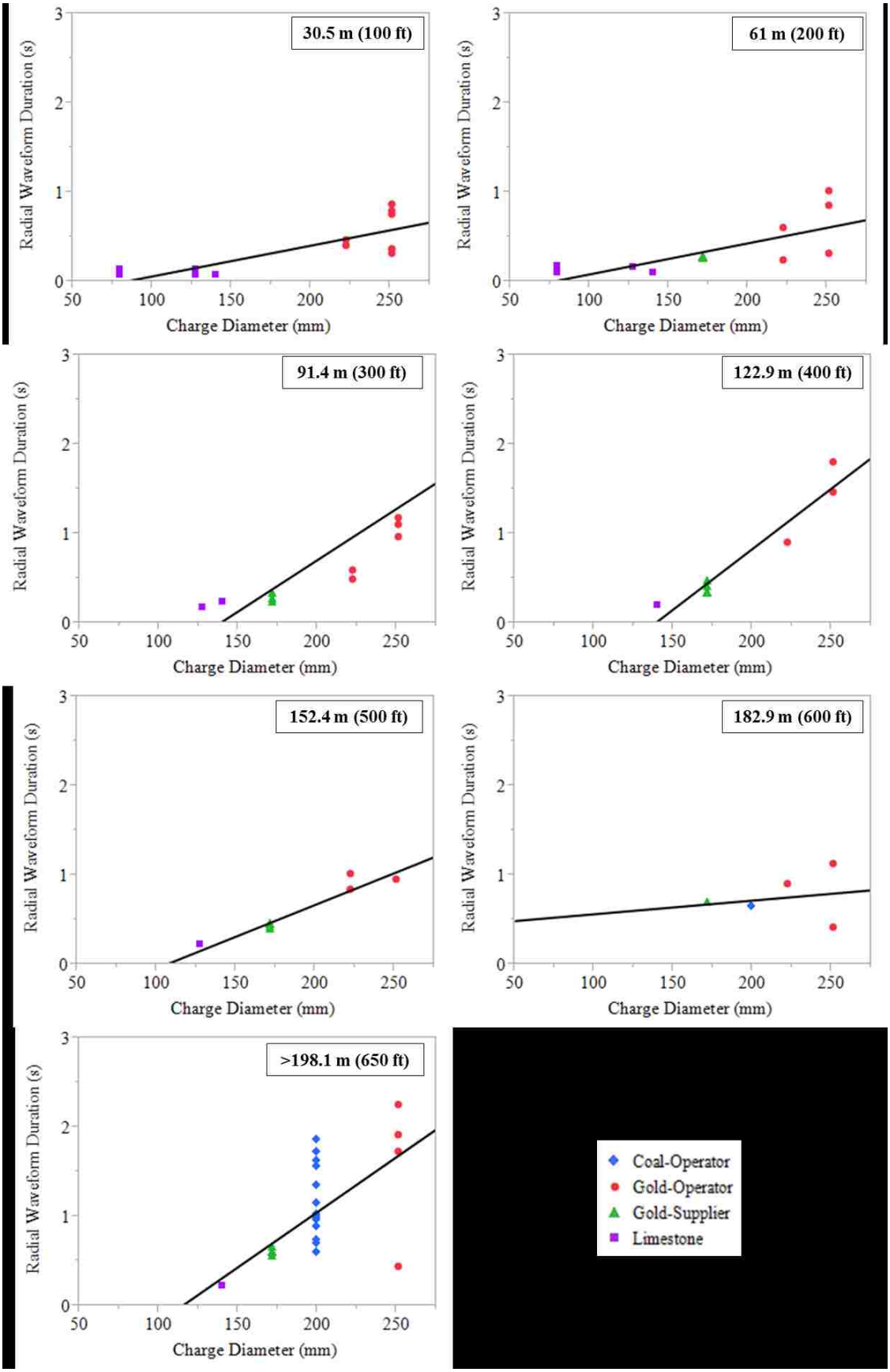
30.5 m (100 ft)
61 m (200 ft)
91.4 m (300 ft)
122.9 m (400 ft)
152.4 m (500 ft)
182.9 m (600 ft)
>198.1 m (650 ft)
Radial Waveform Duration (s)
Charge Diameter (mm)
Coal-Operator
Gold-Operator
Gold-Supplier
Limestone

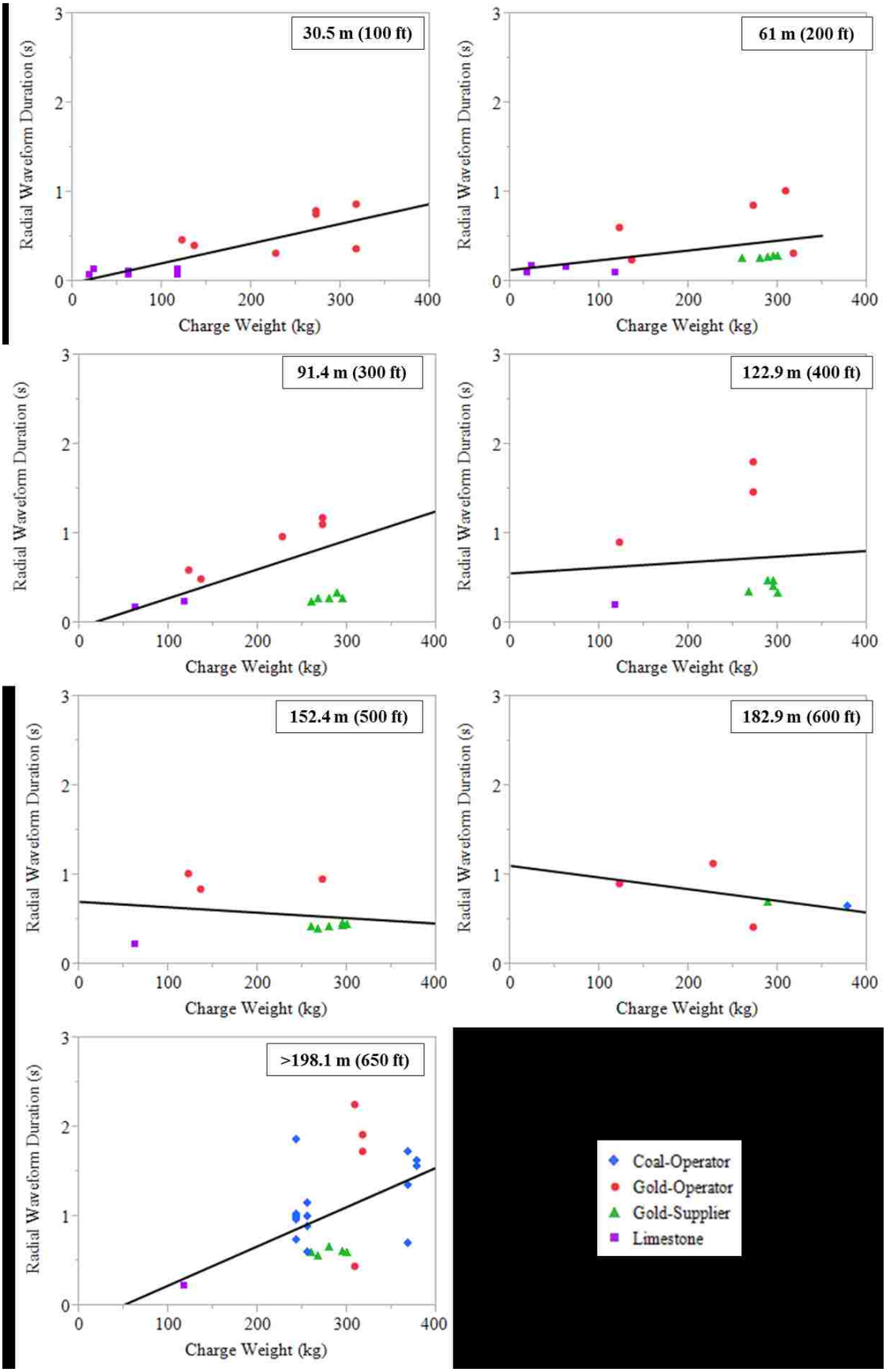
30.5 m (100 ft)
61 m (200 ft)
91.4 m (300 ft)
122.9 m (400 ft)
152.4 m (500 ft)
182.9 m (600 ft)
>198.1 m (650 ft)
Radial Waveform Duration (s)
Charge Weight (kg)
0
1
2
3
0
100
200
300
400
Coal-Operator
Gold-Operator
Gold-Supplier
Limestone

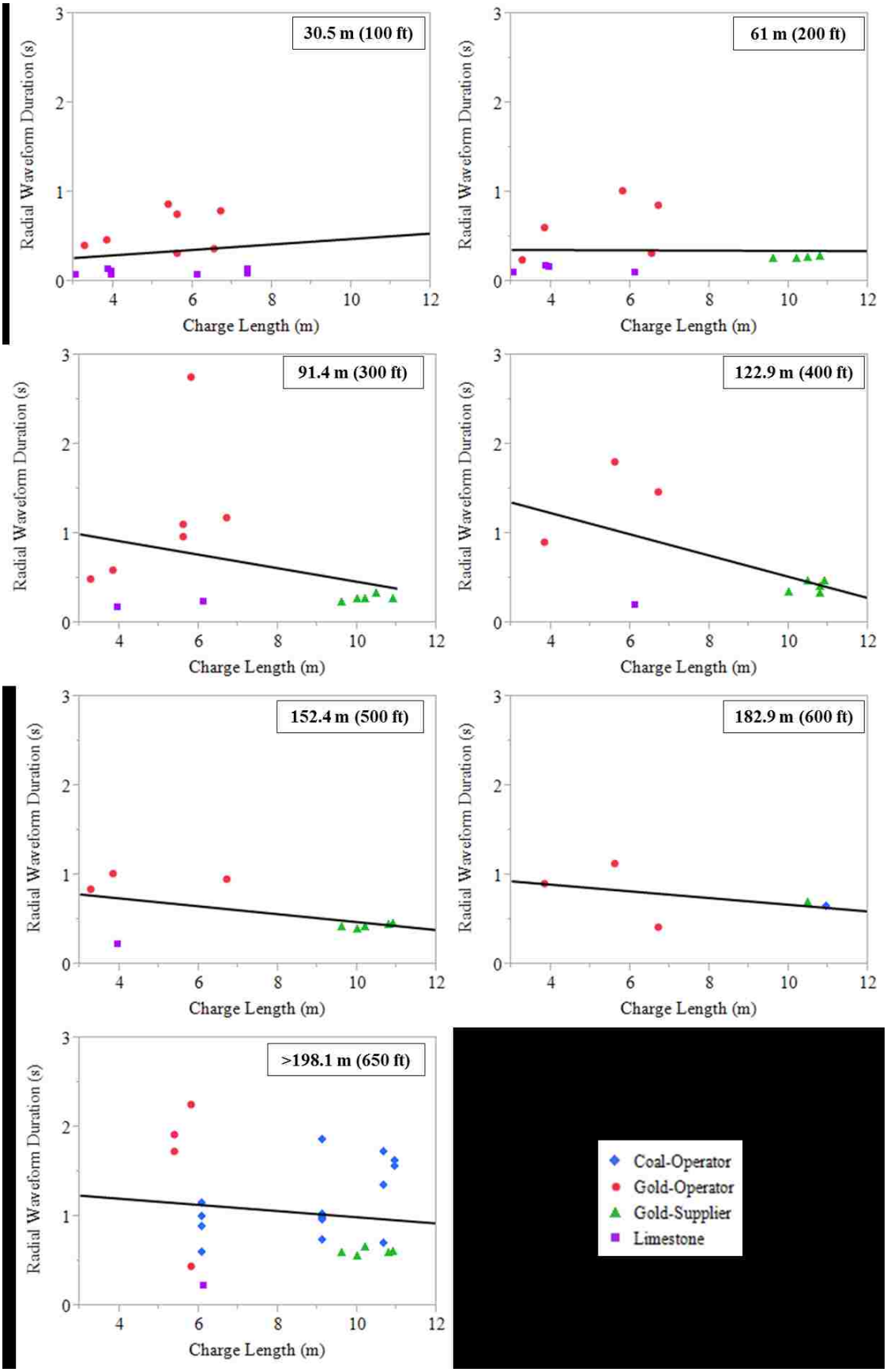
30.5 m (100 ft)
61 m (200 ft)
91.4 m (300 ft)
122.9 m (400 ft)
152.4 m (500 ft)
182.9 m (600 ft)
>198.1 m (650 ft)
Radial Waveform Duration (s)
Charge Length (m)
Coal-Operator
Gold-Operator
Gold-Supplier
Limestone

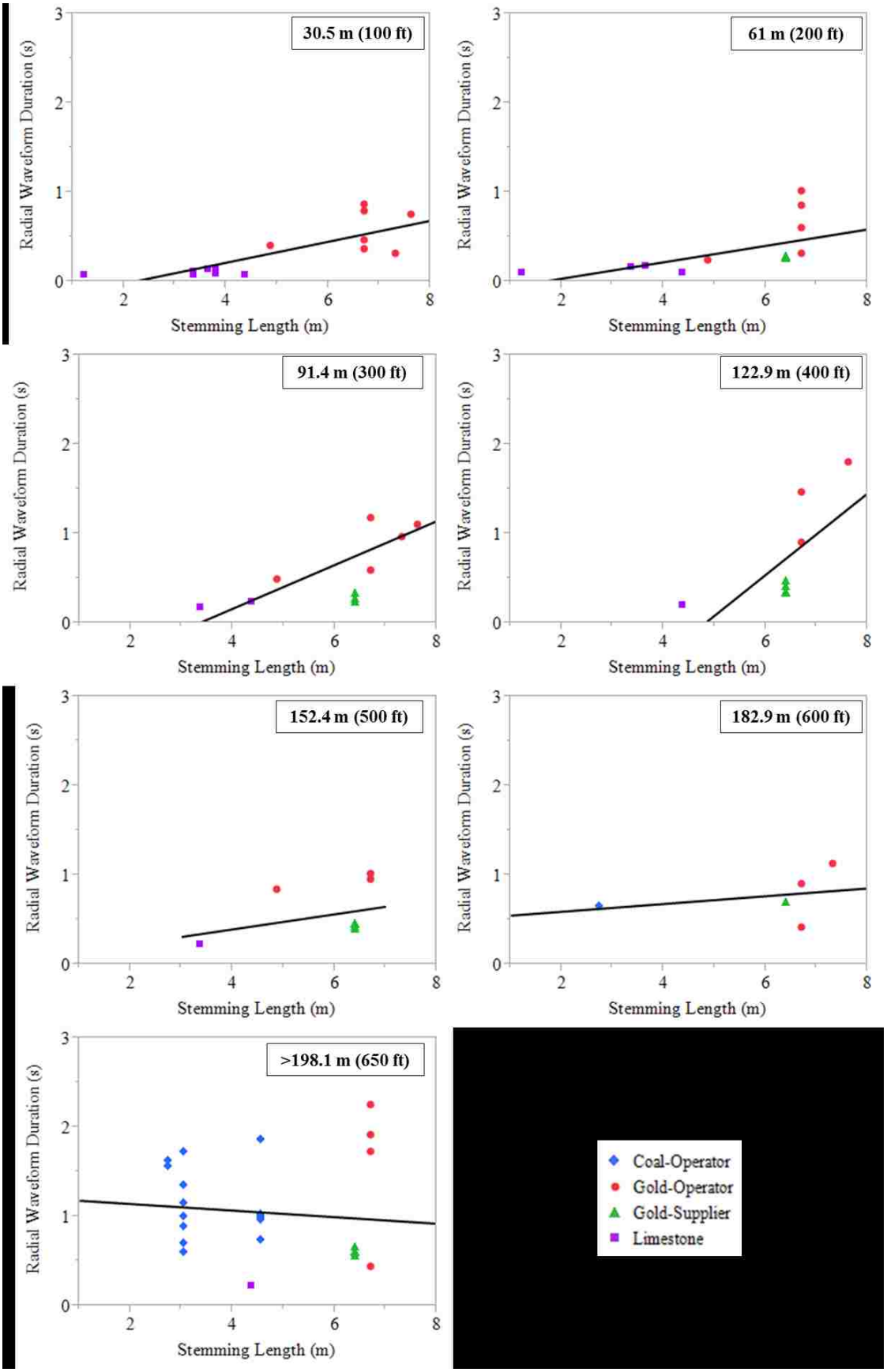
30.5 m (100 ft)
61 m (200 ft)
91.4 m (300 ft)
122.9 m (400 ft)
152.4 m (500 ft)
182.9 m (600 ft)
>198.1 m (650 ft)
Radial Waveform Duration (s)
Stemming Length (m)
Coal-Operator
Gold-Operator
Gold-Supplier
Limestone

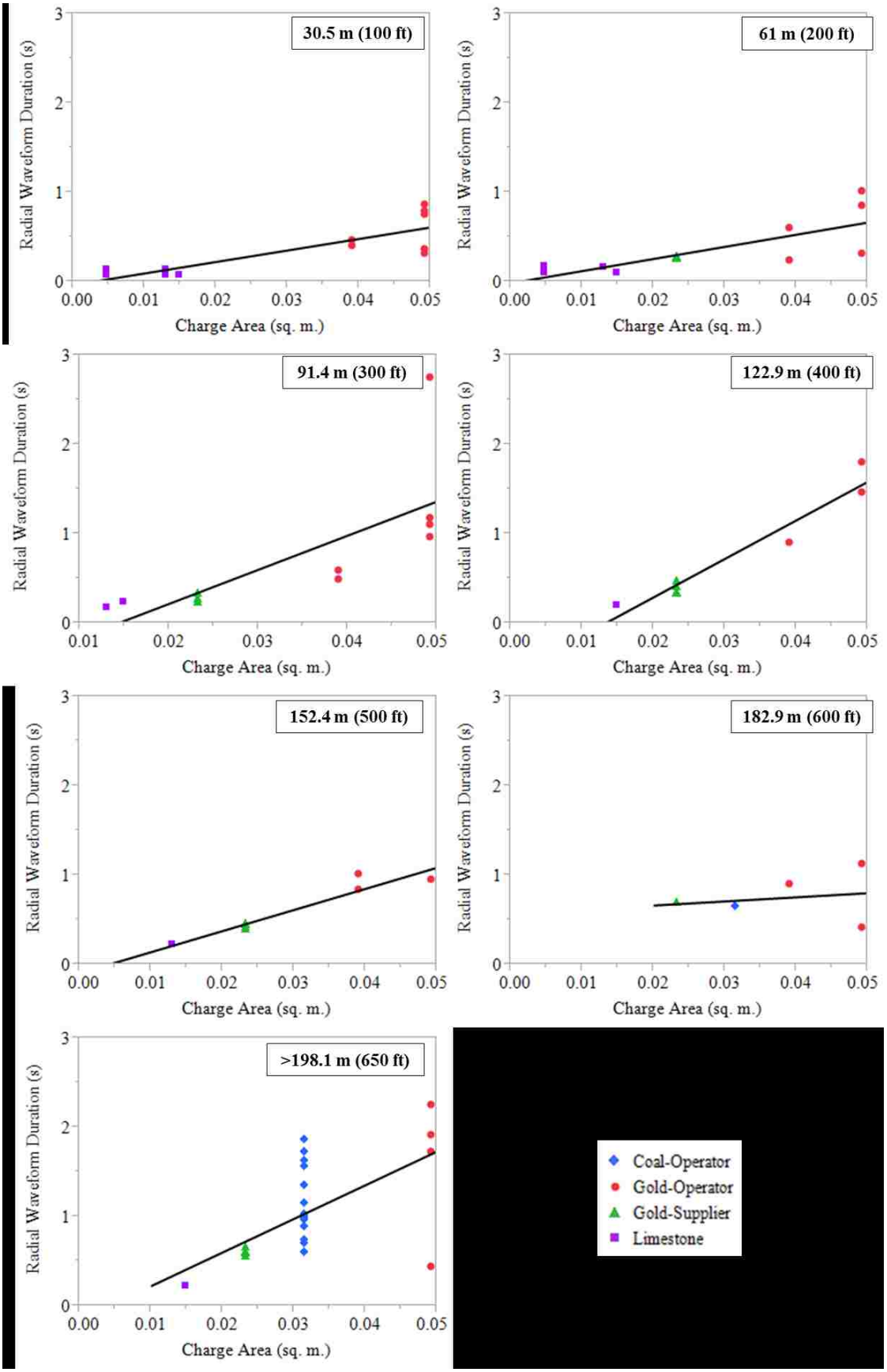
30.5 m (100 ft)
61 m (200 ft)
91.4 m (300 ft)
122.9 m (400 ft)
152.4 m (500 ft)
182.9 m (600 ft)
>198.1 m (650 ft)
Radial Waveform Duration (s)
Charge Area (sq. m.)
Coal-Operator
Gold-Operator
Gold-Supplier
Limestone

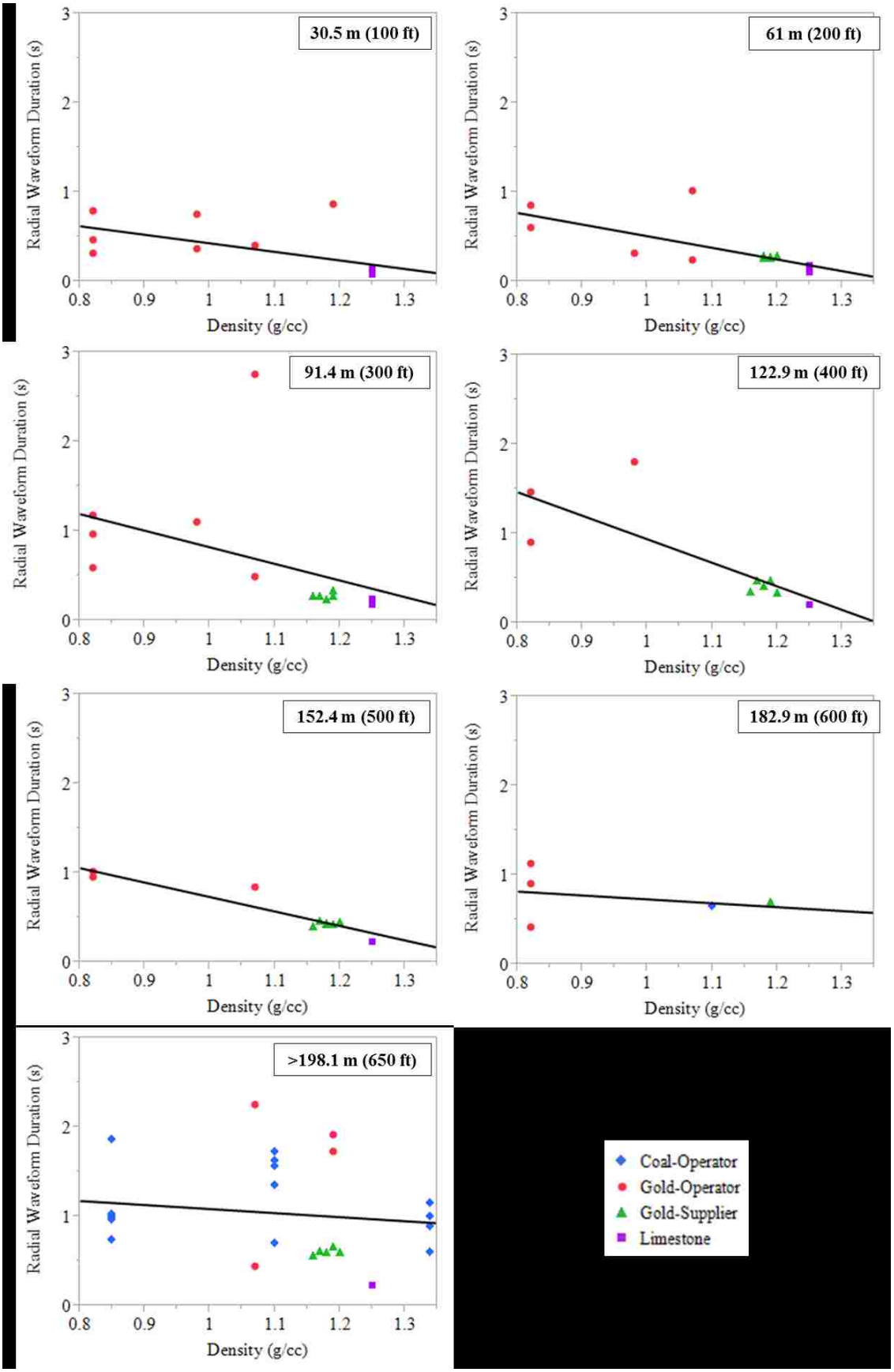
30.5 m (100 ft)
61 m (200 ft)
91.4 m (300 ft)
122.9 m (400 ft)
152.4 m (500 ft)
182.9 m (600 ft)
>198.1 m (650 ft)
Radial Waveform Duration (s)
Density (g/cc)
0
1
2
3
0.8
0.9
1
1.1
1.2
1.3
Coal-Operator
Gold-Operator
Gold-Supplier
Limestone

APPENDIX E

MULTIPLE REGRESSION RESULTS

Appendix E provides the result tables from the multiple regression analyses that were conducted on the signature hole dataset. The tables provide the results of each fit model, including the coefficient, standard error, and p-value of each variable, as well as the R-squared value and adjusted R-squared value for each fit model. The final run provides the statistically significant variables for each respective model.

PPV (within 76 m (250 ft))	Run I			Run II			Run III			Run IV			Run V		
	Coef.	Std Error	P-value	Coef.	Std Error	P-value	Coef.	Std Error	P-value	Coef.	Std Error	P-value	Coef.	Std Error	P-value
Intercept	757.45	270.14	0.0088	675.10	225.25	0.0053	367.10	98.60	0.0008	462.48	53.36	<.0001	470.24	51.65	<.0001
Log (distance from Blast (m))	-109.90	16.74	<.0001	-109.20	16.51	<.0001	-107.48	16.80	<.0001	-101.71	16.10	<.0001	-101.46	15.97	<.0001
Charge Weight (kg)	1.06	0.72	0.1502	0.68	0.25	0.0109	0.46	0.21	0.0348	0.49	0.21	0.0261	0.53	0.20	0.0119
Stemming Length (m)	-38.05	15.32	0.0188	-39.89	14.81	0.0113	-30.70	13.78	0.0330	-27.90	13.63	0.0486	-22.95	11.33	0.0507
Charge Diameter (mm)	3.26	2.12	0.1352	2.43	1.52	0.1200	1.92	1.51	0.2120	0.24	0.36	0.5096			
Charge Cross-Sectional Area (sq. m)	-15241.83	11129.41	0.1810	-9831.21	5661.25	0.0924	-5885.07	5125.94	0.2594						
Explosive Density (g/cc)	-316.64	207.08	0.1367	-244.41	161.44	0.1402									
Charge Length (m)	-12.26	21.63	0.5750												
Rsquare	0.67			0.67			0.64			0.63			0.62		
RSquare Adj	0.60			0.60			0.59			0.58			0.59		

Principal Frequency (Full Dataset)	Run I			Run II			Run III			Run IV			Run V			Run VI			Run VII			Run VIII		
	Coef.	Std Error	P-value	Coef.	Std Error	P-value	Coef.	Std Error	P-value	Coef.	Std Error	P-value	Coef.	Std Error	P-value	Coef.	Std Error	P-value	Coef.	Std Error	P-value	Coef.	Std Error	P-value
Intercept	77.40	26.38	0.0043	78.25	25.32	0.0027	71.76	24.07	0.0037	82.15	22.05	0.0003	66.01	18.93	0.0007	36.37	10.89	0.0012	26.72	4.86	<.0001	16.94	0.84	<.0001
Geology[Gold-Operator]	-22.36	8.58	0.0107	-22.46	8.49	0.0096	-25.47	7.68	0.0013	-21.07	6.50	0.0017	-22.45	6.46	0.0008	-11.10	2.50	<.0001	-9.50	1.91	<.0001	-6.65	1.32	<.0001
Geology[Gold-Supplier]	10.48	6.14	0.0914	10.47	6.11	0.0899	12.53	5.58	0.0273	9.10	4.58	0.0497	6.25	4.12	0.1333	0.07	2.58	0.9785	-0.99	2.34	0.6741	-4.90	1.38	0.0006
Geology[Coal-Operator]	-14.94	4.34	0.0009	-14.77	4.11	0.0005	-14.32	4.06	0.0007	-11.93	3.40	0.0007	-8.15	2.09	0.0002	-6.46	1.92	0.0011	-6.35	1.92	0.0013	-8.59	1.60	<.0001
Charge Length (m)	-6.15	2.60	0.02	-6.22	2.52	0.0153	-4.75	1.80	0.0099	-4.85	1.80	0.0085	-4.69	1.81	0.011	-1.49	0.67	0.0281	-1.32	0.64	0.0438			
Explosive Density (g/cc)	-46.53	18.82	0.0154	-46.92	18.46	0.0128	-37.32	14.47	0.0115	-36.38	14.45	0.0136	-28.89	13.51	0.0351	-7.56	7.63	0.3247						
Charge Weight (kg)	0.13	0.08	0.1182	0.13	0.08	0.1011	0.08	0.05	0.096	0.09	0.04	0.0333	0.08	0.04	0.0603									
Stemming Length (m)	-2.49	1.79	0.1674	-2.46	1.76	0.1661	-2.94	1.66	0.0804	-1.88	1.34	0.1628												
Charge Diameter (mm)	0.27	0.23	0.2459	0.27	0.22	0.2206	0.11	0.10	0.2874															
Charge Cross-Sectional Area (sq. m)	-1019.36	1288.02	0.4308	-1051.98	1253.00	0.4034																		
Log (distance from Blast (m))	0.16	1.32	0.9031																					
Rsquare	0.70			0.70			0.69			0.69			0.68			0.67			0.67			0.65		
RSquare Adj	0.66			0.67			0.67			0.67			0.66			0.65			0.65			0.64		

Principal Frequency (within 76 m (250 ft))	Run I			Run II			Run III			Run IV			Run V			Run VI			Run VII		
	Coef.	Std Error	P-value	Coef.	Std Error	P-value	Coef.	Std Error	P-value	Coef.	Std Error	P-value	Coef.	Std Error	P-value	Coef.	Std Error	P-value	Coef.	Std Error	P-value
Intercept	99.70	58.80	0.1024	96.60	51.13	0.0701	91.67	48.99	0.0722	85.76	47.13	0.0795	49.20	9.74	<.0001	46.10	5.27	<.0001	39.03	3.38	<.0001
Charge Cross-Sectional Area (sq. m)	-2337.26	2183.72	0.2947	-2261.17	2039.67	0.2778	-2192.87	2001.81	0.283	-1174.05	646.66	0.0802	-743.89	349.64	0.042	-617.43	109.88	<.0001	-646.60	111.90	<.0001
Charge Length (m)	-4.83	4.42	0.2845	-4.68	4.13	0.2675	-4.93	4.02	0.2306	-3.34	2.70	0.2256	-2.12	2.20	0.3429	-1.34	0.78	0.0967			
Charge Weight (kg)	0.14	0.15	0.3582	0.13	0.14	0.3379	0.13	0.13	0.3458	0.08	0.10	0.4242	0.03	0.08	0.7055						
Explosive Density (g/cc)	-40.47	41.25	0.336	-39.06	38.60	0.321	-34.86	36.71	0.3506	-24.11	30.41	0.4345									
Charge Diameter (mm)	0.25	0.41	0.5499	0.24	0.39	0.5486	0.20	0.37	0.5946												
Stemming Length (m)	-1.29	3.25	0.6954	-1.33	3.17	0.6793															
Log (distance from Blast (m))	-0.48	4.19	0.91																		
Rsquare	0.58			0.58			0.57			0.57			0.56			0.56			0.51		
RSquare Adj	0.46			0.48			0.50			0.51			0.52			0.53			0.50		

Dominant Frequency (Full Dataset)	Run I			Run II			Run III			Run IV			Run V			Run VI		
	Coef.	Std Error	P-value	Coef.	Std Error	P-value	Coef.	Std Error	P-value	Coef.	Std Error	P-value	Coef.	Std Error	P-value	Coef.	Std Error	P-value
Intercept	97.26	25.58	0.0003	100.32	24.79	0.0001	104.44	22.03	<.0001	65.66	13.00	<.0001	58.73	12.69	<.0001	28.63	7.38	0.0002
Stemming Length (m)	-8.43	1.59	<.0001	-8.35	1.58	<.0001	-7.99	1.25	<.0001	-7.49	1.25	<.0001	-8.22	1.21	<.0001	-6.67	1.12	<.0001
Geology[Coal-Operator]	-22.94	3.76	<.0001	-23.42	3.63	<.0001	-22.93	3.37	<.0001	-20.62	3.26	<.0001	-23.61	2.92	<.0001	-19.83	2.70	<.0001
Geology[Gold-Operator]	-13.85	7.98	0.0863	-13.55	7.93	0.0909	-11.83	6.39	0.0674	0.35	3.05	0.9091	4.52	2.20	0.0427	5.46	2.26	0.0176
Geology[Gold-Supplier]	22.57	5.66	0.0001	22.29	5.61	0.0001	21.08	4.53	<.0001	13.26	2.78	<.0001	10.30	2.36	<.0001	6.57	2.04	0.0018
Log (distance from Blast (m))	4.35	1.23	0.0007	4.14	1.15	0.0006	4.19	1.14	0.0004	4.50	1.15	0.0002	4.32	1.17	0.0004	3.93	1.20	0.0015
Explosive Density (g/cc)	-41.26	18.69	0.0300	-47.23	14.66	0.0018	-48.91	13.87	0.0007	-23.60	7.56	0.0024	-21.79	7.61	0.0053			
Charge Length (m)	-3.68	2.64	0.1668	-4.58	1.99	0.0239	-4.89	1.79	0.0077	-1.28	0.66	0.0557						
Charge Weight (kg)	0.05	0.08	0.5588	0.08	0.06	0.1934	0.09	0.04	0.0337									
Charge Cross-Sectional Area (sq. m)	767.38	1229.44	0.5342	187.62	506.82	0.7122												
Charge Diameter (mm)	-0.11	0.22	0.6058															
Rsquare		0.67			0.67			0.67			0.66			0.64			0.61	
RSquare Adj		0.64			0.64			0.64			0.63			0.62			0.59	

Dominant Frequency (within 76 m (250 ft))	Run I			Run II			Run III			Run IV			Run V			Run VI		
	Coef.	Std Error	P-value	Coef.	Std Error	P-value	Coef.	Std Error	P-value	Coef.	Std Error	P-value	Coef.	Std Error	P-value	Coef.	Std Error	P-value
Intercept	109.67	46.80	0.0281	108.84	36.10	0.0060	89.48	35.54	0.0186	51.36	25.59	0.0553	38.31	22.04	0.0936	11.24	9.37	0.2405
Stemming Length (m)	-9.36	2.44	0.0008	-9.37	2.39	0.0006	-11.01	2.26	<.0001	-11.35	2.31	<.0001	-9.44	1.30	<.0001	-8.26	0.99	<.0001
Log (distance from Blast (m))	13.27	3.06	0.0002	13.30	2.75	<.0001	12.64	2.82	0.0001	12.56	2.89	0.0002	13.31	2.79	<.0001	13.13	2.83	<.0001
Explosive Density (g/cc)	-52.45	34.14	0.1381	-51.68	20.93	0.0210	-48.36	21.61	0.0344	-24.83	15.33	0.1172	-19.39	14.34	0.1874			
Charge Weight (kg)	0.15	0.13	0.2685	0.14	0.06	0.0235	0.06	0.04	0.1035	0.03	0.03	0.3249						
Charge Diameter (mm)	-0.24	0.35	0.5115	-0.25	0.11	0.0296	-0.11	0.07	0.1441									
Charge Length (m)	-3.01	3.97	0.4558	-2.91	1.71	0.1014												
Charge Cross-Sectional Area (sq. m)	-55.91	1938.46	0.9772															
Rsquare		0.79			0.79			0.77			0.75			0.74			0.72	
RSquare Adj		0.73			0.74			0.72			0.71			0.71			0.70	

Duration (Full Dataset)	Run I			Run II			Run III			Run IV			Run V			Run VI			Run VII		
	Coef.	Std Error	P-value	Coef.	Std Error	P-value	Coef.	Std Error	P-value	Coef.	Std Error	P-value	Coef.	Std Error	P-value	Coef.	Std Error	P-value	Coef.	Std Error	P-value
Intercept	-0.16	1.08	0.8800	-0.14	0.71	0.8448	-0.53	0.66	0.4250	0.11	0.48	0.8106	0.06	0.48	0.8939	-0.76	0.26	0.0040	-0.48	0.25	0.0570
Log (distance from Blast (m))	0.26	0.06	<.0001	0.26	0.05	<.0001	0.26	0.05	<.0001	0.26	0.05	<.0001	0.25	0.05	<.0001	0.21	0.05	<.0001	0.24	0.05	<.0001
Geology[Coal-Operator]	0.36	0.17	0.0305	0.36	0.16	0.0284	0.37	0.16	0.0260	0.24	0.14	0.0800	0.04	0.09	0.6722	0.04	0.10	0.7062	0.15	0.09	0.1094
Geology[Gold-Operator]	0.48	0.36	0.1867	0.47	0.34	0.1715	0.84	0.21	0.0001	0.79	0.21	0.0002	0.73	0.21	0.0007	0.32	0.06	<.0001	0.35	0.06	<.0001
Geology[Gold-Supplier]	-0.59	0.25	0.0213	-0.58	0.24	0.0188	-0.83	0.16	<.0001	-0.74	0.15	<.0001	-0.51	0.10	<.0001	-0.37	0.07	<.0001	-0.26	0.06	<.0001
Charge Weight (kg)	0.00	0.00	0.5620	0.00	0.00	0.0744	0.00	0.00	0.0007	0.00	0.00	0.0001	0.00	0.00	0.0006	0.00	0.00	0.0042			
Charge Diameter (mm)	-0.02	0.01	0.0434	-0.02	0.01	0.0081	-0.01	0.00	0.0042	-0.01	0.00	0.0062	-0.01	0.00	0.0476						
Stemming Length (m)	0.14	0.07	0.0574	0.14	0.07	0.0492	0.16	0.07	0.0157	0.12	0.06	0.0464									
Explosive Density (g/cc)	0.55	0.79	0.4872	0.53	0.37	0.1515	0.52	0.37	0.1622												
Charge Cross-Sectional Area (sq. m)	51.41	54.50	0.3482	50.28	37.76	0.1865															
Charge Length (m)	0.00	0.11	0.9769																		
Rsquare			0.66			0.66			0.65			0.65			0.63			0.61			0.58
RSquare Adj			0.62			0.63			0.62			0.62			0.61			0.59			0.56

Duration (within 76 m (250 ft))	Run I			Run II			Run III			Run IV			Run V			Run VI			Run VII		
	Coef.	Std Error	P-value	Coef.	Std Error	P-value	Coef.	Std Error	P-value	Coef.	Std Error	P-value	Coef.	Std Error	P-value	Coef.	Std Error	P-value	Coef.	Std Error	P-value
Intercept	0.22	0.79	0.7798	0.41	0.26	0.1317	0.45	0.25	0.0880	0.48	0.25	0.0633	0.42	0.22	0.0688	0.38	0.22	0.1018	-0.01	0.05	0.8770
Charge Cross-Sectional Area (sq. m)	36.23	32.28	0.2723	30.13	20.73	0.1580	26.16	19.52	0.1913	38.19	12.14	0.0039	36.82	11.74	0.0039	32.48	11.39	0.0078	12.66	1.54	<.0001
Charge Diameter (mm)	-0.01	0.01	0.2058	-0.01	0.00	0.1513	-0.01	0.00	0.1853	-0.01	0.00	0.0345	-0.01	0.00	0.0377	-0.01	0.00	0.0893			
Stemming Length (m)	0.05	0.04	0.2753	0.04	0.04	0.2781	0.04	0.04	0.2855	0.03	0.03	0.4107	0.04	0.03	0.2045						
Charge Weight (kg)	0.00	0.00	0.7992	0.00	0.00	0.4468	0.00	0.00	0.3516	0.00	0.00	0.5838									
Charge Length (m)	-0.02	0.06	0.7619	-0.03	0.04	0.5031	-0.03	0.04	0.4359												
Log (distance from Blast (m))	0.03	0.05	0.5117	0.03	0.05	0.5351															
Explosive Density (g/cc)	0.14	0.57	0.8046																		
Rsquare	0.74			0.74			0.74			0.73			0.73			0.71			0.69		
RSquare Adj	0.67			0.68			0.69			0.70			0.70			0.70			0.68		

BIBLIOGRAPHY

Adhikari, G., Venkatesh, H., Theresraj, A., Roy, S., Balachander, R., Jain, N., & Gupta, R. (2005). *Role of Blast Design Parameters on Ground Vibration and Correlation of Vibration Level to Blasting Damage to Surface Structures.* National Institute of Rock Mechanics.

Ai, H., & Ahrens, T. (2004). Dynamic Tensile Strength of Terrestrial Rocks and Application to Impact Cratering. *Meteoritics & Planetary Science, 39*(2), 233-246.

Ambraseys, N., & Hendron, A. (1968). Dynamic Behavior of Rock Masses. In K. Stagg, & O. Zienkiewicz, *Rock Mechanics in Engineering Practice* (pp. 203-236). London: John Wiley & Sons.

Anderson, D. (2008). Signature Hole Blast Vibration Control - Twenty Years Hence and Beyond. *The Journal of Explosives Engineers, 25*(5).

Anderson, D., Miller, D., & Matheson, G. (1997). Vibration Spectral Mapping. *Seventh High Tech Seminar - State-of-the-Art Blasting Technology, Instrumentation and Explosives Applications.* Orlando, FL: International Society of Explosives Engineers.

Anderson, D., Ritter, A., Winzer, S., & Reil, J. (1985). A Method for Site-Specific Prediction and Control of Ground Vibration from Blasting. *Proceedings of the 11th Conference on Explosives and Blasting Technique.* San Diego, CA: International Society of Explosives Engineers.

Andrieux, P., & Heilig, J. (2000). Near-Field Blast Vibration Monitoring: Practical Considerations and Issues. *The Journal of Explosives Engineering, 12*(6).

Armstrong, L. (2001). *Evaluations of Parameters Effecting Blast Induced Vibrations.* Faculty of Engineering. Wollongong, NSW, Australia: The University of Wollongong.

Bacci, D., & Landim, P. (2002). Statistical Methods Applied to the Anlaysis of Blasting Vibrations in a Diabase Quarry in the City of Campinas, (SP) - Brazil. *Proceedings of the Twenty-Eighth Conference on Explosives and Blasting Technique.* Las Vegas, NV: International Society of Explosives Engineers.

Bernard, T. (2012). The Truth about Signature Hole Method. *Proceedings of the Thirty-Eighth Conference on Explosives and Blasting Technique.* Nashville, TN: International Society of Explosives Engineers.

Birch, W., Pegden, M., & West, R. (2001). An Advanced Blasting Scaled-Distance Model Incorporating Individual Location Response. *Proceedings of the Twenty-Seventh Conference On Explosives And Blasting Technique.* Orlando, FL: International Society of Explosives Engineers.

Blair, B., & Duvall, W. (1954). Evaluation of Gages for Measuring Displacement, Velocity, and Acceleration of Seismic Pulses. *Report of Investigations 5073*. US Bureau of Mines.

Blair, D. (2008). Non-Linear Superposition Models of Blast Vibration. *International Journal of Rock Mechanics & Mining Sciences*(45), 235-2247.

Blair, D. (2014). Blast Vibration Dependence on Charge Length, Velocity of Detonation and Layered Media. *International Journal of Rock Mechanics & Mining Sciences*(65), 29-39.

Bollinger, G. (1971). *Blast Vibration Analysis.* Carbondale, IL: Southern Illinois University Press.

Chiappetta, R. (1994). New Findings on the Impact of an Explosive VOD on Blast Results. *Proceedings of the Twentieth Conference on Explosives and Blasting Technique.* Austin, TX: International Society of Explosives Engineers.

Chock, J. (1996). *Review of Methods for Calculating Pressure Profiles of Explosive Air Blast and its Sample Application.* Master of Science Thesis, Virginia Polytechnic Institute and State University, Department of Aerospace and Ocean Engineering, Blacksburg, VA.

Choudhury, P., & Sitharam, T. (2010). Prediction of Blast Induced Ground Vibration and its Associated Dominating Frequency using a Comprehensive Support Vector Machine Model. *Proceedings Of The Thirty-Sixth Conference On Explosives And Blasting Technique.* Orlando, FL: International Society of Explosives Engineers.

Cooper, P. (1996). *Explosives Engineering.* New York: Wiley-VCH.

Crandell, F. (1949, April). Ground Vibration due to Blasting and Its Effect Upon Structures. *Journal of the Boston Society of Civil Engineers*, 222-245.

Crenwelge, O. (1988). Use of Single Charge Vibration Data to Interpret Explosive Excitation and Ground Transmission Characteristics. *Proceedings of the 14th Conference on Explosives and Blasting Technique.* Anaheim, CA: International Society of Explosives Engineers.

Crenwelge, O., & Peterson, T. (1986). Overburden Blasting Vibrations: Analysis, Prediction, and Control. *Proceedings of the 12th Conference on Explosives and Blasting Technique.* Atlanta, GA: International Society of Explosives Engineers.

Crum, S., Siskind, D., & Eltschlager, K. (1992). Blast Vibration Measurements at Far Distances and Design Influences on Ground Vibrations. *Proceedings of the 18th Conference on Explosives and Blasting Technique.* Orlando, FL: International Society of Explosives Engineers.

Dowding, C. (1985). *Blast Vibration Monitoring and Control.* Englewood Cliffs, NJ: Prentice-Hall.

Duvall, W., & Fogelson, D. (1962). Review of Criteria for Estimating Damage to Residences from Blasting Vibrations. *Report of Investigations 5968*. US Bureau of Mines.

Farnfield, R. (1996). So You Think You Are Monitoring Peak Particle Velocity. *Twenty-Second Conference on Explosives and Blasting Technique.* Orlando, FL: International Society of Explosives Engineers.

Fleetwood, K., & Villaescusa, E. (2011). Non-Ideal Shock Energy Factor versus Powder Factor for Open Pit Blast Design - ANFO and Chemically-Sensitized Emulsion. *EXPLO2011.* Melbourne, Victoria, Australia: Australasian Institute of Mining and Metallurgy.

Fleetwood, K., Villaescusa, E., & Eloranta, J. (2012). Comparison of the Non-Ideal Shock Energies of Sensitised and Unsensitised Bulk ANFO-Emulsion Blends in Intermediate Blasthole Diameters. *Proceedings Of The Thirty-Eighth Conference On Explosives And Blasting Technique.* Nashville, TN: International Society of Explosives Engineers.

Fleetwood, K., Villaescusa, E., & Li, J. (2009). Limitations of Using PPV Damage Models to Predict Rock Mass Damage. *Proceedings of the 35th Conference on Explosives and Blasting Technique.* Denver, CO: International Society of Explosives Engineers.

Froedge, D. (1995). Anomalies in Blast Vibration Propagation. *Sixth High Tech Seminar on Blasting Technology, Instrumentation, and Explosives Applications.* Boston, MA: International Society of Explosives Engineers.

Grady, D. (1998). Shock-Wave Compression of Brittle Solids. *Mechanics of Materials, 29*(3-4), 181-203.

Hudaverdi, T. (2012). Application of Multivariate Analysis for Prediction of Blast-Induced Ground Vibratoins. *Soil Dynamics and Earthquake Engineering, 43*, 300-308.

ISEE. (1998). *Blasters' Handbook* (17th ed.). (R. Hopler, Ed.) Cleveland, OH: International Society of Explosives Engineers.

ISEE. (2009). *Field Practice Guidelines for Blasting Seismographs.* International Society of Explosives Engineers, Standards Committee. Cleveland, OH: International Society of Explosives Engineers.

Iverson, S., Kerkering, C., & Hustrulid, W. (2008). Application of the NIOSH-Modified Holmberg-Persson Approach to Perimeter Blast Design. *Proceedings Of The 34th Conference On Explosives And Blasting Technique.* New Orleans, LA: International Society of Explosives Engineers.

Johansson, C., & Persson, P. (1970). *Detonics of High Explosives.* London: Academic Press.

Katsabanis, P., Pascoal, A., & Rielo, O. (2011). Examination of Dynamic Parameters of Rocks using Hopkinson Bar Experiments. *Proceedings of the 37th Conference on Explosives and Blasting Technique.* San Diego, CA: International Society of Explosives Engineers.

Kirby, I., Chan, J., & Minchinton, A. (2014). Advances in Predicting the Effects of Non-ideal Detonation on Blasting. *Proceedings Of The Fortieth Conference On Explosives And Blasting Technique.* Denver, CO: International Society of Explosives Engineers.

Lee, N. (2011). The Effects of Various Wet-Hole Loading Methods on Powder Factor. *Proceedings Of The Thirty-Seventh Conference On Explosives And Blasting Technique.* San Diego, CA: International Society of Explosives Engineers.

Mohanty, B., & Yang, R. (1997). Blasting Vibrations and Explosives Performance. *Proccedings Of The Thirteenth Mini-Symposium On Explosives And Blasting Research.* Las Vegas, NV: International Society of Explosives Engineers.

Mueller, B., & Boehnke, R. (2004). A New Method for the Prediction of Blast Vibrations and Suggestions with Respect to Uniform Reference Values for Short-Time Vibrations. *Proceedings Of The Thirtieth Conference On Explosives And Blasting Technique.* New Orleans, LA: International Society of Explosives Engineers.

Mullay, J., McGinley, C., & Stancavage, C. (1995). The Use of Statistically Design Experiments to Conduct Effective Small Diameter Crater Studies. *Proceedings of the Twenty-First Conference on Explosives and Blasting Technique.* Nashville, TN: International Society of Explosives Engineers.

Nicholls, H., & Duvall, W. (1966). Effect of Charge Diameter on Explosive Performance. *Report of Investigations 6806*. US Bureau of Mines.

Nicholls, H., Johnson, W., & Duvall, W. (1971). Blasting Vibrations and Their Effects on Structures. *Bulletin 656*. US Bureau of Mines.

Olofsson, S. (2002). *Applied Explosives Technology for Construction and Mining* (2 ed.). Ärla, Sweden: Applex AB.

Oriard, L. (1992). Near Source Attenuation of Seismic Waves from Spacially Distributed Sources. *Proceedings of the 18th Annual Symposium on Explosives and Blasting Research.* Orlando, FL: International Society of Explosives Engineers.

OSM Blasting Performance Standards. (1983). *30 Code of Federal Regulations*. Pittsburgh, PA: Office of Surface Mining Reclamation and Enforcement.

Ozer, U., Karadogan, A., Kalayci, U., Aksoy, M., & Keti, Z. (2012). The Effects of Fault Planes on the Propagation of Vibration Waves. *Proceedings of the Thirty-Eighth Conference on Explosives and Blasting Technique.* Nashville, TN: International Society of Explosives Engineers.

Piersol, A., & Paez, T. (2009). *Harris' Shock and Vibration Handbook* (6th ed.). New York: McGraw-Hill.

Pugliese, J. (1972). Designing Blast Patterns Using Empirical Formulas. *Information Circular 8550*. US Bureau of Mines.

Redpath, B., & Ricketts, T. (1987). An Improved Scaling Procedure for Close-in Blast Motions. *Proceedings of the Thirteenth Conference on Explosives and Blasting Technique.* Miami, FL: International Society of Explosives Engineers.

Rouse, N., Acorn, T., & Worsey, P. (2013). Hole Diameter: Does it Affect Vibration Attenuation? *39th Conference on Explosives and Blasting Technique.* Ft. Worth, TX: International Society of Explosives Engineers.

Sanchidrián, J., Segarra, P., & López, L. (2007). Energy Components in Rock Blasting. *International Journal of Rock Mechanics & Mining Sciences, 44*(1), 130-147.

Segarra, P., Sanchidrián, J., Castillo, I., López, L., & Castedo, R. (2014). Rock-to-Sensor Transmissibility of Vibrations. *Proceedings Of The Fortieth Conference On Explosives And Blasting Technique.* Denver, CO: International Society of Explosives Engineers.

Silva-Castro, J. (2012). *Blast Vibration Modeling Using Improved Signature Hole Technique for Bench Blast.* Doctor of Philosophy Dissertation, University of Kentucky, College of Engineering, Lexington, KY.

Silva-Castro, J., & Lusk, B. (2012, December). Modeling of Signature Waves Based on Fourier Series for Blast Vibration Prediction. *Blasting and Fragmentation, 6*(3), pp. 181-195.

Singh, P., & Narendrula, R. (2007). The Influence of Rock Mass Quality in Controlled Blasting. *26th International Conference on Ground Control in Mining* (pp. 314-319). Morgantown, WV: International Conference on Ground Control in Mining.

Siskind, D., & Fumanti, R. (1974). Blast-Produced Fractures in Lithonia Granite. *Report of Investigations 7901*. US Bureau of Mines.

Siskind, D., Crum, S., & Plis, M. (1993). Blast Vibrations and Other Potential Causes of Damage in Homes Near a Large Surface Coal Mine in Indiana. *Report of Investigations 9455*. US Bureau of Mines.

Siskind, D., Crum, S., Otterness, R., & Kopp, J. (1989). Comparative Study of Blasting Vibrations from Indiana Surface Coal Mines. *Report of Investigations 9226*. US Bureau of Mines.

Siskind, D., Stachura, V., & Nutting, M. (1985). The Generation of Low-Frequency Long-Duration Vibrations from Surface Mine Blasting at Blanford, IN. US Bureau of Mines.

Siskind, D., Stagg, M., Kopp, J., & Dowding, C. (1980). Structural Response and Damage Produced by Ground Vibration from Surface Blasting. *Report of Investigations 8507*. US Bureau of Mines.

Spathis, A. (2010). A Brief Review of Measurement, Modeling and Management of Vibrations Produced by Blasting. *Vibrations from Blasting: Proceedings and Monographs in Engineering.* Water and Earth Sciences, Taylor & Francis Group.

Stagg, M., & Engler, A. (1980). Measurement of Blast-Induced Ground Vibrations and Seismograph Calibration. *Report of Investigations 8506*. US Bureau of Mines.

Stagg, M., Siskind, D., Stevens, M., & Dowding, C. (1984). Effects of Repeated Blasting on a Wood-Frame House. *Report of Investigations 8896*. US Bureau of Mines.

Tariq, S., & Worsey, P. (1996). An Investigation into the Effect of Varying Joint Aperture and Nature of Surface on Presplitting. *Proceedings from the 12th Symposium on Explosives and Blasting Research* (pp. 186-195). Orlando, FL: International Society of Explosives Engineers.

Tawadrous, A. (2014, August). (N. Rouse, Interviewer)

Tawadrous, A., & Katsabanis, P. (2007). Numerical Modeling of the Effect of High Stresses on Blast Induced Damage. *Proceedings of the 33rd Annual Conference on Explosives and Blasting Technique.* Nashville, TN: International Society of Explosives Engineers.

Taylor, L., Fourney, W., & Leiste, H. (2013, December). Close-In Shockwave Characteristics in Saturated Sand. *Blasting and Fragmentation, 7*(3), pp. 183-195.

Torrance, A. (2013). A Study of the Impact of Explosive Quality on Blast Performance. *Proceedings Of The Thirty-Ninth Conference On Explosives And Blasting Technique.* Ft. Worth, TX: International Society of Explosives Engineers.

Use of Explosives: Control of Adverse Effects, 30 CFR 816.67. (1983, September 30).

Walter, E., & Carroll, J. (1981). Lithologic Variation and Vibration Effects. *Proceedings of the Seventh Conference on Explosives and Blasting Technique.* Phoenix, AZ: International Society of Explosives Engineers.

Wheeler, R. (1997). The Analysis of Blast Vibration Data - What is the Current State of the Art? *Seventh High Tech Seminar - Blasting Technology, Instrumentation and Explosives Applications.* Orlando, FL: International Society of Explosives Engineers.

Worsey, P. (1986). Understanding Vibrations From Multihole Blasts Using Short Delay Periods. *Journal of Explosives Engineering, 3*(6), 25-28.

Worsey, P., Giltner, S., Drechsler, T., Ecklecamp, R., & Inman, R. (1996). Vibration Control During the Construction of an In-Pit Lime Kiln. *Proceedings of the Twenty-Second Conference on Explosives and Blasting Technique.* Orlando, FL: International Society of Explosives Engineers.

Wu, Y., Hao, H., Zhou, Y., & Chong, K. (1998). Propagation Characteristics of Blast-Induced Shock Waves in a Jointed Rock Mass. *Soil Dynamics and Earthquake Engineering, 17*, 407-412.

Yan, W., Tham, L., & Yuen, K. (2013). Reliability of Empirical Relation on the Attenuation of Blast-Induced Vibrations. *International Journal of Rock Mechanics & Mining Sciences*(59), 160-165.

Yang, R. (2012). Relationship between Peak Particle Acceleration, Velocity and Displacement of Blast Vibration. *Proceedings of the Thirty-Eighth Conference on Explosives and Blasting Technique.* Nashville, TN: International Society of Explosives Engineers.

Yang, R., & Kay, D. (2011). Multiple Seed Wave (MSW) Vibration Modeling for Tunnel Blasting in Urban Environments. *6th World Conference on Explosives & Blasting.* Lisbon, Portugal: European Federation of Explosives Engineers.

Yang, R., & Lownds, M. (2011). Modeling Effect of Delay Scatter on Peak Particle Velocity of Blast Vibration Using a Multiple Seed Waveform Vibration Model. *Blasting and Fragmentation, 5*(3), 31-45.

Yang, R., & Ray, K. (2014). A Linear Interpolation of Vibration Waveforms for Varying Seed Waveform Vibration Modeling. *Proceedings of the Fortieth Conference on Explosives and Blasting Technique.* Denver, CO: International Society of Explosives Engineers.

Yang, R., & Scovira, D. (2007). A Model for Near-Field Blast Vibration Based on Signal Broadening and Amplitude Attenuation. *EXPLO2007.* Wollongong, New South Wales, Australia: Australasian Institute of Mining and Metallurgy.

Yang, R., & Scovira, D. (2008, July). A Model to Predict Peak Particle Velocity for Near-field Blast Vibration - Based on Dominant Charge, Waveform Broadening, Delay Time Modeling, and Non-Linear Charge Weight Superposition. *Blasting and Fragmentation, 2*(2), pp. 91-116.

Yang, R., & Scovira, D. (2010). A Model for Near and Far-Field Blast Vibration Based on Multiple Seed Waveforms and Transfer Functions. *Proceedings of the 36th Conference on Explosives and Blasting Technique.* Orlando, FL: International Society of Explosives Engineers.

Yang, R., Kay, D., & Kim, G. (2014). Case Examples of Sensor Coupling Effect on Blast Vibration Measurement and Charge Weight Scaling Plot. *Proceedings Of The Fortieth Conference On Explosives And Blasting Technique.* Denver, CO: International Society of Explosives Engineers.

Yang, R., Scovira, D., & Patterson, N. (2009). An Integrated Approach of Signature Hole Vibration Monitoring and Modeling for Quarry Vibration Control. *9th International Symposium on Rock Fragmentation by Blasting.* Granada, Spain: International Society of Explosives Engineers.

Yang, R., Whitaker, T., & Kirkpatrick, S. (2009, April). PPV Management and Frequency Shifting in Soft Ground Near Highwalls to Reduce Blast Damage. *Blasting and Fragmentation, 3*(1), pp. 21-42.

Zhernokletov, M., Glushak, B., Anderson, W., Cherne, F., & Zocher, M. (2006). *Material Properties under Intensive Dynamic Loading.* New York: Springer.

Zhou, R., & Stump, B. (2006). Source Scaling Study of Single-Fired Mining Explosions. *Proceedings of the Thirty-Second Conference on Explosives and Blasting Technique.* Dallas, TX: International Society of Explosives Engineers.

Zhu, Y., Tsvankin, I., & Dewangan, P. (2005). *Physical Modeling and Analysis of P-Wave Attenuation Anistropy in Transversely Isotropic Media.* Colorado School of Mines, Center for Wave Phenomena, Golden, CO.

VITA

Nathan Thomas Rouse attended the University of Missouri-Rolla, earning his Bachelor of Science with Honors in Mining Engineering in 2009 and Master of Science in Explosives Engineering in 2010. This dissertation completes the obligations required of Mr. Rouse for the Doctor of Philosophy in Mining Engineering.

Mr. Rouse has lived in Lexington, KY since 2010, where he is the Staff Mining and Explosives Engineer for Morgan Worldwide Consultants, which is now a division of RESPEC. In 2013 he earned his Professional Engineer License and is currently registered in Kentucky and Ohio. He is also a licensed blaster in Kentucky and Missouri.

Mr. Rouse is a member of the International Society of Explosives Engineers (ISEE) and Society of Mining, Metallurgy, and Exploration. He has published works through both societies, including the Blasting and Fragmentation Journal with the ISEE.